Electron injection into thin insulating and luminescent films on silicon

Richard N. Campbell

TO
MARILYN

ELECTRON INJECTION INTO THIN INSULATING AND LUMINESCENT FILMS ON SILICON

by

Richard N. Campbell Bsc.

submitted in accordance with the regulations of the University of Durham for the degree Doctor of Philosophy.

ABSTRACT

ELECTRON INJECTION INTO THIN INSULATING AND LUMINESCENT FILMS ON SILICON

This thesis describes electron injection into thin films of thermally grown SiO_2 and also Zn_2SiO_4:Mn. Electrons are accelerated to high energies in the depletion field of a reverse biased, shallow (1000 Å deep), planar $p\text{-}n^+$ junction, and directed towards the silicon and thin film interface. The injection process is aided by the additional application of an electric field across the thin films.

The form of the injected current dependence on the field applied across the films and with junction avalanche current is found to be consistent with electron injection from localised microplasmas within the shallow junction. The experimental results indicate that there is a near exponential rise in the injected current with increasing junction current. Previous explanations for similar dependences are shown to have several deficiencies when applied to the present structures. A new model of electron injection is proposed which is based on microplasma switching probabilities. Numerical approximations when applied to the microplasma injection model are shown to give acceptable agreement with experimental results.

The fabrication of the shallow junction injection structures is described in detail and also the thin film formation techniques. A proposed injection structure which should give a more uniform electron injection is also described.

ACKNOWLEDGEMENTS

I should like to thank Professor D. A. Wright for making available the facilities of the Department of Applied Physics and Electronics, Durham University. I am also indebted to Dr. M. J. Morant for his guidance in the experimental work and for his helpful criticism in the preparation of this thesis.

My thanks also go to Mr. F. Spence and all the department's technicians for making possible much of the experimental apparatus.

I should also like to thank Mr. D. Errington for his help in taking the ellipsometer readings.

A special show of thanks must also be given to Mrs. B. Jackson for her hard work in typing the manuscript.

Finally I am especially grateful to the Science Research Council for their financial support during this work.

CONTENTS

CHAPTER ONE - INTRODUCTION		1
1. 1	Integrated Displays	1
1. 2	Bases of Present Work and Properties of Willemite	1
1. 3	Electroluminescence from Willemite	2
1. 4	Outline of Present Research	4
CHAPTER TWO - JUNCTION BREAKDOWN AND HOT ELECTRON INJECTION		6
2. 1	Introduction	6
2. 2	Avalanche Breakdown and Electron Energy Loss Mechanisms	7
2. 3	Scattering in Shallow Junctions	11
2. 4	Properties of Microplasmas	13
2. 5	Electron Emission from p-n Junctions into Vacuum	16
2. 6	Electronic Injection from Silicon into Silicon Dioxide	19
2. 7	Electron Injection from p-n Junctions into Silicon Dioxide	22
2. 8	Conclusions	25
CHAPTER THREE - DESIGN OF HOT ELECTRON INJECTION STRUCTURE		27
3. 1	Introduction	27
3. 2	Impurity Profiles and Junction Breakdown	28
3. 3	The Shallow Diffusion	29
3. 4	Device Geometry	30

CHAPTER FOUR - FABRICATION OF JUNCTION STRUCTURES IN SILICON 31

4. 1 Introduction 31

4. 2 Processing Techniques 31

4. 3 Silicon Cleaning 32

4. 4 The Masking Oxide 32

4. 5 The Phosphorus Diffusions 33

4. 6 Metallisation 36

4. 7 Defects in the Junctions 37

CHAPTER FIVE - MEASUREMENTS OF CURRENT INJECTION INTO SILICON DIOXIDE 39

5. 1 The Injection Structure 39

5. 2 Properties of the Junction Under Reverse Bias 40

5. 3 Measurement of Injection Currents into Silicon Dioxide 42

5. 4 Measurements of Injection Currents with Infra-Red Illumination of the Junction 44

5. 5 Conclusions 45

CHAPTER SIX - DISCUSSION OF THE RESULTS ON ELECTRON INJECTION INTO SILICON DIOXIDE 47

6. 1 Introduction 47

6. 2 The Dependence of the Injected Current on the Oxide Field Strength 47

6. 3 The Dependence of the Injected Current on the Junction Current 54

6. 4 Microplasma Model for Injected Oxide Currents 56

6. 5 Numerical Values for the Microplasma Model 62

6. 6 Discussion of Other Observations 67

6. 7 Conclusions 69

CHAPTER SEVEN - CURRENT INJECTION INTO THIN WILLEMITE FILMS 70

7. 1 Introduction 70

7. 2 High Field Injection 70

7. 3 Willemite Formation Reaction Experiments 72

7. 4 Device for Hot Electron Injection into Willemite 76

7. 5 Results for Electron Injection into Luminescent Films 78

7. 6 Conclusions

CHAPTER EIGHT - CONCLUSIONS AND SUGGESTIONS FOR FURTHER WORK 82

8. 1 Present Research 82

8. 2 Further Research Required 84

8. 3 Conclusion 88

APPENDIX 1 - IMPURITY DIFFUSION PROFILES 89

A1. 1 General Equation 89

A1. 2 The Deposition Stage 90

A1. 3 The Drive-In Stage 90

A1. 4 Step Junction Approximation 90

A1. 5 Numerical Solution 91

APPENDIX 2 - PHOTO-LITHOGRAPHIC PROCEDURES 93

A2. 1 General Procedures 93

A2. 2 Pre-etch Baking and Resist Removal Procedures 94

References 95

CHAPTER ONE

INTRODUCTION

1.1 Integrated Displays

In recent years small area display devices have found wide applications in pocket calculators, digital watches, digital voltmeters, etc. The majority of these displays have been based on $GaAs_x : P_{1-x}$ or GaP light emitting diodes. Liquid crystal displays have found an application where low power dissipation is of primary importance but they have the disadvantage of requiring an external light emitting source and a limited working life. The growth of present displays into areas requiring high resolution and complex character representation or for optical coupling between I.C.'s would appear to be restricted by the necessity for associated circuitry. These are generally silicon integrated circuits performing drive, decoding and memory functions and are coupled externally to the display device. The relative high cost of making such connections and their high failure probability makes them a governing factor in limiting the complexity of display systems. It was realised in the Department that if a thin film, with a light emitting capability, could be formed on a silicon substrate also containing the associated circuitry, then complex integrated interconnections could be made using standard silicon technology. Such a system does not appear to have been studied elsewhere using a direct light emitting film although a similar idea has been suggested using a liquid film on a silicon substrate which acts as one of the electrodes [1].

This thesis forms part of a wider study of possible luminescent films for the described applications. It is necessary to find a material which has a highly efficient light emitting capability and which is also compatible with silicon. One such material is zinc-orthosilicate, doped with manganese, which is known in its natural occurring form as the mineral willemite. This material has been studied earlier in the Department in the form of thin films. This chapter will present some of the findings and the general properties of willemite.

1.2 Bases of Present Work and Properties of Willemite

In a study of the possible methods of forming luminescent films on a silicon substrate, Edwards [2] developed a relatively simple procedure for the formation of willemite by the chemical conversion of thermally grown SiO_2 films.

Willemite has the chemical composition $Zn_2SiO_4:Mn$; it is known to be one of the most efficient cathodluminescent phosphors, second only to ZnS. In a crystalline form willemite has a stable rhombohedral structure with an optical band gap of between 5.4 - 5.5 eV. The characteristic luminescence is peaked in the green at about 5,230 Å and results from the de-excitation of a Mn^{2+} ion which substitutes for the Zn^{2+} ion in the lattice. Most of the early work on willemite was concerned with its properties as a high efficiency cathodluminescent phosphor. It was most commonly prepared in a powder form from zinc compounds, notably zinc oxide, and silica.

The literature shows that, although a definite compound $Zn_2SiO_4:Mn$ exists, the cathodluminescent properties are not critically dependent on the exact composition. The efficiency is not dramatically reduced by an excess of up to 50% silica; similarly the proportion of Mn incorporated can range between 1% and 5%. It has been reported that concentrations of Mn as high as 20% and down to 0.1% still results in a luminescent material. This degree of latitude in composition allowed Edwards to form thin films of willemite on silicon by the single stage vacuum deposition of $ZnF_2 : MnF_2$ onto thermally grown SiO_2 followed by a suitable heat treatment. At temperatures above 900 °C a simple solid state reaction was thought to take place between the deposited film and the thermally grown oxide:- $2ZnF_2 : Mn + 2SiO_2 \rightarrow Zn_2SiO_4:Mn + SiF_4\uparrow$. It was found that the best quality films were obtained by heating in an oxygen atmosphere rather than that of nitrogen or argon. Detailed analysis of the resulting films has shown the structure to be that of willemite polycrystallites in a silica matrix [3]. Measurements of the cathodluminescent emission, made at Newcastle Polytechnic (1083), show the spectrum to be broad and structureless, peaked at 5,230Å with a long wavelength tail. The spectrum was similar to that obtained from a commercially available willemite phosphor powder.

1.3 Electroluminescence from Willemite

Morant [4] has reviewed the luminescent properties of willemite with a view to deducing the conditions necessary for obtaining electroluminescence. It is concluded that willemite may have properties which would make it more suitable than many other phosphors for achieving electroluminescence in thin film structures on silicon. In particular it is thought that luminescence could result from unipolar injection. In order to understand the significance of this it is necessary to consider in more detail the energy levels of the Mn^{2+} ion which are involved in radiative transitions. This has been the subject of much theoretical and practical work by Klick [5, 7] and Garlick [6]. The radiative transitions are from the ^4G excited state of the 3d electrons, in which four of the electrons have parallel spins and one anti-parallel, to the ^6S ground state

in which all five electrons have parallel spins. A diagram of the approximate energy levels of the 3d electrons is shown in Fig. 1.1. Their exact position within the forbidden gap is in some doubt at present. Transitions from higher energy states are non-radiative but there is a probability of an electron losing energy via the ^4G state hence with a radiative transition to the ^6S state. It has been established that radiative transitions in willemite are located entirely within the Mn^{2+} ion.

Of the possible methods of exciting electroluminescence one might be via electron hole recombination or bipolar injection Fig. 1.2a. Electrons and holes are injected from opposite electrodes and if recombination can be achieved within 100Å of a Mn^{2+} ion then there is a high probability of excitation via a resonance transfer of energy. The difficulty of utilizing this procedure lies in the probable low efficiency of the hole injection into willemite from silicon. It is known that hole injection into thermally grown SiO_2 is possible[8] but the higher potential barrier causes the efficiency to be much lower than for the injection of electrons under similar conditions. A similar low efficiency would be expected for hole injection into Zn_2SiO_4. A further complication is that holes would be expected to have a very low mobility in Zn_2SiO_4 as is common in most oxygen dominated phosphors. This would have the effect of limiting the number of Mn^{2+} ions that could be excited to those within a few atomic distances of the hole injecting electrode. The decay time of a Mn^{2+} ion is also known to be quite long, $\simeq$ 10 ms, and this would limit still further the availability of ions for excitation. It is reasonable to conclude, therefore, that bipolar injection is unlikely to be successful as a means of exciting electroluminescence.

It has been noted that one of the features of the radiative mechanism in willemite is that it is located entirely within the Mn^{2+} ion. This means that positive charge need take no direct part thus allowing the possibility of unipolar excitation. In this mechanism luminescence would be excited by the impact collision of a high energy electron with a Mn^{2+} ion, Fig. 1.2b. The lowest energy required for excitation would be 2.65 eV, corresponding to a transition into the 4G excited state. This level has been found to be difficult to excite directly by optical methods and excitation by electron collision may be equally improbable although there is no evidence for this. It is found that the higher energy levels, particularly those above 4.83 eV are the easiest to excite by optical means although they also result in a number of radiationless transitions. Low voltage cathodluminescent experiments, which might have been expected to yield direct information on the levels which could be excited by impact collisions, have been hampered by surface effects apparently

caused by non-luminescent layers on the surface of phosphor powder granules. Cathodluminescence has been observed in willemite powders using electron beam energies as low as 12 eV[9]. It would be expected that the silicon/willemite interface formed in a process such as that developed by Edwards would be less susceptible to the effects which result in the non-luminescence on the free surface of phosphor powders. It has also been shown that if ZnO [9, 10] phosphor powders are produced in a manner such as to reduce the surface effects then cathodluminescence can be produced by bombardment with 4eV electrons. There is thus some hope that the unipolar injection of electrons of comparatively low energies might excite luminescence in either material. This thesis explores this possibility with reference to willemite films on silicon.

1.4 Outline of Present Research

In a thin film structure the simplest way of achieving the electron energies for excitation from thermally injected electrons is by applying a high electric field. It is well known that collision ionisation processes can take place in wide band gap dielectrics under high field bias indicating the attainment of high electron energies. This approach has been investigated by Edwards [2], Davies [11] Husain [107] and the author in an attempt to obtain electroluminescence from thin willemite films. Weak electroluminescence has been observed but the conditions required were found to be non-reproducible. It has been concluded by the author that the willemite formation process results in a residual oxide film being left unreacted between the silicon substrate and the willemite film. The work on this topic is discussed in more detail in Chapter 7, from which it is shown to be highly probable that the thickness of the oxide film is the controlling factor in determining the number and the energies of the electrons which enter the willemite from the silicon. It is probable, therefore, that the nature of the oxide film determined whether or not electroluminescence was obtained in earlier experiments. Control over the oxide film thickness was considered to be impractical without a means of measuring the thickness of films of less than 100 Å. This has since been done as another part of the overall investigation.

A further difficulty in exciting electroluminescence by injection into a high field region is that thermal scattering process can be expected to dominate at energies below 1 - 2 eV. These energy losses make it difficult to accelerate a sufficient number of electrons to the higher energies required for luminescence without using field strengths close to those which result in dielectric breakdown of the film. It was therefore considered that if electrons could be injected into a dielectric with an initial energy of around 2 eV the probability of

accelerating them to higher energies, up to ionisation, would be greatly increased.

The major part of this thesis is concerned with using an avalanching reverse biased p-n junction as a means of providing a population of high energy electrons which can be injected into the conduction band of an insulator. Further acceleration of the electrons may then take place in the film under the action of an applied field. Fig. 1.3 shows a band diagram for such a process. The physics of the resulting energy distribution of the charge carriers in an avalanching p-n junction is considered in Chapter 2. This is followed by a review of the literature on electron injection from silicon p-n junctions into both vacuum and silicon dioxide.

The design of a p-n junction to allow sufficient high energy electrons to reach the silicon/insulator interface is discussed in Chapter 3. The details of the fabrication of the junction are given in Chapter 4.

In order that some insight could be gained into the physics of the injection process an initial series of experiments was performed, injecting electrons into thermally grown SiO_2. The results of these experiments are described in Chapter 5 and discussed in Chapter 6.

In the final part of this investigation thin luminescent films were formed over the junction using a new variation of the process developed by Edwards. Measurements obtained on injecting electrons into these films are presented in Chapter 7.

Chapter 8 presents the conclusions of this investigation and gives some suggestions for further work.

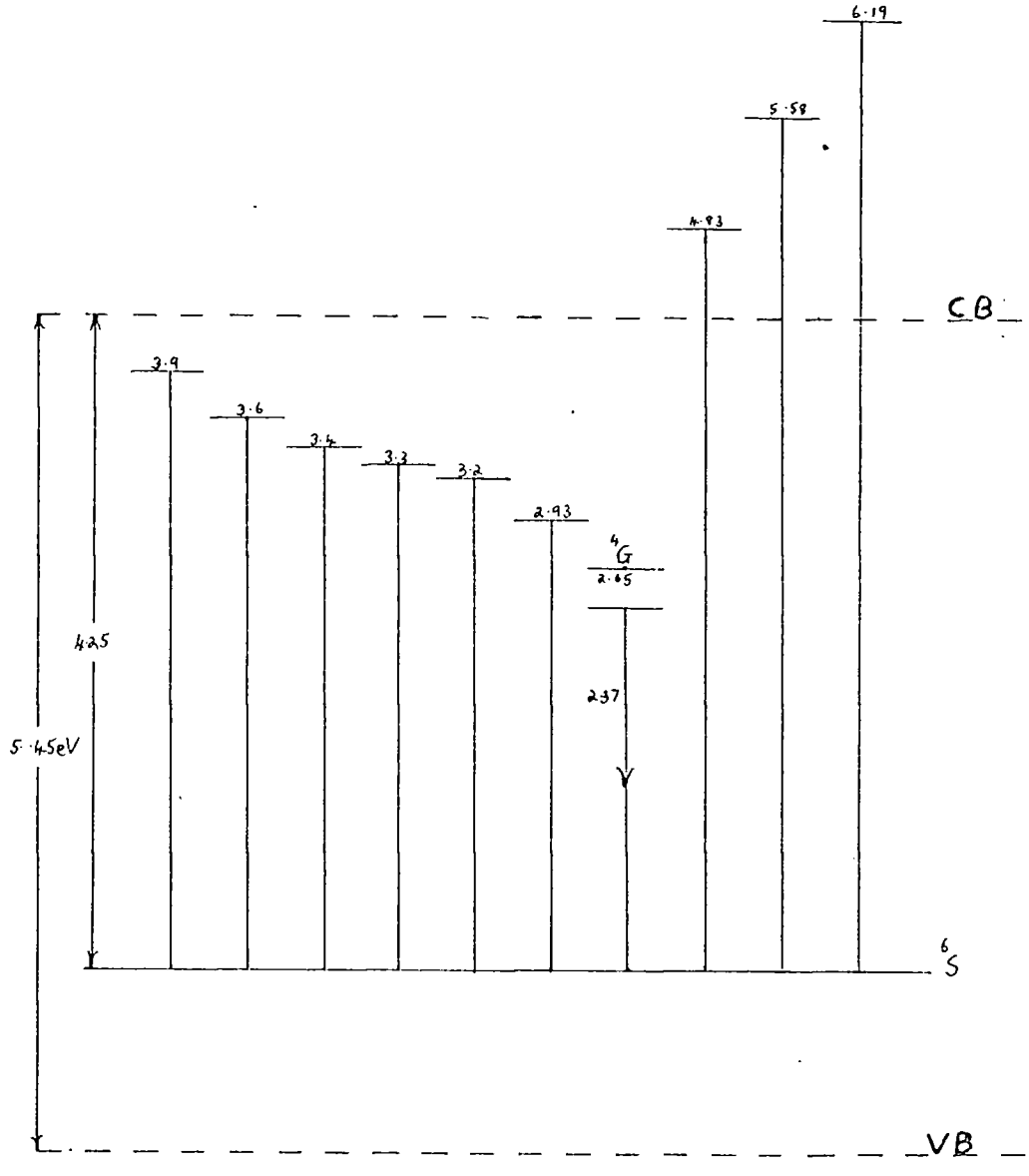

FIG 1.1 ENERGY LEVELS OF 3d ELECTRONS OF Mn^{2+} IN $Zn_2SiO_4:Mn$

Ref 4

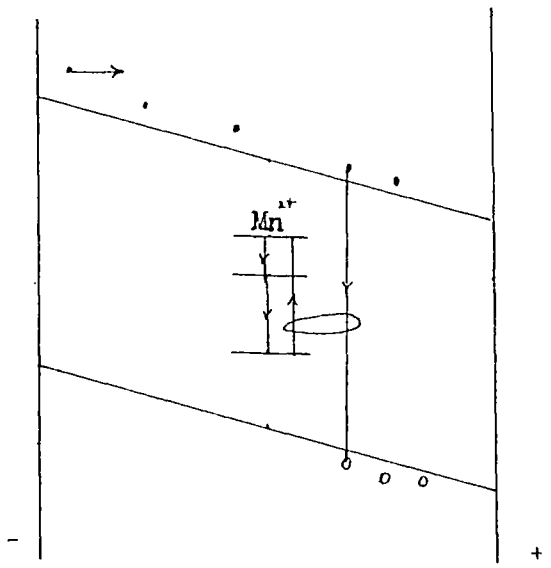

a Bipolar Excitation

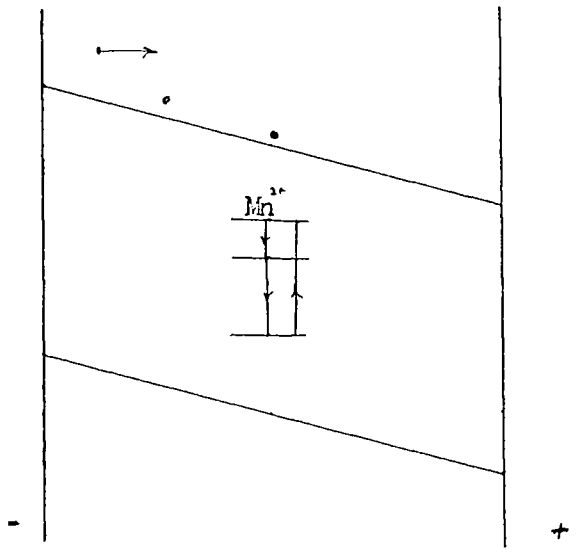

b Unipolar, Impact Excitation

FIG 1.2 ALTERNATIVE MECHANISMS FOR ELECTRONIC EXCITATION OF THE Mn^{2+} ION IN WILLEMITE

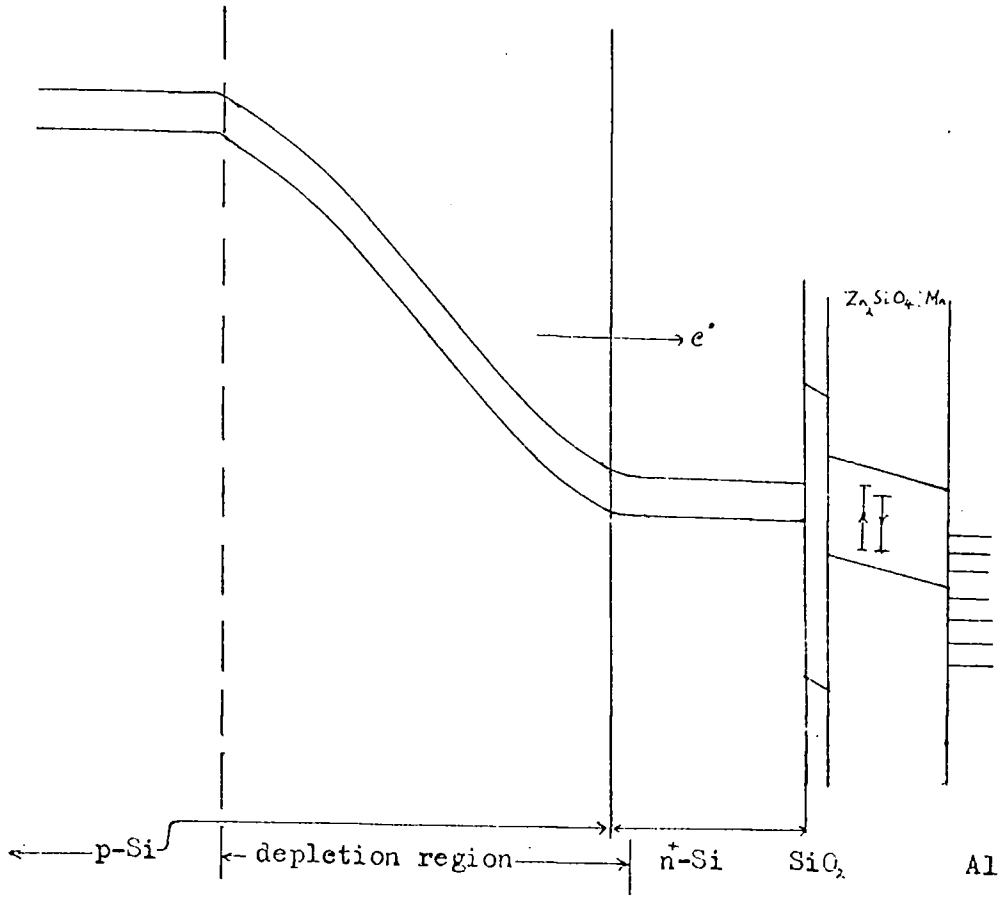

FIG 1.3 ELECTRON INJECTION STRUCTURE USING A REVERSE BIASED pn^+ JUNCTION

CHAPTER TWO

JUNCTION BREAKDOWN AND HOT ELECTRON INJECTION

2.1 Introduction

It was proposed in Chapter I that a possible method of injecting electrons into a thin film of willemite would be to utilize those electrons which had been previously accelerated to high energies in the depletion field of a reverse biased p-n junction. By use of a suitable junction geometry it was considered that it should be possible to arrange for a proportion of the electrons arriving at the silicon-willemite interface to have energies of the same order as the barrier height between the two materials.

There have been several previous reports of electron emission into vacuum and injection into S_iO_2 using the principle of electron acceleration in a depletion field. Some of these reports are described later in this chapter from which it is apparent that the emission or injection efficiencies are generally very low. The primary causes of the low efficiency are the energy loss mechanisms, acting within the silicon, which limit the average energy of the electron population. These energy losses must be allowed for in the design of a junction that will allow electron injection. The following section, 2.2, will review the various energy loss mechanisms in relation to avalanche breakdown of a silicon junction. This will be extended in section 2.3 to include the additional scattering of electrons during transport to the surface from a shallow p-n junction.

Previous work on electron emission into a vacuum from an avalanching p-n junction has shown that the emission originates from localised areas of breakdown known as microplasmas. It will be shown in chapters 2 and 5 that a similar conclusion is reached for injection into insulating films. Interpretation of some of the results will therefore be made with reference to the electrical properties of microplasmas which are reviewed in section 2.4.

In the final sections of this chapter a review is given of previous work by other authors on electron injection from a reverse biased p-n junction into both vacuum and silicon dioxide.

2.2 Avalanche Breakdown and Electron Energy Loss Mechanisms

A thermally or optically excited charge carrier which is created in, or diffuses to the depletion region of a reverse biased p-n junction will be accelerated to a higher energy by the depletion layer field. Once having attained a certain energy it will have a probability of creating an electron-hole pair by impact collision with the valence electrons. The charge carriers thus created can themselves be accelerated and repeat the process leading to a charge carrier multiplication process. If the field is sufficiently high, a situation analogous to that in a gas discharge can exist and the junction is said to be in a state of avalanche breakdown. McKay[11] has analysed this condition in terms of a multiplication coefficient α . This is defined as the number of electron-hole pairs per unit volume produced by a primary hole or electron per unit distance travelled in the direction of charge transport. McKay derived the expression:

$$1 - \frac{1}{M} = \int_0^W \alpha \, dx \qquad ((2.1))$$

for a depletion region of width W.

M is known as the multiplication factor of charge carriers.

At avalanche breakdown $M \to \infty$

$$\text{ie. } \int_0^W \alpha \, dx \to 1$$

The value of α is a property of the material in which the junction is formed. It is found that α varies with field strength and this dependence is due to the energy loss mechanisms to which a carrier is subjected. The principle energy loss mechanisms can be stated as follows:-

(i) scattering by acoustic phonons,
(ii) scattering by impurities,
(iii) scattering by optical phonon emission,
(iv) energy losses in collisions,
(v) energy losses in optical phonon recombinations

These energy loss mechanisms determine the average energy of the charge carrier population created in an avalanching junction. In addition they control the loss of energy as the charge carriers diffuse away from the depletion region. Hence, they determine the maximum junction depth through which electron emission or injection will still occur. A study of α therefore leads to an understanding of the relative importance of the various energy loss mechanisms and has been the subject of much theoretical and experimental work.

In 1954 Wolff[12] presented a theory to describe the experimentally observed dependence of α on the field across a p-n junction in silicon. It was considered that the predominant losses were to optical phonon emission and to ionising collisions. Wolff proposed that the charge carrier population in an avalanching junction was one in which the energy loss in a phonon collision was small compared to the energy gain from the field. Once a charge carrier had attained a threshold energy, ionisation would occur within a very short period. These assumptions resulted in an isotropic description of the charge carrier distribution which allowed Wolff to solve Boltzamann's transport equation by expanding in terms of spherical harmonics and retaining only the first two terms. The velocity distribution function of the carriers could then be written in the form,

$$n(c,\theta) = n_o(c) + n_1(c)\cos\theta \qquad ((2.1))$$

where c represents the magnitude of the charge carrier velocity and θ is the angle its direction makes with the field. Wolff obtained solutions to both n_o and n_1 in low and high energy conditions. The low energy solution represented the situation below an ionisation threshold and involved the assumptions that the m.f.p. for an optical phonon collision was constant, as proposed by Seitz[13]. The high energy solution could only be obtained for a condition in which the charge carriers were a few tenths eV above a threshold energy, such that the m.f.p. for ionisation was much less than for an optical phonon collision. The two solutions were matched in the threshold region such that n_o and n_1 were continuous. Finally, Wolff related the velocity distribution to α and matched it at a single experimental point obtained by McKay[14]. This required an assumption for the value of the threshold energy which was taken to be 2.0eV. A value greater than the 3/2 Eg predicted by simple band theory was chosen to allow for the band structure of silicon. Fig. 2.3. A match was made to McKay's data for an energy of 2.3 eV and a best fit was obtained with a value of the m.f.p. of an optical phonon emission (l_r) of 200A°. The dependence of α on the field (F) was derived as,

$$\alpha = a\exp(-g/F^2) \qquad ((2.2))$$

where a and g are constants. The fit was reasonable at high values but not so good at low fields. The energy distribution of the charge carriers is shown in Fig. 2.1. It is Maxwellian below ionisation with an effective temperature, T_e, given by,

$$T_e = (q l_r F)^2 / 3E_r \qquad ((2.3))$$

where E_r is the optical phonon energy.

In 1960 Chynoweth [15] published results which showed that α varied with field approximately as,

$$\alpha = K \exp(-d/F) \qquad ((2.4))$$

where K and d are constants. In 1961 Shockley[16] proposed a theory which fitted this data over several decades. As in Wolff's theory Shockley considered that optical phonon emission and ionisation were the principle sources of energy loss. According to Shockley's model a charge carrier with energy greater than the threshold energy for ionisation (Ei) is on average, able to make r phonon collisions before ionisation, where $r = \ell_i/\ell_r$ and where ℓ_i is the m.f.p. between ionisation for a charge carrier with energy greater than Ei. The probability of a charge carrier with energy E, greater than Ei, making an ionising collision was derived as,

$$P_1 = 1 - \exp\left(-(E - Ei)/rE_r\right) \qquad ((2.5))$$

It can be seen that as the energy of a charge carrier increases above threshold, taken by Shockley to be 1.1eV, there is an increasing probability of an ionising collision. This is in contrast to Wolff's model in which a charge carrier with energy a few tenths of an eV above threshold, taken to be 2.0eV, has a near certain probability of making an ionising collision.

In his derivation of a relationship for the dependence of α on the junction field, Shockley considers a low field situation in which the random energy of the carriers is of the order of the optical phonon energy. Only those carriers which can travel a distance of Ei/qF without a randomising optical phonon collision are considered to be capable of ionisation. The model neglects all those carriers which reach energies in excess of E_r, but less than Ei, which are scattered but subsequently reach Ei. The probability of a carrier, starting from near zero energy, making an ionising collision was shown to be,

$$P_2 = \exp(-Ei/q\ell_r F) \qquad ((2.6))$$

From which the energy loss per ionisation is found to be,

$$E' = rE_r \exp(-Ei/q\ell_r F) \qquad ((2.7))$$

Equation ((2.7)) was then equated to,

$$E' = qF/\alpha$$

where F/α is the voltage drop per ionisation along the carrier path.

$$\therefore \quad \alpha = (qF/rE_r) \exp(-Ei/q\ell_r F) \qquad ((2.8))$$

The relationship given in ((2.8)) was fitted to Chynoweth's data using the conditions that Ei = 1.1eV and rE_r = 1.1 eV which results in a value for the m.f.p. for an optical phonon emission of 50 Å. In summary it can be stated that Shockley's model leads to a velocity distribution for the carriers which is peaked in the field direction. This peak contains all those electrons which escape randomising collisions.

In 1962 Baraff [17] concluded that the fields encounted in silicon p-n junctions at avalanche breakdown were not high enough to support Wolff's isotropic distribution nor low enough for Shockley's spike to predominate. From a numerical solution of Boltzamann's transport equation Baraff showed that the true situation lies somewhere between the two extremes. He concludes that the charge carrier distribution is probably peaked in the field direction but that the carriers attain high energies essentially by diffusion against the optical phonon drag rather than ballistically as in Shockley's theory.

The models discussed so far have assumed that optical phonon emissions and impact ionisation constitute the greatest energy loss mechanisms. Acoustic phonons are known to predominate only at energies below 1.0 eV and can justifiably be left out of the discussion. Similarly impurity scattering will only be important in relatively impure semiconductors. A statistical study of avalanche breakdown in silicon has been made which also considers energy losses during the recombination of electron-hole pairs. In this study by Sewards and Grannemann [18] it is concluded that energy losses due to recombination dominate below 6 e V. Above ~ 6 eV energy losses through ionisation dominate. The theoretical energy distribution obtained by these authors is shown in Fig. 2.2. It predicts that only a small proportion of the total number of carriers can be expected to gain energies in excess of 3 eV. The distribution is given by

$$fo(E) = A \exp - \frac{(E/Eo)^3}{3} \qquad ((2.9))$$

where A is a constant and Eo is a characteristic energy for silicon. When matched to the breakdown characteristics of commercial junctions Eo was found to be 1.9 eV. The distribution thus predicts a sharper fall off of carriers with increasing energy than given by a simple Maxwellian.

In Chapter 5 a discussion is given of the experimental results obtained in this work for electron injection into SiO_2. In common with other workers, (Section 2.5 and,2.6) the charge carrier distribution is assumed to be Maxwellian although it is shown that there are probably fewer high energy electrons than predicted.

The true distribution is thought to be closer to that predicted by Wolff.

As a further complication to the subject of avalanche breakdown in silicon it must be noted that none of the theories discussed has taken into account the nature of the band structure of silicon. Fig. 2.3. This, as Hodgkinson [19] points out, means that it is not strictly correct to consider a single m.f.p. for ionisation or a well defined threshold energy. In a graphical analysis of the allowed threshold energies in silicon Hodgkinson estimates that a single point in the Brillouin zone exists where ionisation can take place, at a threshold energy of 1.1 eV, but that there is a main threshold covering most of the zone requiring an energy of 2.3 eV.

2.3 Scattering in Shallow Junctions

In the above discussion only the charge carrier distribution within the depletion region has been considered. In the device structure proposed an electron has to move away from the depletion region towards the silicon interface and still retain sufficient energy for emission. With a shallow n^+-p planar junction, as used in this work, the surface n^+ layer can be considered to be field free. In such a situation it is reasonable to expect that an electron will diffuse towards the interface and be subjected to all the energy loss mechanisms discussed earlier. With MO.S. devices or with deep n^+-p structures, such as discussed in Section 2.6, an induced surface field exists within the p- type silicon which can further accelerate electrons.

In 1963 Bartelink et al [20] measured the actual energy distribution of electrons emitted from a shallow planar p-n^+ junction in silicon. Under avalanche conditions the emission was found to originate from areas of localised breakdown or microplasma. The measured distribution was found to decrease exponentially with energy and was assumed to be the tail of a Maxwellian distribution of effective temperature 0.5 eV. This assumption was only justified if an initial assumption is made that the energy distribution of the charge carriers in a microplasma is Maxwellian. If in fact the distribution was that considered by Wolff then an over estimation of the average energy of the charge carriers in a microplasma would result.

In a theoretical analysis Bartelink calculated the flux transport of charge carriers through the field-free n^+ region. He treated the situation as being one of pure diffusion, with electrons losing energy to optical phonons. Ionisation was considered to be an absorptive process in that, once an ionising collision had occured an electron would not have sufficient energy to be emitted. It was shown that if the charge carrier distribution at the junction was Maxwellian then the distribution at the interface would also be Maxwellian but reduced in magnitude by the term,

$$\exp(-L/L_o) \qquad ((2.10))$$

where L is the junction depth and Lo is given by,

$$Lo = \lambda^2 / (1 + rE_r/kT_e)$$

where $\lambda^2 = \ell(\ell_r)$

and $$\frac{1}{\ell} = \frac{1}{\ell_r} + \frac{1}{\ell_i}$$

ℓ_i is the m. f. p. for an ionising collision

ℓ_r is the m. f. p. for an optical phonon emission.

The characteristic length Lo was calculated from the experimentally observed increase in the emitted electron current with decreasing junction depth. A value for Lo of 50 Å was obtained.

In a second part of the experiment Bartelink fitted a theoretical distribution, in which the peak was a function of $r = \ell_i/\ell_r$, to the experimental data. The assumptions of the theory required experimental conditions in which the charge carriers were released into the depletion field within an energy range which was small compared with Er and at a known distance from the silicon surface. This was achieved by reverse biasing the junction below breakdown and photo-exciting carriers into the depletion field. The dependence of the distribution peak on r resulted from the assumption that the number of electrons which could escape with few phonon collisions was small. The probability of escape after many phonon collisions would also be small because of the increase in random walk length and hence the increased probability of an absorptive ionising collision. A fit to the experimental data yielded a value for r = 3.2 and hence values of ℓ_r = 60Å and ℓ_i = 190 Å.

It is apparent from Bartelink's work that the probability of electron emission into a vacuum is very low. The magnitude of the high energy electron population arriving at the interface is reduced by energy losses by a factor approximately given by :-

$$\exp(-L/Lo) \simeq 10^{-10}$$

for a 1000 Å deep junction. The emission probility is further reduced by about an order of magnitude by surface reflection effects. Bartelink obtained an emission probability of about 4×10^{-11} for a 1000 Å deep junction operating with an avalanche current of 25 mA. No information is given how the emission current behaved with changing junction currents. This will be one of the major problems discussed in Chapter 6.

Electron emission probabilities into SiO_2 are not likely to differ very much from those observed for emission into vacuum. The barrier height is smaller and will be further reduced by the field across the oxide, however, this will not be significant compared with the junction depth factor.

Only if the barrier height is reduced to below the ionisation threshold, with for example Cs, can high emission efficiencies be obtained. Injection into SiO_2 might be expected to be further reduced by trapped positive charge and interface states.

2.4 Properties of Microplasmas

The voltage at which a reverse biased junction reaches avalanche breakdown is a function of the relative doping of the p and n regions of the junction. It is found in most practical junctions that the breakdown does not occur uniformly over the entire junction area but in localised regions and at a few tenths of a volt below the voltage expected for uniform junction breakdown. These areas of enhanced carrier multiplication are known as microplasmas. The exact origin of microplasmas is not well established although their electrical properties are well documented [21]. For a microplasma to occur in a junction it is necessary to have a region of localised field intensification within the depletion region. Shockley [16] has proposed that spherical precipitates of SiO_2 could enhance the field locally because of the difference in dielectric constants.

Lawrence [22] has also proposed metal precipitates as being a cause of microplasmas. Dislocations have been considered by Chynoweth and Pearson [23] as being able to distort the field locally such as to cause microplasmas. The subject of the effect of dislocations on p-n junctions has been reviewed more recently by Matare' [24]. It is thought that around a dislocation is a region of dangling bonds where a space charge pipe is built up. This pipe is highly conducting along the axis because of wave-function overlaps of the bonds. Perpendicular to the axis, the pipe possesses blocking properties because of the captured space charge region.

In shallow junctions, microplasmas can usually be located as areas emitting white light, Newman [25]. This emission has been interpreted in terms of the recombination of the high energy charge carriers produced during multiplication in the microplasma. [26] More recently, because of a need to account for an observed angular dependence and polarisation, the emission has been thought to be caused by Bremsstrahlung [27]. That is, the de-acceleration of charge carriers in the lattice colombic field. The emission spectrum was first measured by Chynoweth and McKay [28] and an estimate of T_e = 0.18 eV was made for the effective temperature of the charge carrier population, assuming a Maxwellian distribution.

It was noted that the intensity of the emission increased with current but that there was no change in the emission spectrum.

The most extensive studies of microplasmas have concerned their electrical characteristics. It is observed that if a bias is applied to a junction which is just sufficient to cause a microplasma to switch on then the current is carried in a series of rectangular pulses. These pulses have a very fast rise time ($< 10^{-8}$ secs) and are of constant amplitude but of random interval and duration, τ_1 , for a given bias.[11, 23, 29]. As the voltage is increased the pulse amplitude increases but so does the fraction of time during which the microplasma is on, i.e. carrying a current. Finally, the voltage can be increased to the point where the microplasma is on continuously and the current/voltage characteristics then becomes linear.

Mathematical models to account for these properties have been proposed by McIntyre [30] and later by Haitz[31] with further improvements by Aladinskii [32]. In general four parameters are required to characterise a microplasma. These are:-

(i) The series resistance R_s which is assumed to be constant for a given microplasma. R_s will in general be made up of a space charge component R_{sc} and a spreading resistance component R_{sr}.

The space charge component results from an excess of holes or electrons on opposite sides of the junction boundary after moving away from the region of multiplication, i.e. the region of highest field. McIntyre [30] has considered the case for an abrupt p-n junction and derives the expression,

$$R_{sc} = \frac{2}{\pi \varepsilon \varepsilon_0 v_{ds}} \left(\frac{W^2}{D_m^2} \right) \qquad ((2.11))$$

where, D_m is the diameter of a microplasma whose axis extends over the entire width, W, of the depletion layer, v_{ds} is the saturation drift velocity of the carriers in the field.

The spreading resistance component results from the microplasma current spreading out into the semiconductor bulk. At the low-doped end of the microplasma the current can be considered to be spreading out into a semi-infinite region of resistivity ρ_p. For a microplasma current from a semi-spherical surface area McIntyre derived the expression,

$$R_{srp} = \sqrt{2}(\rho_p / \pi D_m) \qquad ((2.12))$$

At the high-doped end of the microplasma the spreading resistance component is usually unimportant. However, this may not be so for a very shallow junction as used in this work. A second component to the spreading resistance may have to be added, from Phillips[33]

$$R_{srn} = \frac{R_s}{2\pi} \ln \frac{D_s}{D_m} + \frac{R_s}{8\pi} \qquad ((2.13))$$

where Rs is the sheet resistance of the shallow n+ layer and Ds is the diameter of the circular shallow n+ layer.

$$R_{sr} = R_{srp} + R_{srn} \qquad ((2.14))$$

ii) Turn on probability P_{01} In order for a microplasma to switch on it is necessary for a minority carrier to find its way into the depletion field in the region of field intensification. These can be optically or thermally generated carriers which diffuse into the depletion region or are generated within it. They could also be emitted from traps or produced by internal field emission. It is clear that P_{01} is very dependent on illumination and in some circumstances can also be a function of bias voltage although this is usually a much smaller effect. See fig. 2.4 after Maeda et al [34].

iii) The turn off probability P_{10} Once a microplasma has turned on it can be considered to be self sustaining until a small fluctuation in the multiplication process results in more carriers leaving the depletion region than are created within it. If this situation occurs there is a probability that the avalanche will quench. P_{10} will therefore be dependent on the density of carriers within a microplasma and their average transit time across the depletion layer. Fig. 2.5 shows some experimental results for P_{10} against Im and for τ_1 against Vj , where Im is the instantaneous microplasma current, Vj is the junction bias voltage and τ_1 is the average time for which a pulse is on. If τ_1 is small compared with the off time of a pulse then,

$$P_{10} = \frac{1}{\tau_1} \qquad ((2.15))$$

Haitz [35] et al has shown that over three orders of magnitude,

$$\tau_1 = \tau' \exp (Vj/Vo) \qquad ((2.16))$$

where Vo = 0.0204 volts and is constant for a given junction, τ' is given approximately by the transit time for a charge carrier to cross the depletion width with the saturation drift velocity.

iv) The extrapolated breakdown voltage, V_B

Shockley [16] derived an expression for the dependence of the multiplication factor in a uniform junction on the applied voltage near breakdown,

$$\frac{1}{M} = (V_B - Vj)\ (K/V_B) \qquad ((2.17))$$

where K is a constant for a given junction background doping.
At breakdown $Vj \rightarrow V_B$ and

$$\frac{1}{M} \rightarrow 0 \text{ ie. } M \rightarrow \infty$$

Goetzberger et al [36] showed there was no difference in the breakdown behaviour of a microplasma from that of a uniform junction, except that a microplasma switched on a few tenths of a volt below the uniform part of the junction. Haitz [37] found that for a single, strongly illuminated, microplasma, that the value of V_B obtained from the extrapolation of a plot of 1/M against Vj to a zero value of 1/M, was equal to the value of V_B obtained by extrapolating a plot of I_m against Vj (ie. of slope Rs) to $I_m = 0$ as shown in Fig. 2.6. This determines the microplasma breakdown voltage a few tenths of a volt below that of the rest of the junction.

In summary it can be stated that the average current carried by a microplasma on first switching on is determined by the availability of carriers to initiate and sustain an avalanche. This will be enhanced by increasing the total junction current and by injecting carriers into the depletion region for example, by infra-red illumination. In Chapter 6 it will be considered that the current injected into the oxide originates from microplasmas. The parameters discussed above will be used to explain the experimental observations of the dependence of injected oxide current on junction current and infra-red illumination.

2.5 Electron Emission from p-n Junctions into Vacuum

The first observation of electron emission from a reverse biased p-n junction was by Burton [38] in 1957. In this experiment a grown silicon p-n junction was coated with caesium vapour in a vacuum so as to lower the surface work function. An emission current was first observed with a reverse bias of 5 volts and a junction current of 1.0 mA. Maximum emission was not obtained until the junction was avalanched at 40 volts and passing a current of 10.0 mA. Fig. 2.7 shows the emission currents obtained using a pulsed reverse junction bias.

It can be seen that the emission current increased by four orders of magnitude for only a single order of magnitude increase in junction current. No explanation was offered for this effect. Burton noted that the emission currents appeared to be coming from areas of microplasma breakdown and the emission current density was estimated to be greater than 0.05 mA/cm^2. This work was repeated in 1960 under rather better conditions by Simon and Spicer [39]. Emission currents in excess of 1mA were obtained under avalanching junction conditions. It was found that with the junction biased below avalanche the emission current would be increased by photo-exciting carriers in the region of the depletion field. The total emission current was the sum of the field induced emission and the photo-emission. With the junction under avalanching conditions it was found that the emission current could be focussed onto a fluorescent screen and the observed pattern correlated with the microplasma topography of the junction.

Elinson and Lutski [40] have used a retarding potential method to measure the energy distribution of electrons emitted from a silicon p-n junction. The electron emitting device was a bulk p-n junction with a surface n+ layer induced in the p-silicon by a surface caesium layer. The distribution was found to be approximately Maxwellian. The effective temperature of the distribution was found to increase with junction bias and then to saturate. Over the same biasing range the emission current increased exponentially and then also saturated. The increase in the emission current was therefore interpreted in terms of an increase in the average energy of the electron distribution within the silicon. The increase in energy was thought to result from an increase in the field across the surface n+ layer. The explanation was however only qualatative and did not indicate what part of the junction bias was being dropped across the surface junction. Since the junctions appeared to have a very leaky reverse characteristic it is probable that a significant proportion of the junction bias was across a resistive leakage path. The emission was observed to come from microplasmas probably where the n-p junction intersects the surface although this is not indicated.

A similar model involving an increase in the average energy of the electron distribution was used by Goffaux [41] to explain an n^{th} power law increase in emission current with junction current from a SiC junction reported by Patrick and Choyke [42].

The natural surface work function of silicon is about 4.15 eV as shown in Fig. 2.9. In 1958 Tauc [43] detected an emission current from a Si junction which had received no surface treatment to lower the surface

potential. Using a freshly etched junction emissions could be detected in air with a Geiger counter. This observation was substantiated in 1959 by Senitzky [44] who obtained a continuous emission current of 10^{-13} into vacuum from an untreated junction passing a junction current of 100mA. The emitting structure was a 2μ deep, diffused p^+-n junction bevelled at 5^o on one face to expose the junction boundary. Emission was found to originate at the boundary, from areas of microplasma breakdown. The emission currents were found to increase with junction current in an exponential manner asshown in Fig. 2.8. This was interpreted in terms of an increase in the escape probability of an electron with junction field. Present knowledge of microplasmas makes it seem unlikely that there would be a sufficient increase in field across a microplasma to cause a significant increase in the electron escape probability. Senitzky also observed smaller emission currents with the junction biased below the avalanching voltage.

The first observation of an emission current through a shallow planar junction with an untreated surface was by Bartelink in 1963. This experiment has already been described in Section 2.3. Emission appeared to originate from microplasmas when the junction was avalanched. Emission currents of between 10^{-14} A and 10^{-10} A were obtained with a junction current of 25 mA for junction depths ranging between 1200 Å and 700Å. Bartelink did not describe the variation of emission current with junction current but the work was repeated by Bok and Klien [45] who found the emission current to increase exponentially with junction current after an initial sharp rise at breakdown, as shown in Fig. 2.10. No explanation was offered for this observation.

In 1968 Hodgkinson[46] obtained emission currents as large as 10^{-9} A from a diffused planar junction. He also found that the emission current decreased with increasing lattice temperature. This was probably as a result of increased energy losses by the electron population to phonon collisions.

In much of the work described above the authors emphasised that the emission current was very sensitive to surface contamination. Walder[47] investigated the effect of allowing a layer of oxide to grow over the junction surface. A shallow planar junction was fabricated and the oxide allowed to form in the atmosphere over a period of time. As expected the emission current decreased with oxide thickness but at a greater rate than anticipated from scattering considerations. The current was found to decrease with time such that $\log I_e \propto -\log t$. Walder concluded that the decrease was due to charge trapping at the interface and resulting in a retarding field. A surface charge density of 8×10^{12} charges / cm^2 was estimated. When considering injection into SiO_2 this work emphasises the need to form good

quality oxides under clean conditions in order to minimise any reduction in injection efficiency. The following section discusses the effects of traps on electron injection and conduction in silicon dioxide.

2.6 Electronic Injection from Silicon into Silicon Dioxide. Most of the early observations of electrical conduction in SiO_2 films may be interpreted as ionic conduction since this was by far the largest component at the time.[48]. More recently it has been possible to grow thermal SiO_2 which is relatively free from ionic contamination and hence it has been possible to study the electronic component of the conduction. These experiments suggest that SiO_2 thermally grown on silicon can be considered to have a band structure similar to that of a crystalline semiconductor or insulator. The forbidden band-gap has been estimated to be 8.5 eV and the barrier height between Si and SiO_2 to 3.25 eV as shown in Fig. 2.9. Natural electronic conduction is negligible with such a wide band gap so that the observed conduction must result from electron or hole injection at the electrodes.

Photo-excitation was one of the first techniques used to inject electrons into the conduction band of SiO_2. Once in the conduction band the electrons were found to have a relatively high mobility. Goodman[49] used a $Si/SiO_2/Au$ structure to photo- inject electrons into the SiO_2 and then to measure the electron mobility using a Hall technique. The device structure made the mathematical analysis difficult but an average value of 29 $cm^2/Vsec$ for the electron mobility in SiO_2 was estimated.

Current-Voltage curves have also been obtained for the photo-injection of electrons into SiO_2. Although these have been interpreted using the image force lowering model, there has been considerable deviation from this simple model at low and very high fields. In 1966 Goodman [50] interpreted the Current-Voltage characteristics at low fields in terms of traps below the conduction band in SiO_2. Previously Williams [51] had shown that such traps existed about 2.0eV below the SiO_2 conduction band. According to Goodman's model the range an electron could travel before becoming immobilised in a trap would increase with the strength of the applied field. The photo-injected current would then be expected to increase more sharply at low fields, as observed experimentally, than predicted by the image force model alone.

In 1971 Berglund and Powel [52] suggested that this model was probably not correct and proposed a theory in which the field dependence of the emission current at low fields was explained in terms of optical phonon scattering in the potential well between the silicon interface and the classical turning point of the image force barrier. The distance of the

turning point from the interface increases with decreasing applied field, so that the probability of an electron making an optical phonon collision before reaching the turning point is increased at low fields. Thus, in this situation there is a higher probability of an electron being turned back, rather than being injected into the conduction band of the oxide. A value of 35 Å for the mean free path for an optical phonon collision was estimated from the experimental data.

More recent experiments (53 - 55) on the photo-injection of electrons into thermally grown SiO_2 have confirmed the existance of a band of traps spread about 0.5 eV wide approximately 2.0 eV below the conduction band. The density of traps has been estimated to be of the order of $10^{14}/cm^3$. Thomas et al (53) has shown that, once filled, these traps can be emptied by the simultaneous application of U.V. radiation and a high field. There is no evidence that electronic conduction can take place via the traps under the action of a high field alone.

Electron injection from silicon into the conduction band of silicon dioxide has also been achieved by the application of high fields ($> 10^5$V/cm), across the oxide in an M.O.S. structure (56 & 57). The currents obtained have been shown to be dependent only on the applied field and the injecting electrode. That is, independent of oxide thickness and the counter electrode material. This suggests an electrode limited injection mechanism, as expected for a material with such a high band gap and low density of traps. Because of the barrier height of the Si/SiO_2 interface (3.25eV) Schottky emission is not important at room temperature and the Current-Vottage characteristics have been interpreted in terms of Fowler-Nordheim tunnelling.

Lenzlinger and Snow (56) proposed that in the case of electron emission from silicon the surface could be considered to be n-type degenerate regardless of the bulk doping. This allowed use to be made of the Fowler-Nordheim equation for the free electron model and the W.K.B. approximation to the tunnelling probability. The equation was modified to take into account image force lowering and the relative dielectric constant of silicon dioxide. The final expression also contained the effective mass of an electron in the forbidden gap of the oxide. Experiments were performed using oxides ranging in thickness from 640 Å to 5,000 Å grown at 1200 °C in dry oxygen on n-type silicon of resistivity 1 - 10 Ω cm. Current-Voltage measurements were taken of the oxide current and Fowler-Nordheim plots obtained. From the slopes, the value for the effective mass of an electron was derived as $0.42m_o$.

The temperature dependence of the I-V curves was also measured and a theoretical fit made. However, this was found to require a value for the effective mass of 0.96 m_o . An explanation of this discrepancy could not be found unless the barrier height varied with temperature. Similar observations were made in 1972 by Osburn and Weitzman [57].

In the study by Osburn and Weitzman it was found that the I-V curves were not reproducible until the applied field had been cycled several times. As in Lenzlinger and Snow's work it was found that the injected current decayed with time. Lenzlinger and Snow thought that the current decay was a result of traps in the oxide; these were also considered to be responsible for the lower than expected current levels obtained in their experiments. Osburn and Weitzman did not observe such low current levels and proposed that the initial current consisted of injected current plus current released from traps by the applied field. They also found that the rate of current decay increased with applied field which they interpreted in terms of the depth of the traps from which the electrons were released. The flat band voltage was measured before and after injection and no appreciable shift was observed. This was taken to indicate that the traps would need to be located within 0.2 Å of the metal interface. Osburn and Weitzman found that if the devices were annealed after metalisation the current was reduced. In addition if a sample was not annealed the slope of the Fowler-Nordhiem plots gave values for the barrier heights that were 1.5 eV lower than expected. Two models were proposed to account for this observation. In the first it was considered that there were traps levels 1.5 eV below the SiO_2 conduction band which could be annealed out. In the annealed samples electrons could be injected into these traps and may have sufficient mobility to travel through the oxide via the traps. In the light of recent photo-injection experiments on traps, described earlier, it is unlikely that these traps could be the same as those found in normally grown silicon dioxide since there is no evidence of electron conduction via such traps. In Osburn and Weitzmann's experiments, however, it was observed that the apparent barrier lowering effecf was most noticable in those devices on which the aluminium had been deposited using electron beam evaporation. There is some evidence that this type of evaporation technique can produce radiation damage in silicon devices [58] and it is possible that traps induced in this way have properties differing from those found in 'as grown' oxides. Radiation damage has also recently been shown to effect the Si/SiO_2 barrier heights[59]. In the

experiments discussed in this thesis the aluminum , was deposited using electron beam evaporation. (See Chapter 4).

In the second model of Osburn and Weitzmann it was thought that charge introduced into the oxide during metalisation would be able to vary the potential distribution within the oxide such as to produce a non-linear potential against depth profile. It was considered possible that this would alter the shape of the tunnelling barrier resulting in an apparent barrier lowering. More recently [60] scanning photo emission experiments on Si/SiO_2 interfaces show that localised barrier lowering can result from contamination charge in the oxide. Every effort was made in the experimental work contained in this thesis to use clean, oil-free evaporation methods and high purity aluminium. (See Chapter 4).

If very thin oxide films are employed (< 100 Å) it is possible to apply fields to induce electrons to tunnel right through the forbidden gap of the oxide. This property is used in M.N.O.S. [61 & 62] memory devices. In these structures a high field is applied across a sandwich of silicon dioxide and silicon nitride. Electrons tunnel from the silicon, through the oxide and into traps at the oxide-nitride interface. This trapped charge causes a shift in the threshold voltage and hence produces a memory effect.

2.7 Electron Injection from p-n Junctions into Silicon Dioxide

It was shown earlier that electrons could be emitted into a vacuum from a reverse biased p-n junction. This principle has also been used to inject electrons into silicon dioxide. In 1969 Nicollian et al [63] found that if an M.O.S. structure was pulsed at a high frequency and voltage it was possible to invert and avalanche the surface of a p-type silicon substrate as shown in Fig. 2.11. The electron current injected into the oxide was differentiated from the transient capacitance current by the measurement system. The injected oxide current density was found to be linearly proportional to the pulse frequency; values as high as 2×10^{-1} A/cm^2 were measured. A similar experiment was performed by Nicollian and Berglund [64] and the dependence of the injected oxide current on peak field was explained in terms of an image force lowering model. By assuming a Maxwellian distribution of charge carriers in the avalanche pulse, a value of 0.43eV for the effective temperature of the distribution was derived.

Nicollian [65] found that in the above device structures that there was an increase in the electron trapping if water was incorporated into the oxide. After an avalanching sequence a negative charging effect was observed in oxides previously grown in dry oxygen and then exposed to water.

The charge could be removed by heating to 200 ^{o}C for 20 minutes in the presence of water although no change was observed by heating for 30 minutes at 200^{o} C in vacuum or hydrogen, or by exposing to U.V. light. A model was proposed in which electrons were captured at hydrogen ion or water related defects. Steam grown oxides showed increased electron trapping compared with dry oxygen grown oxides. There was also found to be an increase in the surface state density after avalanching. Steady, d.c. electron injection into silicon dioxide has also been observed using M.O.S.T. devices. Erb, Dill and Toombs [66] used an n-channel M.O.S.T. with an additional offset gate as shown in Fig. 2.12. A small part of the drain current could be accelerated towards the silicon-oxide interface by controlling the offset gate field. No avalanching takes place and the oxide current is a function of the drain current and the field induced in the silicon by the gate. Current densities of the order of 2×10^{-4} A/cm^{2} were obtained through the oxide. Verwey [67] has used an n channel M.O.S.T. structure with a forward biased p-n^{+} junction beneath the channel such that electrons could be injected into the region of the channel field and hence be accelerated into the oxide as shown in Fig. 2.13.

Injection of electrons into the gate oxide of an M.O.S.T. device has also been noted during the avalanching of the drain diffusion. Hara et al [68] for example, found that the silicon surface near the drain became more n-type in n-channel devices and inversely for p-channel devices, i.e. avalanching the drain effectively shortened the active channel length. This was shown to be caused by the charging of the gate oxide by injected electrons or holes which were subsequently trapped. This has been used in F.A.M.O.S. [69] memory devices in which current densities of 0.1 A/cm^{2} have been obtained through 1000 Å of oxide.

Verwey et al. [70] has used both npn and pnp transistor structures to measure the injected oxide current during emitter-base breakdown. A field plate was placed above the emitter-base junction and biased positively as shown in Fig. 2.14. In a pnp structure the field plate voltage depletes the emitter surface and gives charge accumulation in the base surface, causing the junction to breakdown at the silicon-silicon dioxide interface. In an npn transistor it is considered that breakdown occurs a few tenths of a micron below the interface because of out diffusion of boron from the base. The oxide current in an npn transistor was found to increase exponentially with applied field whereas in a pnp transistor it increased linearly. It was proposed that the depth of the avalanching region in the npn device was an inverse function of the field and hence the current would be determined by Bartelink's relationship, $I \propto \exp(-L/L_o)$ see Section 2.3. In the pnp device breakdown

takes place at the interface and the current is therefore a linear function of the applied field. This explanation for the pnp device does not however, take into account that the oxide field would result in a lowering of the interface barrier between the silicon and the oxide. This would result in a non-linear dependence of the oxide current field. Verwey also found that electron trapping occured in the oxide resulting in a reduction of the injected current by an order of magnitude in three minutes. The trapping efficiency was estimated to be about 1 electron trapped for 3×10^3 transported.

In a similar experiment Pepper [71] used a p^+–n junction and made a series of measurements of the oxide current against applied oxide field and junction current. As in Verwey's work some trapping effects were observed but in addition it was reported that it was necessary to stabilize the injection current by avalanching the device over a period of time. It was estimated that the charge density of 3.2×10^7 C/cm^2 was at the Si/SiO_2 interface, resulting from trapped charge distributed throughout the oxide. Pepper's results show that he obtained a hundred-fold increase in the injected current for only a three-fold increase in junction current. See Fig. 2.15. Pepper offered no explanation for this observation but considered only the field dependence of the injected current.

It was concluded by Pepper that the observed rate of increase of oxide current with applied oxide field was inconsistent with image-force lowering theory and that the field was not high enough for Fowler-Nordheim tunnelling. The view was taken that an electron would be injected into the oxide if it could gain sufficient energy from the field induced in the silicon surface by the field voltage and the voltage across the junction depletion region. The total field was taken to be that derived by De Graaff [72] for a gate-controlled diode,

$$F = (V_R - V_g') / (\varepsilon_s/\varepsilon_{ox})\, x_o \qquad 2.18$$

where x_o is the oxide thickness,

V_g is the voltage on the field plate,

V_R is the voltage on the diode junction,

and $V_g' = V_g - \phi_{ms} + Q_{ss}\, x_o / \varepsilon_{ox}$,

where Q_{ss} is the charge density at the interface

ϕ_{ms} is the metal/semiconductor work difference

The probability of an electron gaining sufficient energy to be injected was derived in a manner similar to that used by Shockley in his calculation of the charge carrier distribution in an avalanching junction. (Section 2.2).

By integrating the probability an expression for the injected current was obtained,

$$I_{ox} \propto \exp\left[\frac{1}{F_q}\left(\frac{Ei}{\ell_r} + \frac{\phi}{\ell_2} - \frac{Ei}{\ell_2}\right)\right] \qquad ((2.19))$$

where ℓ_r is the optical phonon m. f. p., taken to be 110 Å

ℓ_2 is the combined m. f. p. for phonon scattering and ionisation, taken to be 400 Å.

Ei is the pair production threshold energy, taken to be 1.65 eV.

ϕ is the interfacial barrier height

Good agreement was obtained between this expression and the experimental slope of the graph of oxide current against reciprocal field. This theory is, however, a great simplification and is really only justified in the situation where the junction is biased below avalanche voltage and electrons are generated in the field region by optical or similar means. When the junction is avalanched the charge carriers are thermalised in scattering collisions (Section 2. 2) and the emission probability is no longer valid. Bulucea [73, 74] has more recently proposed a better model of avalanche injection of electrons into the oxide of a gate controlled device similar to Pepper's. In this model Bartelink's theory is extended to take into account the induced interface field and barrier lowering effects.

2. 8 Conclusions

It is generally assumed that the hot electron-hole population in an avalanching junction or microplasma is Maxwellian. The discussion of Section 2. 2 indicates that this is only an approximation and that the true distribution falls off more sharply at higher energies ($\gtrsim$ 2eV).

In the majority of the published work electron injection into a vacuum has been found to originate from microplasmas. Experiments involving electron injection into silicon dioxide have mainly used deep p-n junctions where the origin of the emission is from a localised surface breakdown. The electrical properties of these surface breakdowns is probably the same as described for microplasmas. It is expected that the switching probabilities will greatly influence the average emission current. This must be taken into account when considering the dependence of the emission current on the total junction avalanche current. This dependence has been largely ignored by most workers and will be discussed in Chapter 6 with reference to the device used in this work.

Electron injection into silicon dioxide is generally considered to be electrode limited and the field dependence is usually interpreted in terms of field barrier lowering or Fowler-Nordhiem tunnelling. The presence of traps, distributed throughout the bulk oxide, has been observed to reduce the

injected current by an order of magnitude from its initial level. This effect is less than might be expected for an amorphous insulator. Trapping may be more important in other froms of thin films such as willemite. This may lead to space charge limiting effects.

At the time of writing there have been no reports of electron injection into silicon-dioxide from large area shallow planar junctions. With uniform breakdown this could be expected to give higher injection currents and possibly a higher injection efficiency. This is because of the more favourable geometry giving a depletion field directed towards the interface reducing surface reflections. A shallow n^+p junction will not have the surface induced field as in Pepper's structure thus making an analysis of the results much simpler.

It is one of the objectives of this research to use the information presented in the above review to design a planar junction which will allow electron injection into silicon dioxide. It is hoped that this will lead to a better understanding of some of the injection mechanisms particularly the dependence of the injected current on junction current.

Finally the same design of junction is used to inject high energy electrons into a thin film of willemite as proposed in Chapter 1.

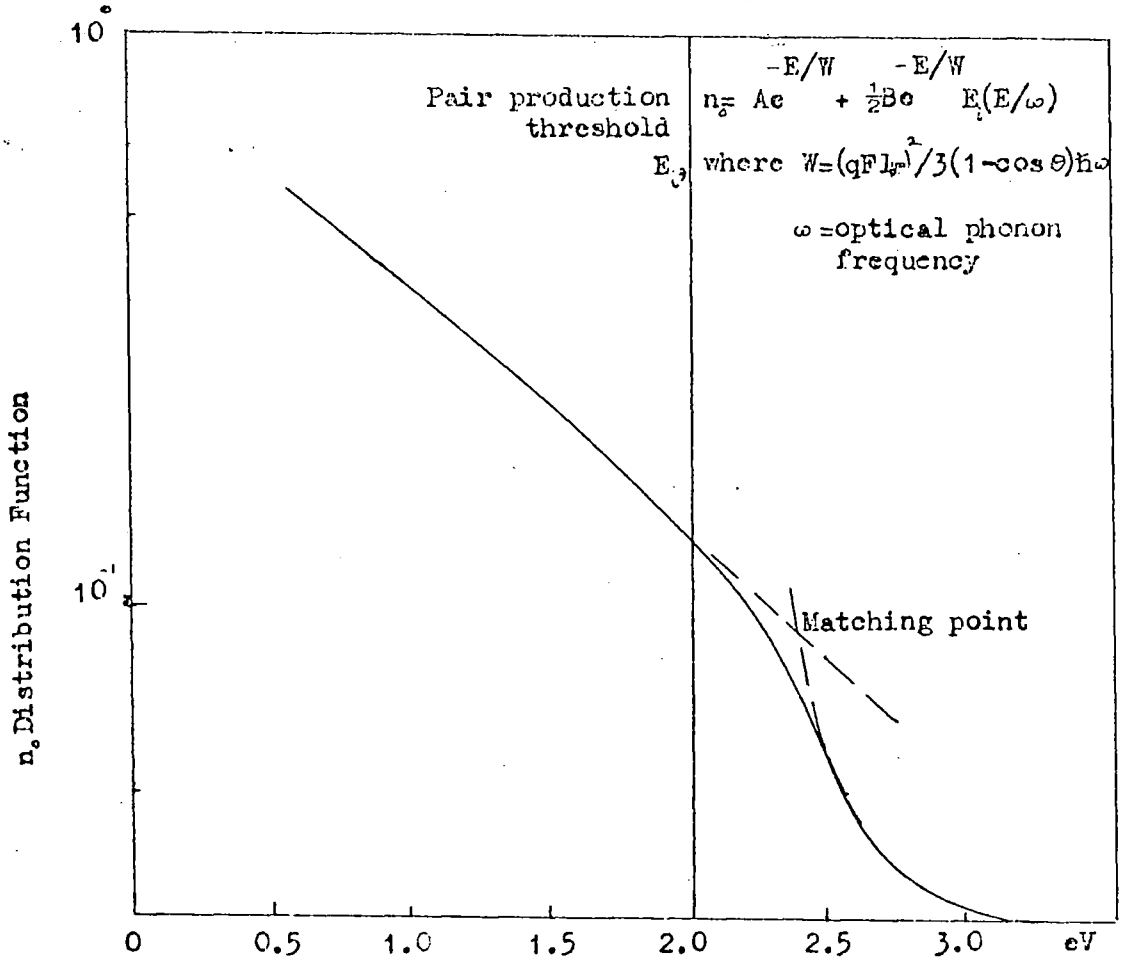

FIG 2.1 FORM OF ENERGY DISTRIBUTION OF AVALANCHING ELECTRONS AFTER WOLFF
Ref 12

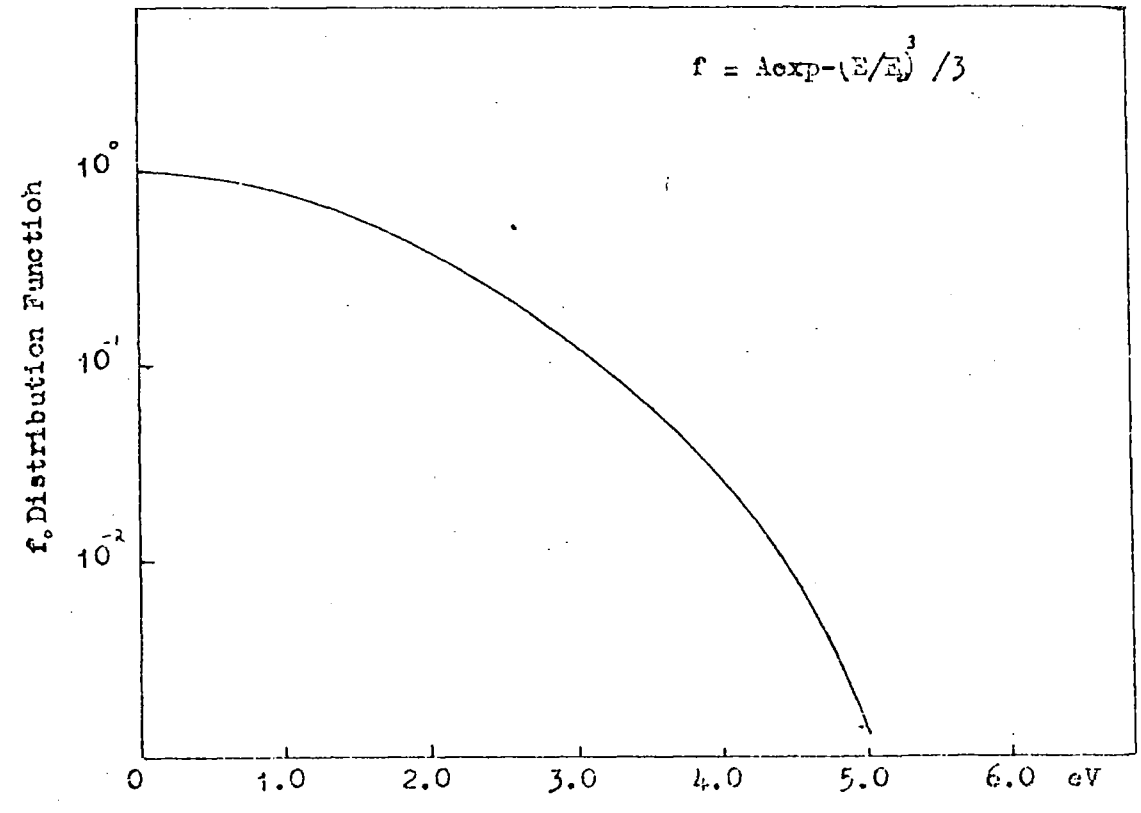

FIG 2.2 FORM OF ENERGY DISTRIBUTION OF AVALANCHING ELECTRONS AFTER SEWARDS et al
Ref 18

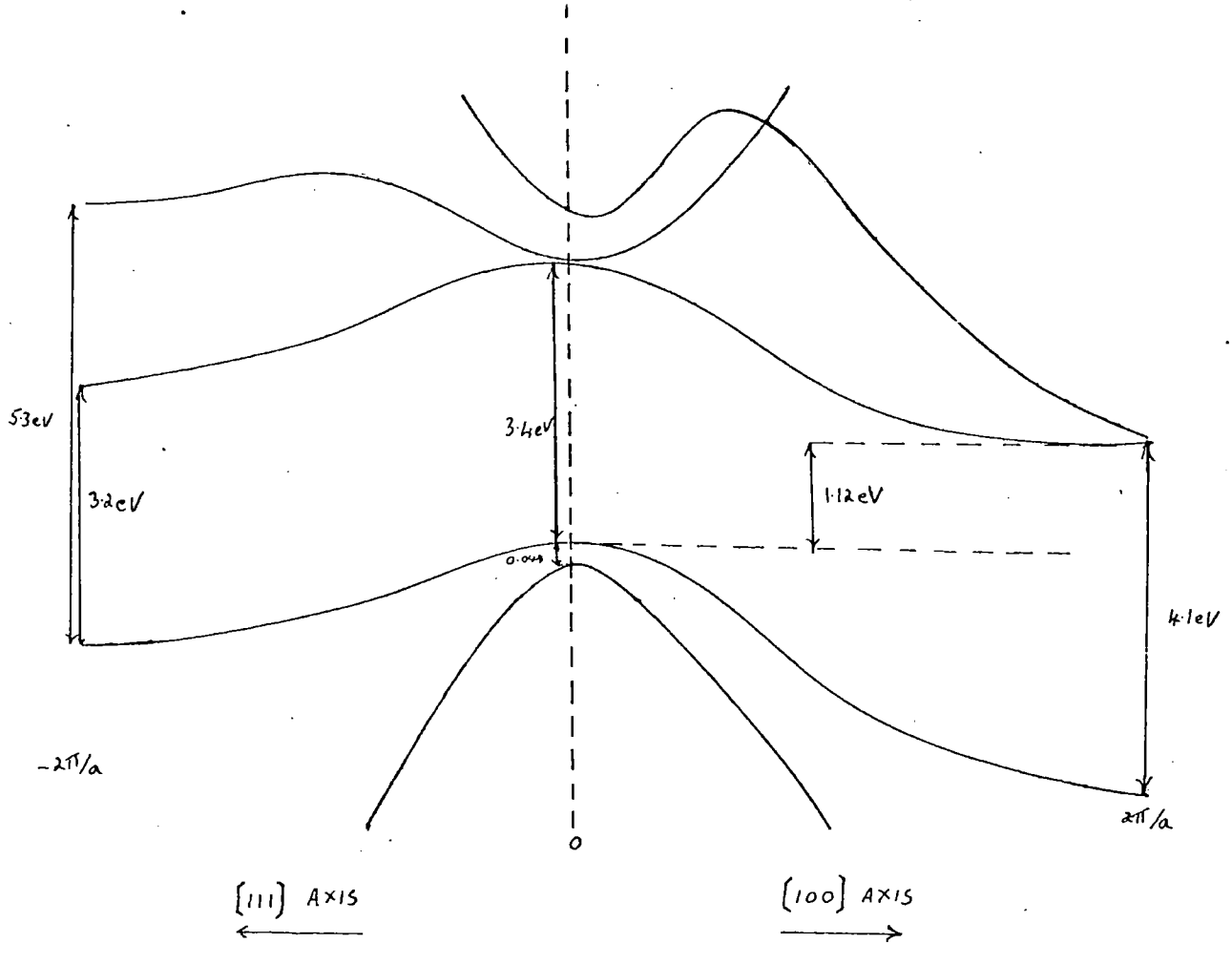

FIG 2.3 BAND STRUCTURE OF SILICON AT 300 °K

Ref 28

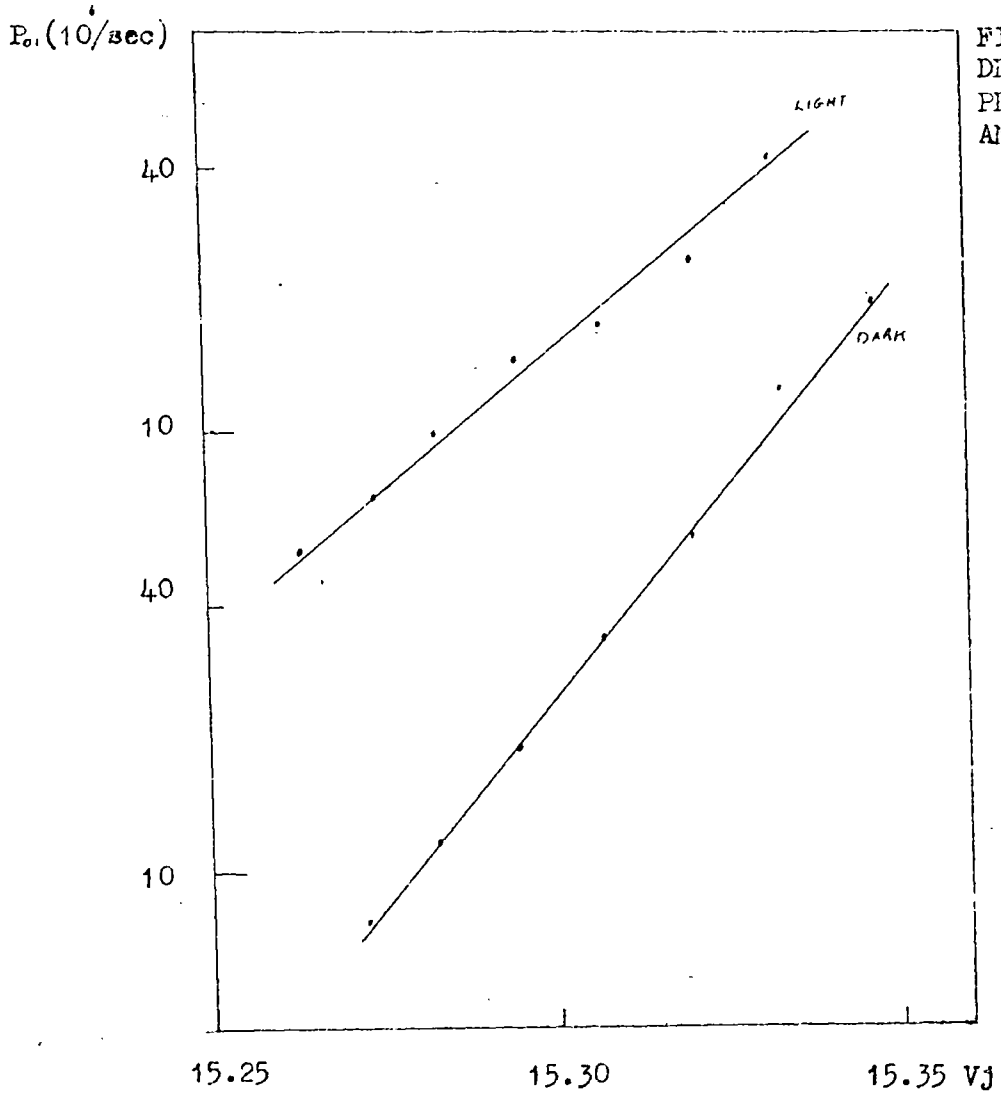

FIG 2.4 Ref 34
DEPENDENCE OF THE TURN-ON PROBABILITY WITH VOLTAGE AND ILLUMINATION

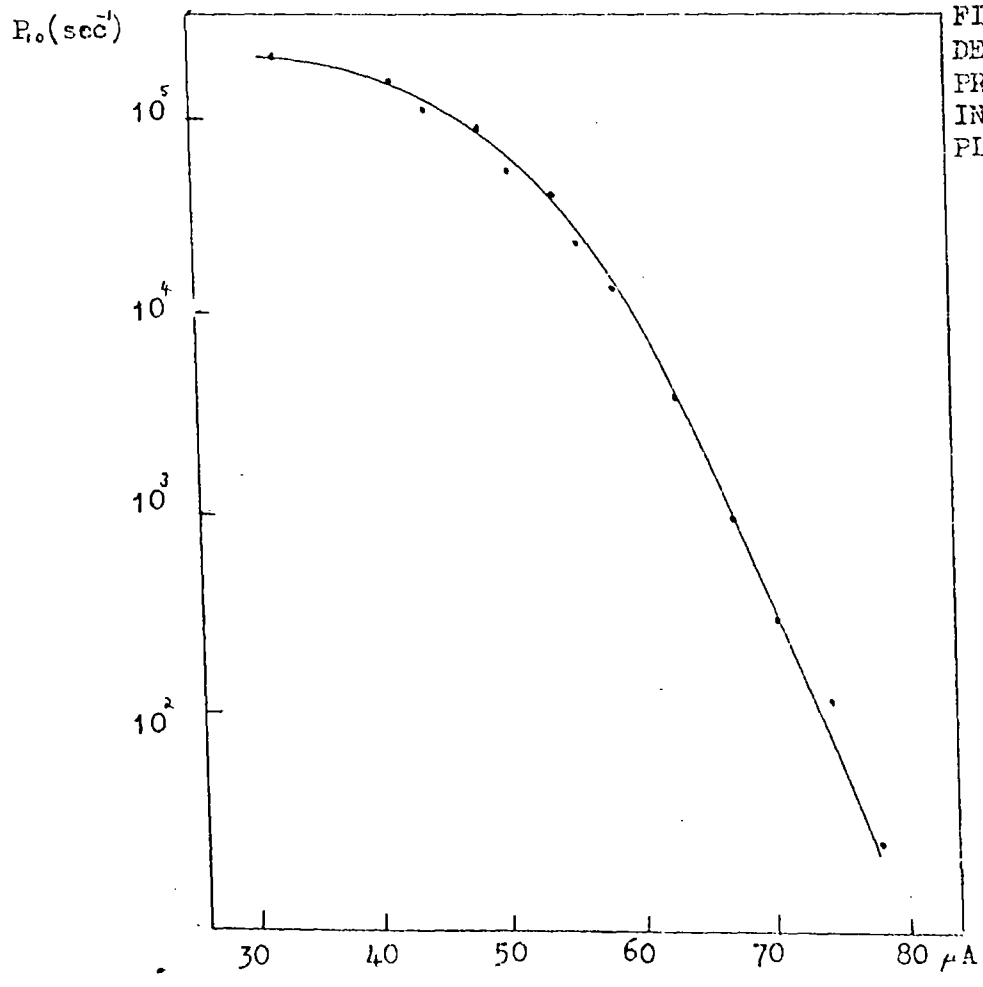

FIG 2.5a Ref 34
DEPENDENCE OF TURN-OFF PROBABILITY WITH THE INSTANTANEOUS MICRO-PLASMA CURRENT

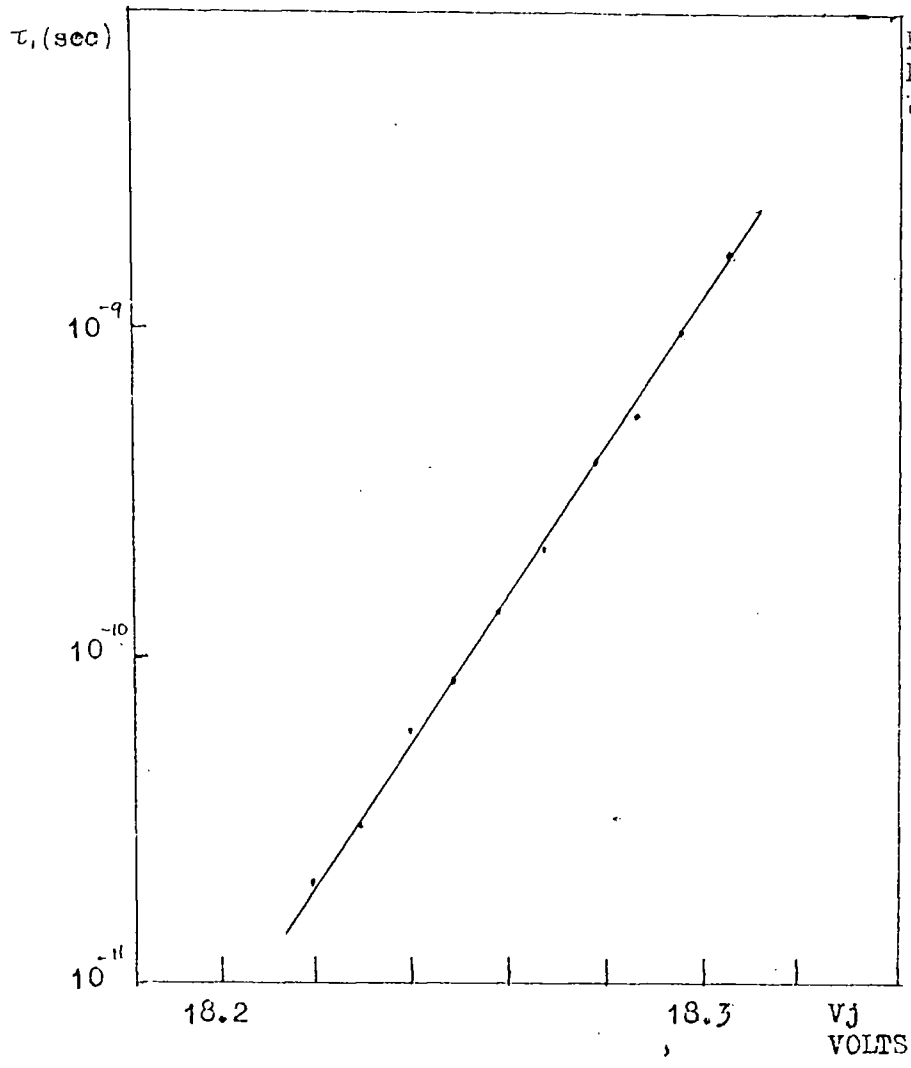

FIG 2.5b Ref 35
DEPENDENCE OF THE ON-TIME WITH APPLIED VOLTAGE

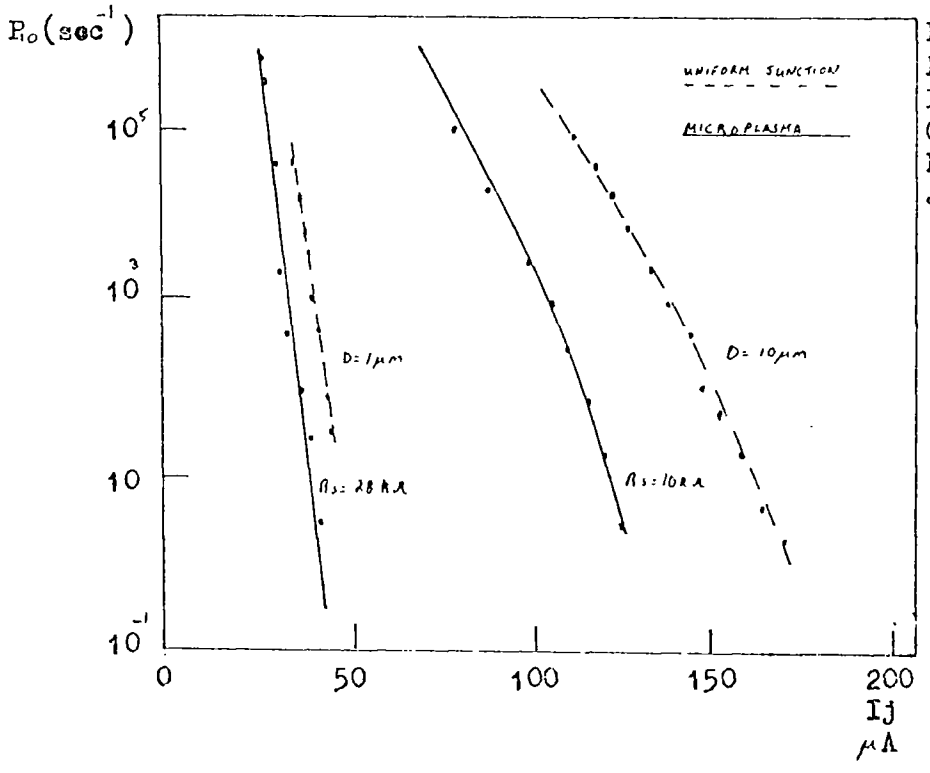

FIG 2.5c Ref 37
DEPENDENCE OF THE TURN-OFF PROBABILITY WITH JUNCTION CURRENT FOR A RANGE OFF MICROPLASMA & UNIFORM JUNCTION DIAMETER

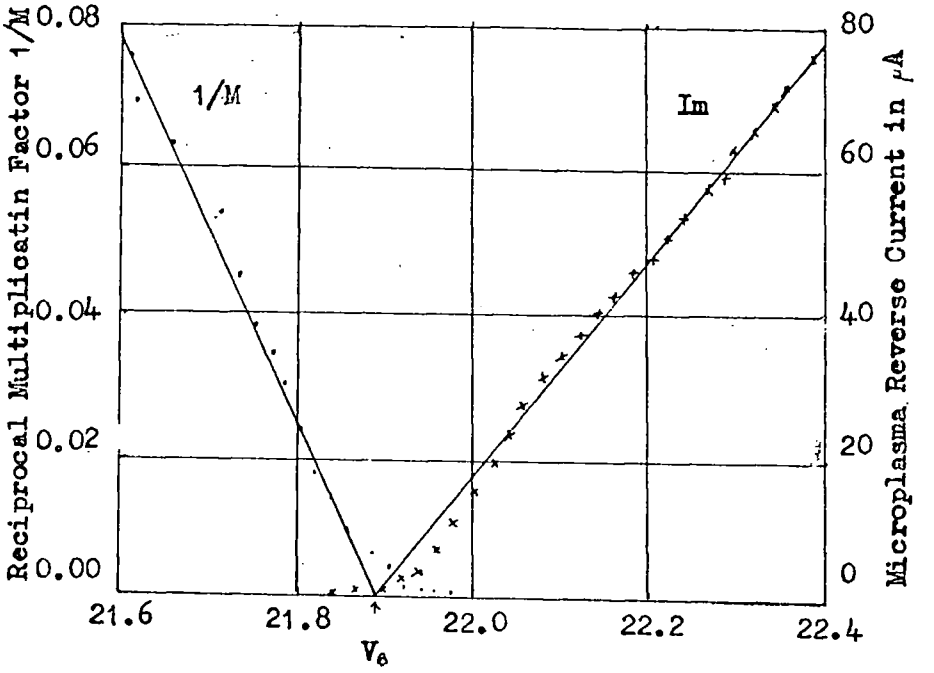

FIG 2.6 DETERMINATION OF THE EXTRAPOLATED BREAKDOWN VOLTAGE

Ref 31

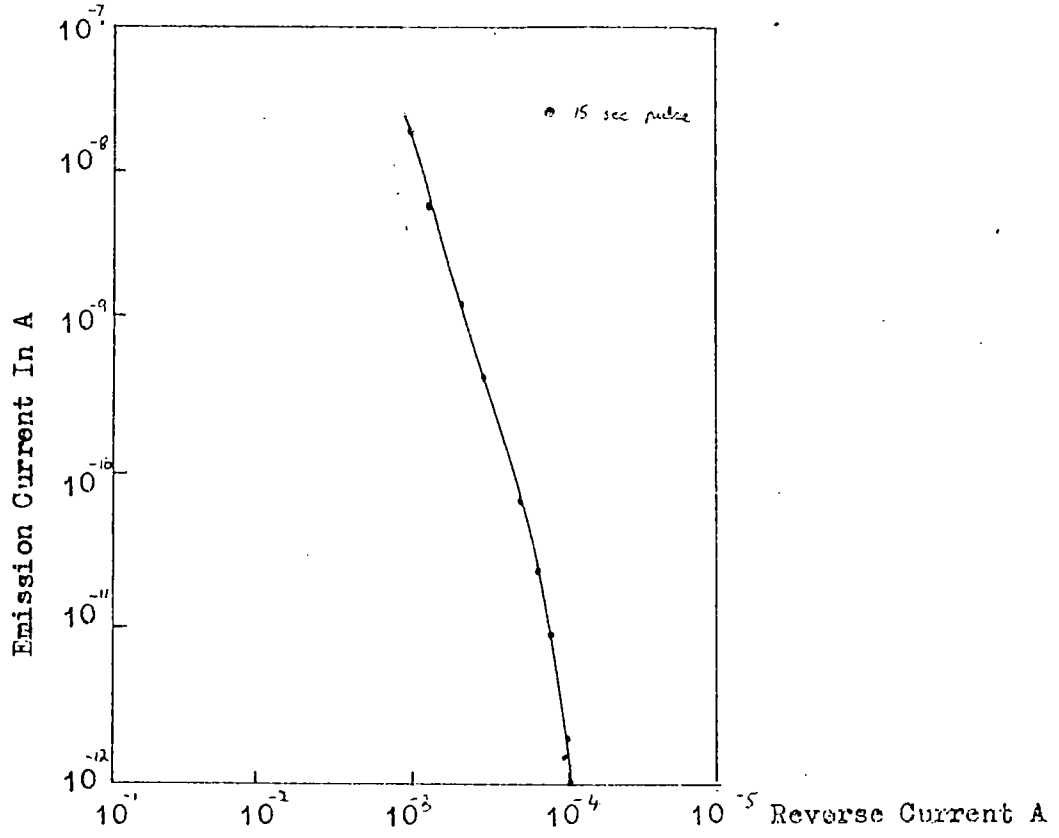

FIG 2.7 ELECTRON EMISSION FROM A Cs COATED SILICON JUNCTION AFTER BURTON Ref 38

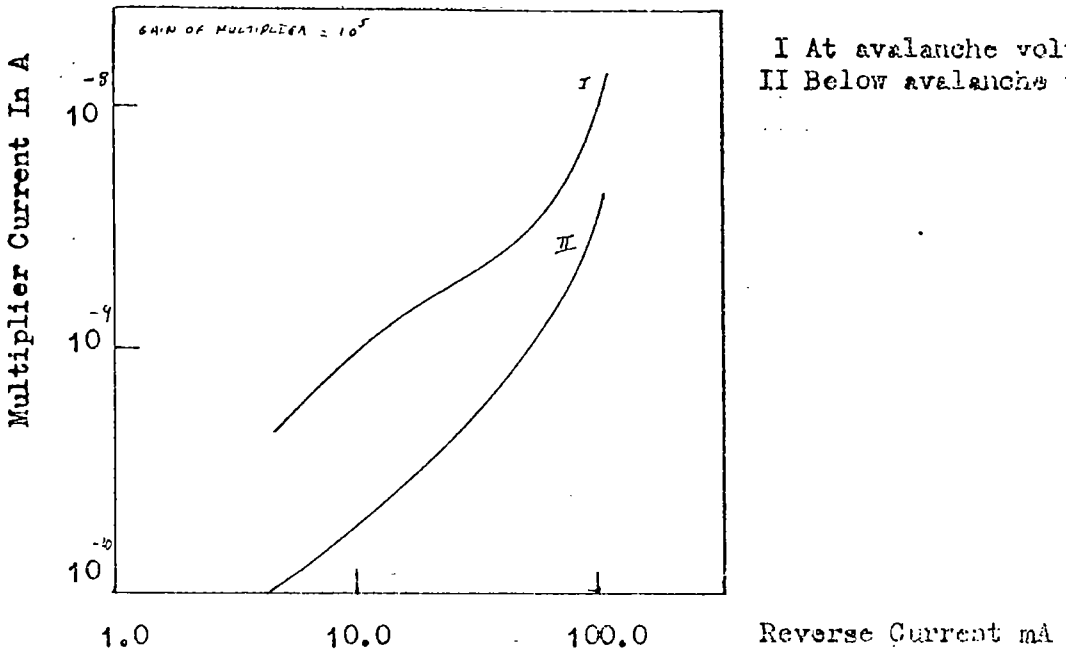

I At avalanche voltage
II Below avalanche voltage

FIG 2.8 ELECTRON EMISSION FROM A CLEAN SILICON JUNCTION AFTER SENITZKY Ref 44

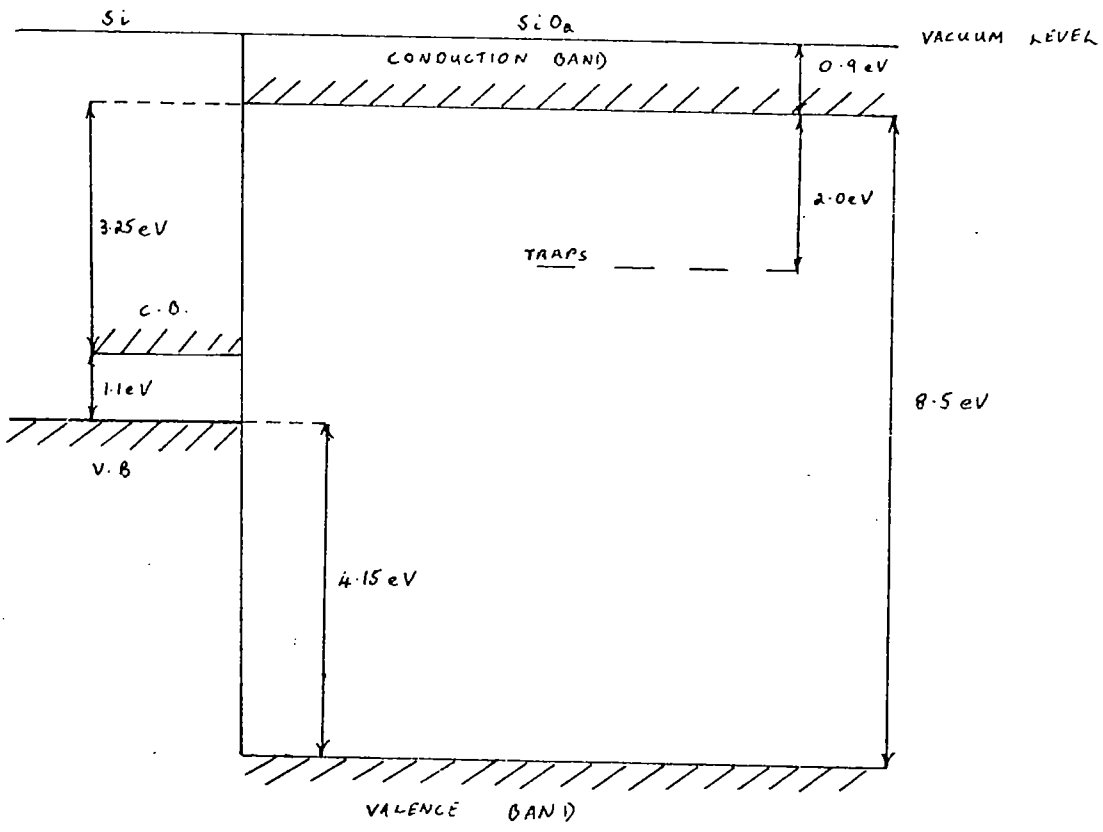

FIG 2.9 ENERGY BAND STRUCTURE OF Si/SiO_2 INTERFACE

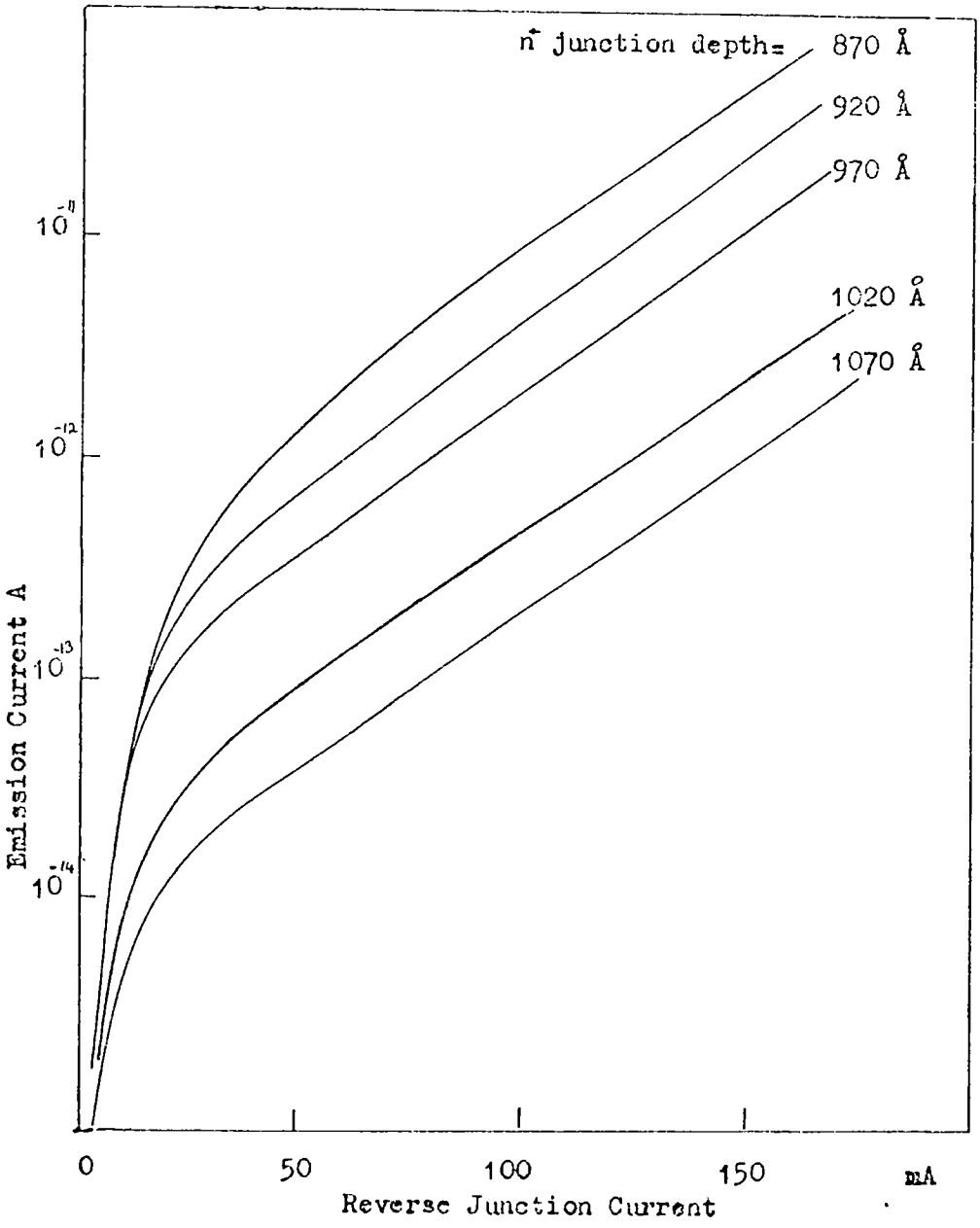

FIG 2.10 ELECTRON INJECTION INTO A VACUUM FROM A SHALLOW AVALANCHING $p\text{-}n^+$ JUNCTION AFTER BOK & KLEIN
Ref 45

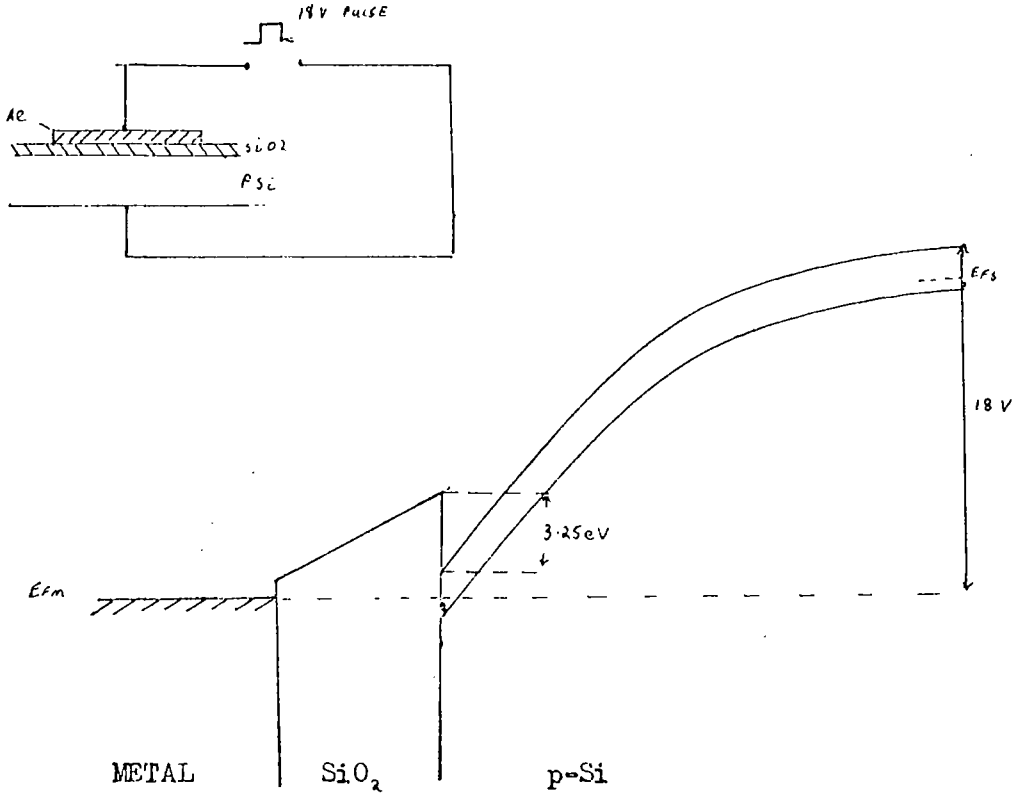

FIG 2.11 BAND STRUCTURE OF SiO_2/Si INTERFACE UNDER PULSE BIAS CONDITIONS ALLOWING ELECTRON INJECTION INTO SiO_2

Ref 63

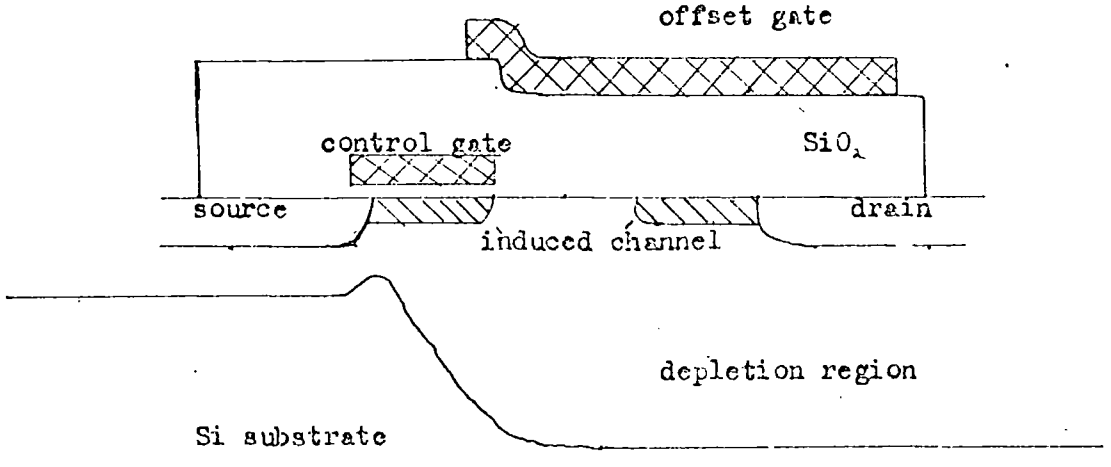

FIG 2.12 MOST OFFSET GATE STRUCTURE FOR ELECTRON INJECTION INTO SiO_2

Ref66

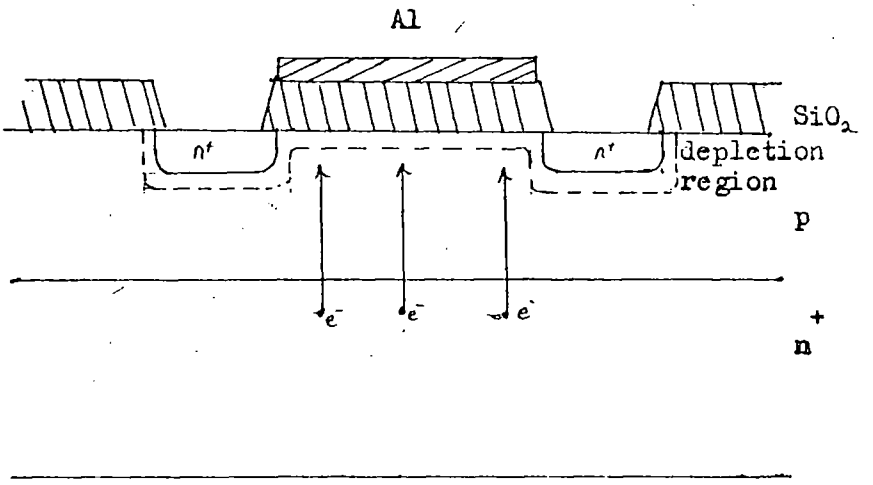

FIG 2.13 M.O.S.T. DEVICE FOR ELECTRON INJECTION INTO SiO_2 WITHOUT AVALANCHE BREAKDOWN

Ref 67

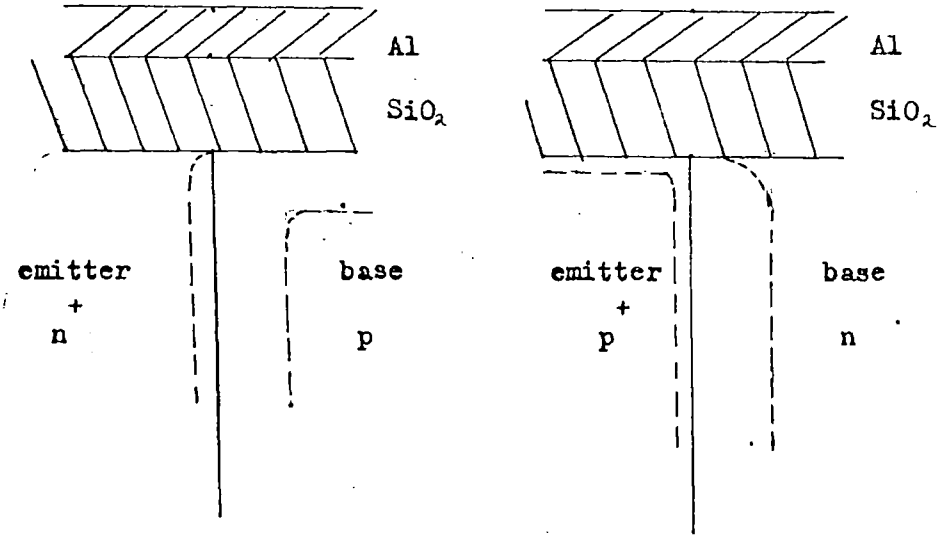

FIG 2.14 EMITTER-BASE STRUCTURE OF npn & pnp TRANSISTORS USED TO OBTAIN AVALANCHE INJECTION OF ELECTRONS

Ref 70

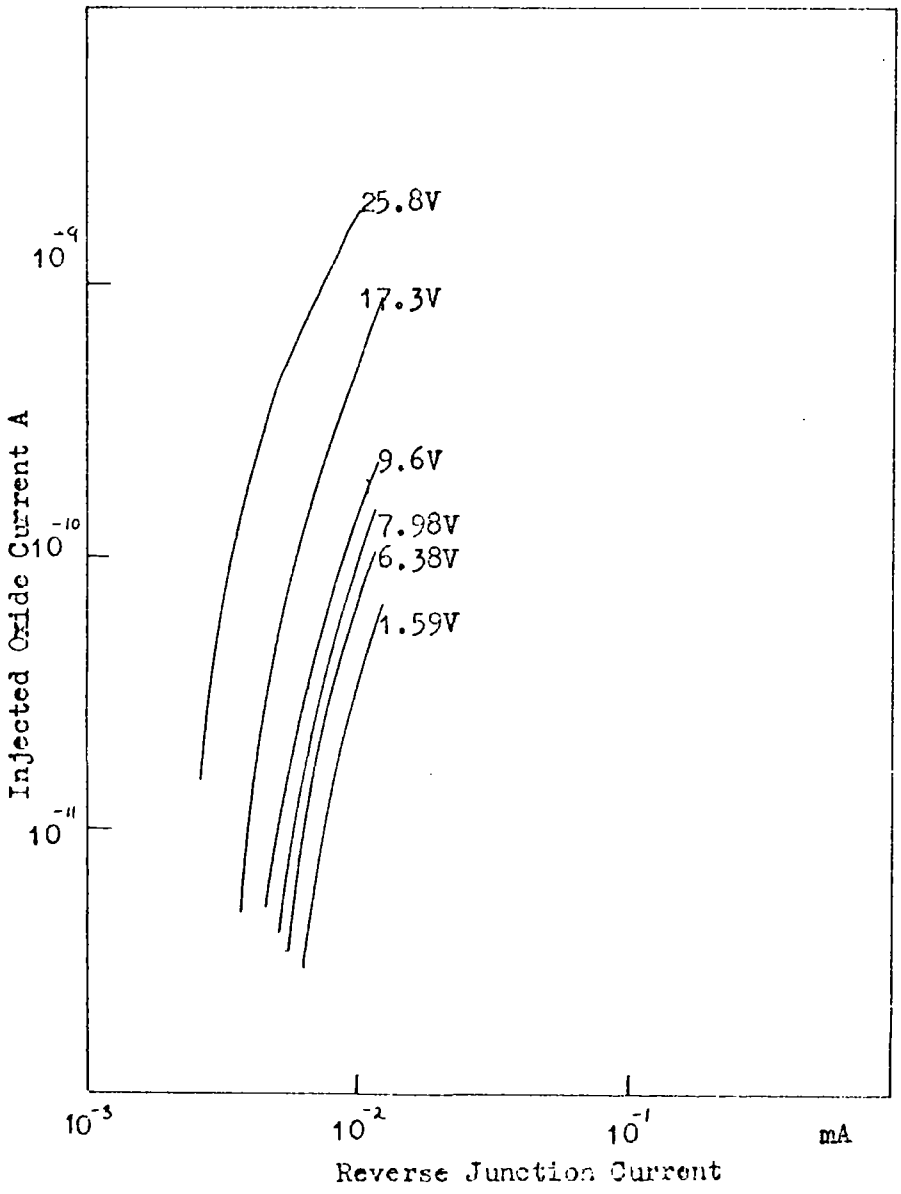

FIG 2.15 ELECTRON INJECTION INTO SiO_2 FROM A BULK p-n JUNCTION USING EDGE EMISSION AFTER PEPPER Ref 71

CHAPTER THREE

DESIGN OF HOT ELECTRON INJECTION STRUCTURE

3.1 Introduction

It has been shown in Chapter 2 that high energy electrons, created in the depletion field of a silicon reverse biased p-n junction, rapidly lose energy during transport away from the junction. In order to achieve electron injection into an overlaying film there must be a finite probability of an electron arriving at the silicon and film interface with an energy greater than the potential step height between the two materials. Bartelink [20] (Sec. 2.3) has shown that for a junction biased in the avalanching mode, the number of high energy electrons arriving at the interface is proportional to exp (-L/Lo). L is the junction depth and Lo is a parameter primarily dependent on the ionising and phonon scattering mean free paths. Order of magnitude calculations, verified by experiment, show that the high energy electrons must originate from depths less than 1000 Å within the silicon if they are to be injected into a vacuum. A similar limitation on depth must apply when considering electron injection into a thin film, although in this case the reduced barrier height should give a more useful current density.

In a display device, electrons thermally generated in the p-type structure, would diffuse towards the depletion layer formed at the junction with an n^+ diffusion. The electrons would gain energy in the reverse biased junction and with sufficient voltage would be increased in an electron avalanche. In this work it was considered that shallow planar junction would be best suited to the fabrication of a display device. If the n^+ layer was sufficiently thin some electrons would reach the surface with enough energy for injection over the interfacial barrier into a surface luminescent film. In practise uniformly avalanching a large area junction is critically dependent on junction quality. It should be possible to obtain a more controlled process by biasing the junction below avalanche and using a buried, forward biased junction, to inject into the reverse biased shallow junction. In this work photo-electric excitation was used to simulate this effect. An alternative structure to the shallow planar junction would have used a deep diffused junction and the surface edge emission of electrons. Such structures might be unsatisfactory from a display point of view as they would have a small and poorly defined emitting area. It was hoped that the planar structure would have the advantages of

From ((3.3)) it can be seen that by making an appropriate choice of $\sqrt{Dt}$, and by control of the sheet resistance Rs, through the deposition stage of diffusion, it is possible to control the value of the impurity profile gradient. Fig. (3. 1) shows the results of computer calculations made by Kennedy [76]. These calculations show that the breakdown voltage of a planar junction changes from a value dependent only on the background impurity concentration, as in a step junction, to a value which is a function of the impurity profile gradient at the junction boundary. By control of this gradient the breakdown voltage of the guard ring can be made higher than that of the shallower region. If it is assumed that the shallow diffusion approximates to an abrupt junction, then Fig. (3. 1) shows that to obtain a breakdown voltage for the guard ring that is significantly higher it is necessary for the impurity profile of the guard ring to be greater than 10^{19} cm^{-4} for a background doping of $5 \times 10^{15}/cm^3$. This requires that $\sqrt{Dt}$ must be greater than 10^{-4}cm; a condition which is satisfied when using phosphorus as the dopant in a four hour drive-in cycle at 1200°C. The initial surface concentration of phosphorus after deposition being $10^{19}/cm^3$. This procedure will result in a junction depth of about 9 μm and a guard ring breakdown voltage of about 120V. The voltage breakdown of an abrupt junction in the same material is about 100V.

3.3 The Shallow Diffusion

Although phosphorus makes an ideal impurity diffusant for the guard ring, an n-type impurity with a much lower diffusion coefficient, such as arsenic, would have been preferable for the shallow junction. Unfortunately this was not possible with the equipment available at the time of this work and both junctions were made by phosphorus diffusion. Calculations based on the data of Kennedy and Murley [77], Fig. (3. 2) show that is possible to use phosphorus to obtain a junction depth of the order of 1000A in a two stage diffusion cycle if the temperature does not exceed 850°C and the duration of each stage is not longer than 5 minutes. In Appendix A 1. 5 it is shown that using the data of Kennedy and Murley that,

$$x_j = (8{\cdot}4\sqrt{Dt}) \qquad ((3.4))$$

assuming that $Dt = D_1t_1 \simeq D_2t_2$ where D_1t_1 and D_2t_2 are the diffusion coefficients and diffusion time for each stage of the deposition and drive-in cycle. The time of each diffusion stage was five minutes at a temperature of 850°C. The surface concentration after deposition was assumed to be $10^{19}/cm^3$. During the work it was found to be advantageous to increase the surface concentration to $10^{20}/cm^3$; however, this had an insignificant effect on the final junction depth.

The limitations imposed by the junction depth have repercussions when considering the formation of oxide and luminescent films over the junction. These will be discussed in Chapters 5 and 7 respectively.

3.4 Device Geometry

The device geometry was defined in the silicon by making use of standard photolithographic techniques. The minimum dimensions of the device are determined primarily by the accuracy of alignment of succeeding masking stages. For this work a mask alignment machine had to be designed and built in the Department. See Fig. A 2.2.

This allowed alignments to be made to an accuracy of 0.1 mm and hence resulted in a device that was larger than desirable. Since the probability of a defect occurring in the junction is proportional to its area, the quality requirements of the diffusion process became more stringent than if a smaller geometry could have been used.

The device to be fabricated is shown in Fig (3.3). The shallow diffused junction is allowed to overlap the guard ring by a margin that is large enough to ensure good electrical contact, and to reduce the probability of the shallow region not being in contact with the guard ring around the whole of its circumference, through an alignment error. Electrical contact is made through an aluminimum contact pattern. Care was taken not to allow the aluminimum to overlay the shallow region as this could result in electrical short circuits due to metal migration through the diffused region. Currents injected into the overlaying film of oxide of willemite were detected by a circular top contact. Connection to the substrate is made via a top contact window through a forward biased n^+ - p junction.

The complete mask set for such a device is shown in Fig. (3.4). It consists of seven masks not all of which are used in a given device. The masks were designed to be used with Shipley positive working photo-resist. Each mask was originally produced 25 times full size in Stabilene 'Cut and Strip' supplied by Keuffel and Esser. From these masters a final mask was produced on a glass high resolution plate in a two stage reduction using standard photographic methods.

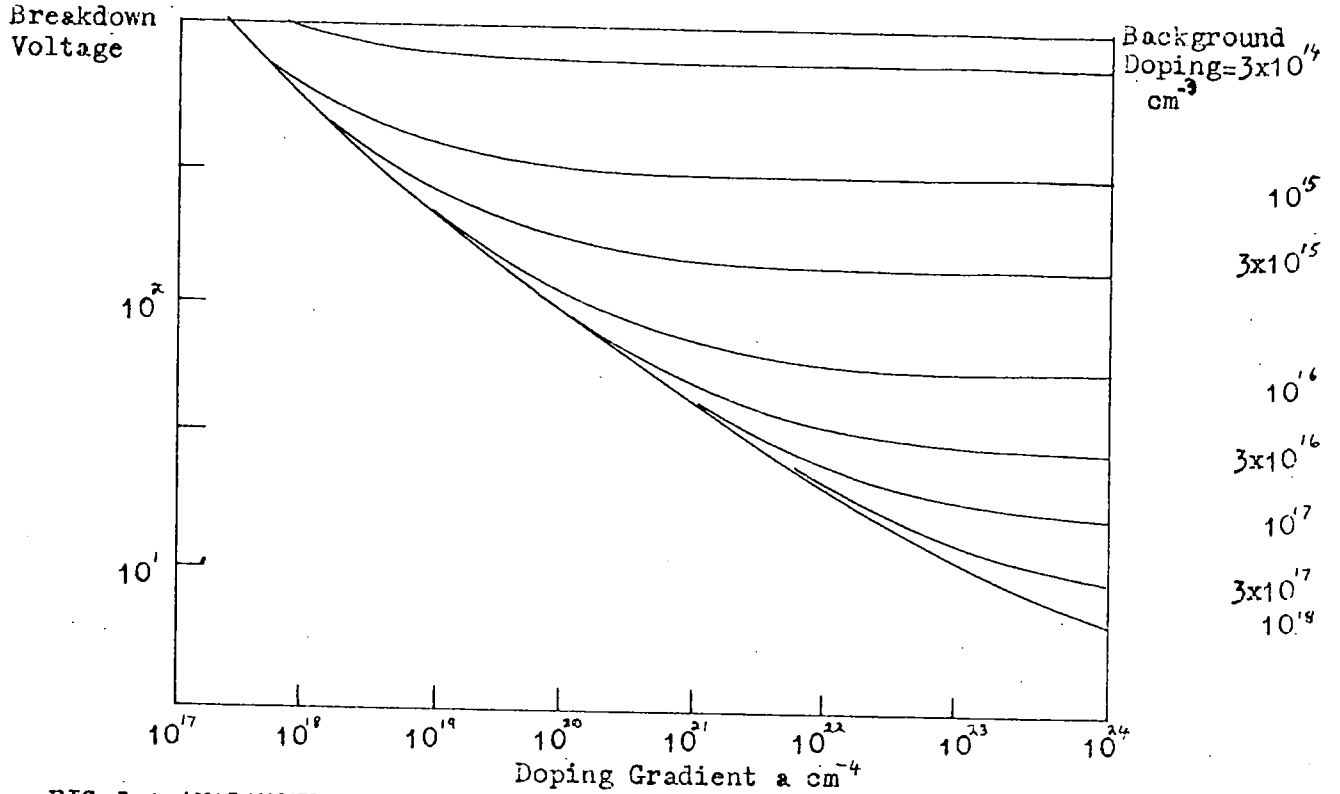

FIG 3.1 AVALANCHE BREAKDOWN VOLTAGE OF A SILICON PLANAR DIFFUSED p-n JUNCTION

Ref 76

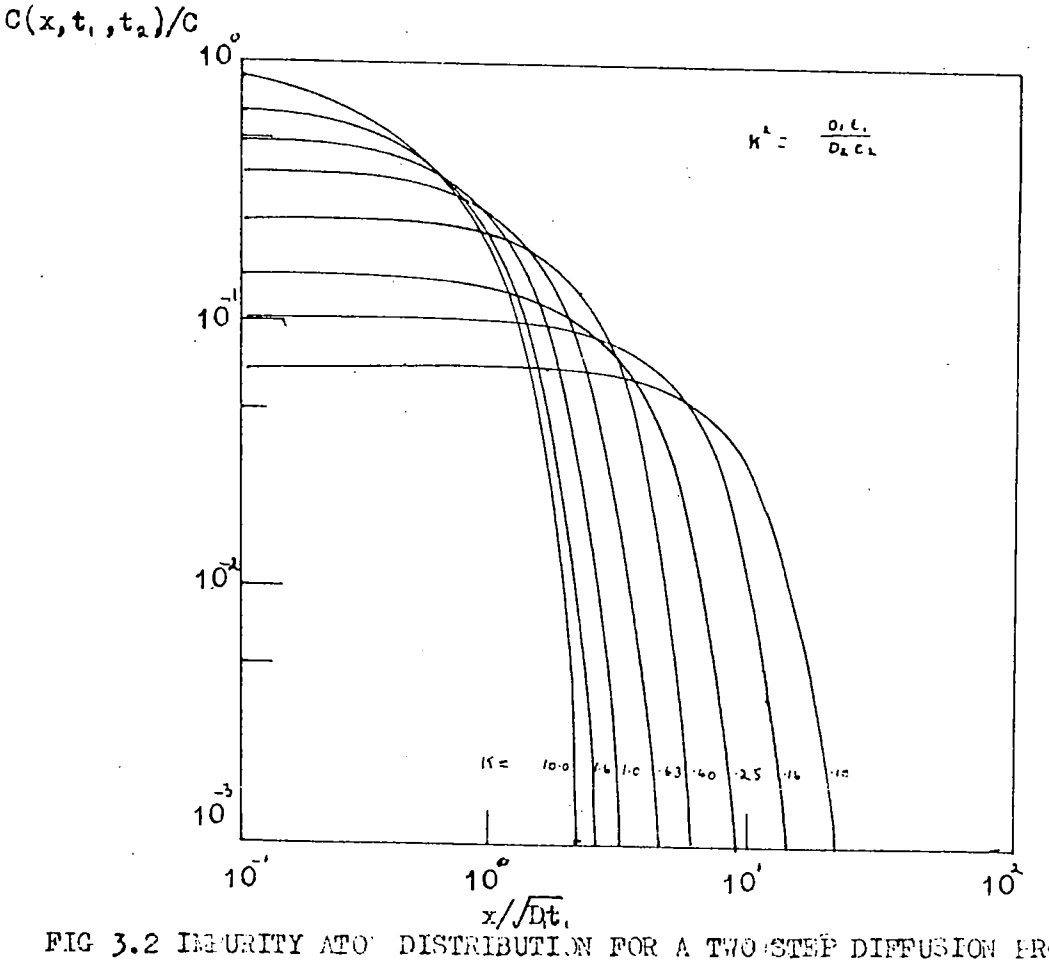

FIG 3.2 IMPURITY ATOM DISTRIBUTION FOR A TWO-STEP DIFFUSION PROCESS

Ref 77

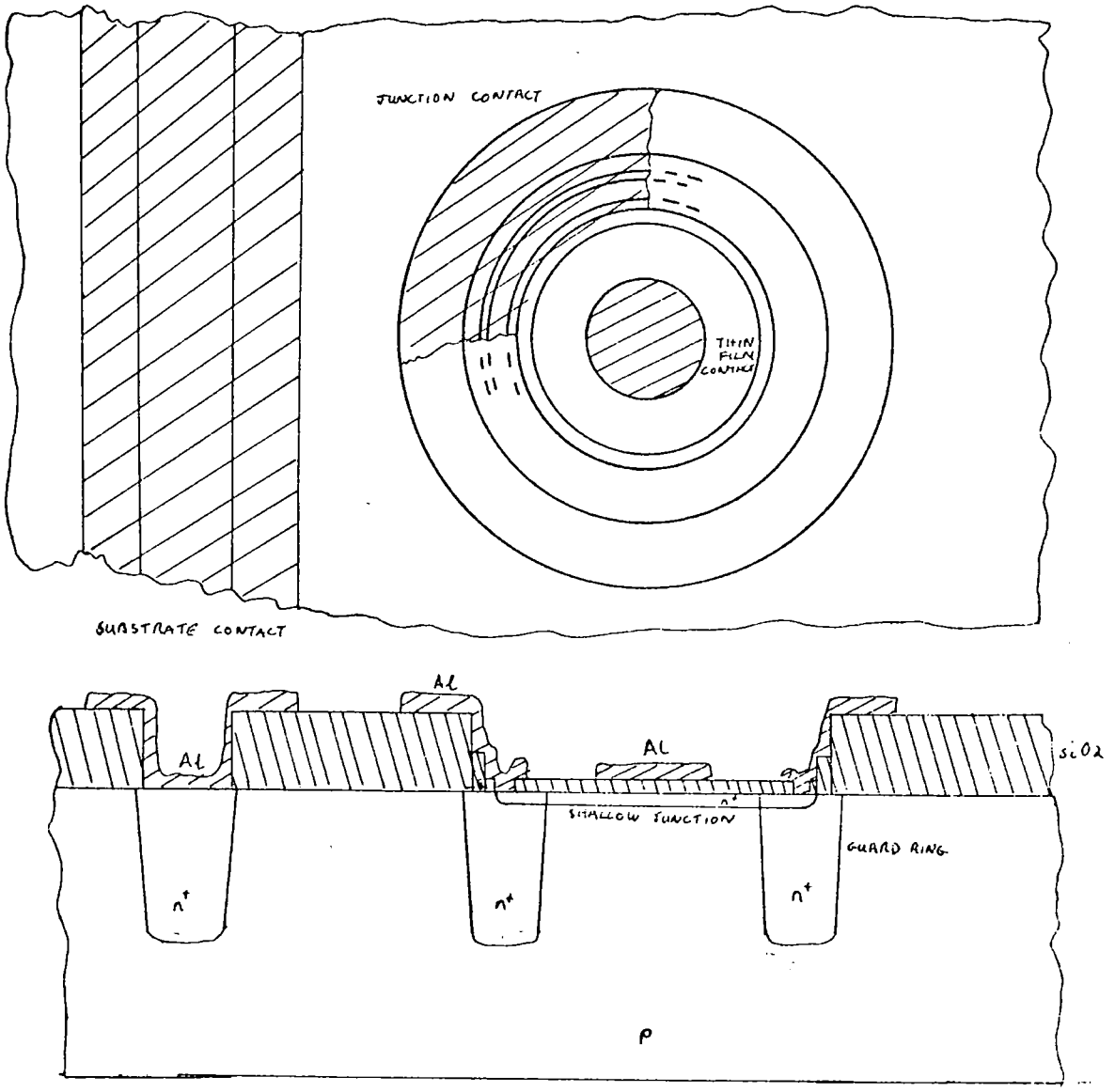

FIG 3.3 PART OF TEST CHIP AND DEVICE STRUCTURE

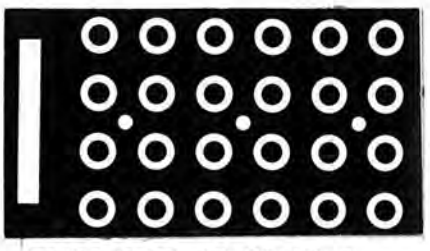

GUARD RING JUNCTION 1

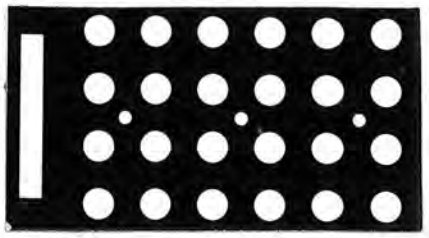

SHALLOW JUNCTION 2

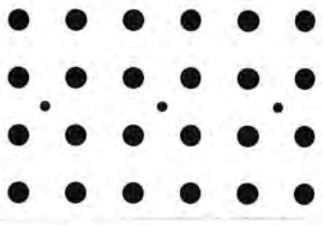

THIN FILM DEFINITION 3

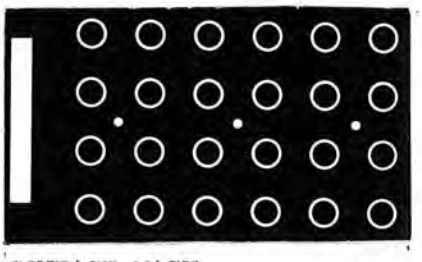

CONTACT MASK 4

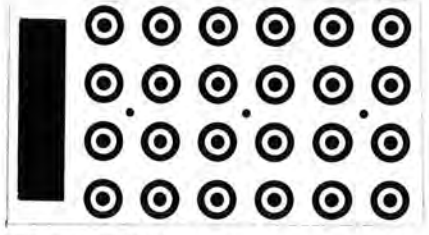

METAL MASK 5

6

OPTIONAL METAL MASKS

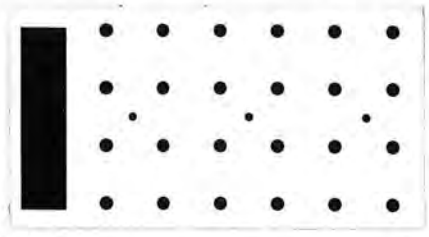

7

FIG 3.4 PHOTO-LITHOGRAPHIC MASK SET

CHAPTER FOUR

FABRICATION OF JUNCTION STRUCTURES IN SILICON

4.1 Introduction

The initial objective of the device fabrication work was to establish a procedure for making shallow $p\text{-}n^+$ junctions which would exhibit uniform breakdown characteristics under reverse bias conditions. In a similar study by Goetzberger et. al.[36] it was established that there is a close correlation between the occurence of structually perfect junctions and the detailed processing employed. In particular it is necessary to avoid contamination of the silicon surface. Similar precautions were taken in the present work. All processing was performed in a Class 10,000 clean room in which the dust particle content was kept to a low level by filtering the air as it entered the room. As an additional precaution against airborne contamination, all furnace loading and photo-lithographic work was performed in laminar flow work benches, having their own air filtering systems. A constant check was kept on the dust particle concentration within the clean room. In all the work, high purity 'ULTRAR' chemicals, supplied by Hopkin & Williams, were used. Water was obtained from an Elgastat recirculating deioniser fitted with a 0.25 micron filter. The resistivity of the water was monitored at 18 M Ω cm at 16°C. Plastic or Pyrex beakers were used for wet processing work, one beaker being reserved for each chemical to reduce cross contamination. Diffusion and oxidation processes were performed in conventional three zone furnaces in which temperatures between 500°C and 1,300°C could be maintained to $\pm$ 0.5°C over a length of 30 cm. Gas supplies were derived from cylinders, dried in a molecular sieve column and filtered (0.5 mm Pore size) before entering the furnace.

The remainder of this Chapter deals with the detailed fabrication procedure of the basic $p\text{-}n^+$ junction structure common to all devices studied. For fabrication details which are peculiar to the oxide, or willemite film covered devices it is necessary to refer to Chapters 5 and 7 respectively.

4.2 Processing Techniques

During this work a strict processing schedule was adhered to, and controlled alterations were made only when necessary. The following description refers to the final procedure which was to yield the greatest reproducibility and the highest incidence of useful devices.

The starting material was 4 - 5 ohm - cm boron doped <111> silicon supplied by Holboken, Belgium. It was nominally dislocation free having less than 100 dislocations/cm^2. The silicon wafers were scribed into chips of 1 cm x 0.5 cm on which an array of 6 x 4 devices could be fabricated using standard photo-lithographic techniques. The detailed procedures used for defining the device geometry are described in Appendix 2. From the point of view of producing microplama free junctions it would have been preferable to process whole wafers (1" Diameter). Scribing the wafers probably introduced a number of dislocations. Unfortunately with the photo-lithographic equipment available this was not possible.

4.3 Silicon Cleaning

The silicon chips were given an initial clean by boiling twice in trichorethane, to remove gross organic contamination. Further cleaning to remove organic plus inorganic contamination was accomplished by immersion in a 50:50 solution of $HCl:H_2O_2$ (HCl - 36% solution, H_2O_2 - 100 vols - 29% w.w.) This clean was followed by a five minute wash in deionised water and then a thirty minute boil in a 50:50 solution of H_2SO_4: H_2O_2 (H_2SO_4 - 98% solution). Since these treatments leave the silicon with an oxidised surface which may contain impurities, the cleaning was completed by immersing the silicon for ten seconds in a 1:10 solution of 48% HF in deionised water. This was followed by a twenty minute wash in running deionised water. In the early experiments the chemical clean was followed by a high temperature wet oxidation to grow about 1 micron of oxide. This was subsequently removed in HF before the masking oxide was grown.. This procedure was meant to remove any surface damage on the silicon which may have been introduced by the manufacturer during final polishing. However, it was found to result in depletion of boron from the silicon surface causing high leakage currents in the final devices. The procedure was therefore discontinued.

4.4 The Masking Oxide

After cleaning, a thick oxide layer was grown on the silicon chip. An oxide layer of about 0.85 microns was necessary to mask against phosphorus diffusion later in the process. The oxide was grown by heating the silicon to 1100°C in a dry oxygen atmosphere for fifteen minutes., followed by 120 minutes in wet oxygen and a final period of fifteen minutes in dry nitrogen. The wet oxygen was produced by bubbling dry oxygen through deionised water contained in a Pyrex flask. The flask was immersed in a water bath maintained at 95° C. The initial oxidation in dry oxygen was necessary to reduce depletion of the silicon surface which would have resulted

from a too rapid oxidation of the bare silicon in wet oxygen. The final stage in dry nitrogen produced an oxide surface suitable for photo resist application. See Appendix 2.

4.5 The Phosphorus Diffusions

The first photo-lithographic stage used mask No.1 , as shown in Fig. 3.4, to define the areas of the guard ring diffusion. This pattern was etched in the oxide using a 4:1 solution of 40% NH_4F : 48%HF. After etching, the resist was removed by boiling for thirty minutes in a 50:50 solution of H_2SO_4:H_2O_2.

The phosphorus doping source used in this work was $POCl_3$. This is a liquid at the temperatures at which it was maintained during this work, ie 23°C and 35°C. $POCl_3$ has an advantage over the solid source P_2O_5, which is also commonly used, in that it allows a better control to be maintained over the surface doping concentration. P_2O_5 normally gives reproducible results only if a saturated surface concentration is obtained. It was considered that surface saturation could result in undue strain in the diffused areas, and hence non-uniform breakdown. (78).

The system used for introducing phosphorus into the silicon is shown in Fig. 4.1. The $POCl_3$ was held in a Pyrex flask which was immersed in a water bath maintained at a constant temperature by heating circulated mains water. The surface doping concentration is a function of the furnace temperature and the partial pressure of phosphorus in the gas stream. The vapour pressure of $POCl_3$ is strongly dependent on temperature, it is given by,

$$\log_{10} P = 7.72 - 1.83 \times 10^3 / T \quad \text{torr} \qquad ((4.1))$$

where P is the vapour pressure and T is in °K.

For the guard ring diffusion the $POCl_3$ source temperature was maintained at $(23^\circ \pm 1)^\circ$ C and at $(35 \pm 1)^\circ$C for the shallow diffusion. The reason for this will be explained later.

A small flow of argon was bubbled through the $POCl_3$ and then combined with the main argon gas flow. A small percentage of oxygen was added to the carrier + $POCl_3$ gas as it entered the furnace tube. The silicon chips were exposed to the phosphorus by pushing them in a quartz boat to the centre of the furnace tube downstream from the gas inlet. The chemical reaction that is thought to take place with the silicon is,

$$4\,POCl_3 + 3O_2 = P_4O_{10} + 6\,Cl_2 \qquad ((4.2))$$

$$P_4O_{10} + 5\,Si = 4\,P + 5\,SiO_2$$

Thus a phosphorus rich glass is formed on the silicon surface from which the phosphorus diffused into the p-type bulk to form the p-n junction. Free chlorine which is also formed in the reaction can etch the silicon surface causing the junction electrical characteristics to be leaky. This can be minimised by controlling the percentage of oxygen in the carrier gas such that

the protective phosphorus glass is formed rapidly. However, if the oxygen concentration is too high the percentage phosphorus content is reduced. This results in high sheet resistance values for the diffused layer. The effect of the oxygen concentration has been studied by Heynes and Wilkerson [79] who found that it was particularly critical for diffusion temperatures less than 1000° C. In this work phosphorus deposition was carried out at 850°C and accordingly the results of Hynes and Wilkerson were followed in using a 0.35% $POCl_3$ concentration and a 3% oxygen concentration in the main argon carrier gas. The percentage of $POCl_3$ vapour picked up by bubbling through argon has been measured to be 76% of the saturated vapour pressure (S.V.P.) In the deposition stage for the guard ring the $POCl_3$ was maintained at 23°C giving a S.V.P. of $POCl_3$ of about 35 torr. The main argon carrier gas flow was chosen to be 500 cc/min so that the argon flow rate required through the $POCl_3$ was calculated to be 45cc/min and the oxygen flow rate 15cc/min.

It was found to be necessary to pre-dope the furnace tube and quartz boat by turning on the $POCl_3$ flow for twenty minutes before beginning a deposition. This allowed the tube and boat to become saturated with phosphorus and in equilibrium with the gas flow when the silicon was placed within the furnace. The silicon was thoroughly dried in an argon atmosphere at about 150°C for thirty minutes before beginning the deposition. If this procedure was omitted the silicon surface could be etched and damaged. See Section 4.7. A silica boat of low thermal capacity was used to transport the silicon to the centre hot zone of the furnace thus minimising any thermal lag in bringing the silicon up to the required temperature. One minute was allowed for thermal equilibrium to be established with a gas flow of just pure argon and oxygen. This reduced non-uniform condensation ofphosphorus on the silicon and in addition allowed a thin protective oxide film to form over the bare silicon. The oxide film was readily converted to a phosphorus glass once the $POCl_3$ flow was started. The deposition stage with the $POCl_3$ flow lasted three minutes after which the $POCl_3$ was turned off and a further one minute allowed for the furnace tube to clear of free phosphorus. It was found that the doping uniformity improved if the silicon chip was placed in the centre of the cross-section of the furnace tube. This was thought to be a result of the convectional gas flows within the tube [80]. It was therefore preferable to perform the deposition on only one device array at a time. A test sample of bare silicon was also included to allow the sheet resistivity and junction depth to be measured.

The deposition cycle results in the formation of a thin film of phosphorus doped glass. Better doping uniformity was achieved if the glass was removed before the junction drive-in diffusion. The phosphorus glass was removed by etching for ten seconds in a solution of 60 cc H_2O , 5cc HF, 3cc HNO_3. This was followed by a twenty minute wash in running deionised water and then blown dry.

The phosphorus accumulated at the silicon surface during the deposition cycle was diffused to a depth of about 9 microns. This was performed in a drive-in cycle at a temperature of 1200°C for 225 minutes in a dry oxygen atmosphere, followed by fifteen minutes in dry nitrogen. As well as giving the required guard ring junction depth this procedure also grows 0.3 microns of oxide over the areas of bare silicon and leaves the surface ready for the second photo-lithographic stage. The sheet resistance of the diffused layer was monitored on the test sample using a four point probe measuring instrument. A typical value was about 100 Ω/□ varying by less than 1% across a 1.0 cm^2 test sample. However, variations as great as 20% were obtained between different batches. The guard ring junction depth was measured by grooving through the n-type surface of the test sample and staining [81] the exposed p-type region as shown in Fig. 4.2a. The depth of the n-type layer was then obtained using an interferometer and sodium light. A value of 8.6 microns was measured for the guard ring depth and, using Irvin's [82] data, an initial surface concentration of phosphorus after deposition was calculated to be $10^{19}/cm^3$.

The second photo-lithographic stage uses mask No. 2 as shown in Fig. 3.4, to define the areas of the shallow junction. In early experiments the phosphorus deposition stage for the shallow diffusion was the same as for the guard ring. However, it was observed that when oxide is grown on heavily phosphorus doped silicon ($> 10^{19}/cm^3$), at temperatures below 900°C, the resulting oxide thickness is greater than that obtained on less heavily doped silicon under the same conditions. Similar results have been reported by Deal and Sklar [83] who conclude that the phosphorus increases the silicon surface affinity for oxygen. It was found in this work that, by using a surface concentration of phosphorus of $10^{20}/cm^3$, an oxide film of 540 Å thickness could be grown at 850°C in five minutes with a wet oxygen atmosphere. It was desirable in the final devices, used for the experiments on electron injection into SiO_2, that the oxide thickness should be greater than 500 Å without driving in the junction beyond 1000 Å. See Chapter 5.

With a surface concentration of $10^{19}/cm^3$ it was only possible to grow oxides of 300 Å under the above conditions. The phosphorus surface concentration was increased to $10^{20}/cm^3$ by raising the temperature of the $POCl_3$ source to 35°C thereby increasing the partial pressure of phosphorus within the furnace tube. After deposition the phosphorus glass was removed as for the guard ring diffusion. The thin oxide or phosphor films covering the shallow junction were formed as described in Chapters 5 and 7 respectively.

4.6 Metallisation

The third photo-lithographic stage used mask No. 4 or 3 as shown in Fig. 3.4 to define the areas where electrical contact is made to the silicon. Mask No. 3 was used if willemite had been formed over the junctions. The etch used was a 4:1 solution of NH_4F:HF if the contact was through silicon dioxide and a 10% solution of glacial acetic acid in deionised water if the contact was to be made through a willemite film. See Appendix 2. After defining the contact windows but before evaporation of the aluminium the junctions were baked at 600° C in dry oxygen for twenty minutes, followed by a 10sec. dip in 10:1, H_2O : HF. This was found to be necessary to reduce the reverse saturation leakage current. If the oxygen bake was omitted the reverse I-V characteristics of the junction were as shown in Fig. 4.3a. The reverse breakdown was sharp but the leakage current was of the order of 0.1 mA. This high saturation leakage is typical of channeling caused by inversion of the p-type surface. The oxygen bake is thought to reduce the number of positive vacancies, in the oxide, at the interface with the silicon surface (84) thus reducing inversion. The oxygen bake reduced the reverse current leakage to less than 1 μA measured at 20V as shown in Fig. 4.3b. A similar bake in dry nitrogen resulted in no such reduction in leakage current which was not therefore considered to be due to water absorption by the oxide.

Electrical contact to the junctions and thin oxide or willemite films was made via an aluminium contact pattern. This was formed in two stages, first by evaporating about 1 micron of high purity aluminium over the silicon surface and then etching in the required contact areas. The aluminium source was of six nines purity and was evaporated from an electron beam heated crucible. The vacuum system was a stainless steel pot covered by a 12" glass bell jar pumped down to a pressure of 2×10^{-7} torr at evaporation. The pumping was oil free using two molecular sieve sorption pumps operated sequentially to a pressure of approximately 10^{-2} torr. High vacuum was reached by the use of a titanium ion pump aided by a titanium sublimation pump. The aluminium film thickness was controlled by timing the evaporation at a fixed electron beam acceleration voltage and current. A calibration

curve of aluminium thickness against time was previously obtained on test samples using an interferometer to measure the thickness.

The metal contact pattern was defined after aluminium evaporation by the fourth photo-lithographic stage using mask No. 5 Fig. 3.4. The aluminium pattern on thin oxide devices was etched using a solution of 80cc H_3PO_4 and 5cc HNO_3. However, since willemite is attacked by all acids an etching procedure employing NaOH had to be used when willemite was present. This is described in Appendix 2 and Chapter 7. The final stage in the manufacture of the devices was to sinter the aluminium in dry nitrogen at 400°C for five minutes to allow the metal to make good electrical contact with the junctions and for good adhesion to the oxide.

4.7 Defects in the Junctions

Several types of junction defects can be attributed to the fabrication processes. These are described briefly below.

Etch pits can be produced in the diffused regions as a result of incomplete drying of the silicon before phosphorus deposition. It is thought that the water combines with the free chlorine from the $POCl_3$ and etches the silicon surface giving triangular etch pits as shown in Fig. 4.4a. Such pits have been observed to be the centre of areas of microplasmas and are thus undesirable when trying to produce junctions with a uniform breakdown.

Star shaped defects have been observed in the diffused guard ring areas after both drive-in and shallow diffusions have been completed. Such defects are shown in Fig. 4.4b, they have also been reported by Stickler and Faust[85]. These star defects have been attributed to the release of high stress resulting from heavy phosphorus concentrations. Evseev et al[86] have shown that the defects are associated with low voltage turn on microplasma breakdown. It is probable that the defects are a contributory factor in the high incidence of microplasma observed at the intersection of the guard ring and shallow junction diffusions.

Oxide islands can sometimes be seen in the etched windows. These are caused by dust particles on the photographic masks during the photo-lithographic stages. Similar effects are caused by dust adhering to the silicon during the shallow junction deposition stages. Fig. 4.4c shows an oxide island observed within the shallow junction area. Such defects are the centre of areas of microplasma breakdown if they occur within the shallow junction because of junction curvature effects. When the junction is reversed biased the area around the oxide island shows up as a ring of bright white indicating localised breakdown.

Some of these defects have occurred in every batch produced; thus the ideal of a shallow junction with uniform breakdown was not achieved. However the process resulted in a yield of about 20% useful devices in which electron

injection could be detected. It is thought that the quality of the junctions was mainly limited by mask defects and the poor alignment tolerences allowed by the masking equipment. Improvements could also be made by fabricating smaller area junctions thus reducing the probability of having a defect within the shallow junction area. The alignment tolerence of the masking equipment did not unfortunately allow this.

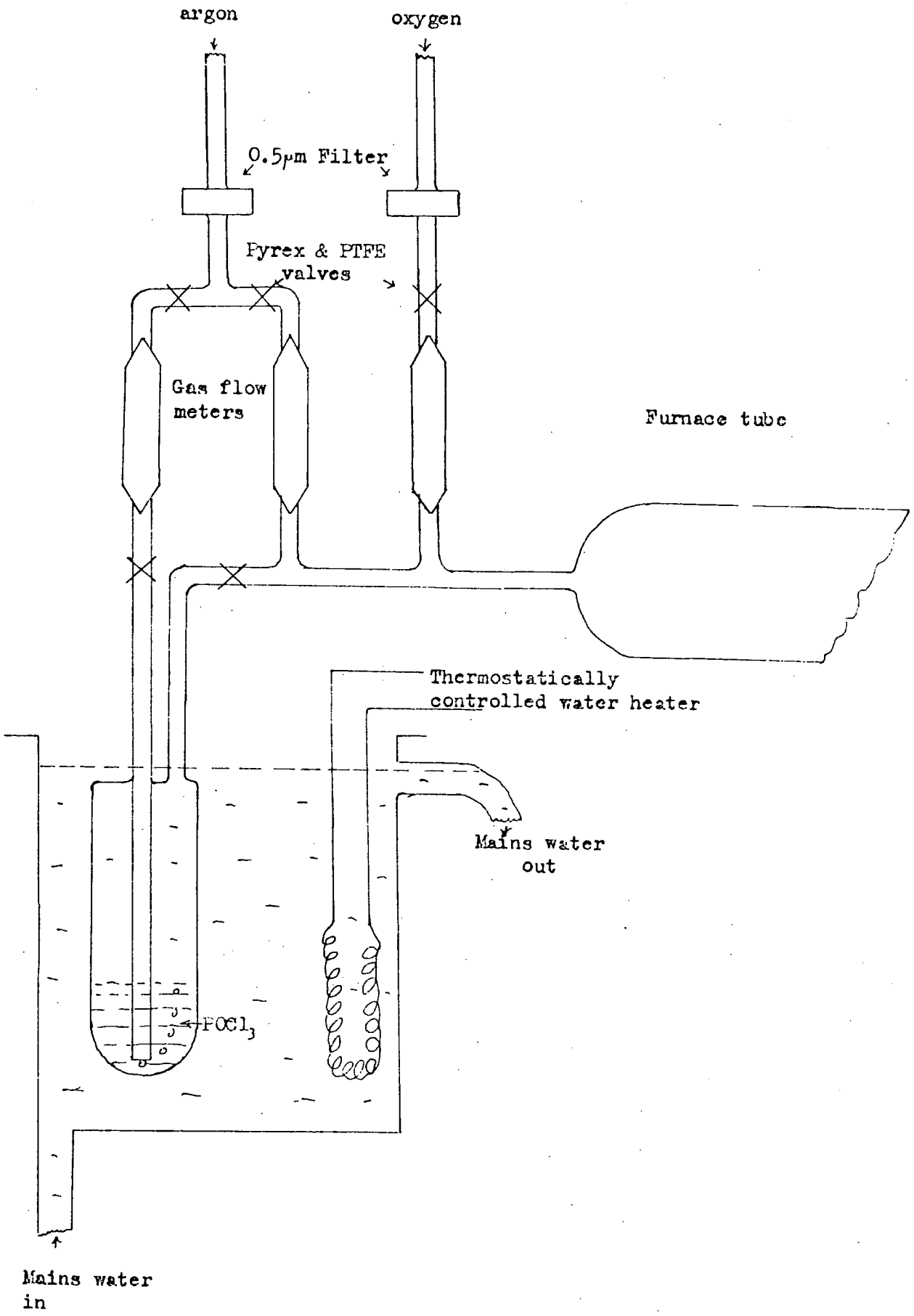

FIG 4.1 GAS TRAIN FOR THE INTRODUCTION OF $POCl_3$ INTO THE FURNACE TUBE

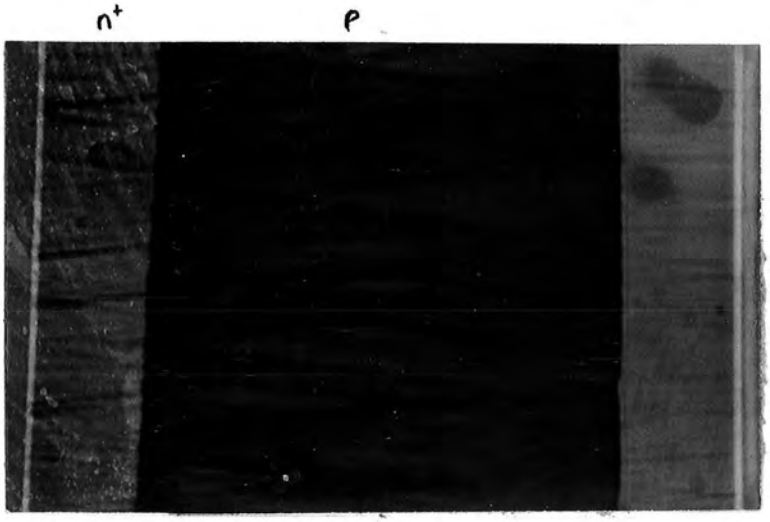

(a) GUARD RING JUNCTION

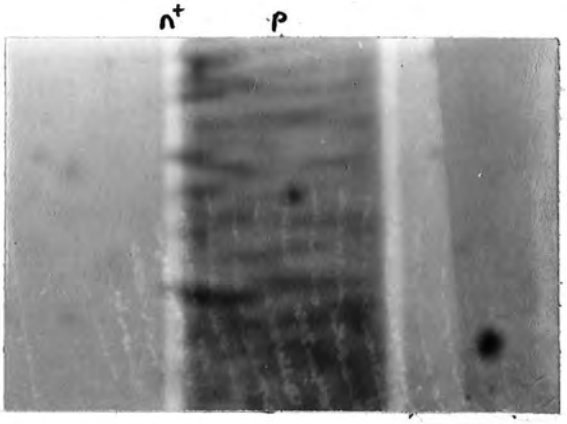

(b) SHALLOW JUNCTION

FIG 4.2 BEVELED AND STAINED JUNCTIONS

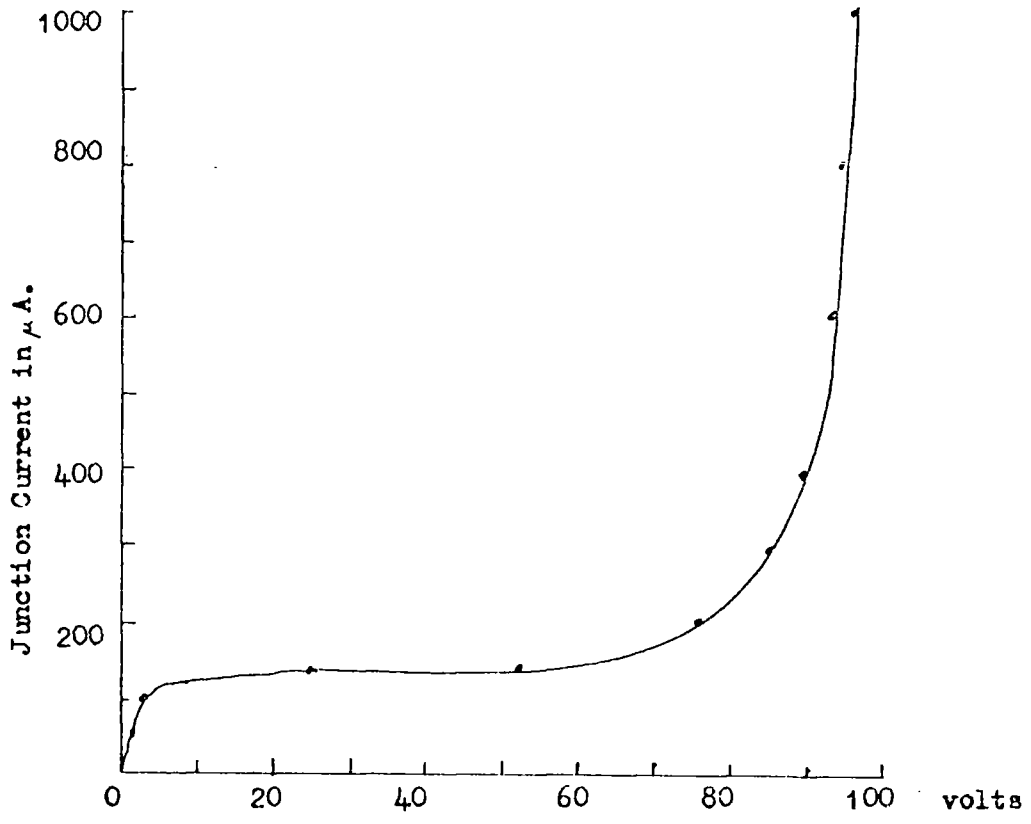

FIG 4.3a DEVICE REVERSE BREAKDOWN CHARACTERISTICS BEFORE AN OXYGEN ANNEAL.

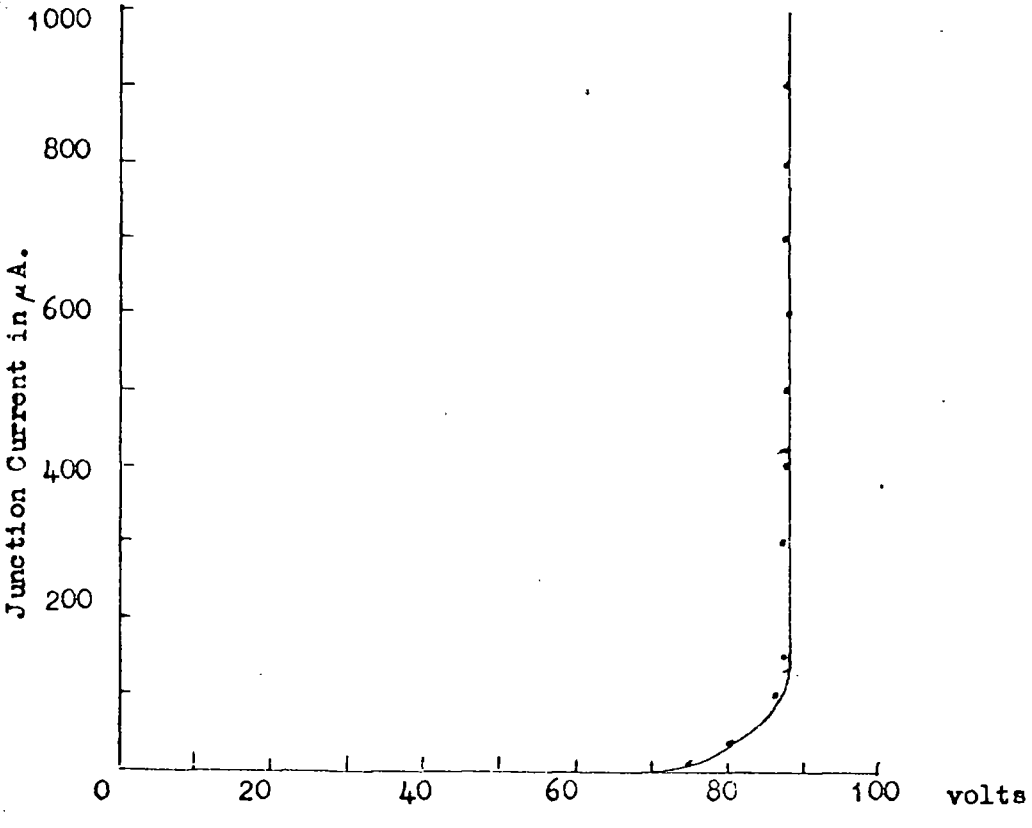

FIG 4.3b DEVICE REVERSE BREAKDOWN CHARACTERISTICS AFTER AN OXYGEN ANNEAL.

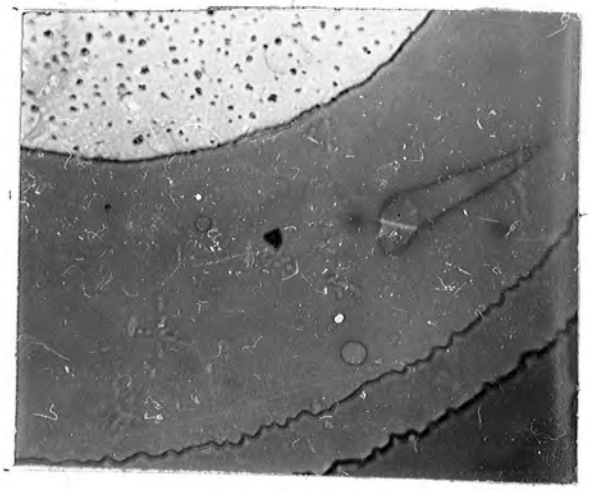

(a) TRIANGULAR ETCH PIT

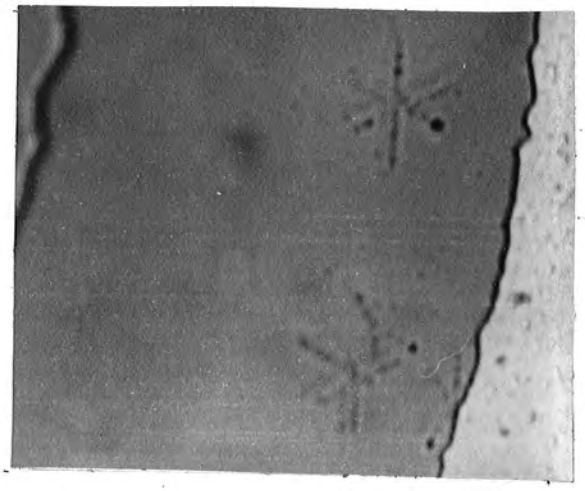

(b) STAR DEFECT

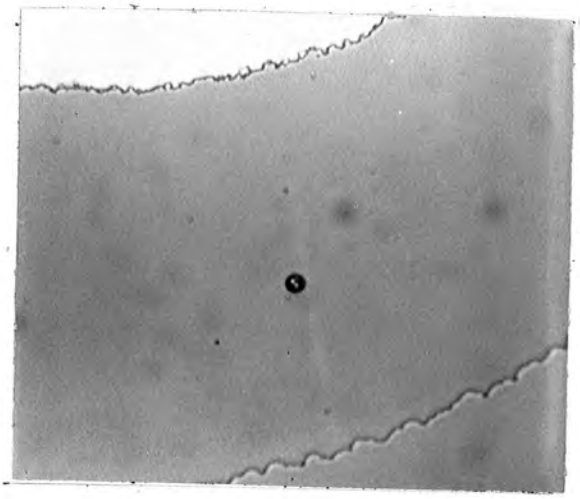

(c) OXIDE ISLAND

FIG 4.4 VISUAL JUNCTION DEFECTS

CHAPTER FIVE

MEASUREMENTS OF CURRENT INJECTION INTO SILICON DIOXIDE

5.1 The Injection Structure

The results presented in this chapter are for charge injection into thermally grown silicon dioxide from the reverse biased, shallow planar p-n junction described in previous chapters. It is, to the author's knowledge, the first reported example of charge injection from a shallow planar junction. All other reports have used deep p-n junctions and have either obtained electron emission from the p-n boundary region, where the junction is exposed at the surface, or employed M.O.S. structures as described in Chapter 2. The discussion in Section 2.2 showed that there is a restriction on the maximum allowable depth for the shallow emitting junction. If the depth is greater than about 1000 Å the probability of an electron reaching the Si/SiO_2 interface, with sufficient energy for injection, becomes vanishingly small. In practice, this limits the heat treatment that can be applied to the device after forming the junction. A too high or prolonged heat treatment would diffuse the junction to a depth of greater than 1000 Å. For injection into a thermally grown oxide overlaying a shallow junction of diffused phosphorus, the heat treatment must be limited to a maximum temperature of 850°C for five minutes. For the structure described in Chapter 4 it was therefore only possible to grow very thin oxide films over the shallow junction region. Ellipsometer readings gave thicknesses of 100 Å for oxide grown in the above conditions in an ambient of dry oxygen, and 300 Å in wet oxygen. Measurements made of currents injected into such thin oxide films were limited by a high incidence of electrical short circuits between the aluminium contact over the oxide and the junction below. This was probably due to pin holes or weaknesses in the oxide caused by process contamination. Where measurements were possible, the injected oxide currents were unstable, displaying large positive swings which eventually resulted in unpredictable breakdown events. Osburn and Weitzmann [57] have observed similar instabilities during a study of high field electronic conduction through silicon dioxide films of less than 400 Å thickness. It was suggested that the instabilities were the result of secondary ionisation collisions within the oxide, their results being in qualatative agreement with a theoretical model proposed by O'Dywer [87].

Osburn and Weitzmann found that high field conduction through oxide films thicker than 400 Å was relatively stable. In order to obtain

more stable measurements in the present work it was therefore desirable to increase the oxide film thickness, but with the same thermal restrictions as stated earlier. It has been found that the initial rate of growth of thermal SiO_2 is increased with a high concentration of phosphorus in the silicon surface[83]. This fitted well with the design of the present structure as the surface phosphorus concentration of the shallow junction could easily be increased by control of the $POCl_3$ source temperature as shown in Section 4.3. To increase the oxide growth rate, the surface phosphorus concentration for the shallow junction diffusion was increased to $10^{20}/cm^3$. This resulted in being able to grow 540 Å of oxide in five minutes at 850°C in an ambient of wet oxygen. The phosphorus glass present after the deposition stage was etched clear before this final oxide was grown. The oxide thickness was measured on an ellipsometer which also gave a value for the refractive index of the oxide of 1.46. Capacitance measurements made at 200 KHZ gave a value for the dielectric constant of 3.9 ± 0.2. These values suggest that oxide grown at the enhanced rate was similar in structure to that normally grown in a steam environment. The sheet resistance of the shallow diffused layer after the oxide growth ranged between 200 and 400 Ω/□ The junction depth was measured by grooving and staining a check sample and was found to be of the order of 1,000 Å. A final fabricated device structure with a thin oxide film over the shallow junction region is shown in Fig. 5.1.

5.2 Properties Of The Junction Under Reverse Bias

Electrical contact to the device was made using micromanipulator probes. The device substrate was held on an insulated, adjustable probing table within a screened chamber as shown in Fig. 5.2. The chamber was continuously flushed with dry nitrogen to reduce junction and surface leakage currents to earth, and to maintain good device characteristics. Thermally grown SiO_2 rapidly absorbs water from the atmosphere and this can lead to a softening of the reverse breakdown characteristics and an increase in the reverse leakage currents. The measurement chamber was kept dark by surrounding it with a black cloth.

The measurement circuit is shown in Fig. 5.3. A constant current generator, connected between the substrate and the guard ring, was used to maintain a known reverse junction current. This supply could provide a current between 0 and 1.0 mA in steps of 0.1 mA or between 1.0 mA and 10.0 mA in steps of 1.0 mA. For some measurements the current source was replaced by a constant voltage supply. The reverse current could then be increased, at a constant reverse bias, byillumination from a

GaAs infra-red emitter located within the probing table, beneath the device. The GaAs lamp could be situated beneath any chosen device on the substrate by means of location marks on the probing table. A Farnell stabilized power supply was used to apply from 0 - 30 V across the thin (540 Å) oxide film. i.e. between the n^+ diffusion and the aluminium thin oxide pad. The area of the contact pad was 0.08 mm^2. Currents of down to 10^{-14}A, through the thin oxide film were measured by a Vibron electrometer connected between the thin oxide contact pad and ground.

The voltage at which avalanche breakdown occurred was about 90±5 V for a typical device. This compares with a breakdown voltage of about 120V for the guard ring structure alone, as shown in Fig. 5.4. It was therefore considered that breakdown was initially taking place within the shallow junction region. This was substantiated by the appearance of small areas of white light within the shallow junction region at avalanche. Some of the properties of these microplasmas have been described in Section 2.4 which will be referred to again in Chapter 6 as the basis for a model to describe the current injection process. The exact origin of microplasmas is not clear but they are generally thought to be associated with precipitates or structural defects within the silicon crystal. In this work microplasmas observed in the shallow junction region have usually been associated with visible defects which were probably introduced during one of the processing procedures. Some of the possible causes of these junction defects are discussed in Section 4.7. A single device may exhibit one or more microplasmas, each being in a well defined region and only becoming visible at a certain junction bias voltage. Occasionally it was observed that a device emitted white light in the form of striations over a large area of the shallow junction. Light emission of this form has also been observed by Goetzberger [36] in a study of structually perfect junctions. It was found by Goetzberger that the orientation of the striation was related to that of the silicon substrate. It is thought that the striations represent areas of uniform junction breakdown and therefore give an indication of the high quality of the shallow diffusion. In all the devices considered in this chapter it was observed that light emission also occurred from the region at the intersection of the guard ring and the shallow junction. This may be the result of strain introduced by the masking oxide at the edge of the diffusion window. These edge microplasmas turned on at a lower voltage than those in the shallow junction and were not of such well defined area since the area of light

emission was observed to increase around the junction perimeter with increasing junction bias.

In was shown in Chapter 2.5 that electron emission into a vacuum is thought to originate from microplasmas. In Chapter 6 it will be considered that electron injection into the silicon dioxide thin films will also be associated with microplasmas. It should be emphasized that none of the junctions produced displayed uniform light emission over the entire shallow junction area. In general, the junctions contained microplasmas so that the area of emission was probably not so great or as well defined as one would have hoped with this structure. Further evidence for charge injection originating from localised areas comes from avalanching junctions to such high currents that destructive breakdown occurred. A typical device was able to sustain a reverse avalanche current of up to about 30 mA without being destroyed. In those devices which gave charge injection into the oxide film, the high current breakdown was accompanied by burning out part of the aluminium contact to the oxide film, as shown in Fig. 5.5b. If the device gave no current injection destructive breakdown was observed at a region away from the aluminium contact and usually at the intersection of the guard ring and the shallow junction as shown in Fig. 5.5a.

5.3 Measurements of Injection Currents into Silicon Dioxide

With zero junction current only very small currents were measured in the oxide film even under high-field conditions. Fig. 5.6 shows that the oxide current was of the order of 10^{-13} A for a field up to 3×10^6 V/cm with the aluminium biased positive with respect to the n^+ surface region. However, if the junction was reverse biased into avalanche, injection currents of the same order could be detected with an applied oxide field well below 1.0×10^6 V/cm. It was found that the injected oxide current increased with both the field and the junction avalanche current. No dependence on junction current was observed when the field polarity across the oxide was reversed showing that the effect was consistent with electron injection from the silicon.

Devices produced early in the research had soft reverse breakdown characteristics and exhibited high leakage currents. In these devices it was necessary to pass junction currents greater than 5 mA before an appreciable oxide current was obtained, as shown in Fig. 5.7. Improvements in processing, such as discussed in Chapter 4, gave devices with sharp breakdown characteristics. With these devices it was possible to obtain oxide currents of up to 10^{-10} A with an applied field of 2×10^6 V/cm and a junction avalanche current of 1.0 mA. If the junction current was increased much beyond 5.0mA

the oxide current became unstable and this usually resulted in a breakdown in the thin oxide film. The oxide current instabilities became more apparent for higher values of the oxide field.

Measurements of the oxide current were usually made with the device in the dark. In this situation with a field of less than 3×10^6V/cm applied across the oxide film, no appreciable oxide current was observed until the underlying junction was biased into avalanche. The condition can be seen from Fig. 5.8 which shows the injected oxide current for three devices plotted against reverse junction current. Each device had a different junction saturation leakage current and in each case the oxide current could only be detected when junction current multiplication occurred and not at the same junction current level.

With zero junction current an oxide current of the order of 10^{-13}A was detected at field strengths above about 3.0×10^6V/cm. This was found to decay by an order of magnitude over a period of hours. A similar fall off in oxide current was observed when the junction was avalanched for about thirty minutes. Initially the oxide current was independent of the reverse bias applied to the junction until the avalanche bias was attained. At this junction bias the oxide current increased rapidly although it was generally unstable, displaying large positive and negative swings. After a period of about thirty minutes the oxide current stabilized and if the junction current was then returned to zero, the oxide current was found to be about an order of magnitude below that recorded before avalanching the junction. For example, with a device from batch R_3 the oxide current was initially 2×10^{-13}A with 20V applied across the oxide film. This decreased to 5×10^{-14}A after avalanching the junction for thirty minutes at 1.0mA. However, by using a lower oxide field, less than 10^6V/cm, and a junction avalanche current of 0.1 mA it was possible to obtain oxide currents that were stable at the initial avalanching of a virgin junction. Fig. 5.9 shows the form of oxide current decay with time for a device avalanched for the first time. The oxide bias voltage was 5.0 V and the junction avalanche current was 0.1 mA. For general measurements it was found to be necessary to stabilize a device by biasing the oxide at 5.0 V and passing an avalanche current of 1.0 mA for thirty minutes. After this treatment the oxide currents were stable and reproducible for both increasing and decreasing oxide field and junction avalanche current. Similar precautions were found to be necessary by Pepper[71] in his study of the currents induced in oxides by avalanching transistor structures.

Fig. 5.10 shows a family of curves for oxide current (I_{ox}) plotted against junction current (I_j), for a range of values of the voltage applied

across the oxide film. The form of the expotential rise in I_{ox} with I_j was typical of all the devices studied for values of junction current up to 1.0mA. Fig. 5.11 shows the oxide current for a device in which the junction was increased to 10.0 mA. For junction currents up to 5.0mA the device shows the same general form of oxide current increase. Beyond 5.0 mA there is a tendency for the oxide current to increase much less rapidly with junction current. This feature was also found in other devices but the point of fall off in the rate of oxide current increase did not necessarily occur at the same junction current nor at the same oxide current level. The greatest oxide bias voltage that could be applied to the device of Fig. 5.11 was 6.0 V. Biasing at 7.0 V caused instabilities to occur in the oxide current and eventually resulted in breakdown of the oxide film. These oxide current instabilities and film ruptures were a general problem when trying to apply high fields and passing oxide currents of greater than 10^{-10}A.

A common feature found in the devices studied was a discontinuity in the rate of increase in the oxide current with junction current. This can be seen in Fig. 5.12 where there is the same form of exponential rise in oxide current but with a discontinuity at I_j = 0.3 mA. A similar feature is shown in Fig. 5.13 and Fig. 5.14 for devices A_1 and A_3 from batch I43. In these examples the discontinuity appeared to coincide with a negative resistance region in the reverse breakdown characteristic of the device. Fig. 5.15 shows the reverse breakdown characteristic for the device A_3.

It has been shown that by avalanching an underlying junction that current injection into the oxide films can be obtained for fields across the oxide of about one third the value required when passing zero junction current. However once avalanche breakdown has been initiated the value of the junction current does not appear to have a strong influence on the rate of increase of oxide current with applied oxide field. Fig. 5.16 shows the oxide current as a function of the field across the oxide for two values of the junction current. It is apparent there is little difference in the field dependence at the two junction currents. This can be taken as an indication that neither the interface energy barrier structure nor the energy population of the charge carriers at the interface is a strong function of the avalanche junction current. This will be discussed further in Chapter 6.

5.4 Measurement of Injection Currents with Infra-Red Illumination of the Junction

In the measurements described so far, current was injected into the oxide at fields of less than 3×10^6 V/cm when the underlying p-n junction was avalanched. It was found that oxide currents could also be

obtained with the junction reverse biased below avalanche potential, if the junction current was enhanced by using an infra-red emitter placed below the junction. Fig. 5.17 shows a typical plot of the injected oxide current against the reverse photo-induced junction current. The junction was reversed biased at 80 V at which bias the reverse leakage current, measured in the dark, was less than 1.0 μA. A bias of 10.0V was applied across the thin oxide and the junction current was controlled by varying the intensity of the infra-red illumination. The oxide currents measured in this way were very stable and it was not necessary to apply the initial stabilizing avalanche required previously. The oxide currents were observed to decay over a period of hours in a manner similar to the high field injection. It is not thought that infra-red emission could itself induce an oxide current since it was noted in Chapter 2 that the electron traps in thermal oxide could only be emptied by the simultaneous application of U.V. radiation and a high field.

The infra-red irradiation of the junction was also found to have an effect on the magnitude of the oxide current obtained at a certain junction current. As expected, when the junction was irradiated, a lower junction bias was required to maintain a constant junction current. However, it was also observed that there was a significant increase in the oxide current for the same junction current as shown in Fig. 5.18. This result was unexpected from current theories of electron injection into silicon dioxide and it will be discussed more fully in Chapter 6.

5.5 Conclusions

The results presented in this chapter demonstrate that the current through a thin silicon dioxide film can be substantially increased by the current in a reverse biased p-n junction beneath the oxide film. This oxide current is shown to be dependent on the junction current, the field applied across the oxide and the junction illumination. It only occurs with a positive potential applied to the surface of the thin oxide film. These results are consistent with electron injection from the avalanching junction.

The decay of oxide current in devices passing a constant avalanche junction current and with a constant bias across the oxide film, probably indicates the presence of electron traps in the oxide. These traps have been observed by other workers as discussed in Chapter 2.6. The oxide current instabilities in devices avalanched for the first time have also been observed elsewhere eg. by Pepper [71]. They are probably the result of creating interface states between the oxide and the silicon or possibly trapping centres around the microplasma region. This will be discussed further in Chapter 6.

Visual observation of the devices under avalanche conditions indicated the presence of microplasmas within the shallow junction. Some of these microplasmas lay beneath the aluminium contact to the thin oxide. It is in such devices that oxide currents have been detected. Microplasmas also appeared at the intersection of the guard ring and the shallow junction. These edge microplasmas were observed to turn on before those within the shallow junction and before any oxide current could be detected. It is therefore reasonable to assume that the injected oxide current is a function of the current carried by the microplasma beneath the oxide contact, and that the junction current is the sum of the currents carried by several microplasmas, plus any leakage currents.

In Chapter 6 an attempt will be made to interpret the dependence of the oxide current on junction current in terms of a model involving electron injection from a microplasma. In addition, the field dependence of the injected oxide current will be discussed in terms of electron transport across or tunnelling through an interfacial barrier between the silicon and the oxide.

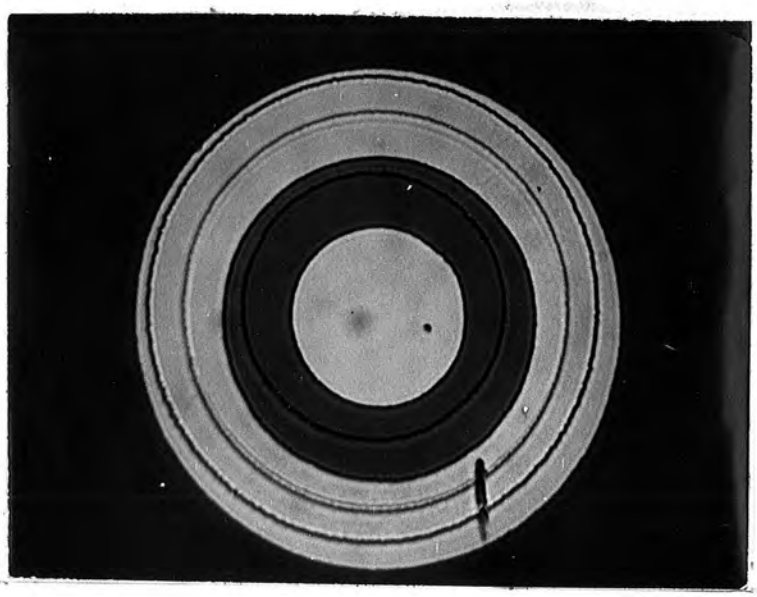

FIG 5·1 COMPLETED DEVICE FOR ELECTRON INJECTION INTO A THIN SiO_2 FILM

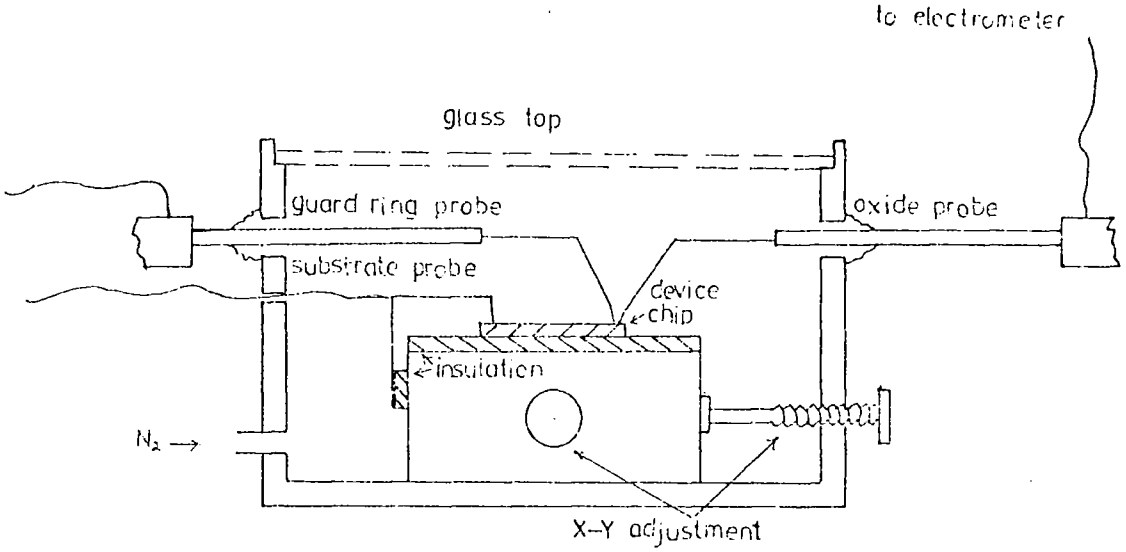

FIG 5.2 SCHEMATIC DIAGRAM OF PROBING ARRANGEMENT

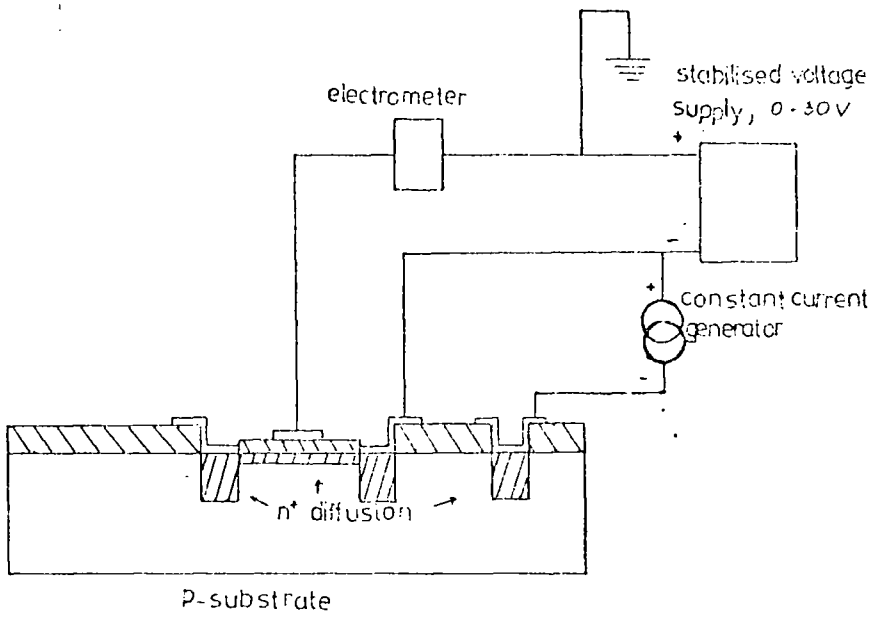

FIG 5.3 ELECTRICAL MEASUREMENT CIRCUIT

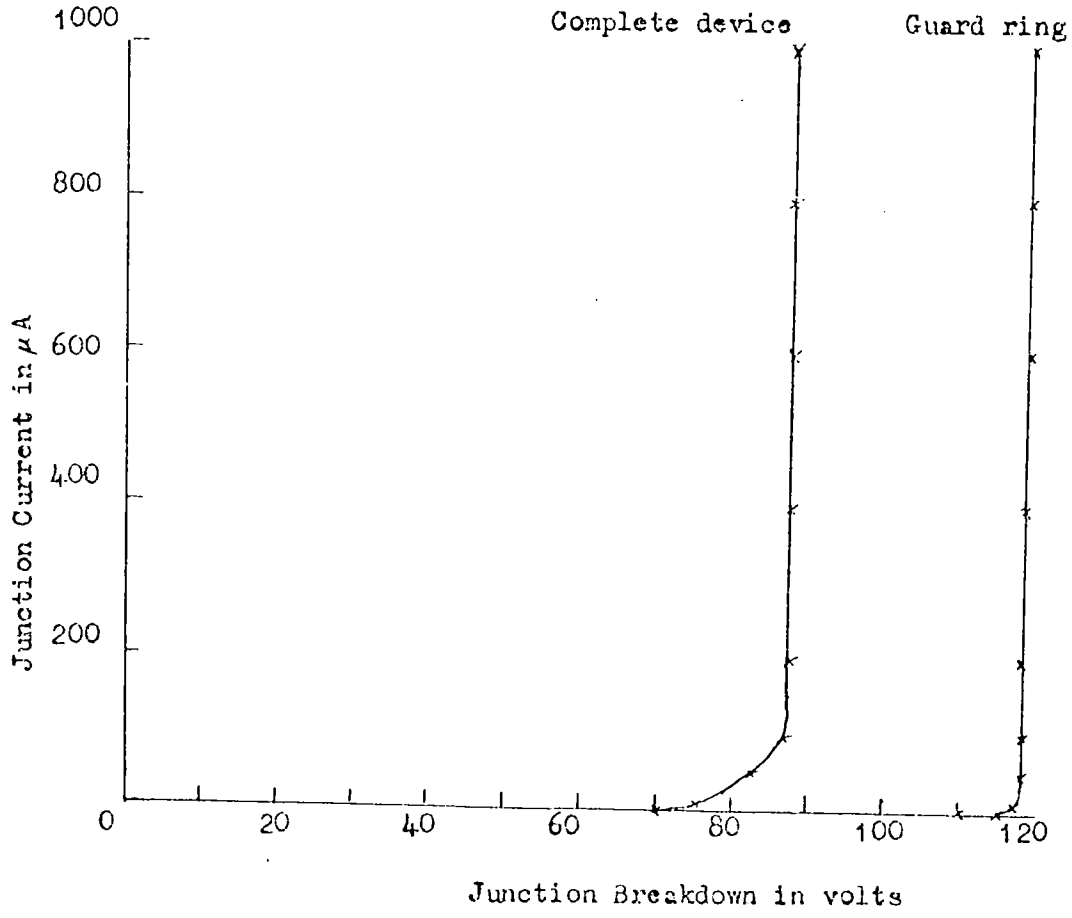

FIG 5.4 JUNCTION BREAKDOWN CHARACTERISTICS OF A COMPLETE DEVICE AND THAT OF THE GUARD RING ALONE.

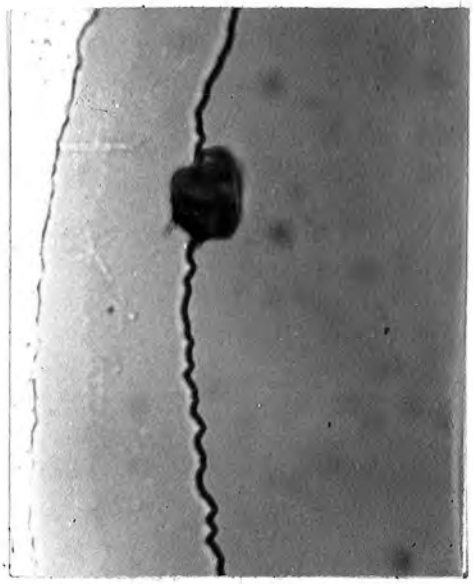

(a) MICROPLASMA AT INTERSECTION OF GUARD RING AND SHALLOW JUNCTIONS

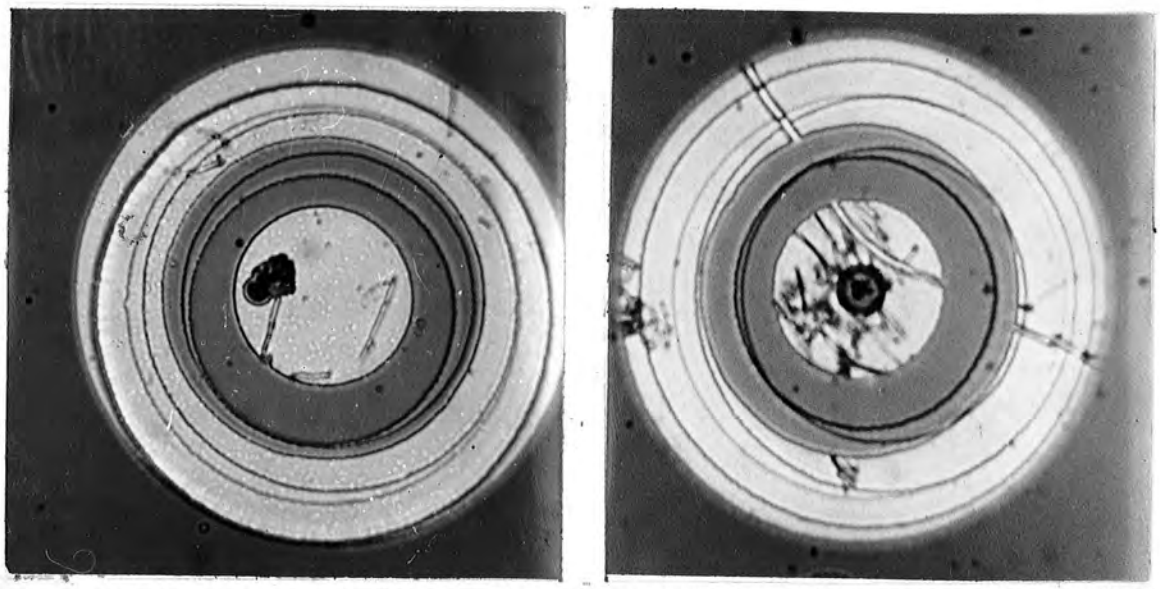

(b) MICROPLASMA IN THE SHALLOW JUNCTION BENEATH THE CENTRAL ALUMINIUM CONTACT

FIG 5.5 DAMAGE CAUSED IN THE REGION OF A MICROPLASMA WHEN THE JUNCTION IS OVERBIASED

FIG 5.6 HIGH FIELD INJECTION INTO OXIDE WITH ZERO JUNCTION CURRENT

(Positive polarity. Oxide thickness 540 Å)

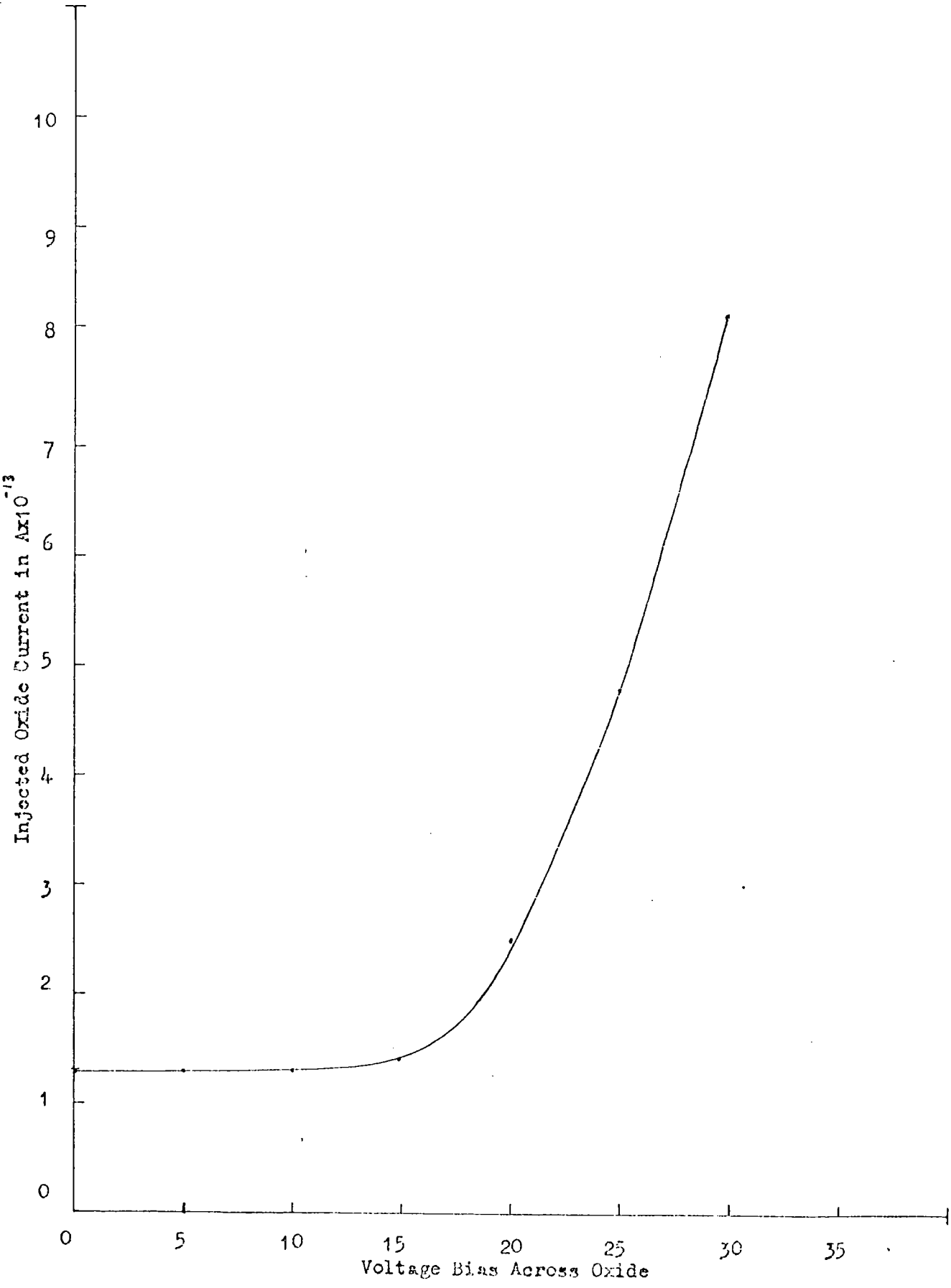

FIG 5.7 INJECTED OXIDE CURRENT FROM JUNCTION STRUCTURES WITH HIGH REVERSE LEAKAGE CURRENTS

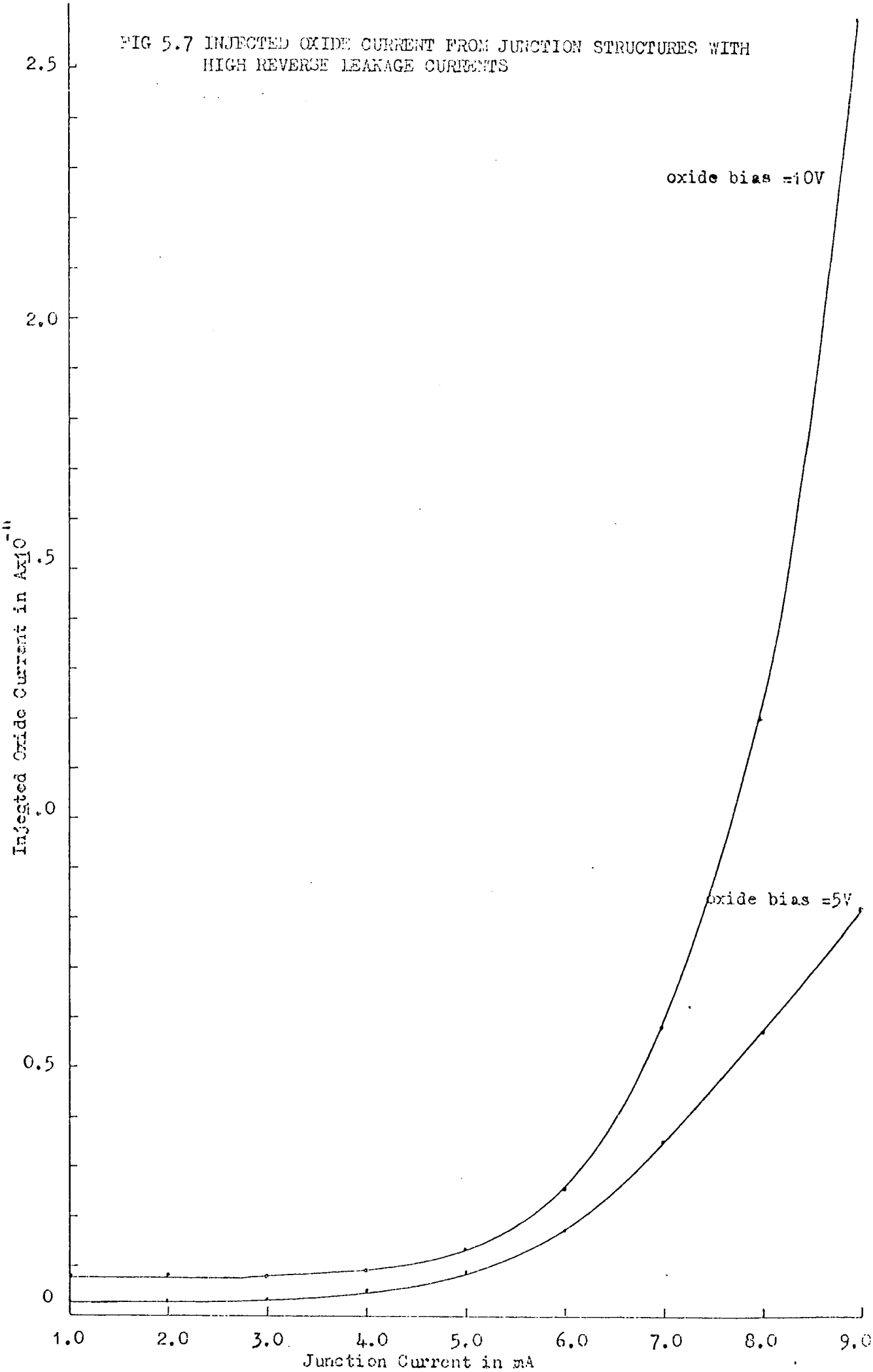

FIG 5.8 INJECTION CHARACTERISTICS OF THREE DEVICES WITH HIGH LEAKAGE CURRENTS SHOWING THAT INJECTION ONLY OCCURS WHEN THE JUNCTION IS AVALANCHED.

(Oxide bias = 10V in each case)

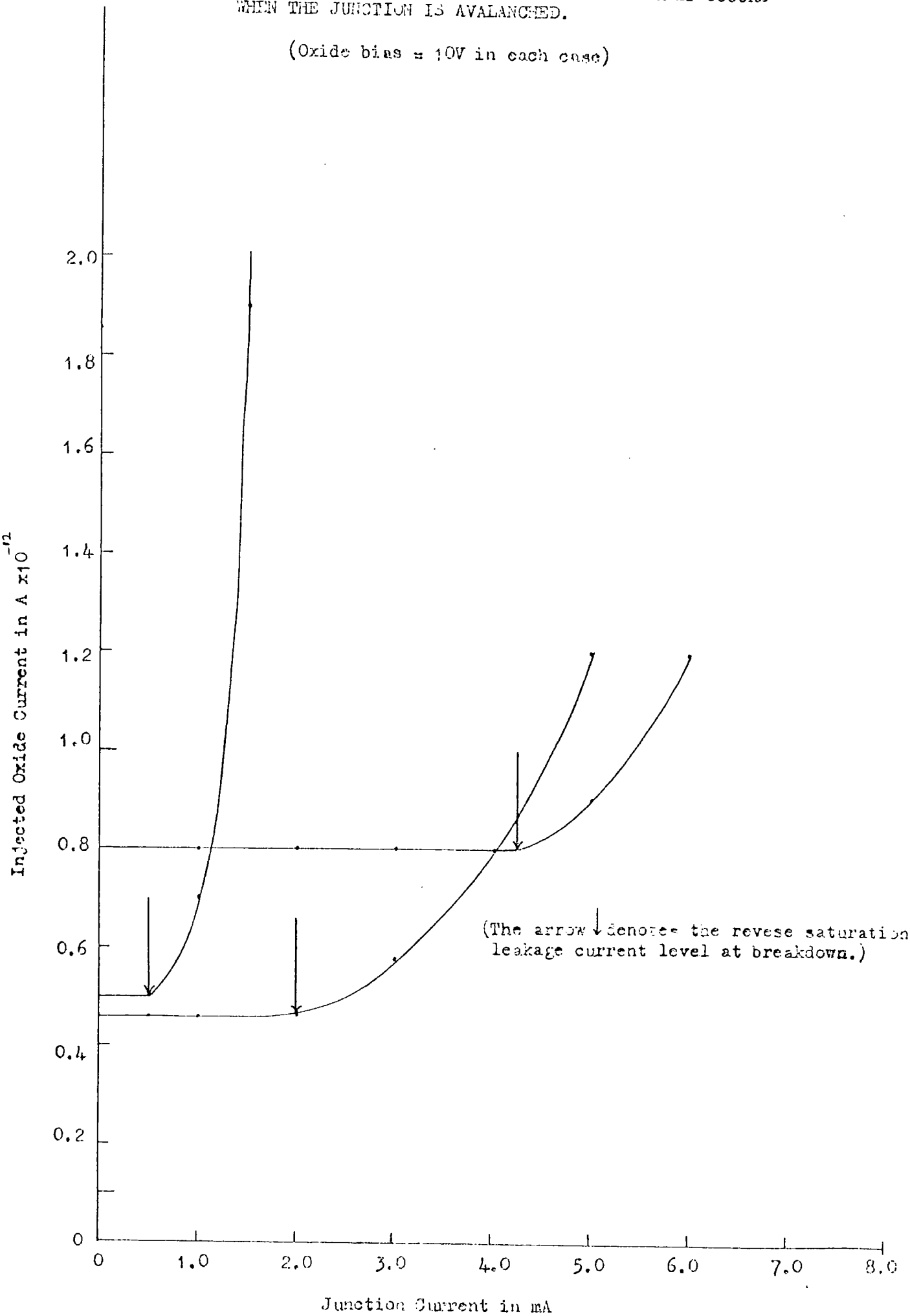

FIG 5.9 DECAY OF OXIDE CURRENT FOR A DEVICE AVALANCHED FOR THE FIRST TIME

(Bias across oxide = 5V. Junction current = 0.1 mA.)

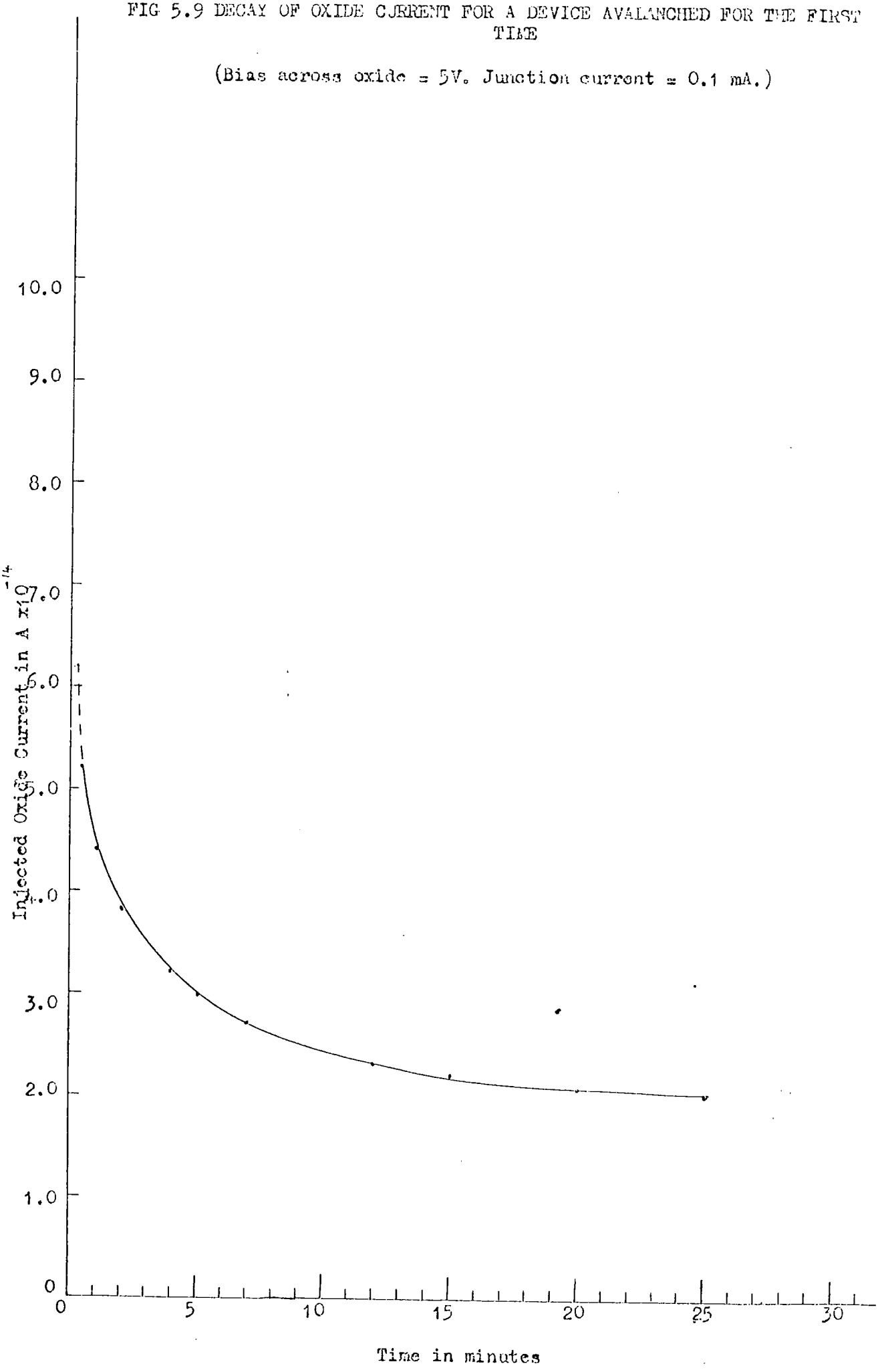

FIG 5.10 INJECTED OXIDE CURRENT AS A FUNCTION OF JUNCTION CURRENT AND OXIDE BIAS

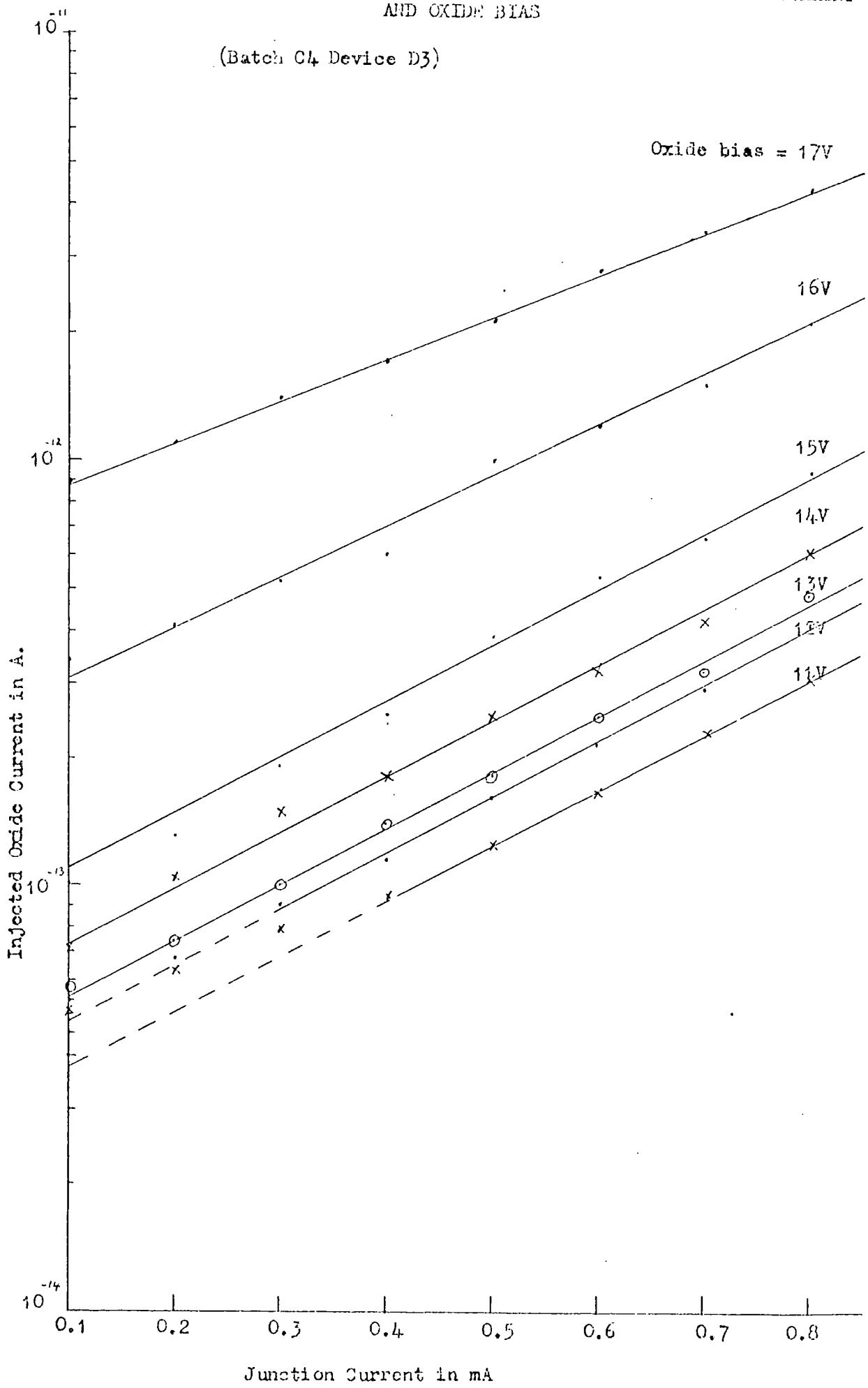

FIG 5.11 INJECTED OXIDE CURRENT FOR HIGH JUNCTION CURRENTS.

(Batch L4 Device C2.)

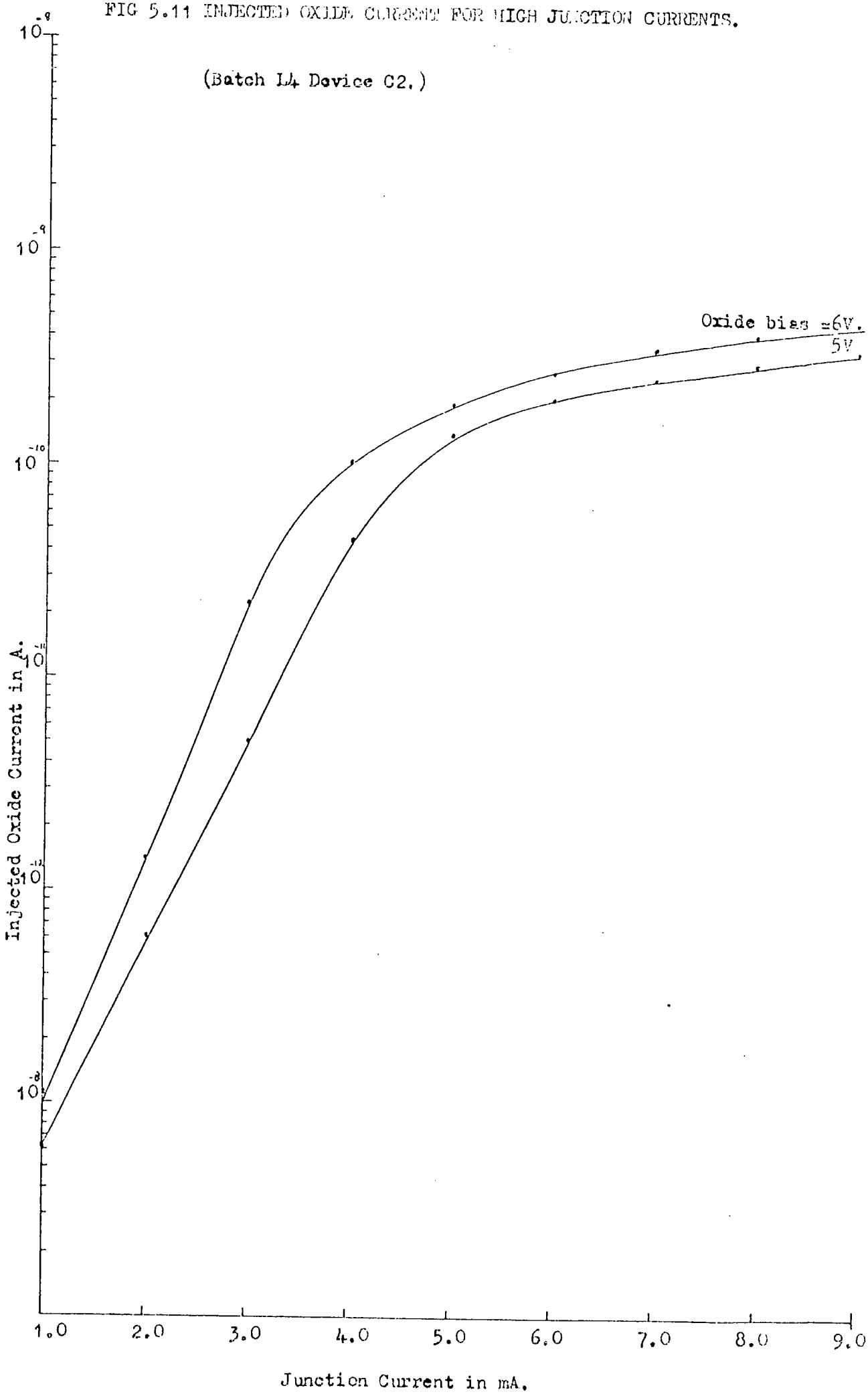

FIG 5.12 INJECTED OXIDE CURRENT AS A FUNCTION OF JUNCTION CURRENT AND OXIDE BIAS SHOWING DISCONTINUITY IN SLOPE

(Batch C4 Device D3.)

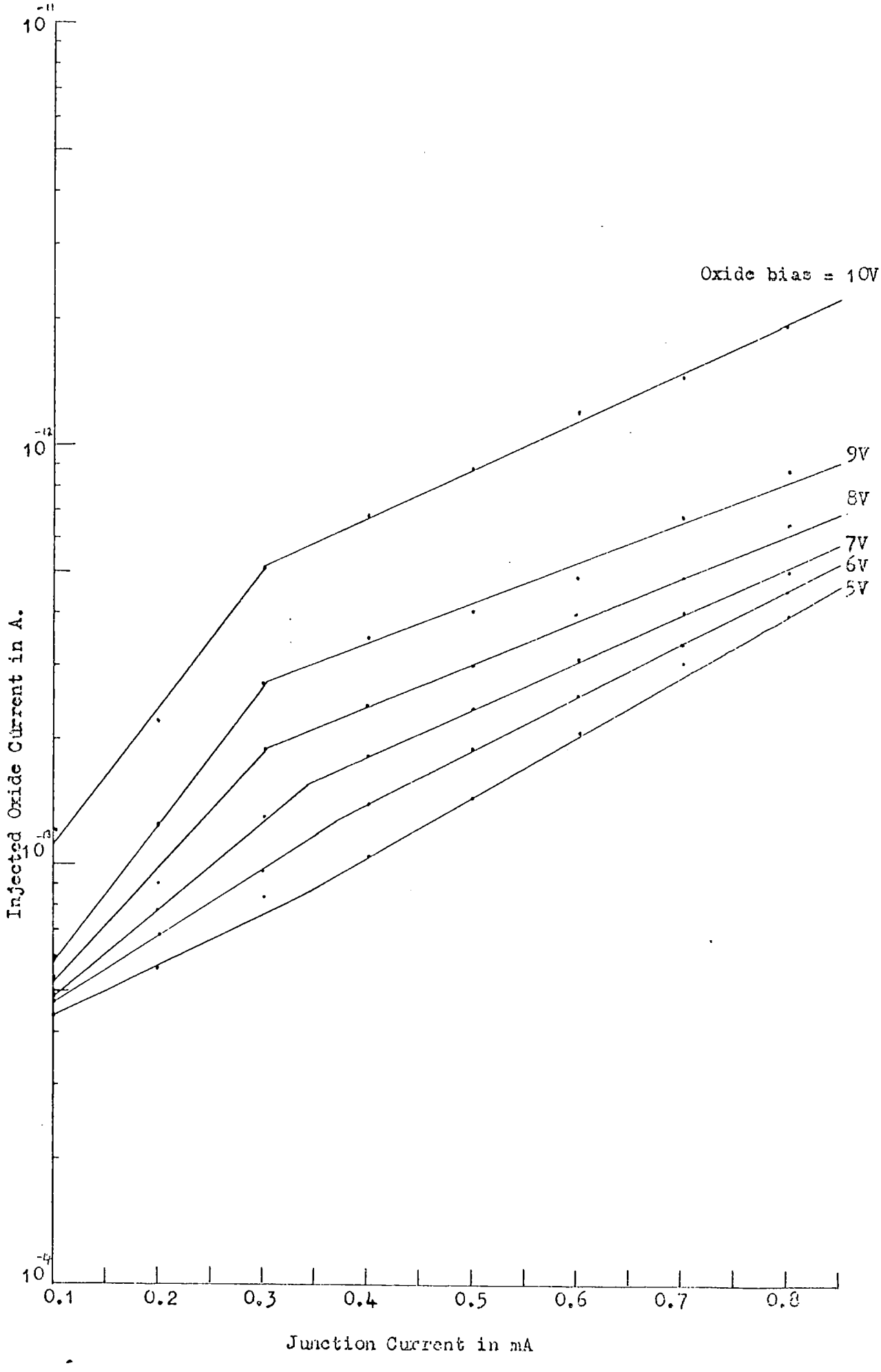

FIG 5.13 INJECTED OXIDE CURRENT AS A FUNCTION OF JUNCTION CURRENT AND OXIDE BIAS SHOWING DISCONTINUITY IN SLOPE.

(Batch I4-3 Device A1.)

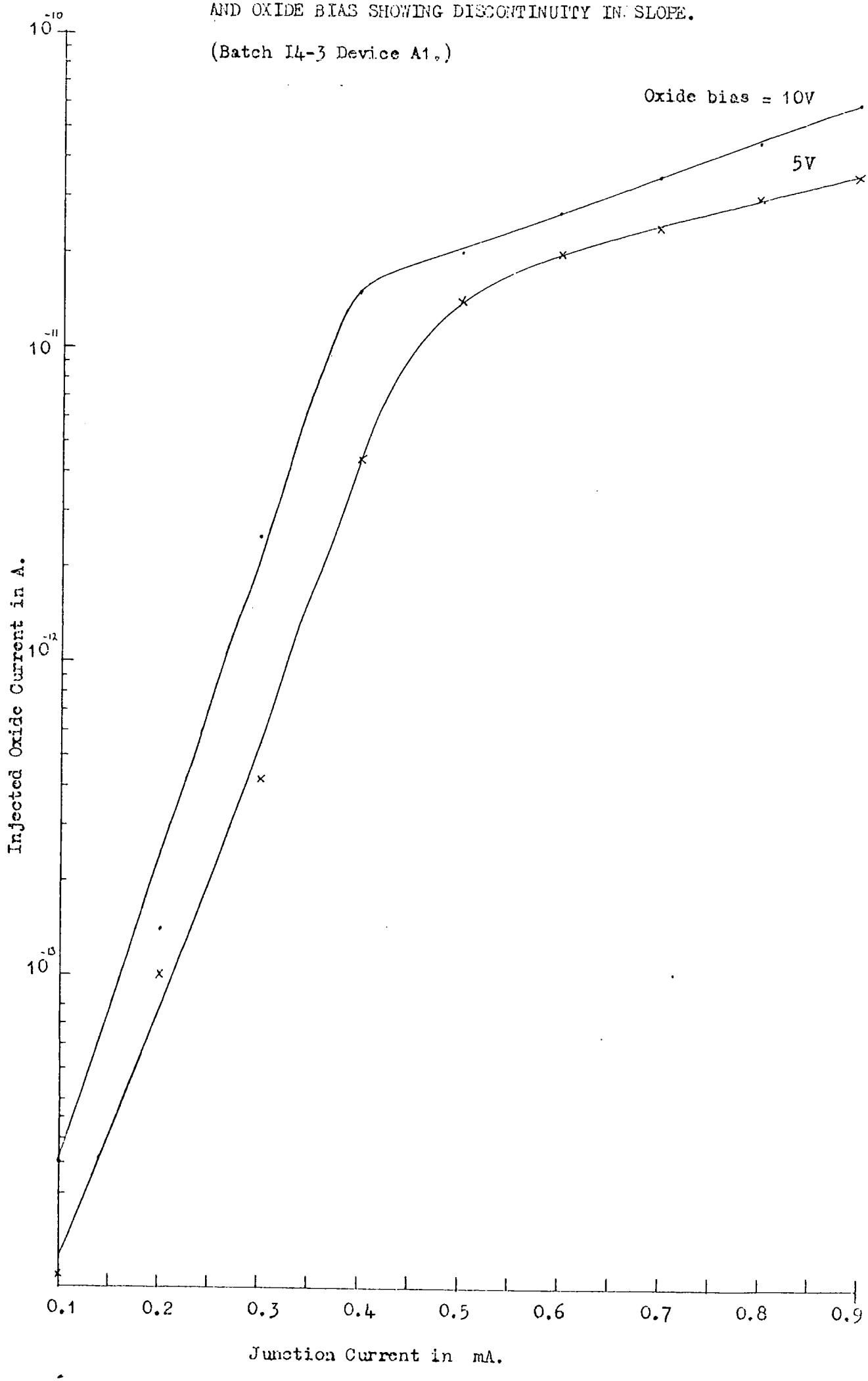

FIG 5.14 INJECTED OXIDE CURRENT AS A FUNCTION OF JUNCTION CURRENT AND OXIDE BIAS SHOWING DISCONTINUITY IN SLOPE.

(Batch I4-3 Device A3.)

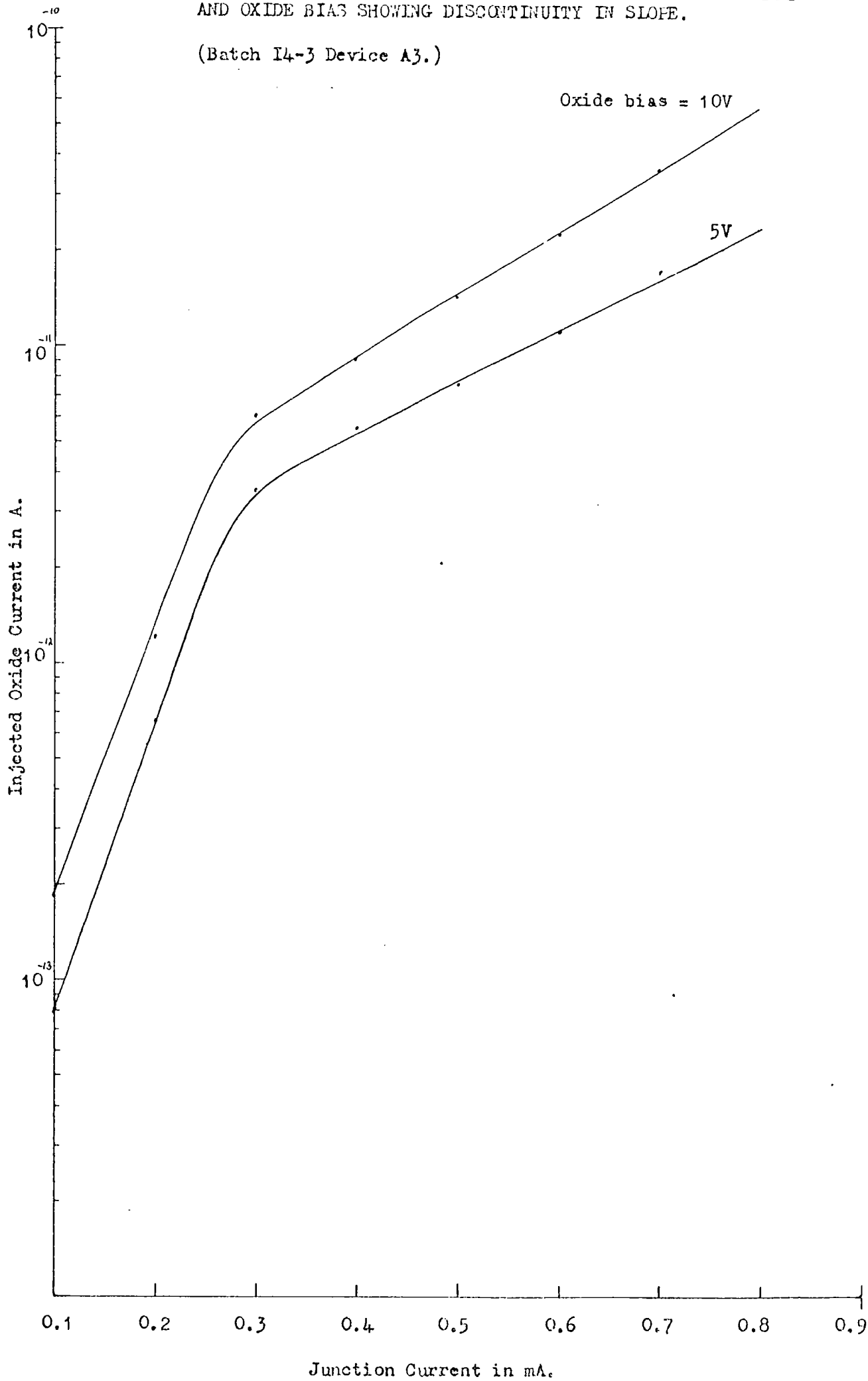

FIG 5.15 REVERSE BREAKDOWN CHARACTERISTIC OF JUNCTION OF DEVICE A3 FROM BATCH I4-3.

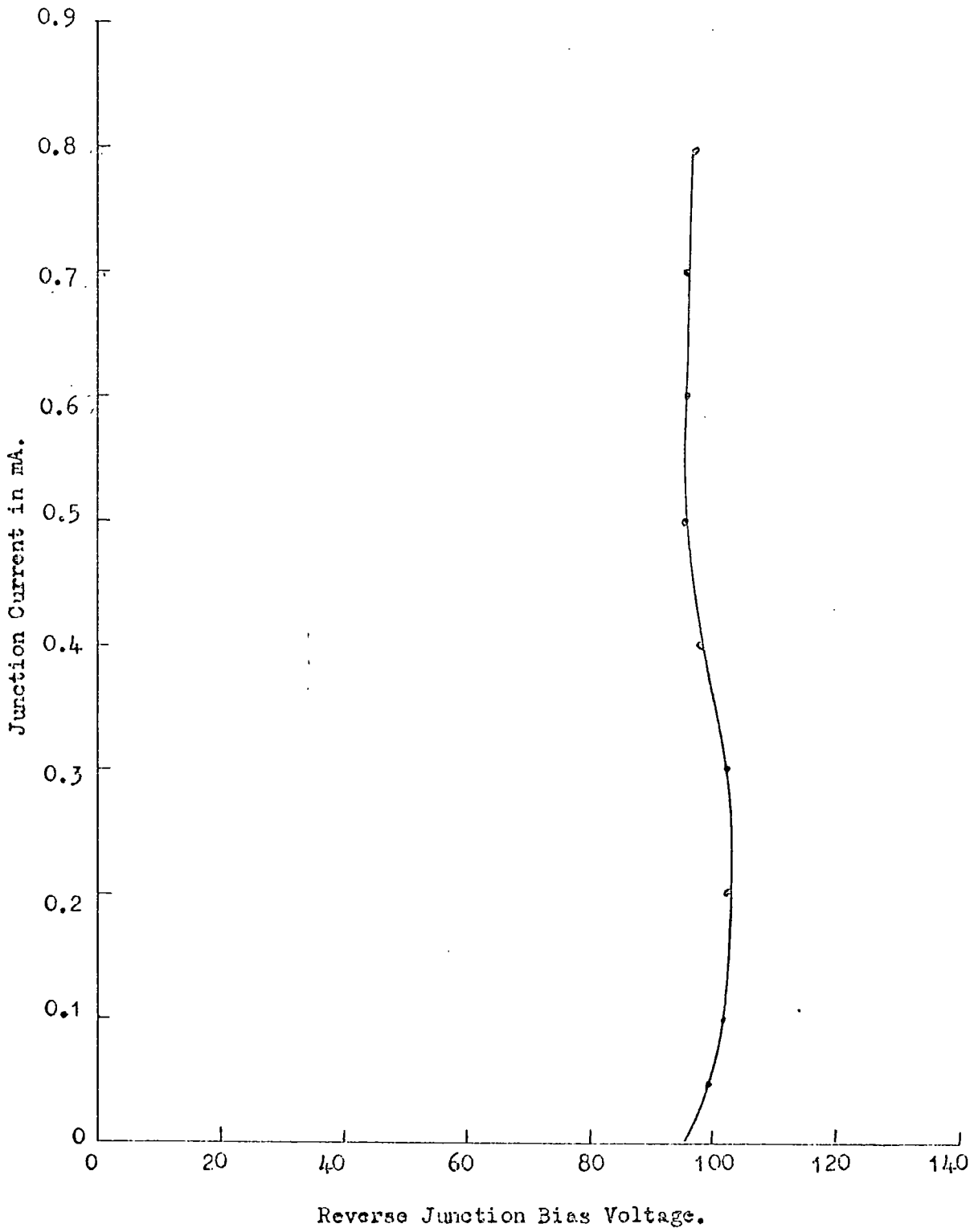

FIG 5.16 INJECTED OXIDE CURRENT AS A FUNCTION OF OXIDE BIAS VOLTAGE.

(Batch C4 Device D3.)

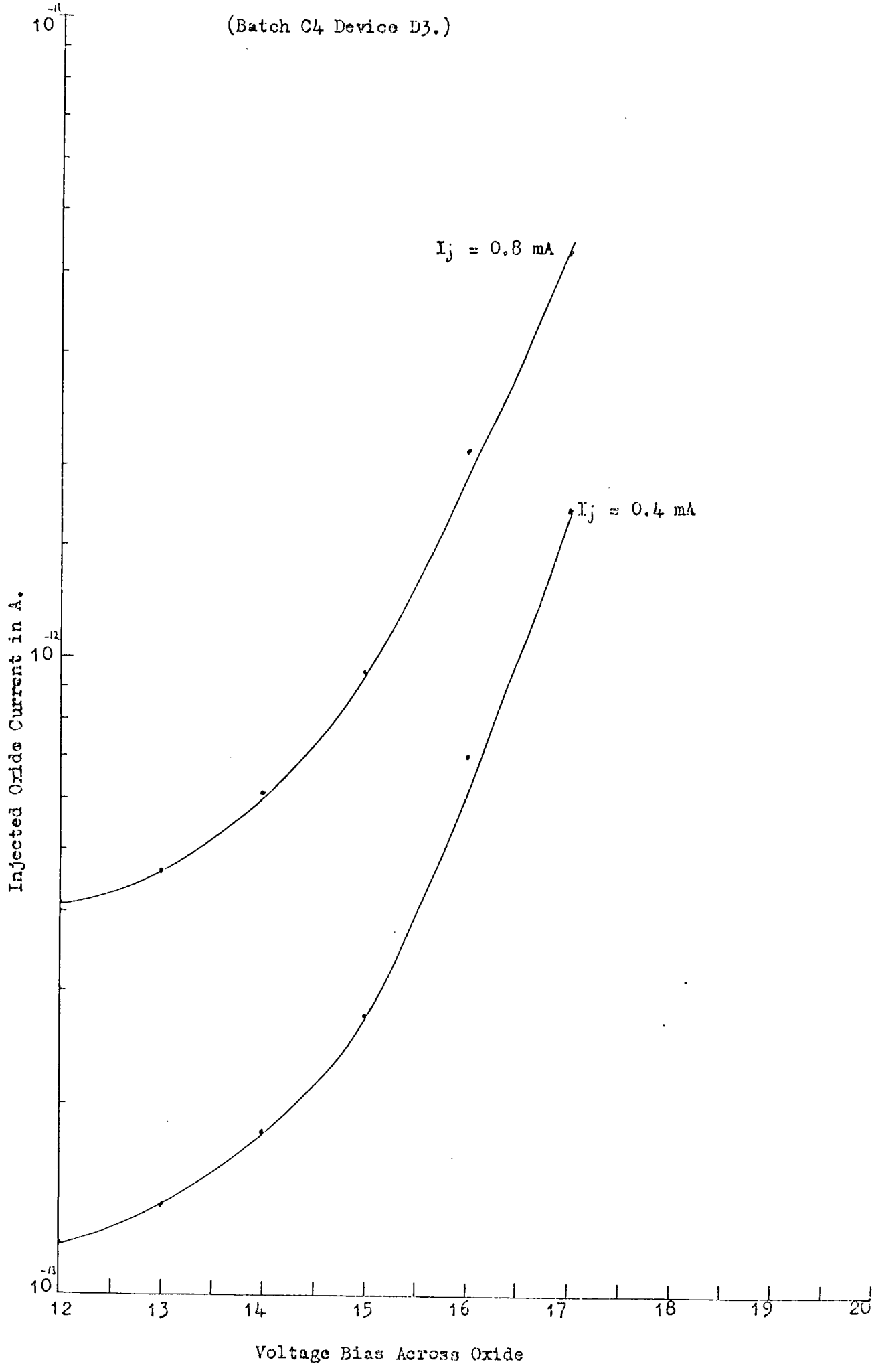

FIG 5.17 INJECTED OXIDE CURRENT AS A FUNCTION OF PHOTO EXCITED JUNCTION CURRENT.

(Junction biased below avalanche voltage @ 80V.)

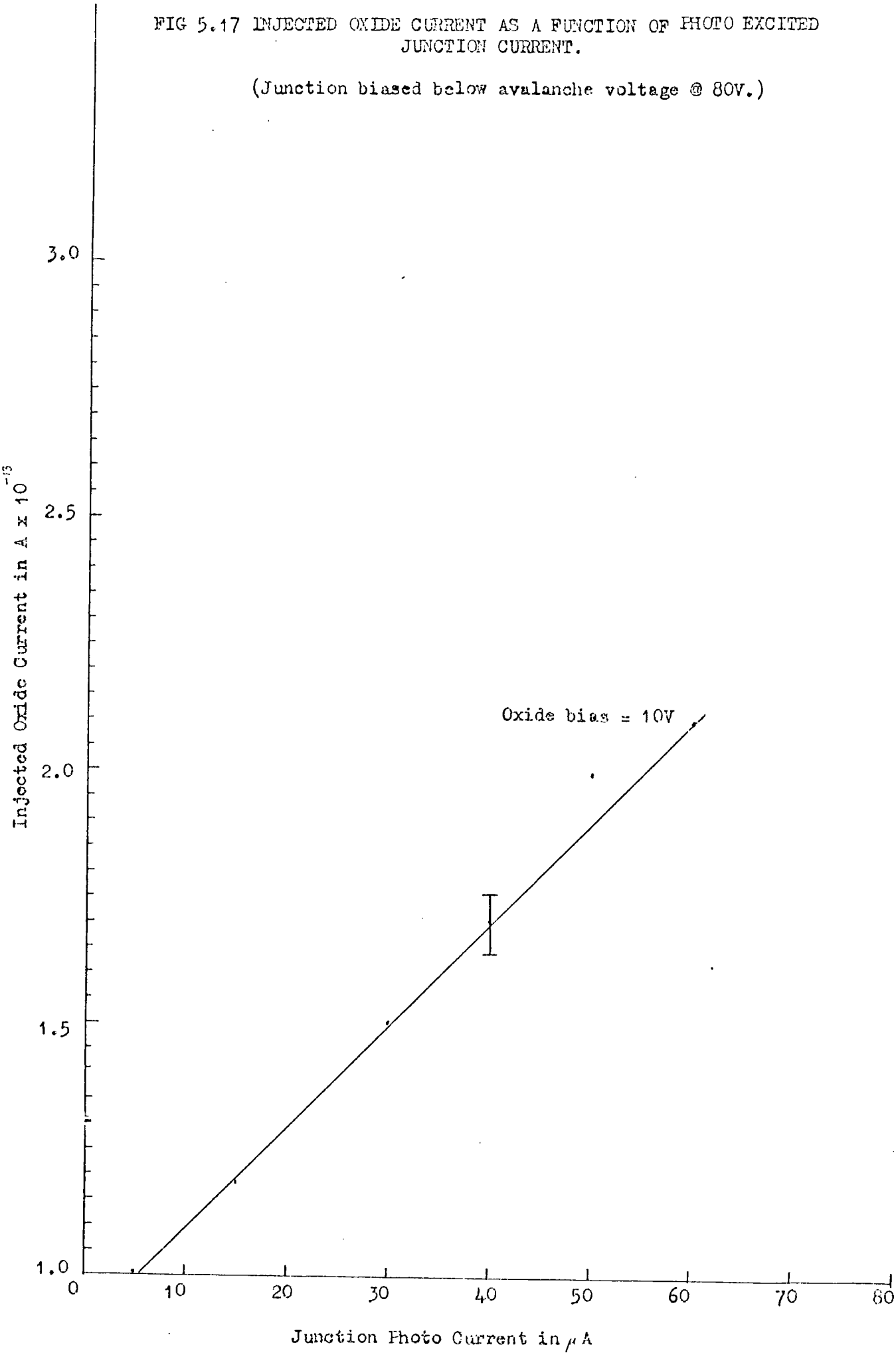

FIG 5.18 EFFECT OF INFRA-RED IRRADIATION OF JUNCTION ON INJECTED CURRENT.

(Batch E4 Device D3.)

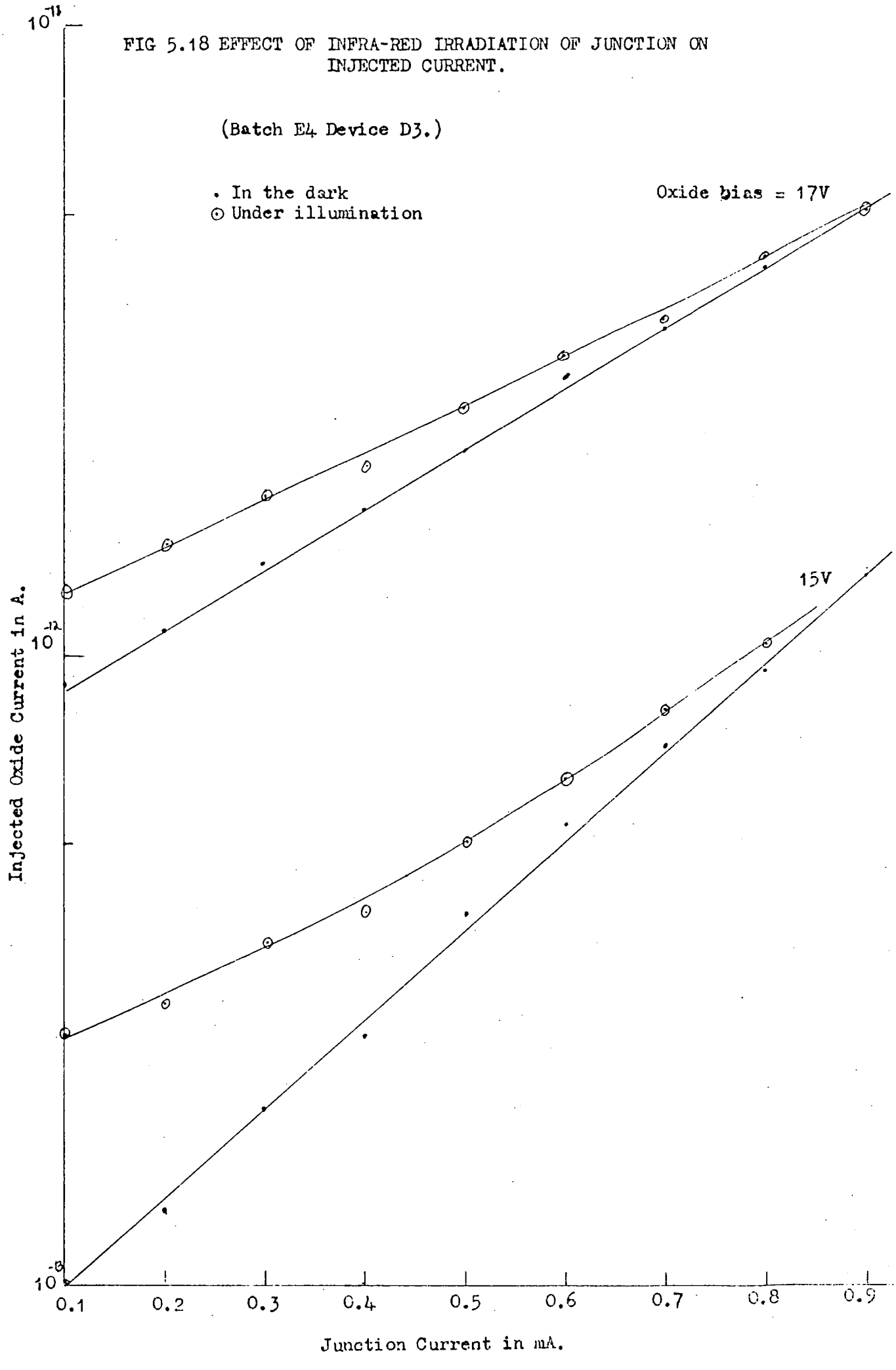

CHAPTER SIX

DISCUSSION OF THE RESULTS ON ELECTRON INJECTION INTO SILICON DIOXIDE

6.1 Introduction

The experiments described in Chapter 5 showed that an appreciable direct current could be maintained through a thin film of SiO_2 formed above a suitable junction structure. This current was shown to be a function of the field applied across the oxide and of the reverse current in the underlying p-n junction. This chapter will examine these dependences, and attempt a physical interpretation in terms of field assisted injection of high energy electrons, from a localised microplasma within the shallow junction.

It was observed that a current could only be detected through the oxide when it was positively biased with respect to the silicon junction. No current ($< 10^{-14}$A) was detected when the bias was reversed. The oxide current was found to be a function of the junction avalanche current so that it must have originated from the junction/oxide interface. This could be interpreted in terms of either electron injection from the silicon or the release of negative ions at the interface. In M.O.S. structures, mobile negative ions are usually associated with hydroxyl ions.[88] However, these ions are generally mobile at room temperature under the action of high fields, so that with the fields ($> 10^6$V/cm used in this work such ionic currents would have been observed even without passing a junction current. Further the high current densities measured in this work are probably greater than those observed for any ion conductivity in SiO_2. It is therefore concluded that the charge conduction through the oxide results from electron injection from the reverse biased p-n junction.

Section 6.2 will show that the increase of the injected current with the field strength in the oxide can be interpreted in terms of the energy distribution of the electrons in the avalanching junction. In Sections 6.3 - 6.5 the apparently exponential increase of injected current with junction current will be explained in terms of the characteristics of the microplasmas which are probably the origin of the injected electrons. Some other observations will be discussed in Section 6.6.

6.2 The Dependence of the Injected Current on the Oxide Field Strength

Examples of high field injection of electrons from silicon into SiO_2 have been given Section 2.6. The field dependence of the oxide current was interpreted there in terms of Fowler-Nordheim tunnelling of thermal electrons from the silicon into the conduction band of the SiO_2. At room

temperature the electron energy was considered to be too low to allow Schottky emission over the 3.25 eV barrier into the oxide. In the present work an avalanching p-n junction is used to create an electron population with an effective temperature much greater than that of the silicon lattice which will be assumed to remain at room temperature. For the majority of the experiments in this work the junction power dissipation is only between 10 and 100 mW. Although a significant proportion of the power is localised in areas of microplasma breakdown it will be assumed that the increase in lattice temperature is insignificant compared with the effective electron temperature.

It was concluded in Chapter 2 that the electron energy distribution in an avalanching junction is probably not well represented by a simple Maxwellian. It is probable that a better distribution function would be one which is Maxwellian below an ionisation threshold energy but which has a rapidly diminishing high energy tail. The tail would result from the greatly increased probability of electrons with energy above threshold making ionising collisions. It is likely that it is these high energy electrons in the tail of the distribution which have been measured by Bartelink[20] and Bok[45] who found them to decrease exponentially with energy. To date there is no complete mathematical representation of the true energy distribution of the electron population in an avalanching junction and it is common to assume it to be Maxwellian - see Chapter 2. In this chapter a comparison will be made between the experimental results from Chapter 5 and those expected from a theoretical consideration of electron injection from a Maxwellian distribution of effective temperature, T_e. It will then be shown that a better fit could be obtained by assuming a truncated Maxwellian distribution of the type described above.

Consider the energy band model of Fig. 6.1, describing the injection structure. A voltage V(x) is applied between the silicon and the surface of the oxide film creating a field $F(x) = V(x)/s$ across the oxide. The silicon surface is heavily doped n-type ($Nd \triangleq 10^{20}/cm^3$) and to a first approximation it can be treated as being degenerate so that field penetration into silicon can be ignored. It is assumed that a Maxwellian distribution of high energy electrons created in the avalanching p-n junction has diffused towards the surface in the manner described by Bartelink[20]. This means that the electron distribution impinging on the Si/SiO_2 interface is also Maxwellian but reduced in magnitude by a factor proportional to $\exp(-L/L_o)$ as given in Section 2.2. If the effective electron temperature is great enough then a proportion of the incident electrons will have sufficient energy to overcome

the interfacial barrier and will be injected into the oxide conduction band. As the field is increased, the barrier height will be reduced according to the classical image force lowering law. This[15] analogous to the Schottky effect and will result in an increase in the injected oxide current according to the relationship,

$$\log_e J(x) \propto \sqrt{F(x)} \qquad ((6.1))$$

It would be expected that, under these conditions, a measurable oxide current would be observed at lower field strengths than would be required by Fowler-Nordheim tunnelling. As the field is further increased, the probability of electrons tunnelling into the conduction band of the oxide becomes significant. The increase in the current with field ceases to be a simple function of image force lowering and will become dominated, at very high fields, by tunnelling effects. In the intermediate field ranges the total oxide current will be a combined function of the two injection mechanisms. Expressions for the two contributions will now be derived.

Consider a small volume dp in momentum space such that,

$$dp^2 = dp_x^2 + dp_y^2 + dp_z^2 \qquad ((6.2))$$

According to Maxwell-Boltzmann statistics the fraction of the electrons in the silicon which have momenta in such a volume is given by,

$$\frac{dN}{N} = \frac{\exp(-p^2/2mkT_e)\, dp_x dp_y dp_z}{\iiint_{-\infty}^{+\infty} \exp(-p^2/2mkT_e)\, dp_x dp_y dp_z} \qquad ((6.3))$$

where N is the total number of electrons per unit volume.

Let $\frac{dN(x)}{N}$ be the fraction of the electrons moving in the direction of the applied field.

Then $$\frac{dN(x)}{N} = (2\pi mkT_e)^{-\frac{1}{2}} \exp(-p(x)^2/2mkT_e)\, dp(x) \qquad ((6.4))$$

Now $$\frac{p(x)^2}{2m} = E(x)$$

therefore $$dp(x) = \frac{m}{p(x)} dE(x) = \frac{dE(x)}{v(x)} \qquad ((6.5))$$

substituting ((6.4)) in ((6.3)) gives,

$$\frac{dN(x)}{N} \cdot v(x) = \left(\frac{1}{2\pi mkT_e}\right)^{\frac{1}{2}} \exp(-E(x)/kT_e)\, dE(x) \qquad ((6.6))$$

Let $$N(x)\, v(x) = n(x)\, E(x) \qquad ((6.7))$$

where $n(x)\, E(x)\, dE(x)$ is the total number of electrons striking unit area of the interface in unit time and having energy in the range $E(x)$, $E(x) + dE(x)$.

$v(x)$: electron velocity in x direction

The number of electrons within a given energy range injected into the oxide will be the product of the number of electrons striking the interface in unit time, and the probability of transmission over or through the interface potential barrier.

Thus the injected current density is given by,

$$J(x) = q\int_0^{\infty} n(x)\, E(x)\, D(E(x))\, dE(x) \qquad ((6.8))$$

where $D(E(x))$ is the transmission probability coefficient.

In a low field situation, and ignoring traps, only those electrons with energies greater than the barrier height ϕ can be injected into the oxide. This is the classical situation in which,

$$D(E(x)) = 0 \text{ for } E(x) < \phi$$

$$D(E(x)) = 1 \text{ for } E(x) \geq \phi$$

Hence $$J(x) = q\int_{\phi}^{\infty} n(x)\, (E(x))\, dE(x) \qquad ((6.9))$$

According to the image force lowering theory the barrier height ϕ, will be lowered with increasing applied oxide field strength according to the relationship,

$$\Delta\phi(F(x)) = (q^3 F(x)/4\pi\, \varepsilon_o\, \varepsilon_{ox})^{\frac{1}{2}} \qquad ((6.10))$$

where $\Delta\phi(F(x)$ is the barrier lowering for an applied field $F(x)$

ε_{ox} is the relative dielectric constant of SiO_2.

Therefore substituting ((6.6)) into ((6.9)), integrating and taking into account image force lowering gives,

$$J(x) = qN\left(\frac{kT_e}{2\pi m}\right)^{\frac{1}{2}} \exp\left(-\left(\phi - (q^3 F(x)/4\pi\, \varepsilon_o\, \varepsilon_{ox})^{\frac{1}{2}}\right)/kT_e\right) \qquad ((6.11))$$

It should be noted that the condition,

$$D(E(x)) = 1 \text{ for } E(x) \geq \phi$$

is the situation where the classical turning point, as determined by the image force effect, is closer to the interface than the mean free path for electron scattering in the oxide. If a scattering event occurs before the classical turning point is reached there is a probability that electrons will be reflected and $D(E(x)) \neq 1$. Bergulund and Powell[52] have considered this situation and conclude that the effect is negligible for fields greater than 10^6V/cm. The present work is concerned with fields greater than 2×10^6V/cm.

Equation ((6.11)) predicts that if $\log_e J(x)$ is plotted against $\sqrt{F(x)}$ a straight line plot of slope, s_1,

$$s_1 = (q^3/4\pi\, \varepsilon_o\, \varepsilon_{ox})^{\frac{1}{2}}/kT_e \qquad ((6.12))$$

will be obtained. Such a plot is shown in Fig. 6.2 for a typical junction avalanche current of 400 μA. It is apparent that only the first few

$$\frac{2}{3}\left(\frac{8m^{*}\pi^{2}}{h^{2}}\right)^{\frac{1}{2}} \cdot \left(\frac{\phi - E(x)}{F(x)}\right)^{3/2} \gg 1$$

then $$D(E(x)) \simeq \frac{4E(x)^{\frac{1}{2}}(\phi - E(x))^{\frac{1}{2}}}{\phi} \exp\left(\frac{-4K_o}{3F(x)}(\phi - E(x))^{3/2}\right) \qquad ((6.15))$$

where D(E(x)) is the transmission coefficient for an electron with energy E (x) through a triangular potential barrier.

and $$K_o = \left(\frac{8m^{*}\pi^{2}}{h^{2}}\right)^{\frac{1}{2}}$$

substituting ((6. 15)) into ((6. 8)) and assuming a Maxwellian distribution of electrons.

$$J(x) = \frac{q4N}{(2\pi m^{*}kT_e)^{\frac{1}{2}}} \int_0^{\infty} E(x)^{\frac{1}{2}} \frac{(\phi - E(x))^{\frac{1}{2}}}{\phi} \exp\left(-\frac{4K_o}{3F(x)}(\phi - E(x))^{3/2} \frac{-E(x)}{kT_e}\right) dE(x). \qquad ((6.16))$$

There is no general solution to Equation ((6. 16)) but Stratton[90] has given a solution for the condition

$$\frac{2K_o\phi^{\frac{1}{2}}}{F(x)} \ll \frac{1}{kT_e}$$

when $$J(x) \simeq \frac{2qNkT_e}{(\pi m^{*}\phi)^{\frac{1}{2}}} \exp\left(\frac{-4K_o\phi^{3/2}}{3F(x)}\right) \qquad ((6.17))$$

Before applying Equation ((6. 17)) it is necessary to examine the inequality used by Stratton. This may be re-written as,

$$F(x) \gg 2\left(\frac{8m^{*}\pi^{2}}{h^{2}}\right)^{\frac{1}{2}} \phi^{\frac{1}{2}} kT_e \qquad ((6.18))$$

This expression requires that for increasing energy the number of electrons with energy E (x) must decrease more sharply than the transmission probability, D (E(x)) increases, i.e. Tunnelling transmission is dominant.

If it is assumed that,

ϕ = 3.25 eV Ref. (52)

m^{*} = 0.42 mo, as the effective mass of an electron in the forbidden gap of SiO_2, Ref. (56).

kT_e = 0.12 eV

Then the inequality ((6. 18)) requires that

$$F(x) \gg 1.4 \times 10^{7} \text{ V/cm}$$

The highest field applied in this work was about 4×10^{6} V/cm so that the solution ((6. 17)) cannot be used. This means that in the region of interest in this work the oxide current is a combination of thermionic and field tunnelling transmission. A complete analytical solution for this region has not yet been obtained and a numerical approach has to be taken.

Fig. 6.3 shows the result of plotting the experimentally obtained values of $\log_e I_{ox}$ against $1/F(x)$. If Equation ((6.17)) had been valid for these results they would have fallen on a straight line of slope, s_2,

$$s_2 = -\frac{4}{3}\left(\frac{8m^*\pi^2}{h^2}\right)\phi^{3/2}$$

The theoretical line given in Fig. 6.3 assumes values for ϕ of 3.25eV and m^* equal to .42 m_o. As expected, the experimental line deviates from this slope increasingly at lower field strengths.

The result of a numerical solution of Equation ((6.14)) is shown in Fig. 6.4 which was calculated using a simple trapizodial rule summation. These calculations assume a value for the barrier height of 3.0 eV which allows for a maximum barrier lowering of 0.3 eV for the fields employed. The experimentally obtained estimate of the effective temperature T_e = 0.12 eV was used and an effective mass of 0.42 m_o. The theoretical plot is fitted to the experimental data for an oxide field of 2.2×10^6 V/cm as shown in Fig. 6.4. However, it is seen that the fit for higher field values becomes increasingly poor. The reason for this discrepancy can be found from an analysis of the summation data. This shows that if a Maxwellian distribution of electrons is assumed then the injected current is being dominated by the number of electrons at the higher energies. The Maxwellian distribution predicts that there will be a significant number of electrons with energies corresponding to the barrier height. At these energies the transmission probability is approaching unity and is varying less sharply with field than at lower energies. However, it was shown in Chapter 2 that the number of electrons at higher energies is probably much less than predicted by a simple Maxwellian because of the probability of ionisation. The result of having fewer electrons at such energies would be a reduction in the magnitude of the oxide current density but an enhanced dependence on the oxide field.

A more quantitative estimate of the effect of the distribution on the field dependence of the injected current can be made for fitting to the experimental results. Consider the electron distribution to be Maxwellian only below the ionisation threshold, $E_i \ll \phi$. Electrons with energies greater than E_i are contained in the high energy tail in which the number of electrons decreases more sharply with energy. The electrons in the tail would be the major contributors to the injected current at low fields when $\log_e I_{ox}$ would be expected to follow a linear dependence with $\sqrt{F(x)}$ as shown above.

The contribution to the injected current coming from the electrons with energies below Ei can be calculated by performing a numerical summation on Equation ((6. 16)) up to the ionisation threshold. This can be fitted to the experimental data at high fields by subtracting from the total measured oxide current a component representing the electrons injected from the tail. In Fig. 6. 15 a fit of the experimental data has been made to each of three summations. The calculated plots represent summations up to 1. 9eV, 2. 1 eV and 2. 3eV respectively. The best fit is obtained by summing to 2. 1 eV which according to the model should represent the ionisation threshold in silicon. This value is very close to the values obtained by other workers for the ionisation threshold in silicon as described in Section 2. 2. It is therefore concluded that the field dependence of the injection current is adequately accounted for at both low and high field strengths.

6. 3 The Dependence of the Injected Current on the Junction Current

The results presented in Chapter 5 showed that the injected oxide current apparently increased exponentially with junction avalanche current. Similar observations of an exponential or power law dependence have been made by other workers for the injection of electrons into both vacuum and silicon dioxide. These reports have been reviewed in Chapter 2; however it is apparent that no satisfactory explanation has been given for such a strong dependence. The observation is either only noted in these reports or a general qualatative explanation has been proposed in terms of an increase in the effective temperature of the charge carrier population. A similar model can be proposed to explain some of the observations of Chapter 5, however, there are several objections which are discussed below. In Section 6. 4 a new model is proposed in terms of microplasma switching probabilities.

If it is assumed that the charge carrier population in an avalanching silicon p-n junctions is Maxwellian, then an incremental change in the effective temperature of the distribution will result in an exponential increase in the number of high energy electrons arriving at the $Si-SiO_2$ interface. An exponential increase in the injected oxide current with junction current would be expected if T_e were proportional to Vj and also I_j proportional to Vj, where T_e is the effective temperature of the electron population, Vj is the junction bias voltage and I_j is the junction current. According to a model by Goffaux [41], the effective temperature of an electron population is a function of the field supporting it. However, a junction avalanche current can be greatly increased by

only a relatively small increase in junction bias which only needs to overcome bulk, space charge and surface layer resistance. Any increase in the effective temperature of the electron population arriving at the interface would only be expected if a significant part of the junction bias was dropped across the surface n-doped layer. A high surface field would not be expected with the shallow $p-n^+$ junctions used in the present work. A qualatative model proposing electron heating in a surface field has been given by Elinson et al [40] to account for an observed increase in the effective temperature of electrons emitted into a vacuum. In Elinson's work the surface p-n junction was formed by the deposition of Cs ions giving a surface doping estimated to be only $5 \times 10^{17}/cm^3$. This compares with the high phosphorus doping of $10^{20}/cm^3$ used in the present work which would be expected to result in a much lower surface field from Elinson's. The influence of the surface field on the effective electron temperature is therefore considered to be negligible in the device structures studied.

The experimental results reported in Chapter 5 indicate that the electron emission originates from areas of localised junction breakdown. Measurements of the radiation emission from such microplasmas can give an indication of the effective temperature of the charge carrier population if a Maxwellian energy distribution is assumed. It would be expected that any increase in the effective temperature of the electron-hole energy distribution with microplasma current would show as a shift in the radiation emission spectrum to higher frequencies. However, this is not observed; for example Chynoweth and McKay [29] report only an increase in the intensity of the emitted radiation with microplasma current.

Further evidence that the charge carrier energy population remains constant with increasing microplasma current comes from the results presented in Fig. 5.9. According to the interface field transmission model proposed in Section 6.2 an increase in the effective temperature of the charge carrier population would reduce the field dependence of the oxide current. This would be observed as a reduction of the slope of the plot of injected oxide current with oxide field for an increasing junction current. The experimental results give no strong indication of such a condition therefore implying a constant charge carrier energy distribution over the junction avalanche current range considered.

A final objection to the model of an increasing effective temperature with avalanche current comes from the observation in Chapter 5 of an increase in the injected oxide current, for a constant avalanche current, during infra-red illumination of the junction. An infra-red emitting source placed beneath the junction results in a decrease in the junction field required to maintain the same junction current. According to the model involving a field dependent effective temperature, illumination with infra-red light should therefore result in a reduction of the average energy of the charge carrier distribution and hence the injected oxide current. In this experiment the reduction in reverse junction bias required to maintain the same junction current as before illumination was less than 0.01V and the effect on electron temperature was probably insignificant . A possible explanation for the increase in oxide current with infra red illumination comes from the fact that the whole junction area is illuminated and not just the microplasma region. Fig. 5.16 shows that carriers generated by infra-red illumination are capable of being accelerated to emission energies in the junction depletion region without avalanching occurring. Thus it is possible that injection under illumination and during avalanching originates from a much larger area than the microplasma regions. However, outside of the microplasma regions the optically generated carriers would undergo little multiplication and the effect of illumination on the $I_{ox} - I_j$ characteristics would be to add a constant component of oxide current for all junction currents. Although the above model gives a qualatative explanation of the experimental observations, the injected oxide current levels obtained generally from, non-avalanching, infra-red illuminated, junctions were insufficient to account for the required additional current component.

It is considered by the author that an adequate model has not yet been proposed to explain the dependence of the oxide injected current on the junction avalanche current, and the dependence on illumination, such as observed for the device structures studied in this work. In the following section a new model is proposed involving microplasma switching probabilities which can best explain the experimental results.

6.4 Microplasma Model for Injected Oxide Currents

In this model it is assumed that electron injection originates from areas of localised breakdown and that microplasma switching probabilities control the oxide injection current. It was noted in Section 2.4 that if a junction is biased at a voltage just above that required to

initiate a microplasma, the current is carried in a random series of pulses. As the bias voltage is increased further the current pulses increase both in amplitude and duration, while the average interval between successive pulses reduces. Eventually the junction bias can be increased to the point where the microplasma is conducting continuously and is behaving as an linear resistance described by Rs. The injection model assumes that the rate of increase in the average current carried by a microplasma can be described by a function primarily controlled by the turn-off probability of the microplasma, ie. an exponential dependence on the junction bias. The measured current injected into the oxide is assumed to be determined by a microplasma in the region of the thin oxide contact. The microplasma current is assumed to be only a small component of the total junction current, which is essentially linear with junction bias over the small range considered. Hence the injection current can increase extremely rapidly with junction current.

In order to put this on a more quantative basis it is necessary to consider the situation of a single microplasma in an otherwise uniform junction. This will then be extended to the practical situation where a junction contains several microplasmas. The following assumptions will be made:-

(i) The manner of breakdown in the microplasma is similar to that of the uniform area of the junction except that the breakdown occurs at a lower voltage.
i.e. The slope of a plot of I/M against Vj is the same for the microplasma region as for the uniform region.

(ii) The junction bias is such that microplasma breakdown is initiated but is insufficient to avalanche the uniform junction area. The microplasma therefore contains most of the high energy electrons so that the oxide current is due to electron injection from the microplasma only.

(iii) The effective temperature of the charge carriers in a microplasma is constant. Over the junction current range considered the variation in junction bias is insufficient to effect significantly the average energy of the electron-hole population.

(iv) A microplasma breakdown is self sustaining until a statistical fluctuation in the multiplication process produces fewer charge carriers than are lost from the depletion region. If this occurs the avalanche will quench and the microplasma is said to have turned off. This implies that the turn off probability is independent of illumination which is only true to a first approximation [34]. In the experimental work reported in Chapter 5 the devices were kept in the dark although for some experiments weak infra-red illumination was used.

(v) The turn-on probability is determined by the generation of minority carriers able to initiate a microplasma. These carriers are considered to be thermally or optically generated and will either be generated within the depletion region or will diffuse into it from the bulk silicon. The generation of carriers from traps via a tunnelling mechanism is not considered to be important in a junction with a high voltage breakdown. The turn-on probability at a constant temperature is therefore assumed to be dependent on illumination but independent of junction bias over the small range of junction avalanche voltage considered.

(vi) The series resistance of the microplasma is considered to be independent of current and to be determined by the model proposed by McIntyre as discussed in Section 2.4. The instaneous current Imm passed by a microplasma at a given junction bias Vj, will therefore be entirely determined by R_s. That is,

$$I_{mm} = (V_j - V_B) / R_s \qquad ((6.17))$$

where V_B is the extrapolated breakdown voltage of the microplasma.

Having made the above assumptions it is now possible to consider in more detail the problemdf a single microplasma in a junction with an otherwise uniform breakdown characteristic. The total junction current can be considered to consist of three components given by:

$$I_j = I_m + MI_s + I_L \qquad ((6.18))$$

where I_m is the average current carried by a microplasma

I_s is the saturation current of the p-n junction

M is the multiplication factor for the unifrom junction area

I_L is the junction leakage current component

The saturation current Is, results from the diffusion of carriers into the depletion region and from the generation of carriers within the depletion region.

ie. $I_s = (I_{diff} + I_{gen})$ ((6. 19))

The multiplication factor for the uniform junction area M, will be dependent on the difference between the microplasma breakdown voltage V_B, and the breakdown voltage of the uniform junction V_B', as shown in Fig. 2. 6.

The leakage current I_L can be due to many effects, for example, defects in the junction, surface leakage due to inversion and surface leakage due to water contamination of the oxide. The precise voltage dependence of I_L is indeterminant and may well vary from junction to junction. In the present work the junction breakdown was sharp and the reverse leakage current was found to be independent of voltage. The magnitude of the leakage current was greater than expected from consideration of Equation ((6. 19)) as shown in Section 6. 5 and was typical of a channel effect due to surface inversion. It was therefore considered reasonable to assume that for the devices considered I_L is independent of voltage and equal to

$$I_L = (I_{sat} - I_s) \qquad ((6.20))$$

where I_{sat} is an experimental measurement of the junction leakage current.

The average current carried by a microplasma is dependent on its series resistance and the average ratio of the current pulse duration to the pulse cycle. The current-voltage characteristics of a single microplasma have been measured by Haitz [35] as shown in Fig. 2. 6. The slope of the linear region is R_s, the series resistance of the microplasma. By extrapolating the microplasma current -voltage characteristic to zero current the extrapolated breakdown voltage V_B, of the microplasma is defined, as described in Section 2. 4. Haitz found that this value was equal to the breakdown voltage obtained from an extrapolation of a plot of I/M against Vj to I/M = O (ie. M = ∞ at breakdown). A plot of I/M against Vj can also be drawn for the uniform area of the junction and according to assumption (ii) this will be parallel to the plot for the

microplasma but intersecting the voltage axis at V_B' where $V_B' > V_B$.

The experimental results obtained by Haitz show a deviation from the theoretical slope R_s near breakdown. This deviation is caused by the on-off switching of the current pulses resulting in a reduced average microplasma current. The measurements made by Haitz were for an illuminated microplasma, thus increasing the turn-on probability. For a junction in the dark the deviation from the ohmic slope would be apparent at greater values of the junction bias voltage. It should be noted however, that the amplitude of a microplasma current pulse is determined only by R_s.

The average current carried in a microplasma is given by,

$$I_m = I_{mm} \times \frac{\tau_1}{\tau_1 + \tau_0} \qquad ((6.21))$$

where I_{mm} is the amplitude of a microplasma current pulse

τ_1 is the average current pulse length

τ_0 is the average interval between current pulses.

$$\tau_1 = \frac{1}{P_{10}} \qquad ((6.22))$$

where P_{10} is the turn-off probability of the microplasma and, according to assumption (iv), is a function of $(V_j - V_B)$ but independent of illumination.

$$\tau_0 = \frac{1}{P_{01}} \qquad ((6.23))$$

where P_{01} is the turn-on probability of the microplasma and, according to assumption (v), is independent of $(V_j - V_B)$ but is increased by illumination.

Therefore we can write,

$$\left(\frac{\tau_1}{\tau_1 + \tau_0}\right) = \left(\frac{\frac{1}{P_{10}}}{\frac{1}{P_{10}} + \frac{1}{P_{01}}}\right) = \left(\frac{P_{01}}{P_{01} + P_{10}}\right) \qquad ((6.24))$$

Thus the average current carried in a microplasma is,

$$I_m = I_{mm}\left(\frac{P_{01}}{P_{01} + P_{10}}\right) = I_{mm}\left(\frac{1}{1 + \frac{P_{10}}{P_{01}}}\right) \qquad ((6.25))$$

From experimental measurements on localised microplasmas with breakdowns of about 18 V Haitz [35] has deduced that,

$$\tau_1 = \tau' \exp (V_j - V_B) / V_o \qquad ((6.26))$$

where τ' is of the order of the transist time for a carrier through the depletion region.

Vo is a characteristic voltage for the microplasma under study and is determined from the slope of the experimental graph of $\log_e \tau_1$ against $(V_j - V_B)$.

Therefore by substituting ((6.26)) into ((6.25)) and by putting ,

$$P' = \frac{1}{\tau'}$$

we obtain

$$I_m = I_{mm} \left(\frac{1}{1 + \left(\frac{P'}{P_{o1}}\right) \exp - (V_j - V_B)/V_o} \right) \qquad ((6.27))$$

That part of Equation ((6.27)) contained in brackets is of the same form as the Fermi-Dirac distribution function, and it will tend to unity as the junction bias is increased beyond that necessary to initiate the microplasma. That is, when

$$\left(\frac{1}{1 + \left(\frac{P'}{P_{o1}}\right) \exp - (V_j - V_B)/V_o} \right) \rightarrow 1$$

then $I_m \rightarrow I_{mm}$

and the microplasma is conducting continuously.

According to the assumptions (ii) and (iii) made for the injection model, the injected oxide current is proportional to the mciro-plasma current.

Therefore we can write,

$$I_{ox} = \gamma I_m$$

where γ is a constant representing the injection efficiency which will be dependent on the injection structure geometry.

Equation ((6.18)) gave the total junction current as

$$I_j = I_m + M I_s + I_L$$

therefore,

$$\frac{I_{ox}}{I_j} = \frac{\gamma I_m}{I_m + M I_s + I_L} \qquad ((6.28))$$

where $$I_m = I_{mm} \Big/ \left(1 + \left(\frac{P'}{P_{o1}}\right) \exp - \frac{(V_j - V_B)}{V_o}\right.$$

In the experimental work described in Chapter 5 it was observed that the junctions contained several microplasmas at the intersection of the shallow junction and the guard ring. In general these edge microplasmas turned on before any microplasma within the shallow junction area and in this work they will therefore be considered to be conducting continuously before any oxide current is detected. The current carried by these edge microplasmas will therefore be determined by their parallel combined resistance when conducting. Thus, for a device containing edge microplasmas and a single injecting microplasma within the collecting region of the electrode to the thin oxide,

$$\frac{I_{ox}}{I_j} = \frac{\gamma I_m}{I_m + M I_s + I_L + I_{me}} \qquad ((6.29))$$

where I_{me} is the current carried by the edge microplasmas.

6.5 Numerical Values for the Microplasmas Model

In the following section an attempt is made to calculate numerical values for the parameters used in Section 6.4. Where possible these calculations are based on junction parameters and constants typical for the devices fabricated in the present work. Where direct measurements have not been possible reasonable estimates from other authors work are used. The junction parameters and constants for the present devices are summarised in Table 6.1.

Equation ((6.27)) gives,

$$I_m = I_{mm}\left(1 \Big/ \left(1+\left(\frac{P'}{P_{o1}}\right)\right)\exp -(V_j - V_B)/V_o\right)$$

P_{o1} will be determined by the probability of the arrival of a minority carrier in the region of localised field enhancement and the probability of it being accelerated to ionisation energy.

The probability of a minority carrier arriving in the region of localised field enhancement will be determined approximately by the thermal generation current density.

Hence,

$$P_{o1} = \frac{I_s}{q}\ \frac{A_m}{A_s}\ P_i' \qquad ((6.30))$$

where A_m is the cross sectional area of the microplasma within the depletion region of the shallow junction

A_s is the area of the shallow junction

I_s is the thermal generation current of the shallow junction.

P_i' is the probability of a thermally generated carrier in the region of field enhancement being able to initiate a microplasma.

The thermal generation current is, can be considered to consist of two components.

(i) I_{diff}, which results from the diffusion of thermally generated carriers from the bulk silicon into the depletion region.

(ii) I_{gen}, resulting from carriers thermally generated within the depletion region and those carriers field emitted from traps in the depletion region.

Thus, $$I_s = I_{diff} + I_{gen} \qquad ((6.31))$$

From Ref(91)

$$I_{diff} = \frac{q A_s D_n n_p}{\sqrt{D_n \tau_n}} \qquad ((6.32))$$

where τ_n is the minority carrier lifetime of electrons in p-type silicon

n_p is the electron concentration in p-type silicon

D_h is the diffusion constant for electrons in silicon

Now $$D_h = \frac{kT \mu_n}{q} \qquad ((6.33))$$

where μ_n is the mobility of electrons in silicon,

therefore assuming that,

$A_s = 0.18\ mm^2$

$\tau_n = 10^{-6}$ sec

$\mu_n = 1,350\ cm^2/V$ sec

$n_p = 4.5 \times 10^4\ cm^{-3}$ for p-type Si of 4-5 Ω cm resistivity

then $$I_{diff} = 7.7 \times 10^{-14}\ A \qquad ((6.34))$$

If we neglect the effect of traps as given in assumption (v) of Section 6.4 then from Ref. (91)

$$I_{gen} = \frac{q A_s n_i W}{2 \tau_o} \qquad ((6.35))$$

where W is the depletion width at breakdown voltage

n_i is the intrinsic carrier concentration in silicon

τ_o is the average minority carrier lifetime within the depletion region

therefore assuming that,

$\tau_o \simeq 10^{-6}$ sec

$n_i = 1.5 \times 10^{10}$ cm $^{-3}$ @ 300° K

$W = 4.0$ μm @ 90V

$A_s = 0.18$ mm^2

then $$I_{gen} = 8.7 \times 10^{-10} A \qquad ((6.36))$$

Thus $$I_s \simeq 10^{-9} A \qquad ((6.37))$$

If only those carriers which escape an optical phonon collision are considered to be able to attain ionising energies, then the probability of a thermally generated carrier in the region of field enhancement being able to initiate a microplasma is given by

$$P_i = \exp(-E_i/q\ell_r F) \qquad ((6.38))$$

where E_i is the ionisation threshold energy

ℓ_r is the m. f. p. for an optical phonon collision

F is the field strength at avalanche

If a value for F of 3×10^5 V/cm is assumed and also Wolff's values for $E_i = 2.3$ eV and $\ell_r = 200$ Å are taken then,

$$P_i \simeq 2 \times 10^{-2} \qquad ((6.39))$$

By using Equation ((6.30)) and taking the values calculated for $I_s \simeq 10^{-9}$A and for $P_i \simeq 2 \times 10^{-2}$, we can now calculate the turn on probability for microplasmas of different diameters. The diameters of microplasmas found in the experimental work were estimated from photographs to range from between 5 μm and 25 μm .

In table 6.3 below P_{01} has been calculated for microplasmas of 5 μm , 10 μm and 25 μm diameter

TABLE 6.3 CALCULATIONS OF TURN-ON PROBABILITIES

Diameter of microplasma, μm	5	10	25
Area of microplasma, cm^2	1.96×10^{-7}	7.86×10^{-7}	4.91×10^{-6}
P_{01}, sec^{-1}	4.1×10^3	1.7×10^4	1.1×10^5

The parameter P' can be calculated from the transit time for a carrier to cross the depletion region.

$$\frac{1}{P'} \simeq \tau' = W/v_{ds} \qquad ((6.40))$$

Where V_{ds} is the saturation drift velocity of an electron in silicon, taken to be $\simeq 10^7$ cm/sec.

therefore $$\tau' = 4 \times 10^{-11} \text{ secs}$$

$$P' = 2.5 \times 10^{10} \text{ sec}^{-1} \qquad ((6.41))$$

For microplasmas of diameter 5, 10 and 25 μm the respective values of P'/P_{01} are 6.1×10^6, 1.5×10^6 and 2.3×10^5.

The parameter Vo is a constant for a given microplasma and controls the rate of decrease in the turn off probability with increasing junction bias above that required to initiate the microplasma. An avalanche will quench primarily because of a fluctuation in the number of ionising collisions produced by carriers in passing through the microplasma's space charge region. It can be deduced therefore that Vo is a function of the multiplication factor M which is known to increase with avalanche breakdown values as given in Equation ((2.17)). Vo should be measured directly for the microplasma under study. However this was not possible with the equipment available and a value of 0.02 V measured by Haitz for 18 V breakdown microplasmas is assumed in this work. This value is considered to be sufficiently accurate to illustrate the main features of the injection model although a direct measurement of Vo is required to validate the model completely. It can also be seen from Haitz's results that there is an increase in Vo with increasing microplasma diameter, however the variation is very small and the value of Vo will be assumed to be constant in this work.

The values for the microplasma current pulse amplitude can be calculated from Equation ((6.17)) which gives,

$$I_m = (V_j - V_B) R_s$$

where R_s is the series resistance of the microplasma and is given by

$$R_s = R_{sc} + R_{srp} + R_{srn}$$

R_{sc} is given by Equation ((2.11))

R_{srp} is given by Equation ((2.12))

R_{srn} is given by Equation ((2.13))

Therefore using the above equations the series resistance for microplasmas of diameters 5, 10 and 25 μm can be calculated to be 4×10^4, 1.1×10^4 and 2.4×10^3 ohm respectively.

The above values of microplasma series resistance and also the turn-on probability are summarised in Table 6.2.

The parameters calculated in this section can now be used to calculate the average current carried by microplasmas of 5, 10 and 25 μm diameter. This has been done in Fig. 6.6 which shows the average current carried by microplasmas for increasing bias beyond that required to initiate turn-on. It can be seen that the microplasma current increases approximately exponentially from initial turn-on, but is tending to become linear at higher bias values as the turn-off probability decreases and becomes comparable in magnitude to the turn-on probability.

It was shown earlier that illuminating a junction with infra-red light results in an increase in the bulk generation of carriers. This will increase the turn-on probability of the microplasma. The theoretical effect of this is illustrated in Fig. 6.7 where the turn-on probability of a 25 μm diameter microplasma has been assumed to have been increased by a factor of ten by illumination.

The plot shown in Fig. 6.7 shows some similarity with the results contained in Chapter 5 if it is assumed that the total junction current is a near linear function of the junction bias voltage over the given bias range. From Fig. 4.3b it can be seen that this is a reasonable assumption since a typical junction has an linear characteristic in the avalanche bias region for currents greater than 100 μ A. In the next paragraph an arbitary but reasonable set of conditions will be introduced to illustrate the effect of plotting the current carried by a single microplasma against the sum of the junction current components considered in Section 6.4.

Consider a junction with a uniform breakdown at 90V. Let it contain, within the collecting region of the contact to the thin oxide, a single microplasma of 25 μm diameter which first turns on at 89.7 V. Assume that the junction also contains microplasmas at the intersection of the shallow junction and the guard ring which are conducting continuously and passing together a current of 100 μ A when the junction is biased at 89.8 V. Let the parallel combined current voltage characteristics of these edge microplasmas be linear for currents greater than 100 μ A with a resistive slope of 100 Ω .

The effect of the multiplication factor on the bulk generation current can be calculated from Equation ((2.17)), ie.

$$\frac{1}{M} = (V_B' - Vj)\,(K/V_B')$$

K is dependent on the background doping and for the devices under study is approximately 2 as given by Bulucea [92]. This contribution to the junction

current only becomes appreciable compared with the edge microplasma current for a junction bias within 0.2 v of the breakdown of the uniform junction area, ie when $M > 200$ and $MI_s > 0.1\ \mu$ A.

The surface leakage current was approximately $1\ \mu$ A and constant over the junction bias range even close to breakdown. Therefore in this example the surface leakage is considered to be constant which neglects carrier multiplication and possible breakdown in surface inversion layers.

The result of plotting the current carried by a 25 μm diameter microplasma against the total junction current considered in the above example is shown in Fig. 6.8. Also plotted is the result obtained by increasing the turn-on probability by a factor of 10 with illumination. Similar results are obtained by considering 10 and 5μm diameter microplasmas except that the microplasma current levels are reduced by about one and two orders of magnitude respectively for a given junction current. Another notable effect is that the characteristic is more nearly exponential over a wider junction current range.

Considering the arbitary nature of the assumptions the theoretical plot compares favourably with that obtained experimentally in Fig. 5.9. There is some deviation in Fig. 6.8 away from a true exponential dependence at higher junction current values. This reflects the choice of the turn on condition for the microplasma which is beginning to saturate. It may be noted that Pepper's results have a dependence of this form as shown in Fig. 2.15. According to the model proposed in Section 6.4 the injected oxide current is calculated from the microplasma current by multiplying by a factor γ. The results presented in Fig. 6.8 would indicate that γ is of the order of 10^{-9}. This value compares with a range of 10^{-8} to 10^{-15} calculated from Bartelink's results and assuming a junction depth of $(0.1 \pm 0.03)\ \mu$m. The agreement is therefore quite good even assuming one injecting microplasma.

6.6 Discussion of Other Observations

In Fig. 5.10 it is shown that for an injected oxide current of greater than 10^{-10} A there is a fall off in its rate of increase with junction current. This observation is readily explained on the microplasma injection model as being the condition where the turn-off probability has decreased to such an extent that the microplasma is conducting continuously. It is not considered that the current is being space charge limited since the current density is only of the order of 2×10^{-5} A/cm^2, assuming a

microplasma diameter of 25 μm diameter. A pure lower space charge limited current in a trap free insulator [93] would be given by,

$$J = \frac{9}{8} \frac{\mu_{ox} \varepsilon_o \varepsilon_{ox} V(x)^2}{s^3} \qquad ((6.42))$$

where μ_{ox} is the electron mobility in the oxide
s is the oxide thickness
$V(x)$ is the voltage applied across the oxide

Assuming $\mu_{ox} = 30\ cm^2/Vsec$
$s = 540^{\circ}A$
$V(x) = 5\ V$

then $J \simeq 2 \times 10^6\ A/cm^2$

The presence of traps in the oxide will reduce the current density required for space charge limitation. However, the density of traps in thermal silicon dioxide has been estimated [53] to be only of the order of $5 \times 10^{13}\ cm^{-3}$. Verwey and De Maagt [94] have obtained current densities of $10A/cm^2$ from surface avalanched p^+-n diodes for which the current injection characteristics are consistent with an electrode limited rather than a bulk limited process.

Several of the plots of oxide injection current against junction current shown in Chapter 5 have a discontinuity in the characteristics. The explanation for this is not clear but it appears to be associated with a negative resistance region in the diode breakdown characteristic, possibly caused by a surface avalanche effect.

In Fig. 5.16 it is shown that the injected oxide current increases linearly with photo-excited junction current. It would be expected that this injection characteristic would differ from that obtained from an avalanching junction since there is probably a continuous and uniform injection of electrons from the whole shallow junction area. These injected electrons result from electrons photo-excited in the bulk silicon which diffuse to the depletion field where they are accelerated to injection energies but undergo little multiplication. Since junction avalanching is not required to achieve a population of high energy electrons injection can take place over the whole junction area because, at the junction bias used, defects will not cause localised microplasmas. This effect will be discussed further in Chapter 8.

6.7 Conclusion

The theoretical model presented in this chapter is consistent with the experimental observations of Chapter 5. The process of electron injection from a microplasma is, to the author's knowledge, the only quantative explanation ever given for such a rapid variation of injected current in SiO_2 with avalanching junction current. Further work is however necessary to validate the microplasma model completely. In particular it is desirable that devices with only a single microplasma should be produced so as to accurately measure the turn-on and turn-off probabilities. This would allow an unequivocal fit of the theoretical model to the experimental data to be obtained.

TABLE 6.1 TYPICAL JUNCTION PARAMETERS

REGION	SURFACE DOPING/cm^2		SHEET RESISTANCE	JUNCTION DEPTH	DEPLETION WIDTH		BREAKDOWN VOLTAGE	JUNCTION AREA	BULK THERMAL DIFFUSION CURRENT	BULK THERMAL GENERATION CURRENT	LEAKAGE CURRENT
	p	n^+	ohm/□	μm	0V BIAS	90V BIAS			A	A	A
TOTAL JUNCTION	-	-	-	-	-	-	90V	$0.5mm^2$	$2.2x10^{-13}$	$4.7x10^{-9}$	10^{-6}
GUARD RING	$5x10^{15}$	10^{19}	100	8.6	$1.5\mu m$	$10\mu m$	120V	$0.32mm^2$	$1.4x10^{-13}$	$3.8x10^{-9}$	-
SHALLOW JUNCTION	$5x10^{15}$	10^{19}	200	(0.1 ± 0.03)	$0.4\mu m$	$4\mu m$	90V	$0.18mm^2$	$7.7x10^{-14}$	$8.7x10^{-10}$	-

TABLE 6.2 MICROPLASMA PARAMETERS

MICROPLASMA DIAMETER μm	R_{sc} ohm	R_{srp} ohm	R_{srn} ohm	R_s ohm	P_{o1}	P'	P'/P_{o1}	V_o	K
5	$3.5x10^4$	$4.5x10^3$	$1.5x10^2$	$4x10^4$	$4.1x10^3$	$2.5x10^{10}$	$6.1x10^6$	0.02	2
10	$8.8x10^3$	$2.3x10^3$	$1.3x10^2$	$1.1x10^4$	$1.7x10^4$	$2.5x10^{10}$	$1.5x10^6$	0.02	2
25	$1.4x10^3$	$9.0x10^2$	$1.0x10^2$	$2.4x10^3$	$1.1x10^5$	$2.5x10^{10}$	$2.3x10^5$	0.02	2

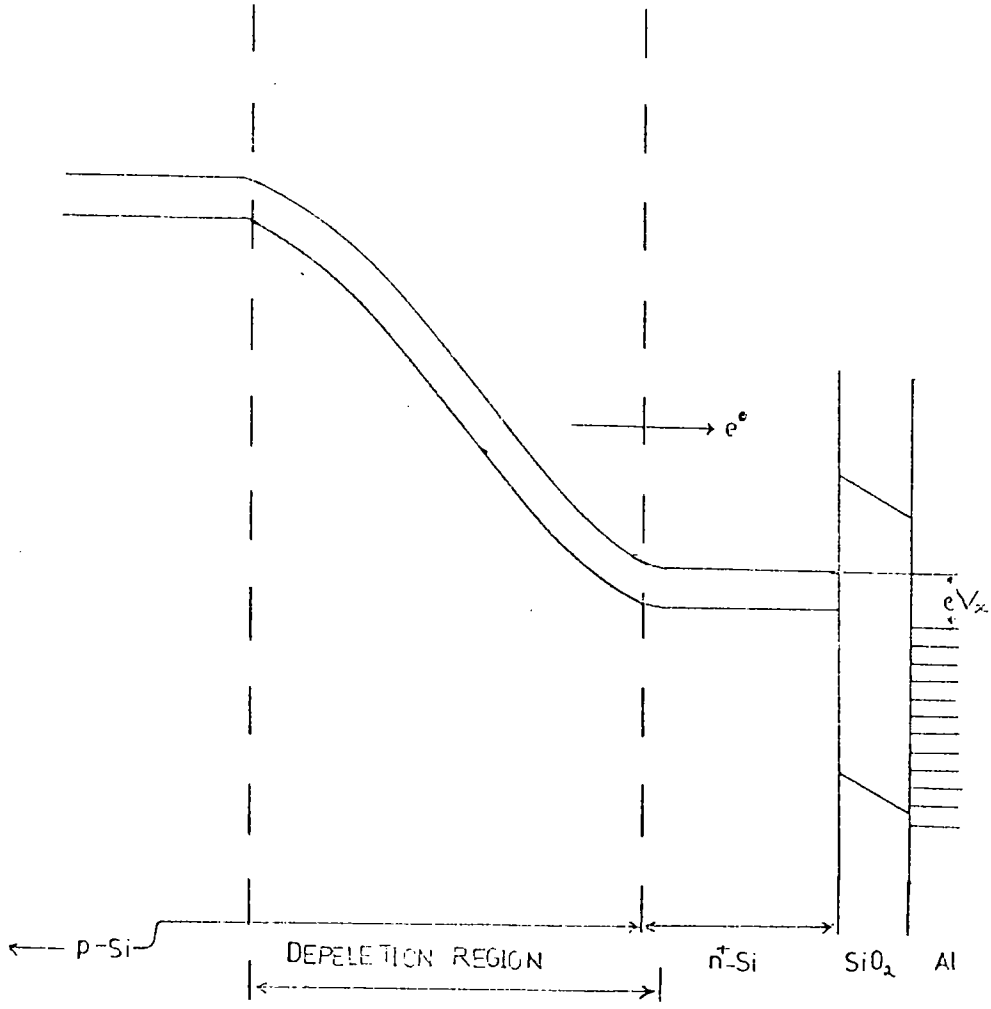

FIG 6.1 BAND STRUCTURE FOR ELECTRON INJECTION INTO SiO_2

FIG 6.2 DEPENDENCE OF THE INJECTED OXIDE CURRENT ON THE SQUARE ROOT OF THE APPLIED FIELD.

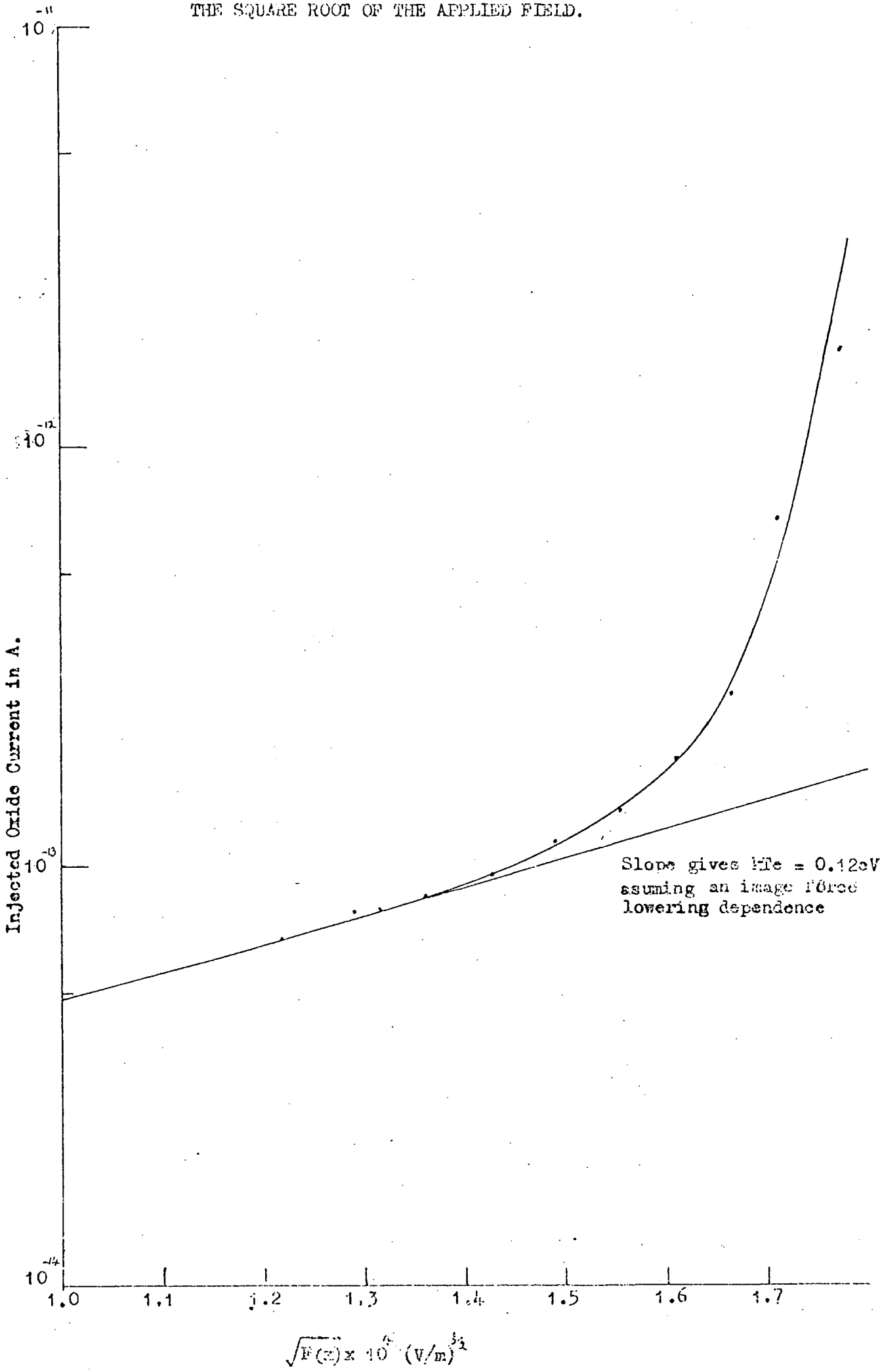

FIG 6.3 DEPENDENCE OF THE INJECTED OXIDE CURRENT ON THE RECIPROCAL OF THE APPLIED FIELD.

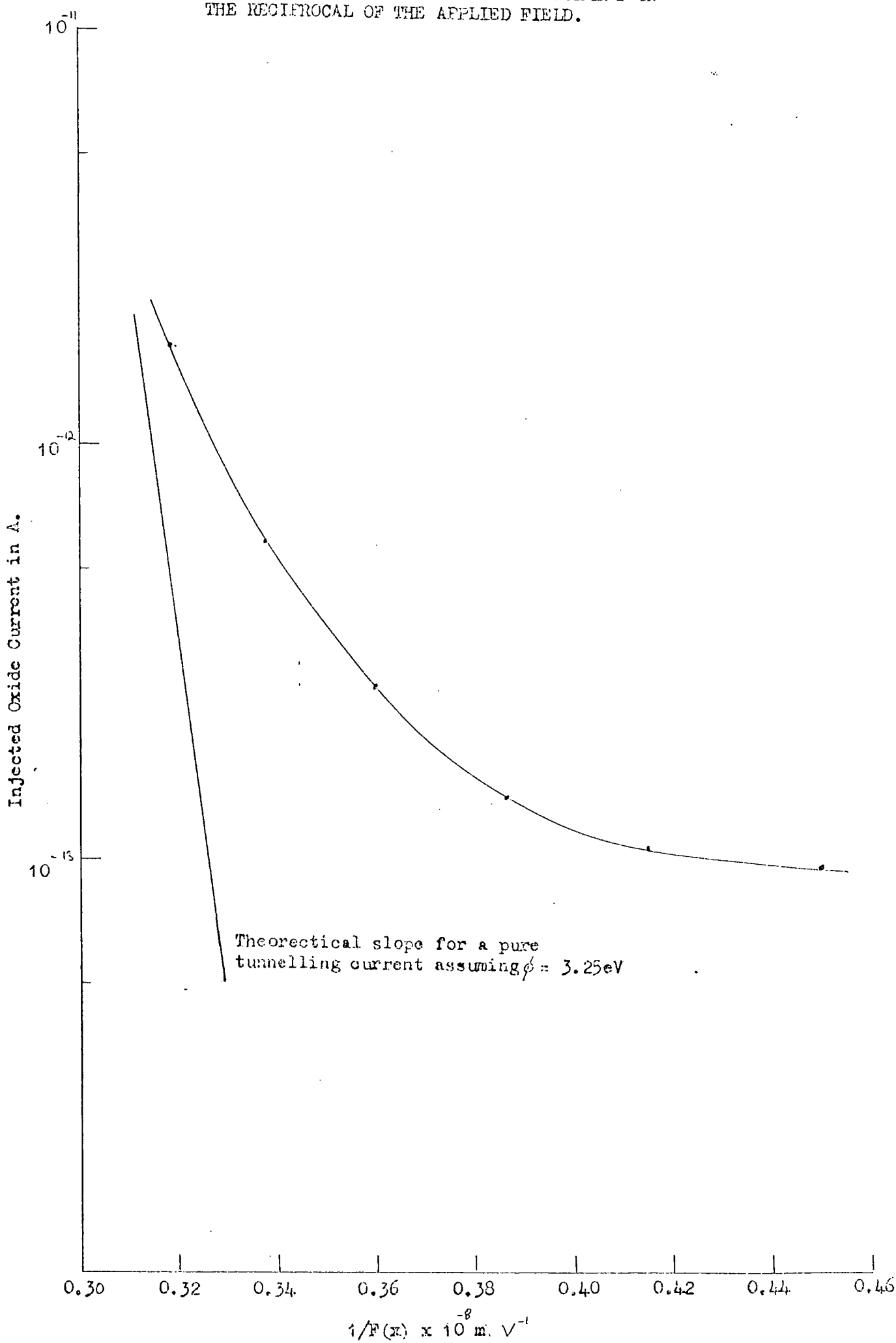

FIG 6.4 RATE OF INCREASE OF INJECTED OXIDE CURRENT WITH APPLIED FIELD. COMPARISON OF EXPERIMENT AND CALCULATED SUMMATION FOR E(x)= 0 TO E(x)= 3.0 eV.

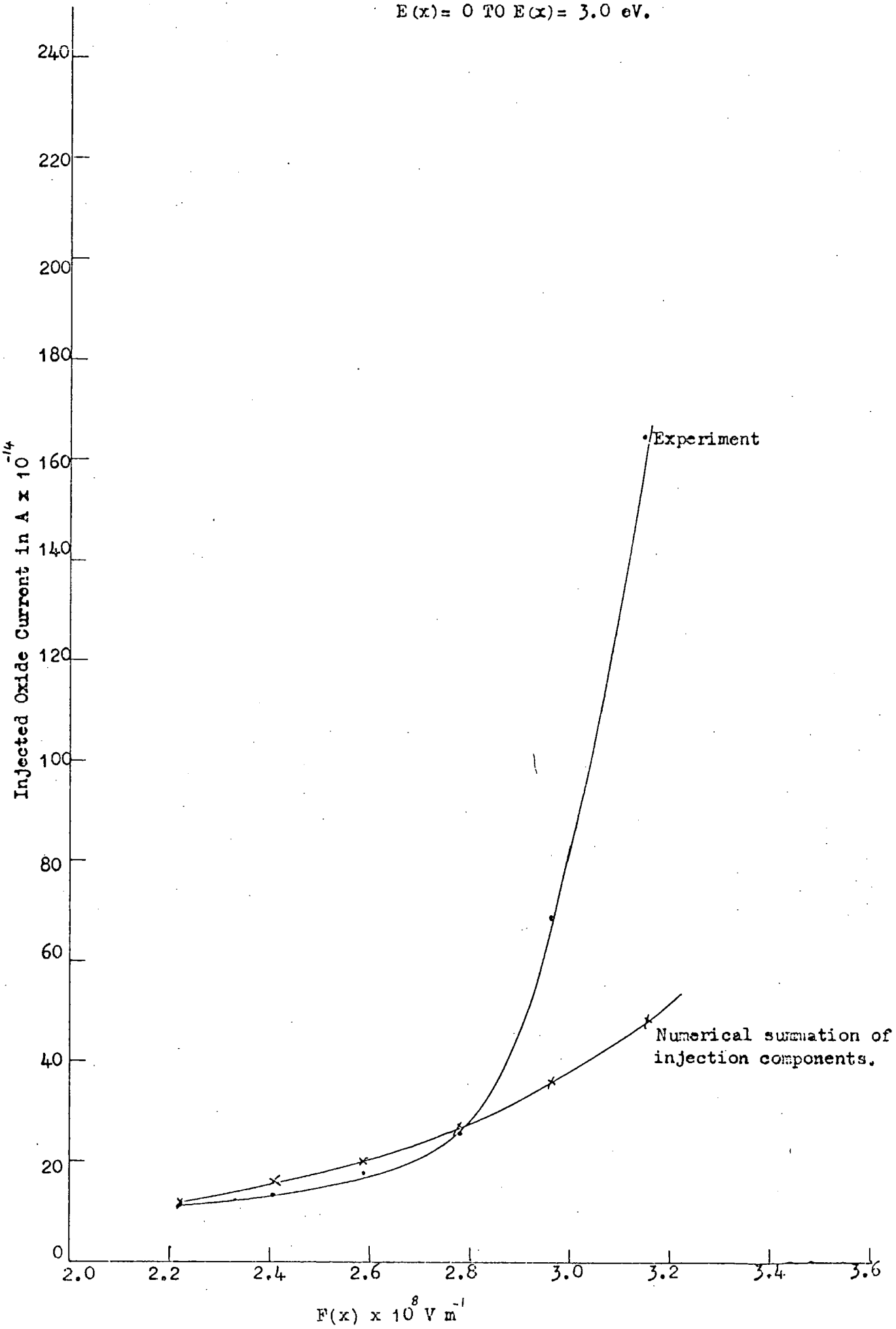

FIG 6.5 RATE OF INCREASE OF INJECTED OXIDE CURRENT WITH APPLIED FIELD.
COMPARISON OF EXPERIMENT AND CALCULATED SUMMATION FOR
E(x) = 0 TO E(x) = Ei .
(ϕ = 3.0eV , kTe = .12 eV.)

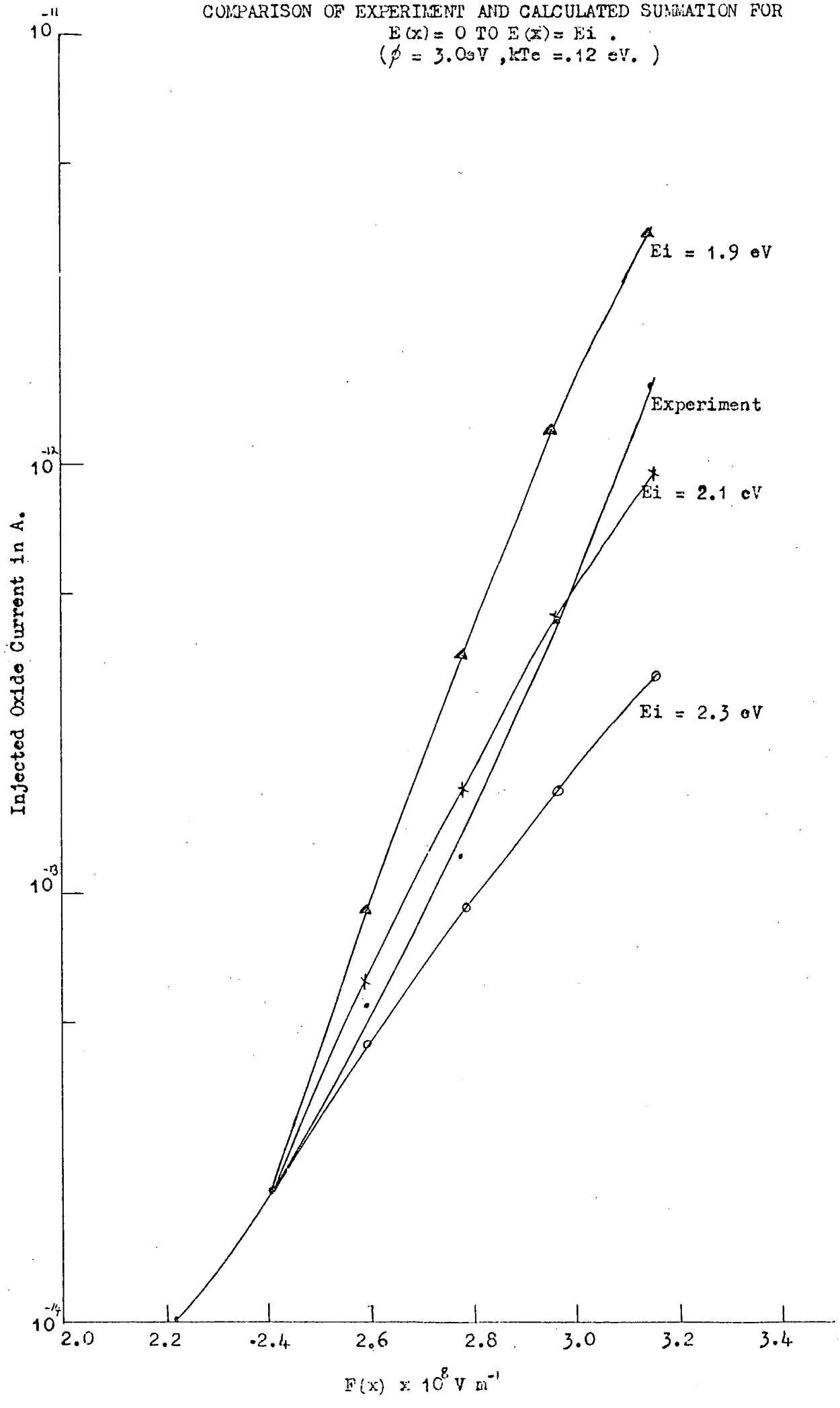

FIG 6.6 VARIATION OF MICROPLASMA CURRENT WITH INCREASING BIAS ABOVE TURN-ON.

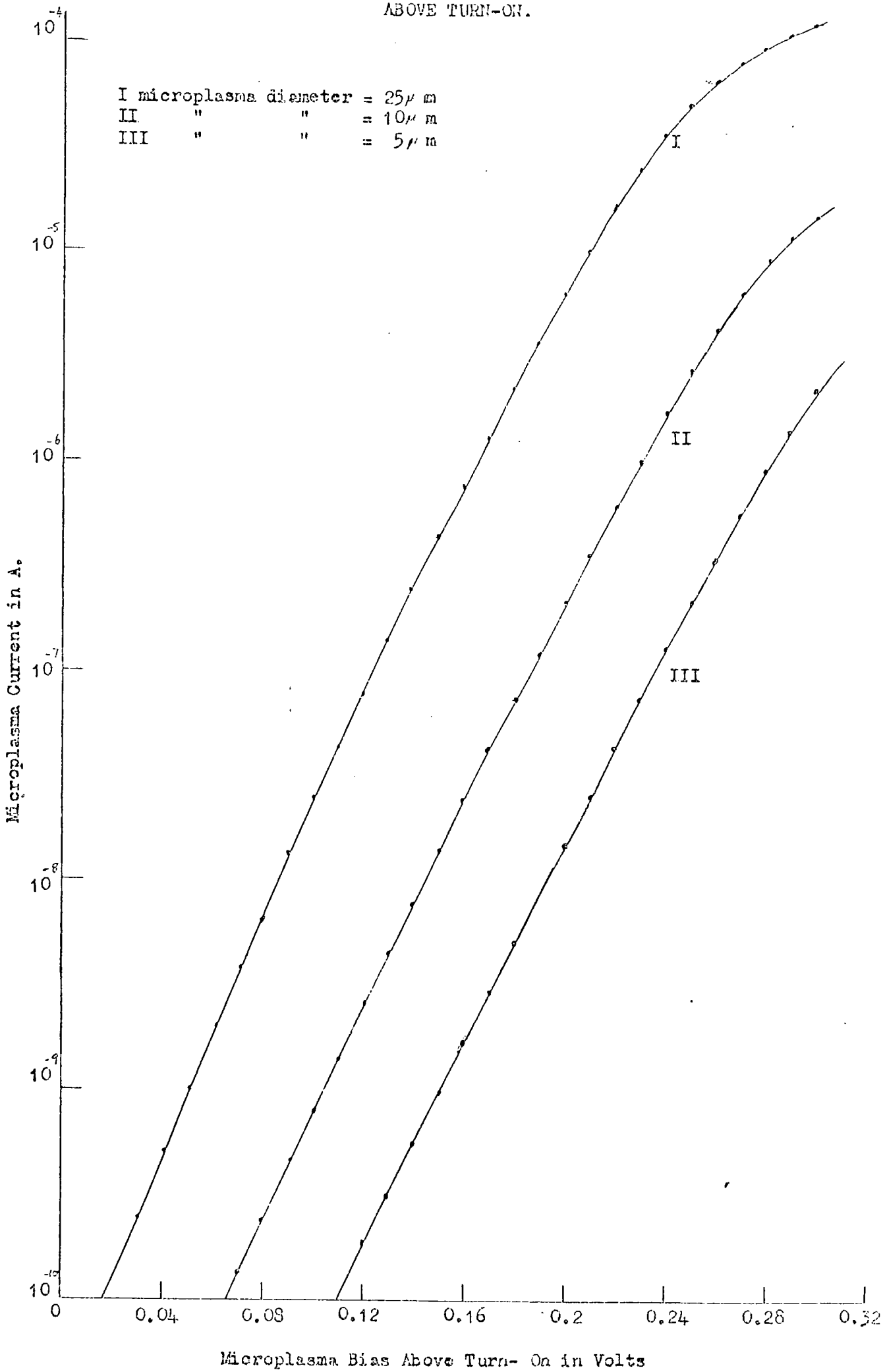

FIG 6.7 EFFECT OF INCREASING TURN-ON PROBABILITY ON THE MICROPLASMA CURRENT.

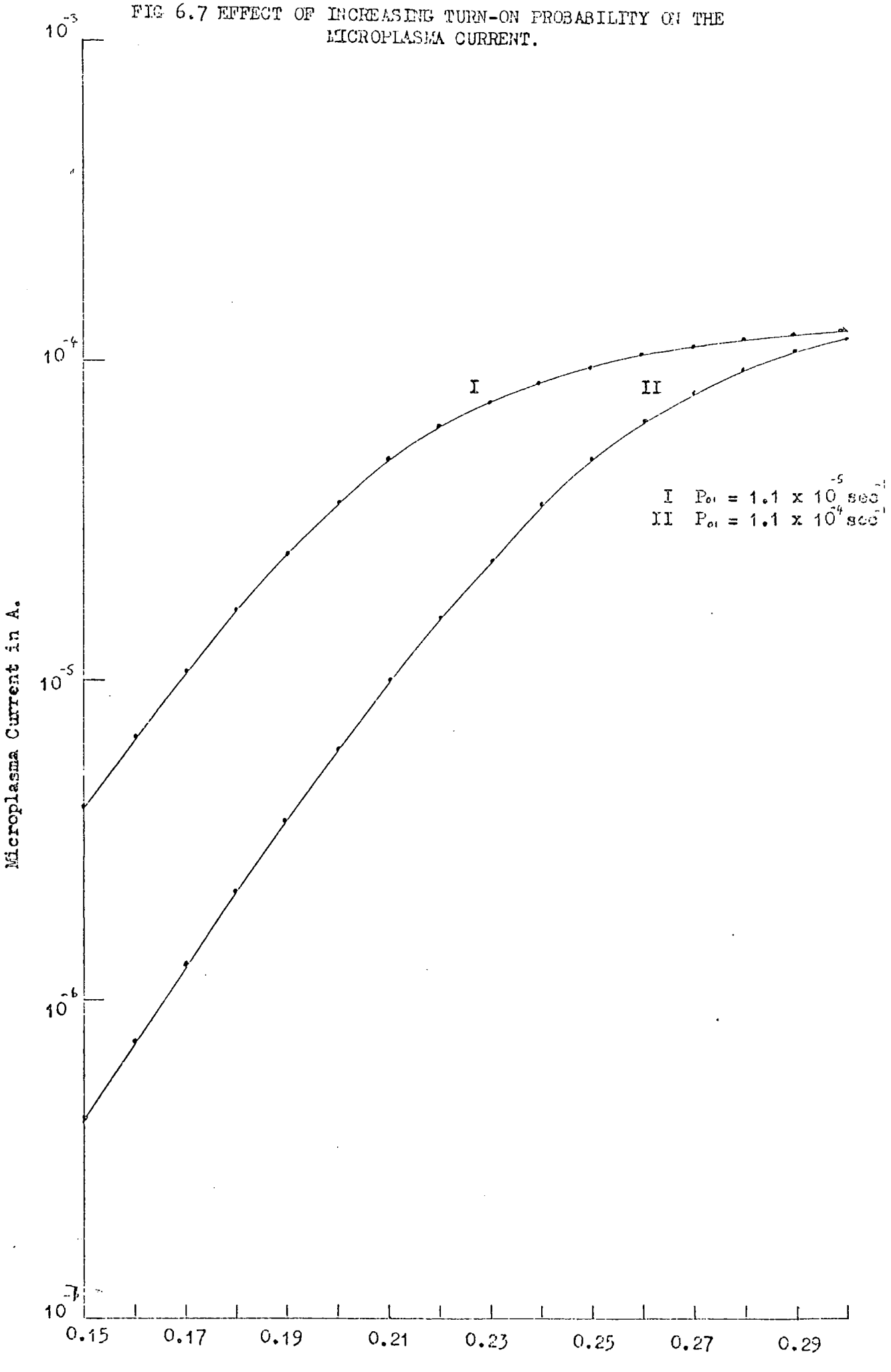

FIG 6.8 THEORETICAL PLOT OF INJECTED OXIDE CURRENT AGAINST JUNCTION CURRENT, DERIVED FROM THE MICROPLASMA MODEL OF ELECTRON INJECTION.

(Microplasma diameter = 25 μ m, $\gamma = 10^{-5}$)

I Junction in the dark
II Junction illuminated.

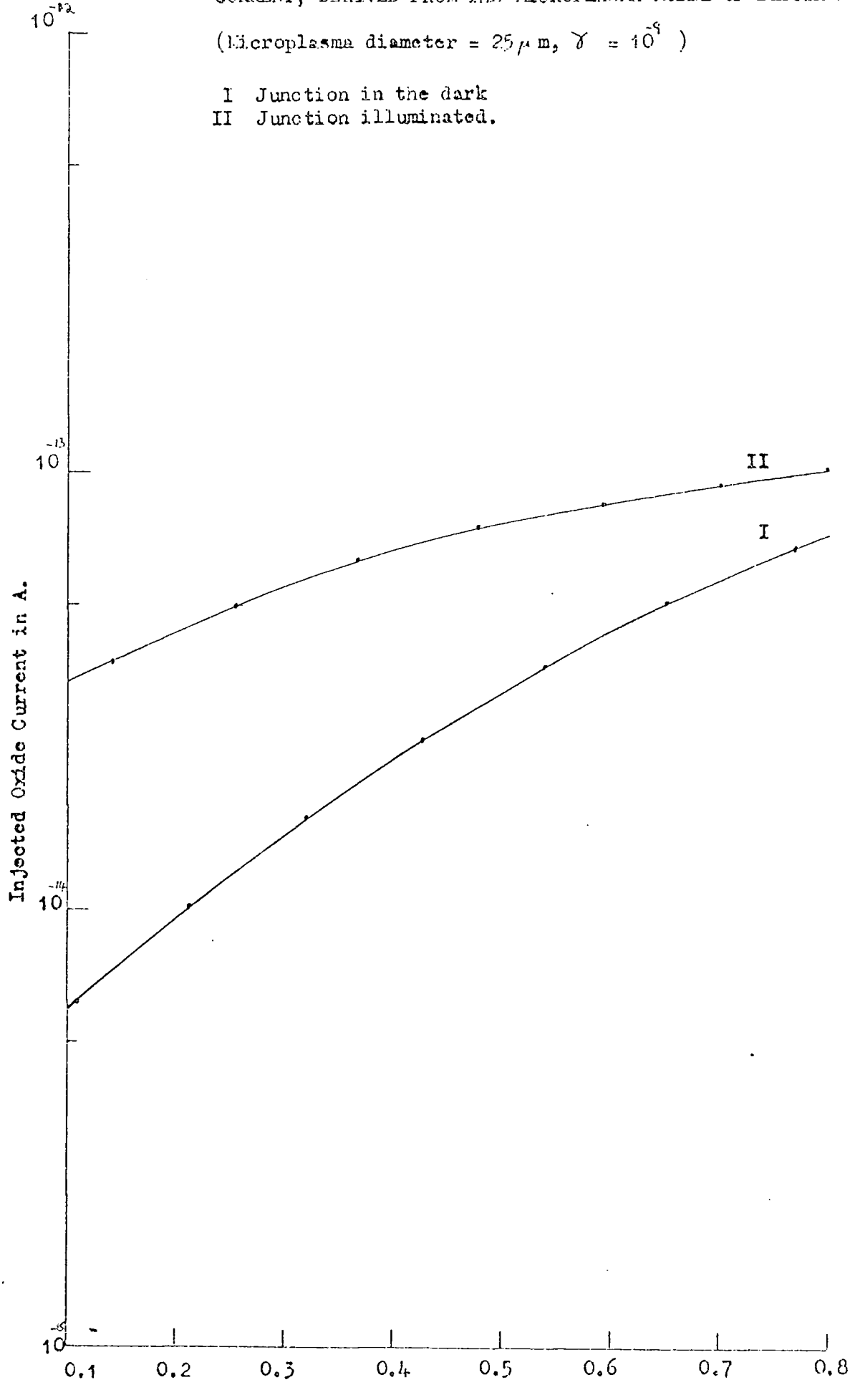

CHAPTER SEVEN

CURRENT INJECTION INTO THIN WILLEMITE FILMS

7. 1 Introduction

The final objective of the present work was to investigate electron injection into a thin film of willemite by using a p-n^+ injection structure, similar to that described in Chapter 5. Before embarking on this course some initial experiments were completed on simple structures of thin ($<$ 1000 Å thick) films of willemite on uniformly doped, p-type silicon substrates, of approximately 1 Ω -cm resistivity. This work was necessary to tie in with earlier results, obtained by Edwards [2] and Davies [95], and to optimise the willemite formation reaction which could then be used in conjuction with the injecting p-n^+ junction structure.

The following two sections of this chapter are concerned with the work on thin willemite films themselves. Section 7. 4 describes the fabrication of a p-n^+ device used for the injection of electrons into a luminescent film and Section 7. 5 describes the results obtained for this injection.

7. 2 High Field Injection

Edward's original work established that thin films of willemite ($Zn_2 SiO_4$:Mn) could be formed on a silicon substrate by the conversion of a thermally grown silicon dioxide film as described in Chapter 1. These films were shown to have a high light emitting capability when bombarded with high energy ions or electrons. It was further shown that the films could exhibit weak electroluminescence (EL) if a high field was applied across the willemite, between the silicon substrate and an aluminium contact. Edwards only observed EL with the metal biased positive with respect to the silicon substrate. His C-V measurements showed that mobile positive ions were present in the films and it was proposed that these could accumulate at the willemite-silicon interface, under the action of a positive bias to the metal. It was considered that the positive ions were possibly being prevented from discharging at the interface by the presence of a layer of uncoverted silicon dioxide. Edward's proposed that a locally enhanced field would result at the interface, which allowed electrons to tunnel into the willemite and hence to excite luminescence on impact with a Mn^{2+} ion, as shown in the band diagram of Fig. 7. 1.

More recent work by Davies [96], using much improved processing control has indicated that Edward's results may have been misleading because

of contamination introduced during the willemite film formation. Davies' results indicate that electron injection into the willemite is controlled by thin insulating films at the silicon-willemite interface, (possibly SiO_2) and/or at the willemite-aluminium interface, (possibly AlO_3, ZnO or unreacted ZnF_2). Davies has obtained many I-V and C-V plots which are consistent with electron tunnelling into the willemite through such insulating films, in addition EL has also been observed with both biasing polarities. A typical current-voltage characteristic obtained by Davies is shown in Fig. 7.2. The polarity shown is that of the aluminium with respect to the silicon substrate. A similar form of I-V characteristic has since been obtained by the author. The plots shown in Fig. 7.3 and 7.4 were obtained by using an aluminium contact of 0.5 mm diameter on a willemite film about 1000 Å thick. With a negative bias applied to the aluminium the I-V curves were reproducible with repeated increasing and decreasing cycles of bias. The curves had a characteristic shape, showing a steeply rising current in the middle voltage range which begins to flatten off at the highest applied voltages. The currents obtained for a positive polarity were, in general, non-reproducible for repeated bias cycles. There were frequent irreversible switching events leading to higher current levels for a constant applied voltage. Davies observed that thin film structures with a reasonably stable I-V characteristics, had a positive current curve which tended towards that obtained with negative polarity at the highest field values. The instabilities obtained in the present work for a positive polarities made it difficult to confirm this observation. It can be seen from the curves that, for a given thin film sturcture, a higher threshold voltage is required for an appreciable current flow under positive bias than for a negative bias. This threshold voltage was not constant and it varied greatly from sample to sample. The current magnitudes for a given positive or negative bias were fairly consistent for samples made on the same substrate but could vary by several orders of magnitude from batch to batch. In the majority of films a current of a few microamps was obtained by applying a bias of greater than $\pm$ 20V. Electroluminescence occurred in some of these samples under positive applied bias but there was no strong correlation between its incidence and the current level. During the present work EL was never observed with a negative bias. Fig. 7.5 shows I-V curves with positive bias applied to each of three aluminium dots on the same willemite film. All showed electroluminescence which was observed as a region of green light emitted from around the edge of the contact when passing a

current of about 1 μ A.

Davies has observed EL for both negative and positive polarities and he considered that for negative bias electrons were tunnelling into the willemite through a thin insulating film beneath the aluminium contact. In the present work the films were washed in an ammonia solution before metalisation in order to remove any ZnO or excess ZnF_2. This procedure was not followed by Davies; however, there is no direct evidence that films washed in ammonia cannot give electroluminescence with negative bias but unwashed films can give electroluminescence.

In some films very high currents of several hundred microamps could be obtained, although electroluminescence was never observed from these samples. The I-V characteristics of these high current samples were essentially ohmic with a resistance of the order of 1 meg-ohm. It is the authors hypothesis that the willemite films produced were relatively conducting compared with an insulating film of silicon oxide at the silicon interface. Although crystalline willemite is an insulator of band gap 5.5eV, it is possible that conduction occurs around the surface of crystalites of willemite embedded in a matrix of silicon dioxide. Electron microscope pictures taken by Edwards and Rusby [3] show the films to be of this nature. The high current samples could therefore be considered to have either a ruptured interface oxide film or the oxide film is absent. The low currents normally obtained are thought to be limited primarily by the thin interface oxide film so that current injection into the willemite, under positive bias, occurs by electron tunnelling from the silicon. A voltage applied between the silicon substrate and the aluminium contact will be dropped primarily across the oxide film resulting in a high field at the interface. Therefore according to the proposed model reproducible electroluminescence can only be achieved in a high field device through accurate control of the insulating film thickness. In a device which uses a reverse biased p-n junction as a source of high energy electrons, the interface film thickness should be minimised or ideally eliminated. Section 7.3 describes some simple experiments which were performed to obtain some understanding of the parameters which control the thickness of the oxide film at the silicon-willemite interface.

7.3 Willemite Formation Reaction Experiments

The methods used for forming thin films of willemite on a silicon substrate were based on those developed by Morant & Edwards [97] although many improvements were made in the processing techniques in order to reduce contamination. Silicon substrates of 1 Ω-cm, p-type were oxidised

in a conventional furnace at 1,000°C. When an oxide film of the required thickness had been grown, usually between 500 and 1,000 Å, the substrates were transferred immediately to a high vacuum deposition system. The vacuum was contained by a 12" glass bell jar and was pumped to a pressure of less than 10^{-6} torr by an oil diffusion pump incorporating a liquid air cold trap. A composite film of ZnF_2 and MnF_2 was coevaporated onto the oxidised silicon surface from a platinium crucible at a temperature of 855°C. At this temperature the relative vapour pressures of ZnF_2 and MnF_2 are about 100:1. An evaporation period of 10 mins resulted in a film of ZnF_2:MnF_2 about 600 Å thick. Finally the willemite film was formed by reacting together the SiO_2 and the ZnF_2:MnF_2 at a temperature between 900°C and 1100° C in either an oxygen or argon atmosphere. It was found that the lower the reaction temperature the longer the time required to produce the maximum luminescence, as excited with a Tesla coil in a simple discharge system and judged by eye. At 900°C the time taken to reach maximum luminescence was about 20 minutes compared to two minutes taken at 1100°C. Although in Edward's process the reaction was completed in an oxygen atmosphere it was found by the author that there was no detectable difference in the luminescence intensity between films formed in oxygen and those formed in argon. However, it was also found that luminescent films could be formed on a non-oxidised silicon surface by baking the ZnF_2:MnF_2 films in oxygen but not in argon. The luminescence obtained from films formed on non-oxidised silicon were never as intense as those obtained by the conventional process.

These initial observations, described above, indicate that the willemite formation process is a function of time, temperature and gas ambient during the reaction. Experiments were devised to discover approximately how the willemite reaction progresses with time. Six samples were produced with a thick initial oxide thickness of 7,000 Å. A 600 Å thick film of ZnF_2:MnF_2 was evaporated onto the oxidised surface in a standard evaporation cycle. The samples were then baked for periods of 10, 30 or 60 minutes at temperatures of either 900°C or 1100°C in an argon ambient to prevent additional oxide growth. Any ZnO or unreacted ZnF_2 on the surface after baking was removed by washing the samples in ammonia. A solution of 1% glacial acetic acid in deionised water, which was found to etch willemite in a well controlled manner, was used to remove part of the willemite film thickness. Each sample was etched for five seconds, quenched in deionised water, dried and examined

by cathodoluminescence. This procedure was repeated until no luminescence was observed, thus the number of etching cycles gave an indication of the film thickness. The results showed that for the samples baked at 900°C, the willemite film thickness increased at a rate that was very approximately proportional to $\sqrt{t}$,where t is the time of the reaction bake. This suggests that a diffusion process controls the willemite reaction growth. The thickness of the willemite formed at 1100°C appeared to be constant on each sample indicating that there may be a maximum film thickness that can be achieved by this method.

A further experiment was made in which the thickness of the oxide remaining after the removal of the willemite was measured from its capacitance. Eight samples were produced with an initial oxide thickness of 1000 Å. A thickness of 600 Å of ZnF_2:MnF_2 was deposited in a standard evaporation cycle and the samples were baked for periods of 2, 5, 10 and 20 minutes in argon at temperatures of either 900°C or 1100°C , The willemite film was etched away and an array of aluminium dots was evaporated over the residual oxide film. The average value of the oxide thickness was estimated from the average capacitance of ten dots as shown in Table 7. 1. An accuracy of only ± 15% was expected because of the variation in dot area.

	Reaction Time (Minutes)			
Reaction Temperature	2	5	10	20
900°C	950 Å	900 Å	800 Å	700 Å
1100°C	640 Å	560 Å	560 Å	560 Å

TABLE 7. 1 RESIDUAL OXIDE THICKNESS AFTER WILLEMITE REACTIONS FORMED ON INITIAL OXIDE THICKNESS OF 1000 Å.

These results substantiate the earlier findings that there is a maximum thickness of willemite that can be formed at 1100°C. If this result also occurs when the willemite is formed on thinner oxides, such as batch D1 shown in Fig. 7. 5 where the initial oxide was 600 Å and the willemite reaction was at 1100°C for twenty minutes, then the residual oxide thickness would be approximately (160 ± 70) Å. However it was not possible to verify this because the very thin

oxides ruptured when measuring the capitance.

A further parameter which was thought to be able to influence the residual oxide thickness was the amount of ZnF_2:MnF_2 deposited. Two samples were prepared with an initial oxide thickness of 2700 Å. Five evaporations were completed on each sample. depositing a 300 Å film of ZnF_2:MnF_2 in each run. In the first evaporation only 1/5th of the total sample area was exposed to the evaporant. The area of exposure was increased with each successive run to give a single sample with a ZnF_2:MnF_2 film thickness ranging from 300 Å to 1500 Å in steps of 300 Å. One of the samples was baked for $1\frac{1}{2}$ hours at 900°C in argon and the other in oxygen. With both samples it was found that the final films produced by using initial thickness of ZnF_2:MnF_2 greater than 900 Å were cracked, flaky and non-luminescent. Once these films were washed in an ammonia solution the normal appearance of the willemite film was revealed, as formed in the standard reaction. After drying these films were also found to be cathodoluminescent. The areas on which only 300 Å of ZnF_2:MnF_2 were deposited gave a noticably less bright cathodoluminescence than the remainder of the sample. It was also observed that after etching away the willemite films there was a step in the underlying oxide thickness between the areas of the 300 Å and 600 Å ZnF_2:MnF_2 film depositions. No steps were observed between the remaining areas showing that the optimum thickness of ZnF_2:MnF_2 in this reaction is about 600 Å. The thickness of the residual oxide film left under the area of thickest ZnF_2:MnF_2 deposition was judged from its interference colour and from sodium light interometer measurements to be about 2,000 Å for the argon baked sample and about 200 to 300 Å greater for the oxygen baked sample. This would indicate that either additional oxide growth had occured beneath the willemite in the oxygen baked sample or that less oxide had been consumed. However, the method of estimating film thickness was not sufficiently sensitive to allow a more detailed investigation of the effect of the ZnF_2:MnF_2 film thickness on the residual oxide thickness after willemite formation.

The experiments described above show that the parameters, ZnF_2:MnF_2 film thickness, reaction temperature, time of reaction and ambient gas during the reaction all influence the growth of the willemite films. However, the experiments give very little quantative information and they highlight the need for much more sensitive film thickness measurements techniques if there is to be sufficient control over the willemite reaction process, to give reproducible electroluminescence. Since the work described in this thesis was

done an ellipsometer has been built in the Department which has allowed precise measurements to be made of the willemite and residual oxide thicknesses. This later work will be described elsewhere in a forthcoming thesis [98]. In the present work it was considered that an electroluminescent device, based on hot electron injection from a reversed biased p-n junction into thin willemite films, would be less critically dependent on the residual oxide film thickness. This is because the p-n junction injection structure would determine the electron injection energy and current independently of the residual oxide thickness. An ideal device would have zero residual oxide; however, experiments have not yet indicated if this is possible. In the injection devices described in the following sections the residual oxide thickness has been measured to be less than 100 Å.

7.4 Device for Hot Electron Injection into Willemite

The basic p-n junction structure used in this work is the same as that described in Chapter 3 and used for electron injection into SiO_2. Instead of oxide a thin film of willemite was formed over the shallow junction area, and it was hoped to excite luminescence by the direct impact collision of a Mn^{2+} ion by a high energy electron injected from an avalanching junction. The lowest theoretical electron energy necessary for the direct impact excitation of a Mn^{2+} ion in Zn_2SiO_4 is 2.64 eV. A form of 'internal cathodoluminescence' may therefore be possible since electron injection into SiO_2 over a 3.25 eV barrier has already been demonstrated in Chapter 5. It is probably more reasonable to expect that higher electron energies would be required which could, perhaps, be produced by the additional application of a field across the willemite film.

The major problem in fabricating devices with a thin film of willemite over the shallow junction area was that the best cathodoluminescent films were formed in periods in excess of ten minutes at a minium temperature of 900°C. Such a heat treatment would be expected to drive in the phosphorus diffusion to a depth greater than 0.25 μm and hence no electron injection would be expected. This would have been much less of a problem if arsenic could have been used in place of the phosphorus for the shallow diffusion; however this was not possible at the time of this work. The problem was resolved in a less satisfactory manner by the discovery by the author that cathodoluminescent films could be formed by depositing 600 Å of ZnF_2:MnF_2 on to non-oxidised silicon and heating to 850°C in a wet oxygen atmosphere. After the reaction was complete there was a non-luminescent surface on the films which could be removed by washing in an ammonia solution. This process left a film about 500 Å thick which was cathodoluminescent but

less bright than those described earlier and giving a more yellow, light emission. Pfeiffer et al [99] has also reported a yellow light emitting form of willemite produced in a reaction of ZnO with SiO_2 at 850°C. Under an optical microscope the film structure was very granular as can be seen in Fig. 7.6b. Despite the poorer quality of the films from those normally produced the luminescence was unaffected by the presence of phosphorus in the silicon junction and they were considered adequate for an initial investigation. Ellipsometer measurements showed there to be an oxide layer under the luminescent film of 80 Å thickness which should be thin enough to allow a high proportion of the high energy electrons to conduct through and into the willemite.

The luminescent films produced in the above reaction were found to be compatible with the standard photo-lithography used in modern silicon technology and described in Appendix 2. The luminescent film was first formed over the entire area of the silicon sample. Mask 3 as shown in Fig. 3.4 was then used to define areas of willemite only in the shallow junction area by exposing Shipley photo-resist. The exposed resist was baked on the film at 90°C for twenty minutes and then an etch of 10% glacial acetic acid in deionised water was used to remove the unwanted willemite film. After etching, the photo-resist was cleared from the willemite by using Shipley ion free remover. The luminescence of the remaining film was unaffected by the photo-lithographic procedure.

After definition of the willemite pattern the devices were completed by defining the aluminium metal contact pattern. This presented a problem with the willemite thin film devices since the phosphoric acid normally used to define the aluminium also attacked the luminescent films. This problem was resolved by using a solution of NaOH to etch the aluminium as described in Appendix 2. However, this etching procedure required that the photo-resist should be baked on the aluminium at 120°C for thirty minutes which made it very difficult to remove without also destroying the luminescent or aluminium films. Shipley photo-resist remover could be used if a very tight control was maintained over the temperature of the removing solution and the time of the removal period, as described in Appendix 2. Another method of defining the metal contact pattern was to form a reverse photo-resist pattern on the sample before evaporating the aluminium. The aluminium adheres very strongly to the areas of oxide and luminescent film, where the photo-resist has been developed away, and after evaporation the remaining photo-resist and the overlaying metal could be removed by immersion in acetone. However, the metal definition quality was not as

good by this method as obtained by etching in NaOH.

A typical finished device is shown in Fig. 7.6a. The formation of the luminescent film above the shallow junction produced no change in the measured sheet resistance which was of the order of 200 Ω / □ . The final depth of the shallow junction was of the order of 1000 Å. The reverse bias characteristics of the junctions were, in general, much softer than those obtained for the thin oxide covered devices although the point of avalanche was usually apparent, as shown in Fig. 7.15. The degradation of the junction characteristics may have been caused by Zn diffusing into the silicon. It has been shown by Goetzberger and Shockley [100] that metal precipitates can be responsible for soft junction characteristics. Another feature of the junctions produced with luminescent films compared with those with thin oxide films was that visible microplasmas were much less in evidence. However, in all junctions avalanche breakdown voltage had to be reached before any injection could be detected.

7.5 Results for Electron Injection into Luminescent Films

The circuit used for the detection and measurement of the currents injected into thin luminescent films was the same as that shown in Chapter 5, and used for injected currents into SiO_2. A family of curves is shown in Figs. 7.7, 7.8, and 7.9 for the injected film current I_f against the junction current I_j for a range of positive voltages applied across the film. In most devices no injected current was detected with junction currents of less than 1.0 mA although one exception is shown in Fig. 7.10. The probable reason for the higher junction current requirement was the high leakage characteristics of the junctions. It was noted that the device, for which the injection characteristics are shown in Fig. 7.10, had a much harder junction breakdown than was normal. It was found that on all the devices measured, that an injection current could be detected by applying a voltage across the luminescent film as low as 1.0 V, which was much less than that required for the oxide covered devices discussed in Chapter 5. A further difference between the injection characteristics obtained with the luminescent film devices and the thin oxide devices was that the rate of increase of the injection current with film bias was not constant but increased with junction current. The injected current in the luminescent film devices increased almost exponentially with junction current, as in the oxide devices. However, the different reverse junction characteristics do not allow a meaningful comparison to be made for the rates of increase in injected current with junction current. At the highest junction current levels there is evidence of a fall off in the rate of increase of the injected current level. This usually occurs for injected current levels of the order

of 10^{-10} A but this value can vary considerably from device to device.

A common feature of the injection characteristics obtained with luminescent films was an irreversible switching event as shown in Fig. 7. 10. A series of these switching events can also be seen in the results of Fig. 7. 11. In this device the switching was not observed until the junction current was increased from zero in a second cycle. A few devices also showed both positive and negative switching as shown in Fig. 7. 12. The instabilities observed in the luminescent films were similar to those obtained when measuring currents in very thin silicon dioxide films of less than 300 Å thick, as discussed in Chapter 5. None of the devices tested were able to withstand a film bias voltage of greater than 8. 0V without a breakdown event. Once breakdown had occurred the resistivity across the film dropped, such that a current of 1 μA could be passed using a film bias of 1 volt and with zero junction current. The nature of this I-V characteristic was similar to that obtained with the earlier thin film structures described in Section 7. 2, where it was considered that was either no oxide between the willemite and the silicon or that the oxide had ruptured.

One sample from batch W2 included several devices which gave a small light output when the junction was avalanched. The light emission was extremely weak and could only be seen by dark accustoming the eye. The light emission was quite unlike that previously associated with microplasmas which was usually from a well defined area and a white emission. In the W2 devices the light appeared to be coming from a large part of theshallow junction, not covered by the aluminium, and was a diffuse, yellowish emission. A photomultiplier tube was placed over the device and the light output was measured giving the results shown in Fig. 7. 13. The light output was found to increase smoothly with junction current but there was no increase in intensity with bias applied across the film. The absence of any variation in light intensity with film bias may have been because the field was not being sustained across the luminescent film itself or because any increase below the aluminium contact could not be seen. An attempt was therefore made to fabricate devices with half the film contact of thin enough aluminium to be semitransparent, using masks 6 and 7 as shown in Fig. 3. 4. These experiments were unsuccessful since no light output from the willemite was observed in this case and time did not allow further devices to be made.

For the device showing light output it was found that the light intensity fell off after the device had been operating for about ten minutes. The intensity recovered after the junction current had been turned off for a few minutes indicating that a heating effect was the cause of the fall off.

A hundred volt pulse was applied to the junction causing it to avalanche, at the same time the light output was monitored by a photomultiplier connected to an oscilloscope. The voltage pulse to the junction is shown in Fig. 7. 13a and the photomultiplier output pulse is shown in Fig. 7. 13b. It can be seen that the photomultiplier pulse was very noisy which is characteristic of microplasma pulses observed by other workers[101].

7. 6 Conclusions

The initial work with simple thin film structures indicated that, the willemite reaction process described resulted in thin films that had a much higher conductivity than would be expected for single crystal willemite. A possible explanation was that the films consisted of willemite crystallites in a silicon oxide matrix, and that conduction was occurring across the surface of interconnecting crystallites. It was considered that in the majority of the films, electron injection from the silicon was being limited by a thin oxide film between the silicon and the willemite. Therefore electroluminescence could only be achieved in a high field injection structure if the interfacial oxide film thickness was optimised. Under favourable conditions of both applied bias and oxide film thickness at the interface electrons could tunnel from the silicon into the willemite and excite luminescence.

A procedure was devised for the fabrication of a p-n junction structure for the injection of high energy electrons into a luminescent film. It was found that the reverse bias characteristics of the junctions were degraded by the luminescent film reaction. This necessitated using a higher junction current, before injection into the luminescent films was observed, than had been used for injection into silicon dioxide. However, the form of the injection had similar characteristics for both types of film.

The results obtained for injection into luminescent films show that unpredictable breakdown events could occur. These were similar to those described in Chapter 5, which were observed using very thin silicon dioxide films less than 300 Å thick, and those observed by Osburn and Weitzmann[57] during high field injection. In the present willemite film devices, later ellipsometer measurements showed there to be a residual silicon dioxide thickness of less than 100 Å. It is therefore possible that the electron injection in these devices was also being limited and that the breakdown events were occurring at weak points in the oxide films. Some of these breakdowns must have been self healing[102] as the current usually switched to a higher level without resulting in a short circuit.

The dependence of injection on junction current was consistent with the model of electron injection from a microplasma as proposed in Chapter 6. However, the emission of light from some of the films or junctions suggests that injection may be occurring from a larger area. The observed increase in the rate of injected current with junction current at higher film bias voltages may be accounted for by the conducting nature of the luminescent film. This would mean that the current collecting area of the aluminium contact is also a function of the film bias.

The emission of light from some samples was encouraging, although the exact origin is not yet clear. The high noise level observed in the pulsing experiments indicate that the emission was associated with microplasma behaviour. However, the emission may be a result of electron-hole recombination in the avalanching junction, and not hot electron injection from a microplasma exciting a luminescent centre in the willemite film. Since the emission was from a greater area than previously observed from avalanching junctions, and was a yellow rather than a white light, electron-hole recombination in the junction is considered to be an unlikely origin of the emission. The yellow colour of the emission was similar to the cathodoluminescence appearance of the films, although an exact judgement was difficult due to the very low intensity. More work is therefore necessary to establish the exact origin of the emission. In Chapter 8 methods will be discussed for fabricating devices with more efficient luminescent films.

The work discussed in this Chapter is mainly exploratory, but it has been successful in solving some of the technological problems in making a hot electron injection luminescent device. Further problems have been highlighted which are also discussed in Chapter 8. The work therefore provides a useful base for future work involving more detailed measurements which could be compared with the results obtained from electron injection into silicon dioxide thin films.

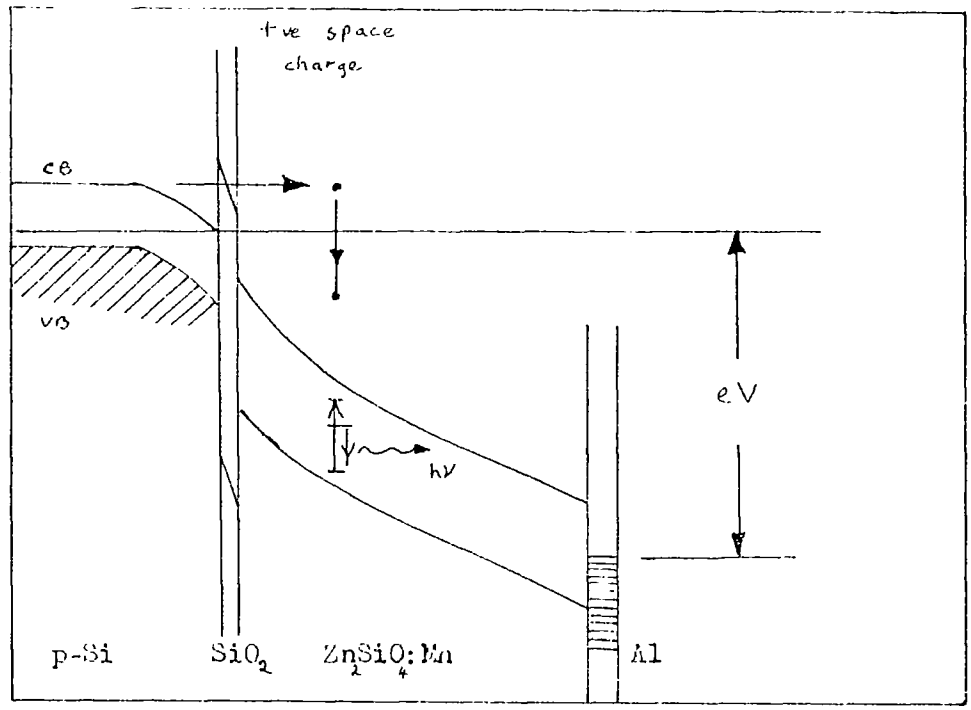

FIG 7.1 Ref.2
EDWARDS' SPACE CHARGE MODEL FOR ELECTRON INJECTION INTO WILLEMITE WITH A POSITIVE APPLIED VOLTAGE.

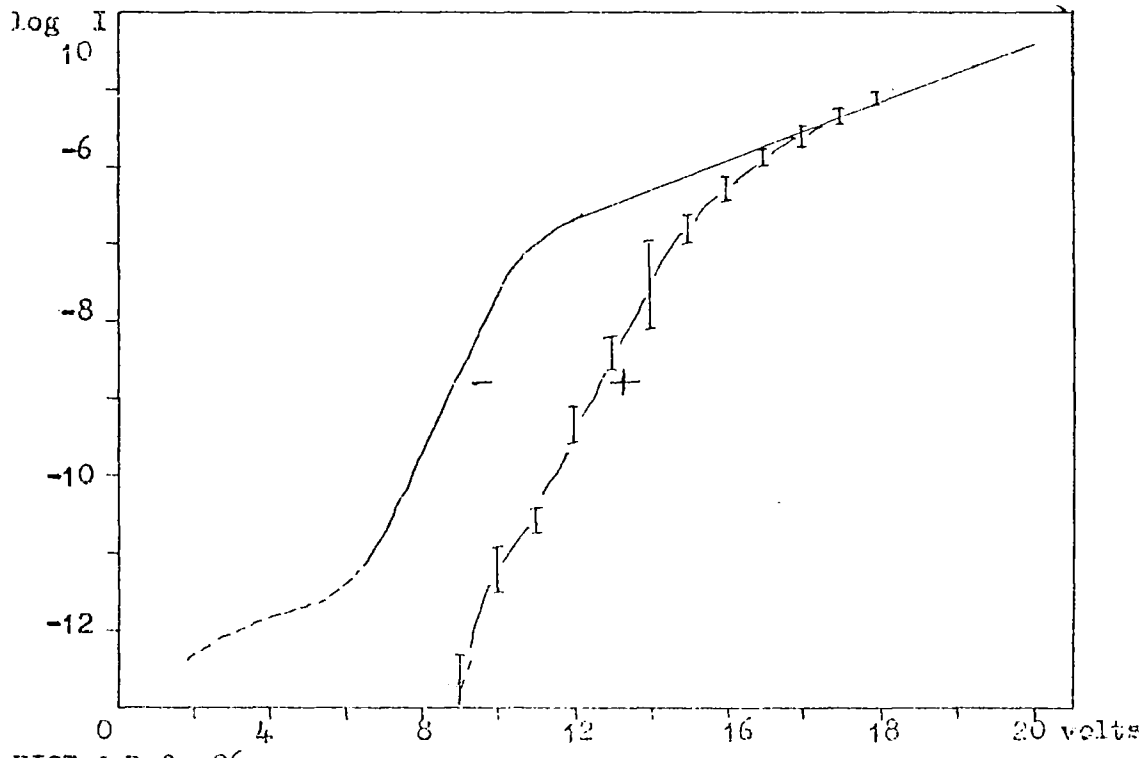

FIG7.2 Ref. 96
I-V CURVES OBTAINED BY DAVIES FOR POSITIVE AND NEGATIVE VOLTAGES APPLIED TO THIN WILLEMITE FILMS ON SILICON.

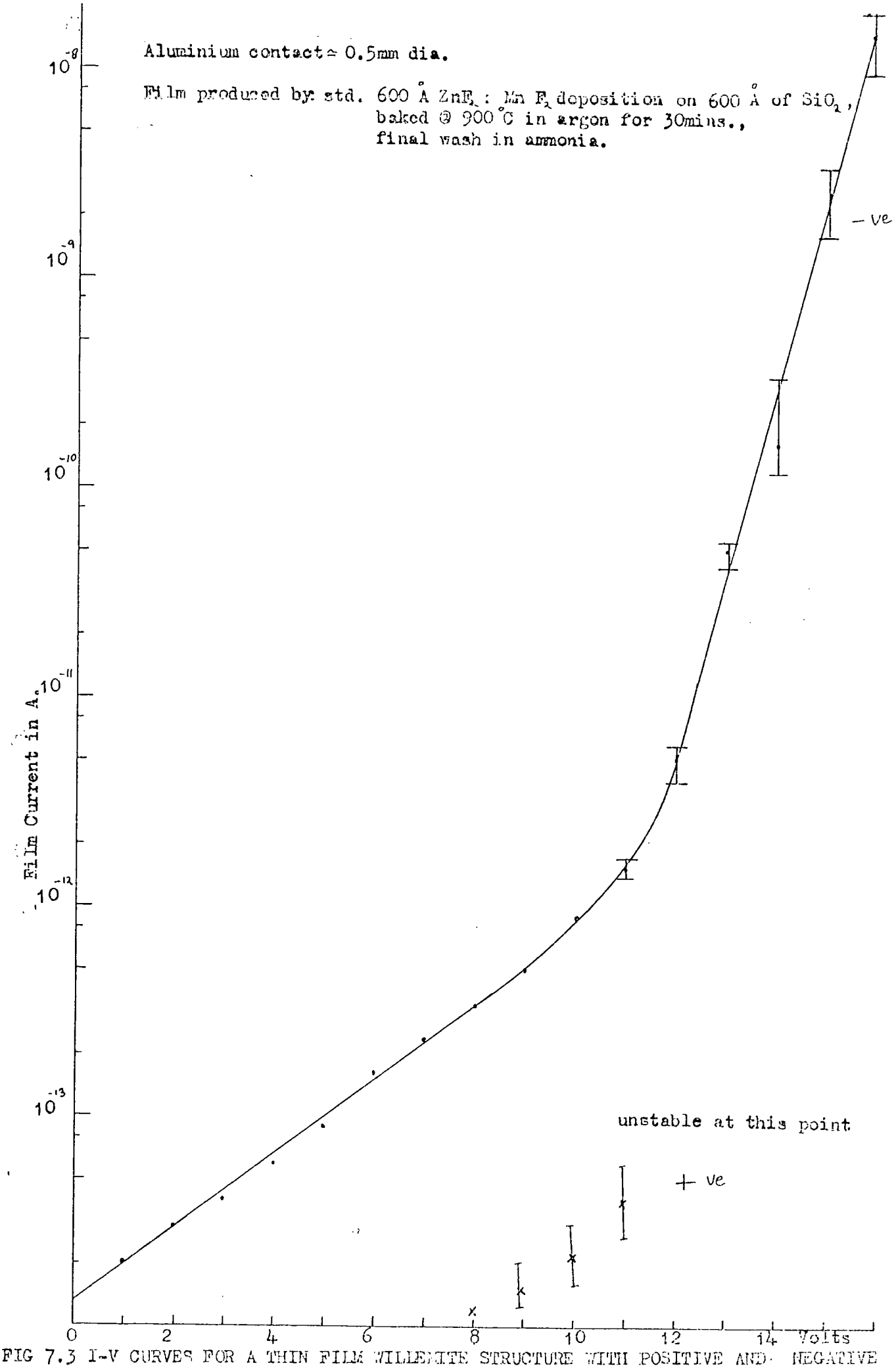

FIG 7.3 I-V CURVES FOR A THIN FILM WILLEMITE STRUCTURE WITH POSITIVE AND NEGATIVE APPLIED VOLTAGES.

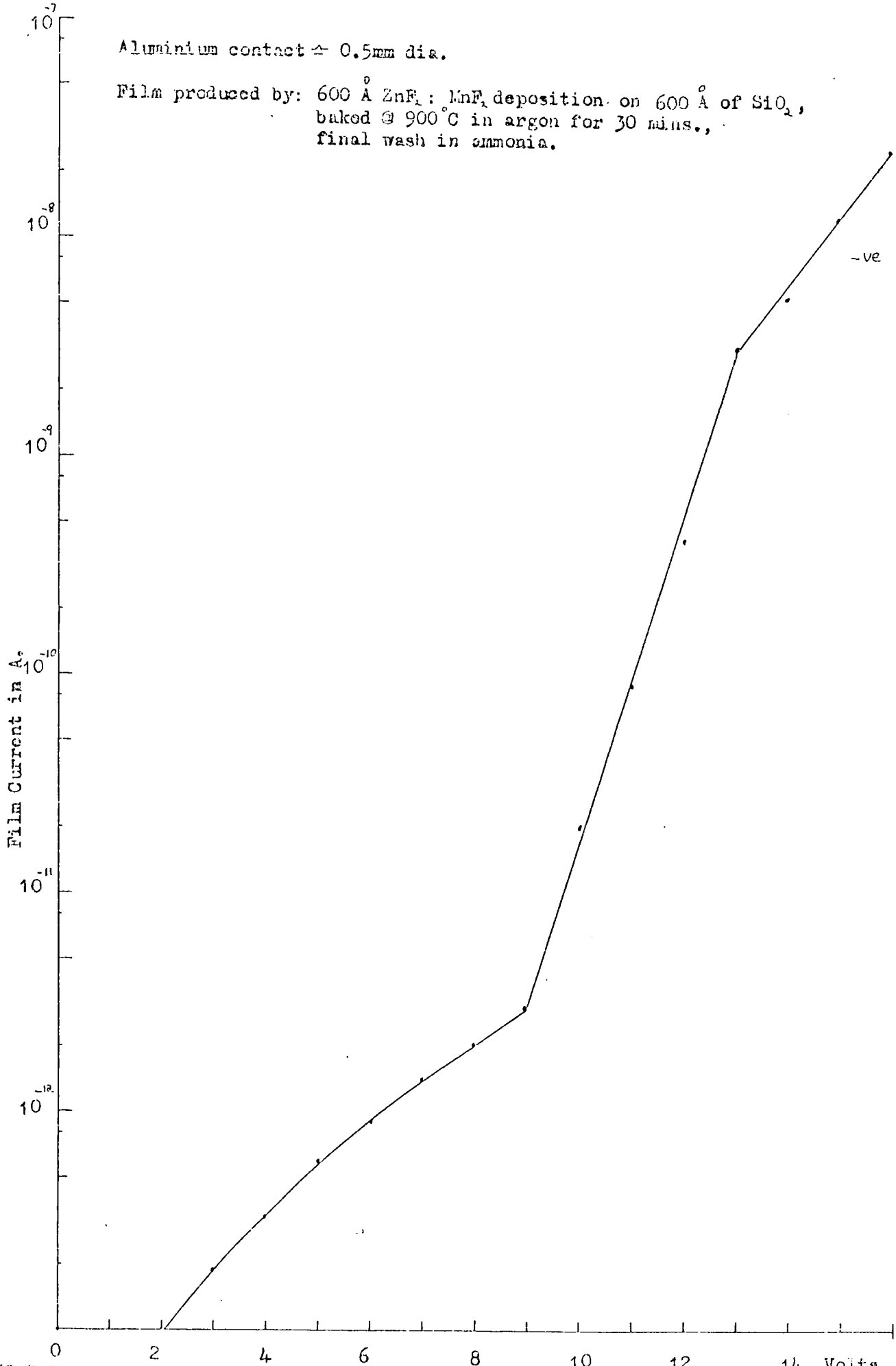

FIG 7.4 I-V CURVE FOR THIN FILM WILLEMITE STRUCTURE WITH NEGATIVE APPLIED VOLTAGE

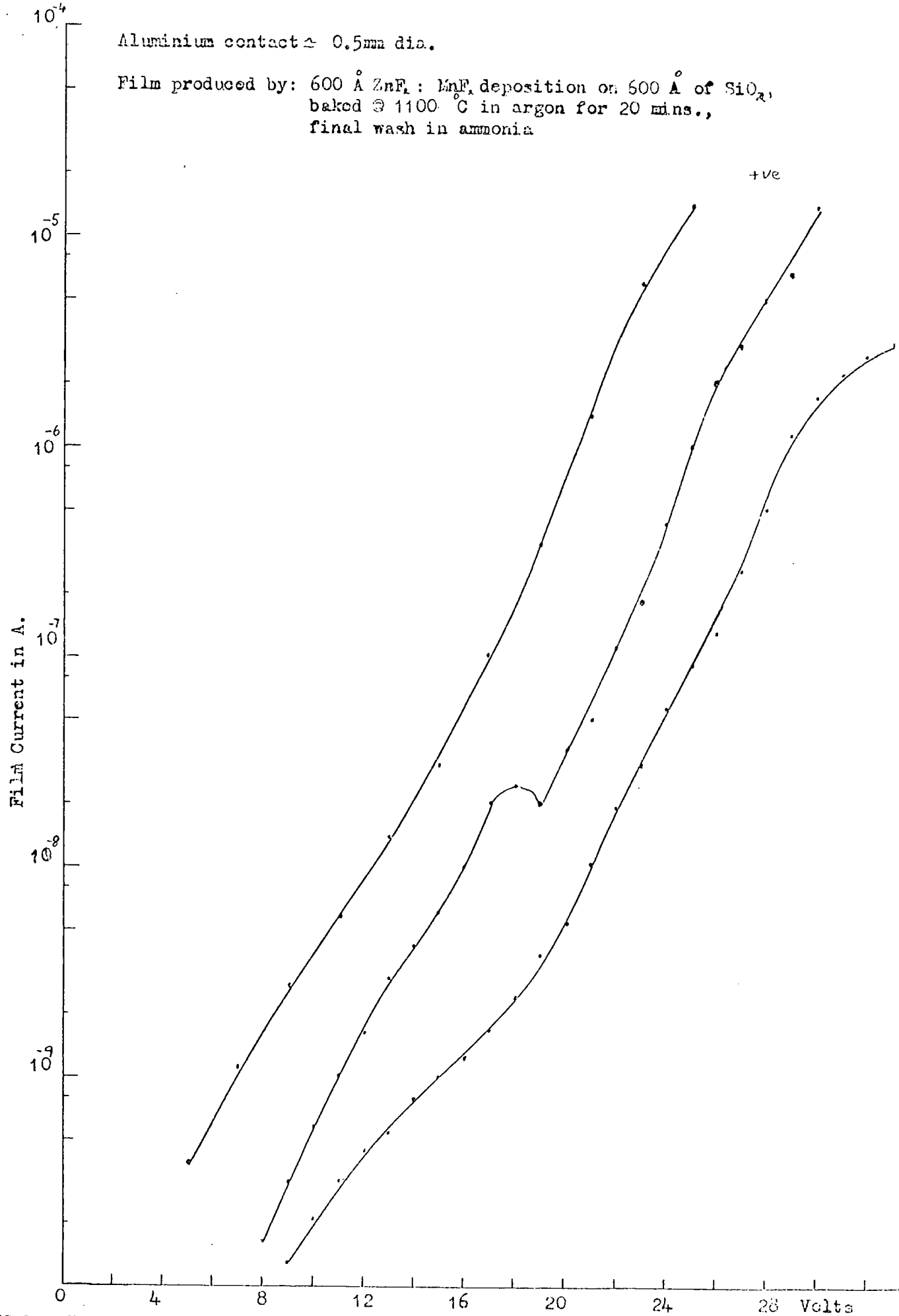

FIG 7.5 I-V CURVES FOR THREE CONTACTS ON THE SAME FILM, ALL OF WHICH GAVE EL WITH POSITIVE APPLIED VOLTAGE.

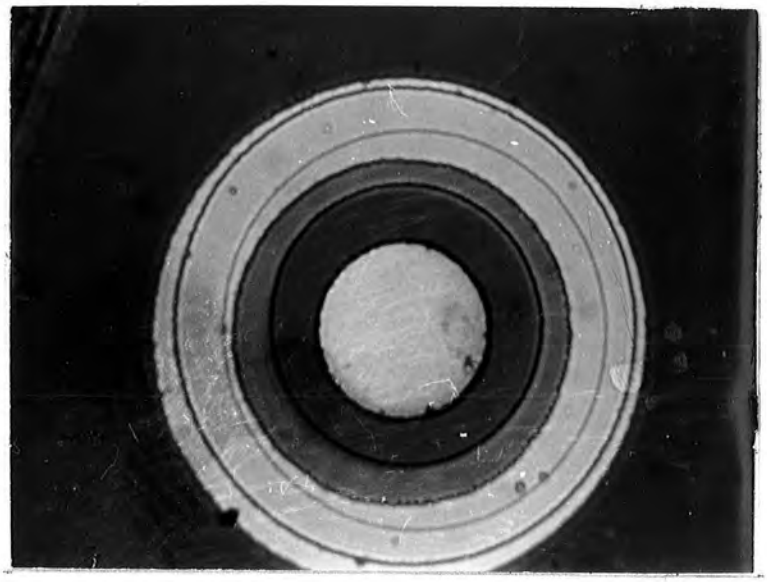

FIG 7.6 a COMPLETED DEVICE WITH WILLEMITE FILM

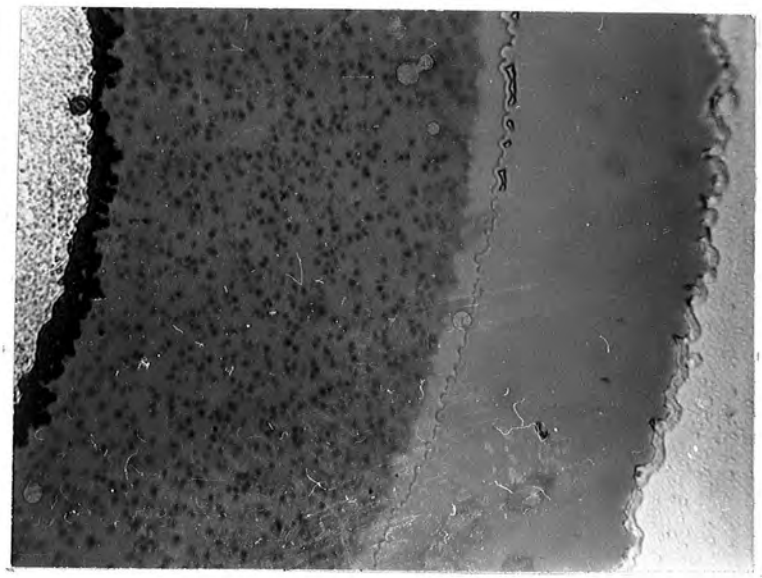

FIG 7.6 b ENLARGEMENT OF WILLEMITE FILM
SHOWING GRANULAR EFFECT

FIG 7.7 INJECTION INTO LUMINESCENT FILM USING A pn JUNCTION DEVICE
(With positive voltage bias to the film.)

Batch W2 Device A1
Film produced by: 600 Å ZnF_2 : MnF_2 depositon on P doped Si,
baked @ 850°C in wet O_2 for 5mins.
final wash in ammonia.

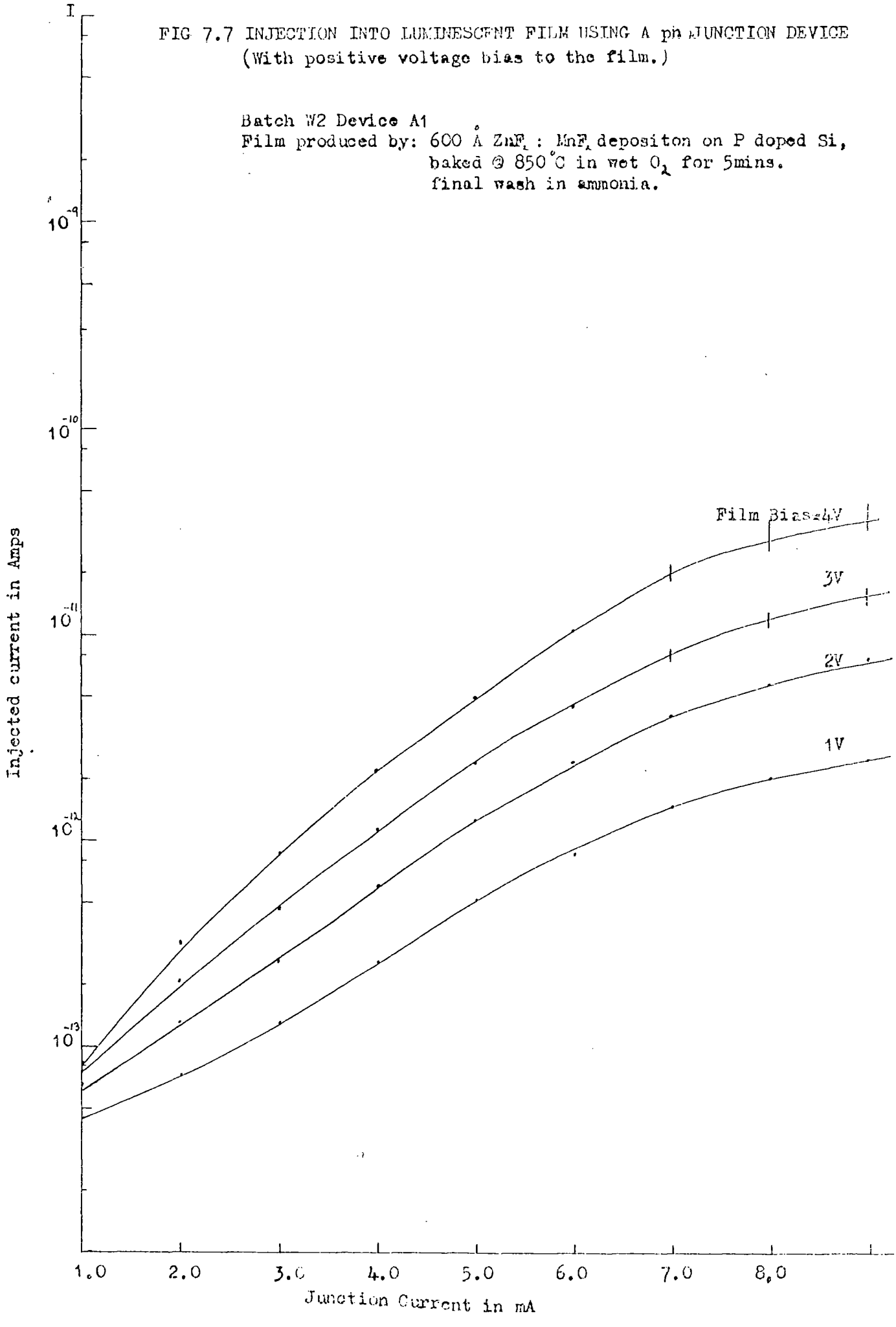

FIG 7.8 INJECTION INTO LUMINESCENT FILM USING A pn JUNCTION DEVICE
(With positive voltage to the film.)

Batch W2 Device A3
Film produced as in FIG 7.7

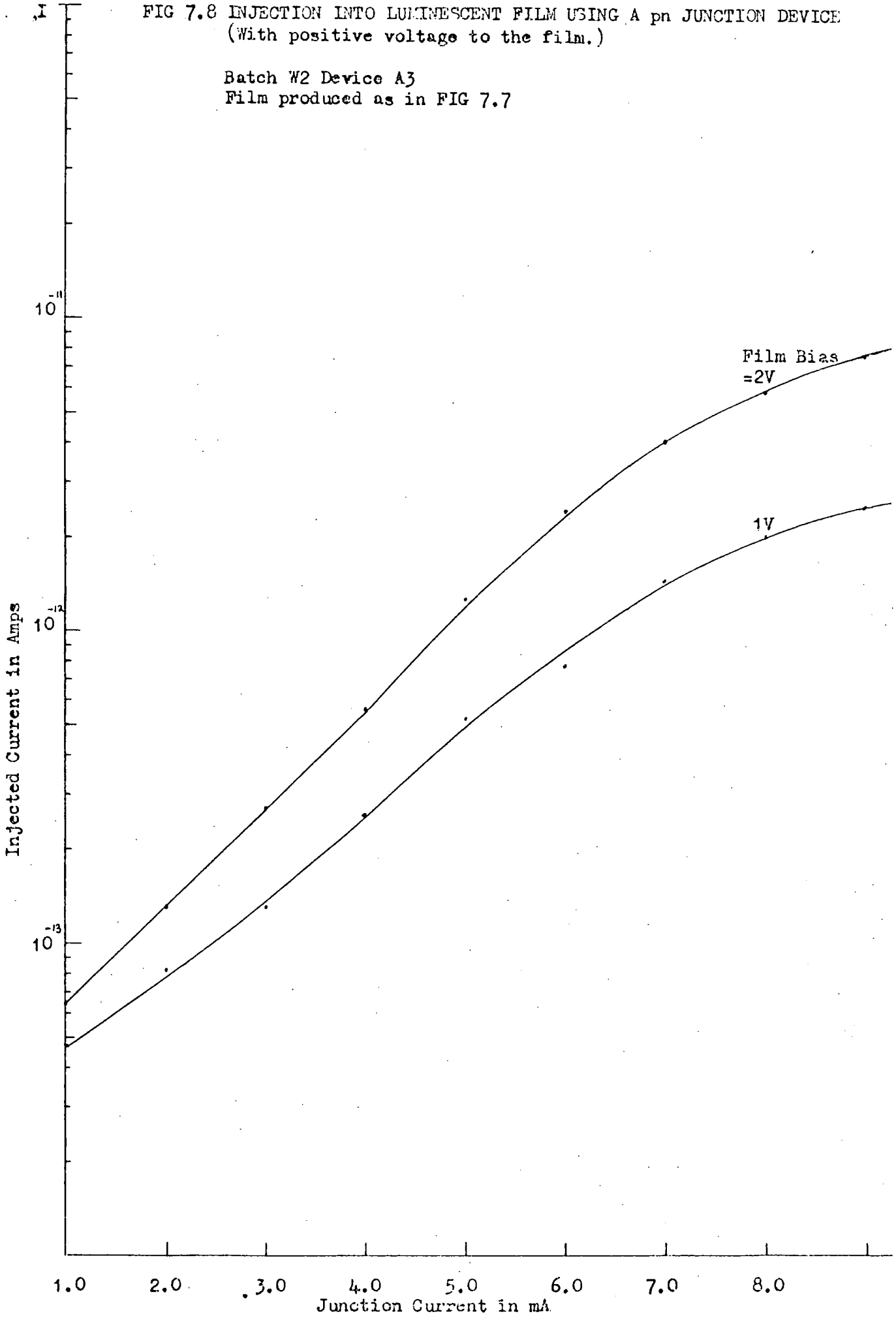

FIG 7.9 INJECTION INTO LUMINESCENT FILM USING A pn JUNCTION DEVICE
(With positive voltage bias to the film.)

Batch W3 Device C3
Film produced as in FIG 7.7

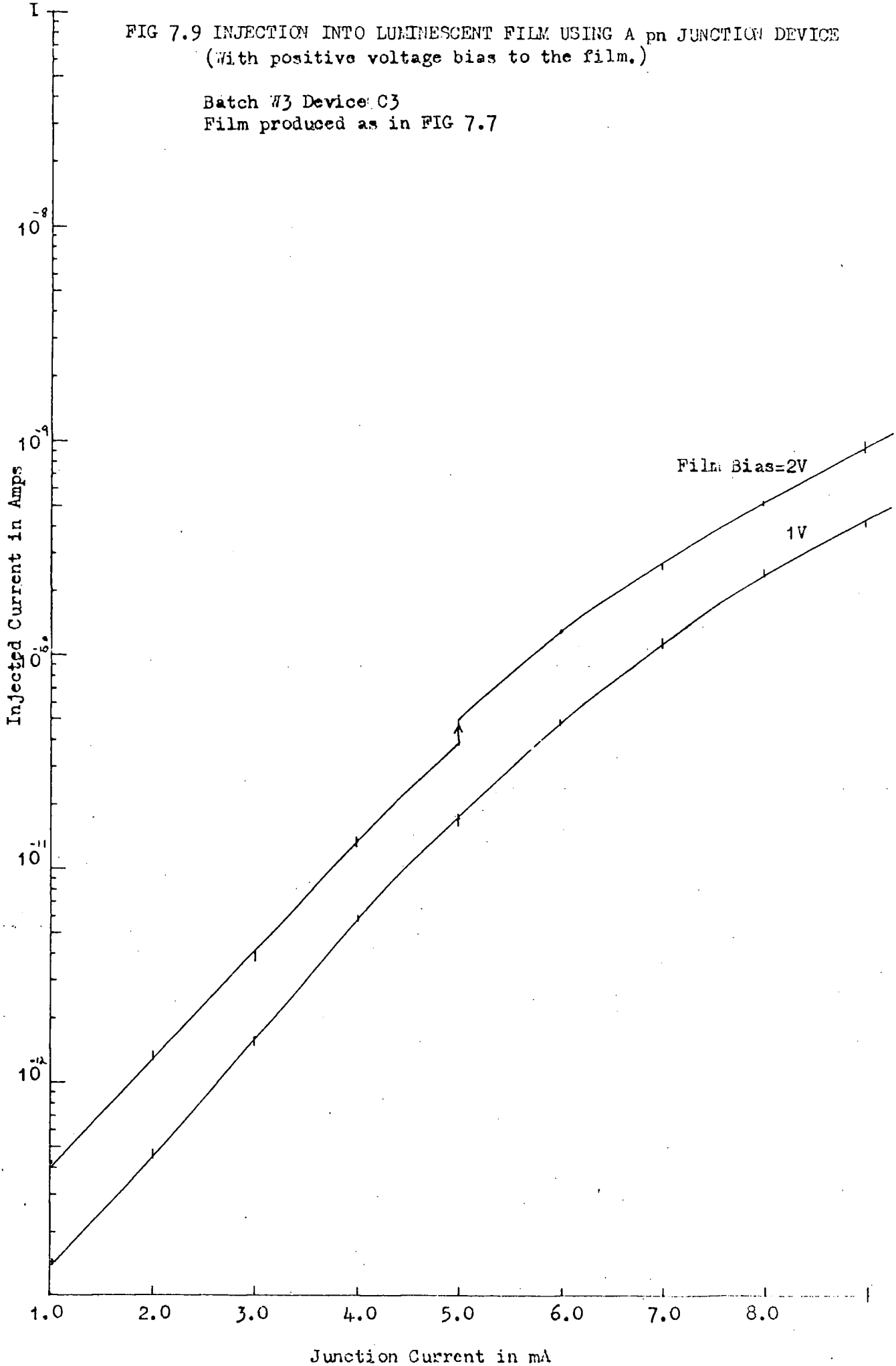

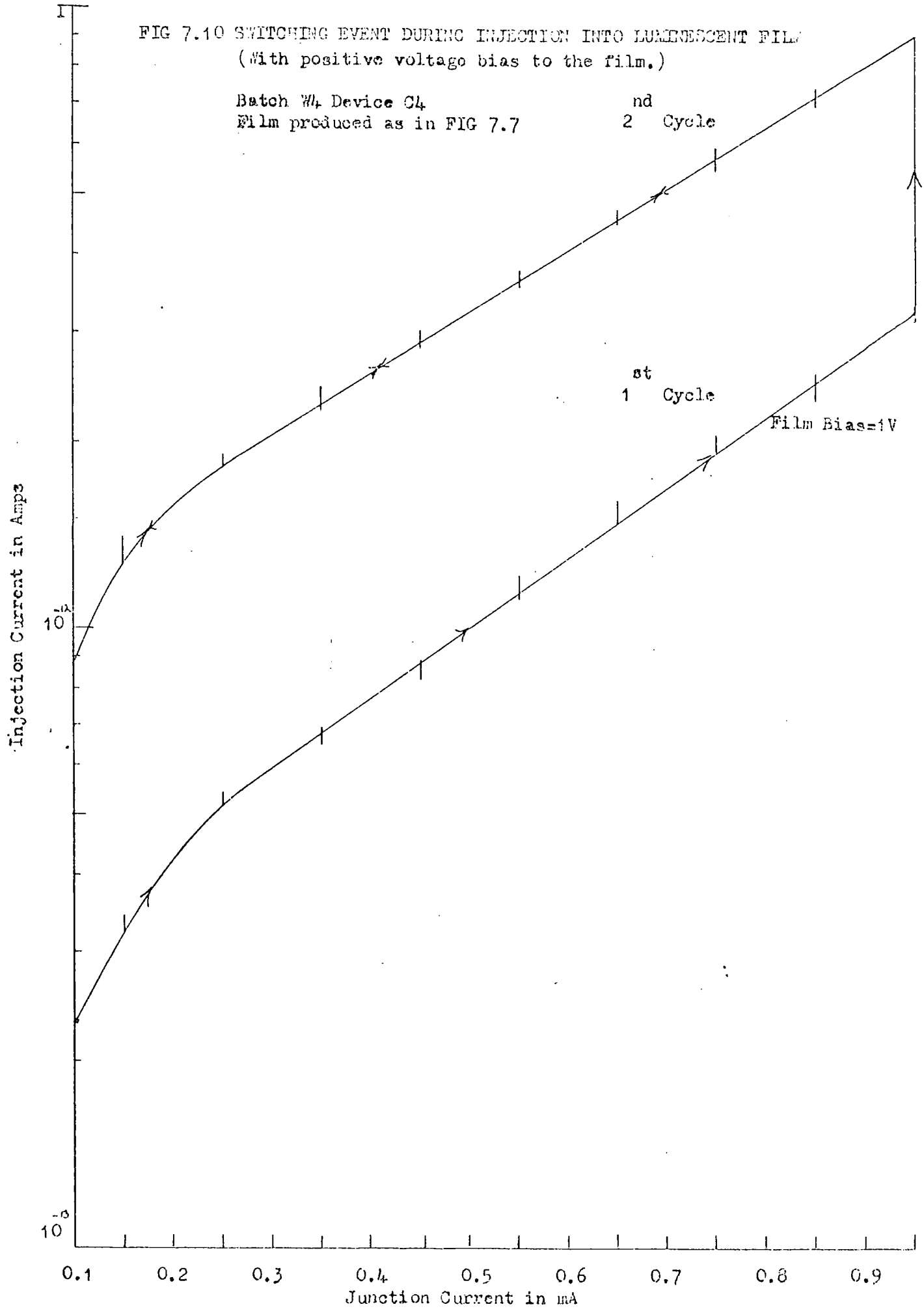
FIG 7.10 SWITCHING EVENT DURING INJECTION INTO LUMINESCENT FILM
(With positive voltage bias to the film.)
Batch W4 Device C4
Film produced as in FIG 7.7
2nd Cycle
1st Cycle
Film Bias=1V
Injection Current in Amps
10^-4
10^-5
0.1
0.2
0.3
0.4
0.5
0.6
0.7
0.8
0.9
Junction Current in mA

FIG 7.11 A SERIES OF SWITCHING EVENTS DURING INJECTION INTO LUMINESCENT FILMS
(With positive voltage bias to the film.)

Batch W6 Device B2
Film produced as in FIG 7.7

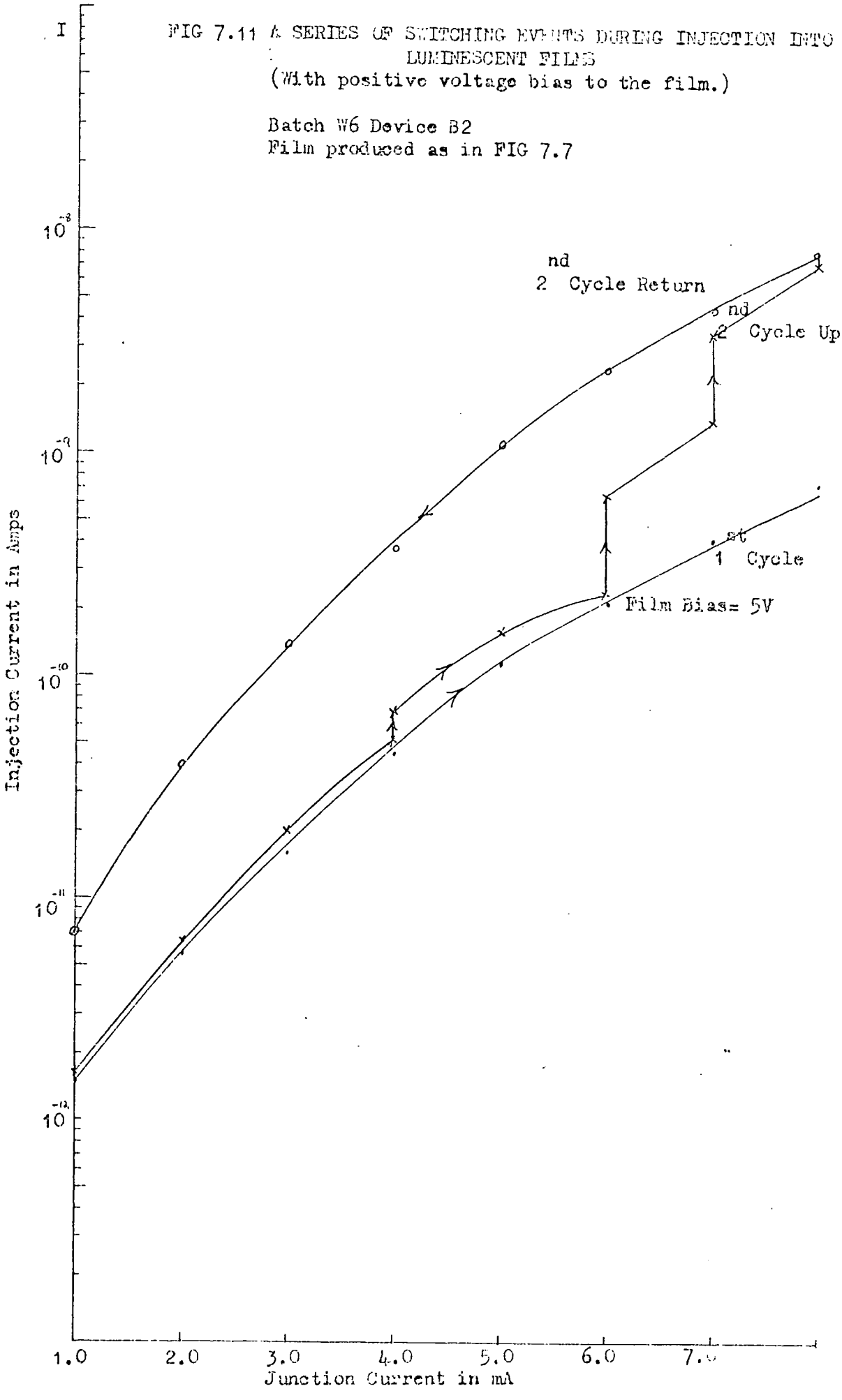

FIG 7.12 SWITCHING EVENTS TO HIGHER & LOWER CURRENT LEVELS
(With positive voltage bias to the film.)

Batch W4 Device A2
Film produced as in FIG 7.7

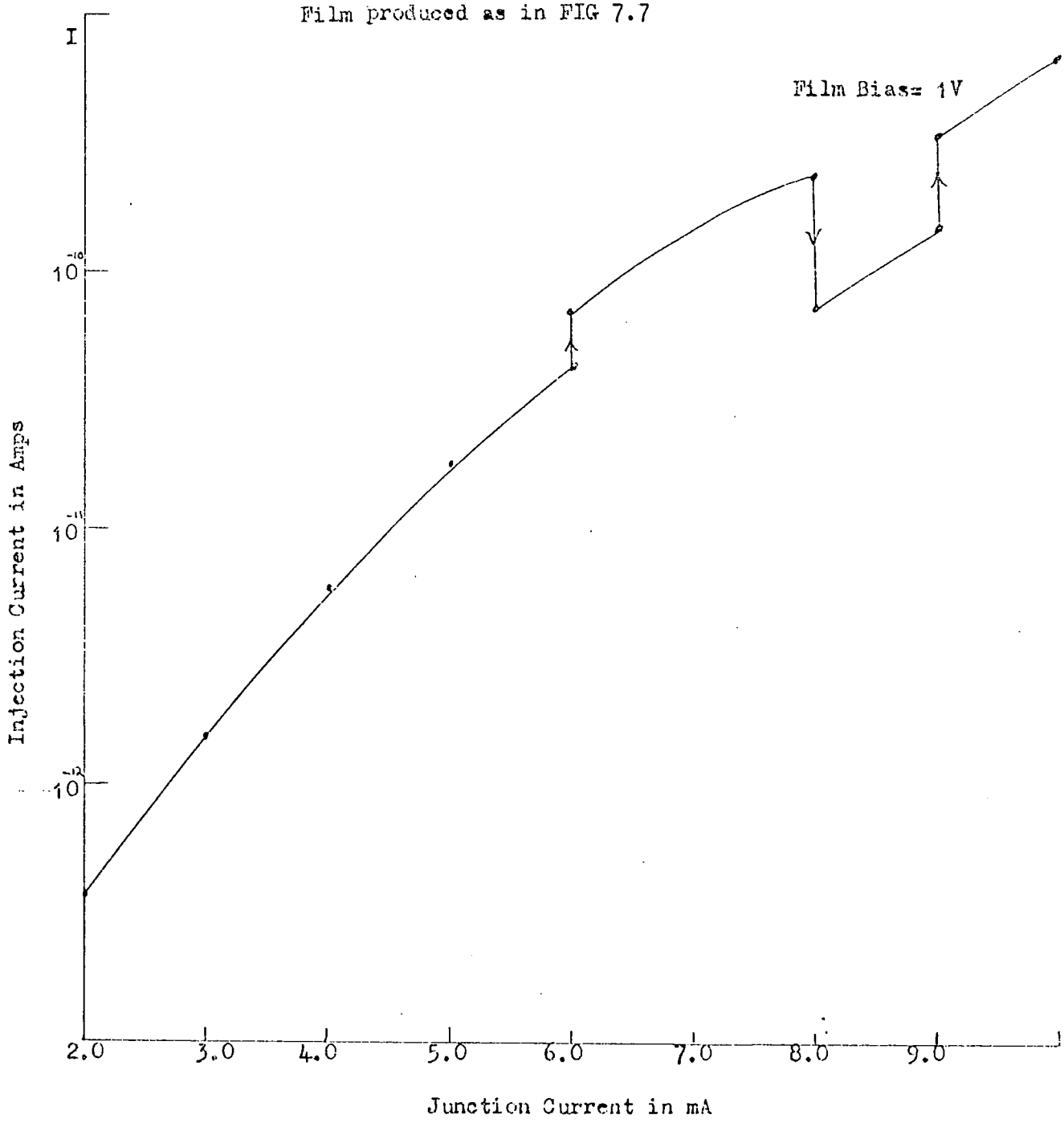

FIG 7.13 PHOTO-MULTIPLIER OUTPUT DUE TO LIGHT FROM A LIGHT EMITTING DEVICE.

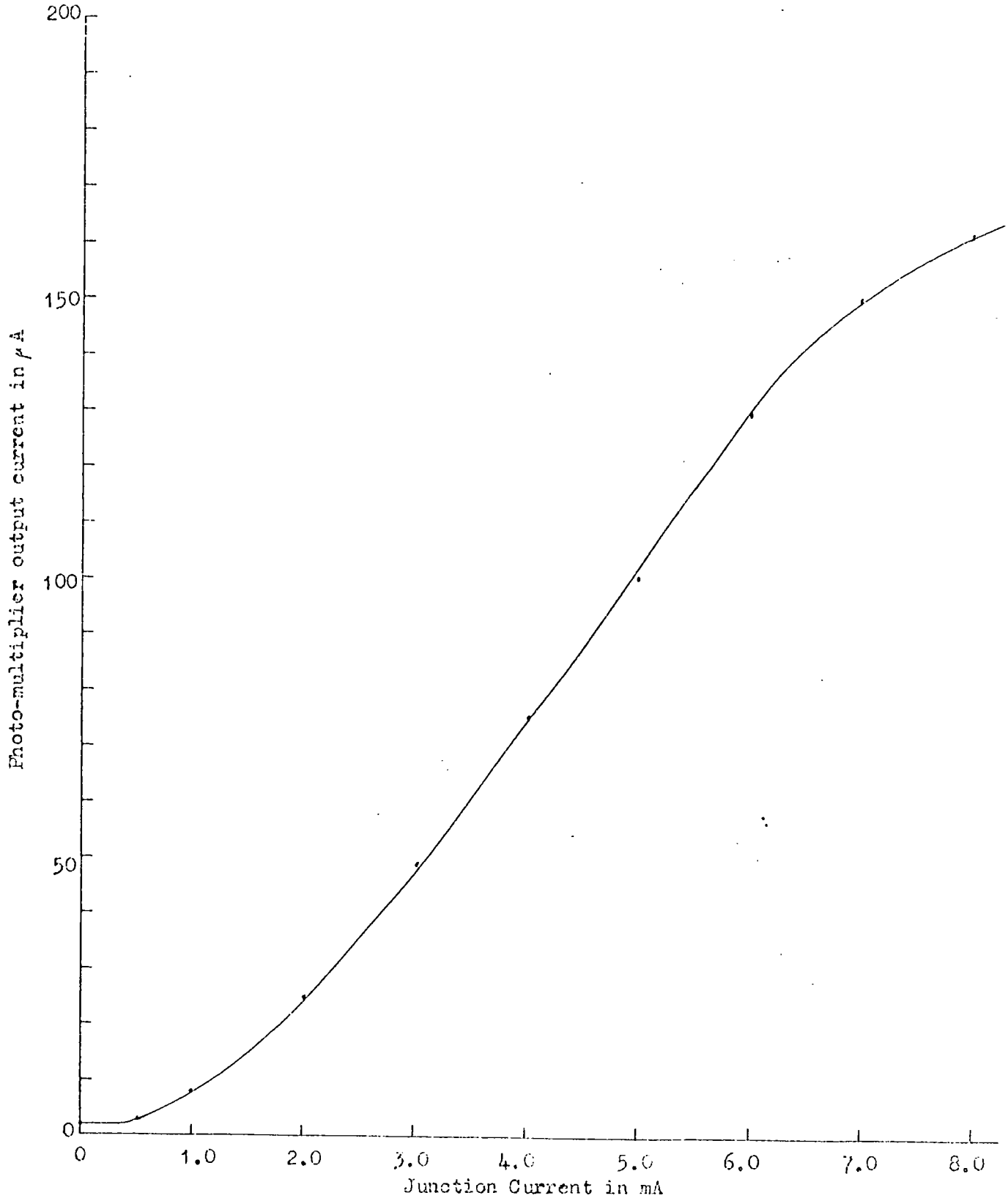

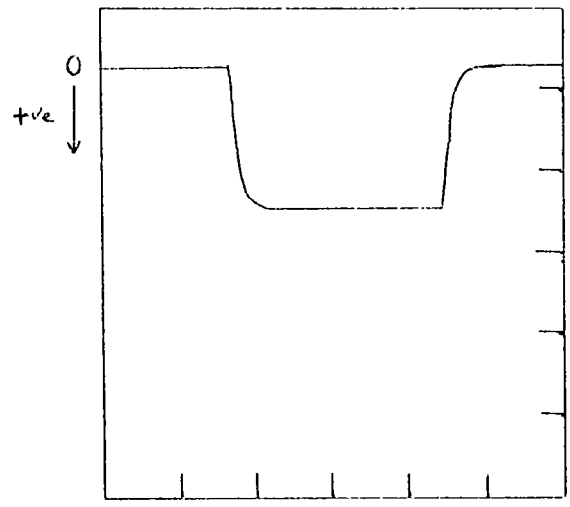

HORIZ. 10 m sec/cm

VERT. 50 V/cm

POSITIVE INPUT PULSE APPLIED TO THE n-TYPE GUARD RING OF THE DEVICE.

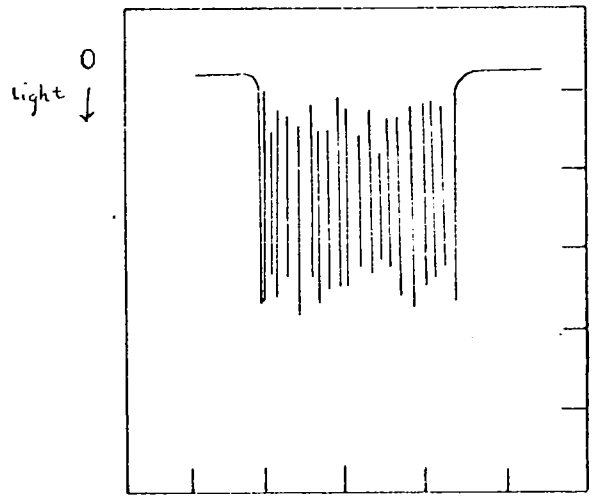

HORIZ. 10 m sec/cm

VERT. 5 V/cm

OUTPUT PULSE FROM PHOTO-MULTIPLIER

FIG 7.14 OSCILLOSOPE TRACES FOR A PULSE APPLIED TO THE INJECTION DEVICE

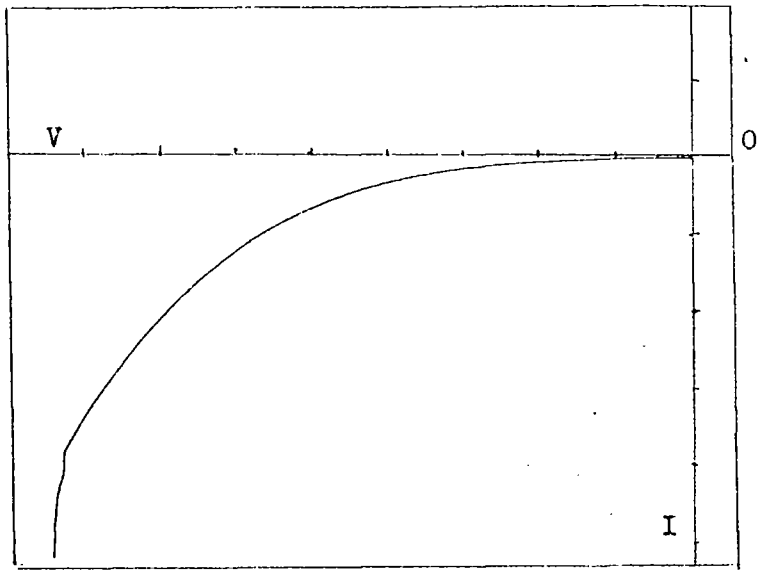

HORIZ 10 V/cm

VERT. 0.1mA/cm

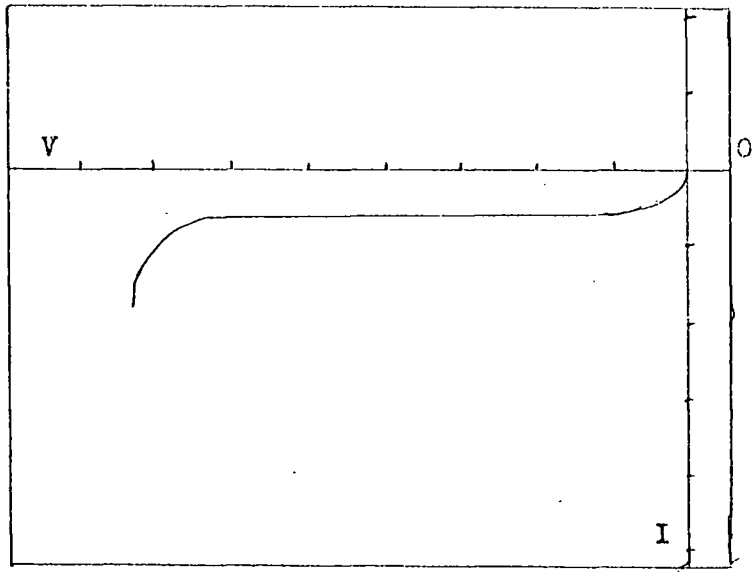

HORIZ. 10 V/cm

VERT. 0.5mA/cm

FIG 7.15 TYPICAL REVERSE BIAS JUNCTION CHARATERISTICS FOR DEVICES ON WHICH THE SHALLOW $p\text{-}n^{+}$ JUNCTION IS COVERED WITH A WILLEMITE THIN FILM.

(Taken from an oscillosope curve tracer)

CHAPTER EIGHT

CONCLUSIONS AND SUGGESTIONS FOR FURTHER WORK

8.1 Present Research

The greater part of this thesis has been concerned with consideration of the use of a reverse biased p-n junction to accelerate electrons to high energy, and to inject those electrons into the conduction band of thin films of SiO_2 and luminescent Zn_2SiO_4:Mn. This is believed to be the first time that electron injection into thin films from a shallow planar junction has been reported. All previous published works, on injection into SiO_2, have exploited avalanching at the surface boundary region of deep p-n junctions or pulsed surface avalanched M.O.S. structures.

The interpretation of the experimental results indicate that electron injection occurs from micropiasmas, and that the electron-hole population could be approximated by a Maxwellian energy distribution. An exact mathematical description is not yet available, but the results presented in Chapters 5 and 6, suggest that the true distribution probably contains fewer charge carriers with energies greater than 2.0 eV than is predicted by a simple Maxwellian. In Section 6.2 a good fit was made at low oxide fields to Schottky emission theory and an estimate of 0.12 eV obtained for the effective temperature of the distribution. At higher fields electron injection via a tunnelling mechanism was more dominant. A reasonable fit to tunnelling theory was made in Section 6.3 by assuming a Maxwellian distribution of carriers up to an ionising threshold energy of 2.1 eV. A future mathematical description of the charge carrier energy distribution in an avalanching junction will probably require a statistical analysis approach and take into account the energy band structure of silicon.

The present work, and previously published results, [56 & 57] indicate that electron injection into thermally grown SiO_2 is electrode limited and not bulk limited. Once injected into the conduction band, a small proportion of the electrons are captured in trapping centres, although the majority are able to transport through a thickness of several hundred angstroms of oxide and be captured by a metal electrode on the oxide surface. It is shown in Chapter 6 that the dependence found for the junction electron injection on the applied oxide field is well explained by transmission at the interfacial barrier. At low fields the dependence is a function of the image force lowering of the interface barrier height (Schottky effect) and at

higher fields becomes increasingly dependent on the electron tunnelling probability.

The dependence of the injected current on the junction current is more difficult to explain. When the junction is avalanched the injected current initially rises very rapidly and is not linearly dependent on the junction current as might be expected. A similar result has been found for example, by Bok[45] and Pepper,[71] for electron injection into vacuum and silicon dioxide, but was never explained by these authors. It has been argued [40, 42] that the rapid increase in injected current results from an increase in the average energy of the electron population as the junction current is increased. This has however, never been put on a quantative basis and has been discounted in the present work for at least the device structure studied. A new model is proposed in terms of electron injection from a switching microplasma which gives a good quantative fit to the observed almost exponential rise of the injected current with junction current. The microplasma model is also shown to be consistent with the observed fall off in the rate of increase in injected current at high junction current levels, and the observed rise in injected current level when the junction is illuminated with infra-red light. Further work is however, necessary to validate the microplasma model completely.

The work described in Chapter 7 on the high field electron injection into thin willemite films shows that the appearance of luminescence is probably determined by the thickness of an unreacted film of silicon oxide between the silicon and the willemite. The experimental results indicate that the willemite films were several orders of magnitude more conducting than the oxide film and that the energy of the injected electrons was controlled by the field across the interface oxide. Further work is necessary to discover the optimum thickness of the oxide film in high field luminescent devices. However, in the experiments made so far it is shown that the oxide film is always present after the willemite formation reaction. In the present work a luminescent film is formed over a shallow p-n junction electron injection structure by a reaction of ZnF_2:MnF_2 on bare silicon in a wet oxidising atmosphere. Even this procedure has been shown to result in an interfacial oxide film thickness of 80 Å. This oxide film may well limit the injection efficiency of high energy electrons into the luminescent film and be a fundamental limitation to a luminescent device.

Electron injection into the luminescent films from a reverse biased p-n junction shows essentially the same characteristics as injection into SiO_2. The major differences were in the higher injected current levels

and the observations of frequent switching events. These observations probably result from the conducting nature of the luminescent film which in turn result in a large part of the applied voltage being dropped across the thin interfacial oxide film. The work described in Chapter 7 shows that high energy electrons can be injected into a thin luminescent films from a reverse biased p-n junction. However, insufficient work has yet been completed to show conclusively whether this electron injection can result in the excitation of a luminescent centre within the film.

8.2 Further Research Required

The model proposed in Chapter 6 describing electron injection from microplasmas into thin insulating or luminescent films is at present only tentative. It has been shown that under reasonable assumed conditions the microplasma model can explain the experimental observations. In order, to gain more confidence in the model it is necessary to measure directly some of the parameters which were either estimated or taken from other published works. The current knowledge of microplasmas is very limited. The main observations have been made with low voltage ($\sim$ 25V) breakdown junctions such as described by Goetzberger[36]. As a result many of the deductions made in the present work are based on the behaviour of microplasmas found in this type of junction; very little is known of the behaviour of microplasmas in 100 V breakdown junctions. In particular the dependence of the microplasma's turn-on and turn-off probabilities with junction bias and illumination needs to be measured. It would also be desirable to measure the current multiplication factor of the uniform junction, in the voltage bias region to initiate the microplasma. It should be possible to build a measurement system which is able to distinguish between the total pulsed current carried by the microplasmas and the steady current carried by the remainder of the junction.

In order to simplify measurements and to make an unambiguous fit of the data to the model it is necessary to fabricate devices with a limited number of microplasmas: idealy they would have a single microplasma in the collecting region of the metal electrode. It was noted in Chapter 5 that the junctions tended to breakdown initially at the intersection of the shallow junction with the guard ring, and that this was probably as a result of strain induced defects. The number of edge microplasmas might be reduced by improvements in processing techniques, e.g. by reducing the rate at which the silicon substrates are pushed into or pulled from the hot zone of the furnace. It has also been shown that the number of strain

induced defects can be affected by the percentage of oxygen in the carrier gas during the initial push of the silicon into the hot zone of the furnace. It is thought that strain introduced in this part of the process cycle is a function of the initial growth rate of oxide on the silicon. It may also be possible to reduce the number of defects by processing whole silicon slices as supplied by the manufacturer rather than the scribed chips used in this work.

The work described above is concerned with validating the micro-plasma injection model. In the longer term the work should concentrate on the original goal of using high energy electron injection to obtain light emission from a thin luminescent film. The work described in this thesis has been successful in achieving electron injection into both SiO_2 and luminescent Zn_2SiO_4: M_n. The electron injection structure should now be improved with a view to obtaining a more uniform injection and hopefully exciting light emission in the luminescent film.

One of the major problems in fabricating the injection structures discussed in the present work was to form the luminescent films while maintaining a junction depth of less than 1000 Å. The willemite reaction process results in a maximum luminescence when formed at a temperature greater than 900 °C in a time longer than ten minutes. If such a reaction process had been used on the present structures it would have resulted in a shallow junction depth considerably greater than 1000 Å and hence no detectable electron injection would have been obtained. The problem was resolved as described in Chapter 7, by using a low temperature (850°C), wet reaction process to form a luminescent film. However, the films produced had a lower luminescent efficiency than those produced by Edwards' process. The luminescent films probably consisted of a form of zinic-orthosilicate as reported by Pfeiffer [99] however, further work on the analysis of the films is required to confirm this. Because of the low electron injection efficiency it would have been preferable to use a luminescent film of the highest luminescent efficiency. It may be possible to vacuum deposit such a film of willemite but it would probably require the use of a multiple source evaporation to obtain a film of the correct composition for luminescence. Such a system would have the advantage of not diffusing in the shallow junction although a post evaporation anneal might still be required to locate the Mn ions in the correct lattice sites. A vacuum evaporation system may also have the disadvantage of producing a poorer quality interface than is formed in a thermal growth reaction.

Another possible solution to the problem of forming willemite over a

shallow $p\text{-}n^+$ junction would be to use Edward's method for the film reaction but to use an n-type impurity with a low diffusion constant to form the junction. For example arsenic has a much lower diffusion constant than the phosphorus impurity used in the present work. The value of D at 1000 °C for arsenic is approximately $10^{-2}\ \mu/h^{\frac{1}{2}}$ compared with a value of $8 \times 10^{-2}\ \mu/h^{\frac{1}{2}}$ for phosphorus. (102) Arsenic also has the advantage of having an atomic radius well matched to the silicon lattice thus reducing strain effects. The tetrahedral radius of an arsenic impurity atom is 1.18 Å and for phosphorus it is 1.1 Å, these values compare with a radius of 1.17 Å for host silicon atom. (See Ref: 103, 104.) Unfortunately arsenic is not compatible with the open tube diffusion methods which were available at the time of this work and could not therefore be investigated. Some more recent work has been started in the Department using a spin-on arsenic source.

Probably the most attractive method of forming the shallow junction is to use ion implantation techniques. This would have the advantage of allowing the luminescent film to be formed before implanting the n-type impurity through the film to form the shallow junction. Only a low temperature bake at approximately 700°C would be required to anneal out the damage in the silicon lattice and to put the impurity into an electrically active site. It is not known what would be the damage effect of subjecting a luminescent willemite film to a high energy ion beam of around 100 KeV. Mayer et al (105) have obtained electron emission into vacuum from shallow ion implanted junctions. The methods employed were however crude by present day techniques and considerable loss in injection efficiency was found compared with conventionally produced junctions. This loss of efficiency was probably caused by junction damage resulting from the Cs and Na ion beam accelerated at 15-45 KeV. It is now possible to produce high quality junctions using phosphorus or arsenic as the impurity.

The work suggested above assumes that willemite is still considered by the author as the most suitable luminescent material for the device structure studied. This remains so because although epitaxial ZnS growth has been obtained on silicon, the conditions for electroluminescence are difficult to achieve (106) because of the necessity of bipolar recombination and the influence of impurities and defects in the films. It was considered in Chapter 1 that luminescence could be achieved in willemite using unipolar direct impact excitation of the Mn^{2+} ion, thus making it ideal for the device structure studied. Willemite also has the advantage of being

completely compatible with present day silicon device technology, as has been demonstrated in this thesis. The main disadvantage with willemite is the presence of the interfacial oxide film when using the present reaction process.

In a practical luminescent device it is desirable that electron injection should be achieved from the entire shallow junction area. A uniform emitting structure would also be useful in the verification of the electron injection model since the area of emission would be well defined. The device process procedures described in this thesis have been shown to be unsuitable for making large area, defect free, junctions. It is considered that it would be more practical to fabricate devices with a shallow junction diameter of approximately 100 μm. Making small area junctions would require the introducation of a high resolution and a more controlled masking procedure. It would be required to be abie to align successive mask stages within a tolerance of $\pm$ 10μm.

This thesis has not considered the effect of substrate doping on the injection device performance. It may be that a lower junction breakdown voltage ($\sim$ 10V) would be more suitable in making large area uniform emitting junctions. A lower value of junction breakdown means a narrower depletion layer width and hence the possibility of accelerating electrons to emission energies within the scattering mean free paths. In order to achieve a reasonable injection current such a device would require the additional injection of carriers into the depletion region by either infra-red excitation or by a forward biased n^+-p junction. This is also discussed below.

The problems caused by defects in the junction area only become apparent when avalanche breakdown is used to create a population of high energy electrons. It was shown in Chapter 5 that infra - red illumination can be used to create electron-hole pairs in the bulk silicon. In a reverse biased, infra-red illuminated junction the electrons which diffuse into the depletion field are able to gain sufficient energy to be injected into the SiO_2 film. In the experiment described in Chapter 5 the depletion field is well below the critical value required for avalanche breakdown and hence, localised enhanced multiplication does not significantly influence the injected current magnitude. In such a situation electron injection is probably occurring from the whole area of the shallow junction. It was noted in the experiment description that the injected current magnitude was a function of the infra-red illumination intensity. However, the maximum intensity available from the infra-red source was insufficient to achieve a high injection current level.

To increase the injected current density an improved injection structure can be devised which uses a forward biased p-n junction buried beneath the accelerating junction i.e. a p-n-p-n^+ structure as shown in Fig. 8.1. The buried, forward biased, junction would be the electron source, replacing the infra-red emitter used earlier. By forward biasing the buried junction minority carrier electrons would be injected into the intermediate p-type region and diffuse to the depletion field of the surface reverse biased p-n^+ junction. If the buried junction is placed within an electron diffusion length of the surface junction, which is easily done in making planar transistors, it should be possible to obtain a high density of energetic electrons directed towards the silicon surface. A structure such as described above does not rely on an avalanching junction to create the population of high energy electrons, it is therefore less susceptible to junction defects, and hence results in a more uniform electron injection. The current injection from such a device would also be easily controlled by means of the forward bias applied to the buried injector. Investigation of this type of device should be a long term aim of the research. It does however, require the facilities for epitaxial growth which are not available in the Department.

8.3 Conclusion

The work presented in this thesis has demonstrated the occurrence of electron injection into thin insulating films of SiO_2 and luminescent Zn_2SiO_4:Mn from a silicon planar p-n^+ junction. A model of the injection process has been presented which is consistent with the experimental results. It is proposed that a more uniform electron injecting structure could be made by reducing the defect levels during processing and by also reducing the junction area. Further work is also necessary to investigate the properties of low voltage breakdown junctions. A more sophisticated electron injection device is described which should allow a high density of electron injection while operating the accelerating junction below avalanche breakdown voltage. This device would be more difficult to make but far less sensitive to process induced defects.

It is concluded that willemite is still one of the best luminescent materials for use with a high energy unipolar injection structure. Methods are proposed for the formation of willemite films of optimum luminescent efficiency without driving in the injecting p-n^+ junction beyond 1000Å from the silicon surface. This will increase the probability of a high energy electron entering the willemite and making a radiative collision.

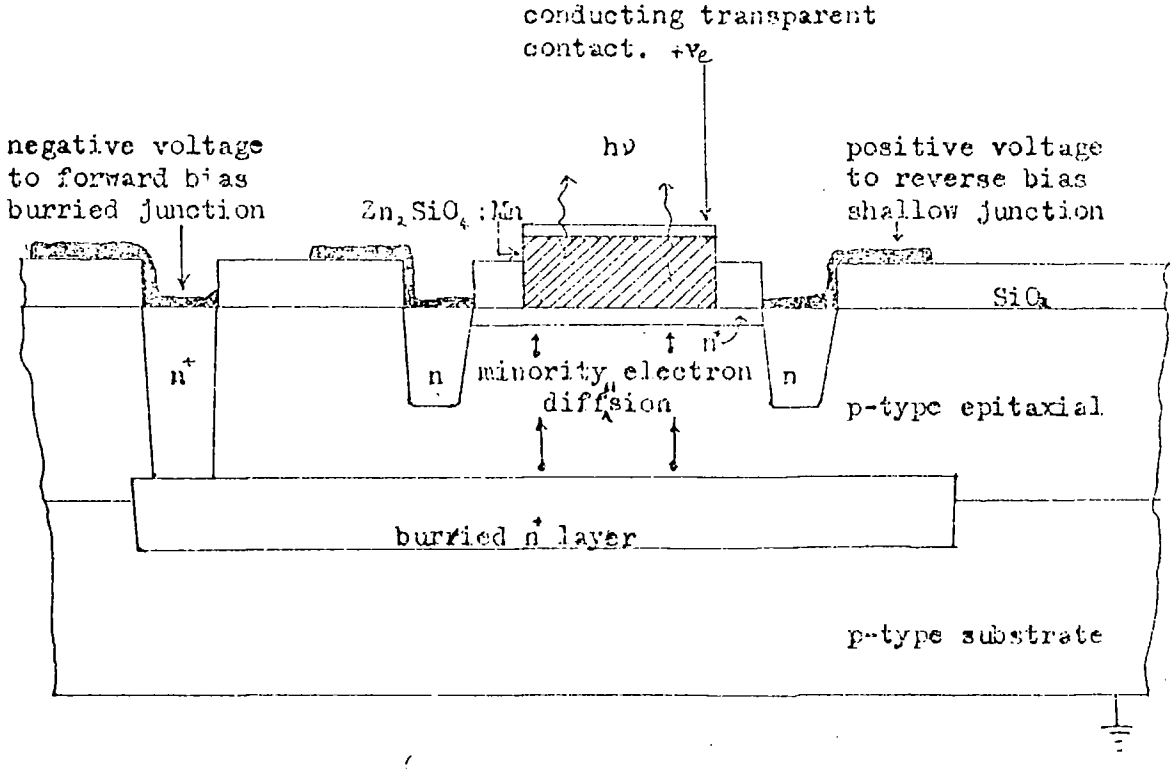

FIG 8.1 SECTION OF PROPOSED HOT-ELECTRON INJECTION STRUCTURE USING A BURRIED FORWARD BIASED p-n JUNCTION.

APPENDIX 1

IMPURITY DIFFUSION PROFILES

A1. 1 General Equation

In this section we shall consider the one dimensional solution to Fick's laws describing isotropic diffusion.

Fick's first law states:-

$$J = -D \nabla N, \qquad ((A1.1))$$

where J is the flux density of diffusing atoms

N is the concentration of diffusing atoms

D is the diffusion coefficient.

For the one dimensional case

$$J = -D \frac{\partial N}{\partial x} \qquad ((A1.2))$$

If we consider mass continuity through a small element of a solid and if material is neither formed or lost in this element it can be shown that:-

$$\frac{\partial N}{\partial t} = -\frac{\partial J}{\partial x} \qquad ((A1.3))$$

$$\frac{\partial N}{\partial t} = \frac{\partial}{\partial x}\left(D \frac{\partial N}{\partial x}\right) \qquad ((A1.4))$$

If D is assumed to be constant

$$\frac{\partial N}{\partial t} = D \frac{\partial^2 N}{\partial x^2} \qquad ((A1.5))$$

By considering certain limiting boundary conditions it is possible to obtain solutions to (A1. 5). Some of these solutions will be given below where they are applicable to the work contained in this thesis.

A1. 2 The Deposition Stage

In this situation a silicon wafer is in thermal equilibrium with a carrier gas containing a constant partial vapour pressure of the required dopent. According to Henry's Law the surface concentration of the impurity within the solid is proportional to the partial pressure of the impurity within the gas, up to the solid solubility. To a first approximation we can neglect the time taken for an equilibrium situation to arise between the gas and the silicon and consider the surface concentration to be constant throughout the deposition state.

Thus $N(x>0, t=0) = 0$

$N(x=0, t\geq 0) = N_0$

and the solution to (A1·5) becomes

$$N(x,t) = N_0 \operatorname{erfc}\left(\frac{x}{2\sqrt{D_1 t_1}}\right) \qquad ((A1.6))$$

where D_1 = diffusion constant for deposition

t_1 = time of deposition

A1. 3 The Drive-In Stage

In this work the deposition is followed by a further diffusion in an oxidising ambient such that the total number of impurities within the silicon remains constant.

Thus:
$$\left.\frac{\partial N}{\partial x}\right|_{x,t} = 0$$

$$N(\infty, t) = 0$$

The initial state for the drive-in diffusion is set by the deposition diffusion.

$$N(x,0) = N_b \operatorname{erfc}\left(\frac{x}{2\sqrt{(D_1 t_1)}}\right)$$

A closed analytical solution to (A1. 5) under these conditions has not been obtained. Approximations can be made however, and numerical solutions are possible.

A1. 4 Step Junction Approximation

If a step junction approximation is made for the error function deposition distribution, a solution of (A1. 5) can be obtained which holds if

$$\sqrt{(D_2 t_2)} \gg \sqrt{(D_1 t_1)}$$

where D_2 = diffusion constant for Drive in

t_2 = time of Drive-in

Thus:-

$$\left.\frac{\partial N}{\partial x}\right|_{x,t} = 0$$

$$N(\infty, t) = 0$$

$$N(x, o) = \begin{cases} N & 0 \leq x < h \\ 0 & x \geq h \end{cases}$$

where $h << x_j$

The solution to (A1. 5) is then given by

$$N(x,t) = \frac{Q}{\sqrt{\pi D_2 t_2}} \exp(-x^2/4D_2t_2) \qquad ((A1.7))$$

where Q is the total number of impurities within unit area of the silicon.

(Al. 7) can be rewritten as,

$$N(x, t) = N_o \exp(-x^2/4D_2t_2) \qquad ((A18))$$

Or in terms of the sheet resistance of the diffused layer,

$$\frac{1}{R'_s} = \mu_{av} q Q \qquad ((A\ 1.9))$$

where R'_s is the sheet resistance in $\Omega/\square$

μ_{av} is the average electron mobility in diffused layer in $cm^2/V\,sec$

q is the charge on an electron in coulombs

Thus $N(x) = \frac{1}{R'_s q \mu_{av} \sqrt{D_2 t_2 \pi}} \exp(-x^2/4D_2t_2)$ ((A1. 10))

A 1.5 Numerical Solution

In the shallow diffusion $\sqrt{D_1 t_1} \simeq \sqrt{D_2 t_2}$ and in this case equation (A1. 7) is not applicable. Kennedy and Murley[77] have obtained a numerical solution to the two step diffusion problem where the distribution after the deposition stage is given by,

$$N(x, o) = N_o \operatorname{erfc}\left(x / 2\sqrt{D_1 t_1}\right)$$

A graphical representation of the solution is given in Fig. (3. 2) for the diffusion encounted in the fabrication of the shallow junctions

$$\sqrt{D_1 t_1} \simeq \sqrt{D_2 t_2}$$

$$\frac{N_B}{N_o} \simeq \frac{5 \times 10^{15}}{10^{19}} \simeq 10^{-3}$$

where N_B is the background substrate doping

Thus from the graph Fig. (3. 2)

$$xj = (8{\cdot}4\sqrt{D_1 t_1}) \qquad \text{(A1. 11)}$$

It must be emphasised , however, that this still only an order of magnitude solution. No account has been taken for the time required for the silicon to reach thermal equilibrium with the carrier gas, or the redistribution of impurities during diffusion, or the dependence of the diffusion coefficient on the impurity concentration and oxide growth rate, all of which may introduce considerable errors with a very short diffusion time.

APPENDIX 2

PHOTO-LITHOGRAPHIC PROCEDURES

A2. 1 General Procedure

In this work Shipley AZ 1350 positive working photo resist was used throughout. This had the advantage over other types in that it could be easily removed in acetone, or if baked, in an alkali remover. Other resists required acid removal treatments which would destroy the willemite films.

Shipley AZ 1350 resist is supplied ready for use without the need for thinning. It was applied directly on to the oxidised silicon surface from a syringe fitted with a sub-micron filter. Before resist application the silicon was baked above 120°C to render the surface free from all traces of absorbed water which could result in poor adhesion and hence under-cutting. It was found to be desirable that this baking should take place in an atmosphere of dry nitrogen. If this was not done, incomplete develop - ment of the resist could sometimes result, leaving a thin film of resist in the pattern areas. The baking could be omitted if the resist was spun on within fifteen minutes of the silicon leaving a furnace. Where possible oxidation treatments finished with a fifteen minute period in dry nitrogen.

A resist film of about 5, 000 Å was formed on the oxidised silicon surface by spinning the silicon at a constant rotation speed of 4, 000 r. p. m. for thirty seconds. A spinner incorporating a vacuum chuck was designed for this purpose by the author as shown in Fig. A2. 1. It was found to be preferable to set the spinner rotating before the resist was applied. An alternative method was to flood the silicon with resist and then to spin off the surplus. This was found to result in a considerable build-up of resist at the silicon edges causing the masks to be out of contact giving poor image definition in the resist. Following application, the resist was dried for ten minutes at 65°C. A small stainless steel oven which allowed evaporation of the resist solvents was designed for this purpose by the author.

The pattern to be etched in the oxide or willemite films was defined in the photo-resist by exposure to U. V. light through the in contact, emulsion, glass mask. An apparatus enabling the mask to be aligned with a pattern previously etched in the silicon surface film was also designed by the author and is shown schematicly in Fig. A2. 2. The resist image was developed by immersion in Shipley ion-free developer for three minutes. This was followed by a wash in deionised water and by examination for defects under a micro-scope. Excess resist on the back face of the silicon was removed with acetone.

This was important in the etching stage. The thickness of oxide on the back of the silicon was the same as that in the regions to be etched on the front. A clean silicon surface, without oxide, is hydrophobic thus when the etchant runs off the back of the silicon the etching is complete. The final stage before etching was to wash the silicon for ten minutes in running dionised water and then to bake the resist in order to increase its resistance to the etchant. The time and temperature of the pre-etch bake varied according to the type of film to be etched as described in Section A2. 2. Similarly the removal of the resist depends on the baking treatment.

A2. 2 Pre-etch Baking and Resist Removal Procedures

(i) The etchant used for SiO_2 is a 4:1 solution of NH_4F:HF. This requires that the resist be baked for thirty minutes at a temperature of 150°C before etching the SiO_2.

After etching, the resist is best removed by boiling in a 50:50 solution of H_2SO_4:H_2O_2. This also leaves the silicon surface clean and ready for the next diffusion stage.

(ii) The willemite films are readily attacked by all acids but a controlled etch can be obtained using a 10% solution of glacial acid in deionised water. This requires that the resist be baked for twenty minutes at 120°C before etching the willemite.

It was possible to remove the resist in acetone after this bake but the use of Shipley ion-free resist remover at 50°C was preferable as this also removed excess ZnF_2 and ZnO.

(iii) Aluminium was best etched in a 80:5 solution of H_3PO_4:HNO_3. A pre-etch bake is not required.

Resist removal was best accomplished using acetone.

(iv) With aluminium overlaying a willemite film it was not possible to use an acid etch and a solution of 2% NaOH in deionised water was used. This is a strongly alkali solution and readily attacks the resist if it is not baked on at 150°C for thirty minutes.

Removal of the resist was accomplished by using Shipley ion-free resist remover at 50°C. Care was necessary to establish a minimum removal time for each batch using a pilot sample since the remover can attack the aluminium with prolonged exposure.

Chemical concentrations used above: -

H_2O_2 - 100 vols, 29% W. W.
H_2SO_4 - 98%
HF - 40% solution
NH_4F - 40% solution
HNO_3 - 69 -71% W. W.

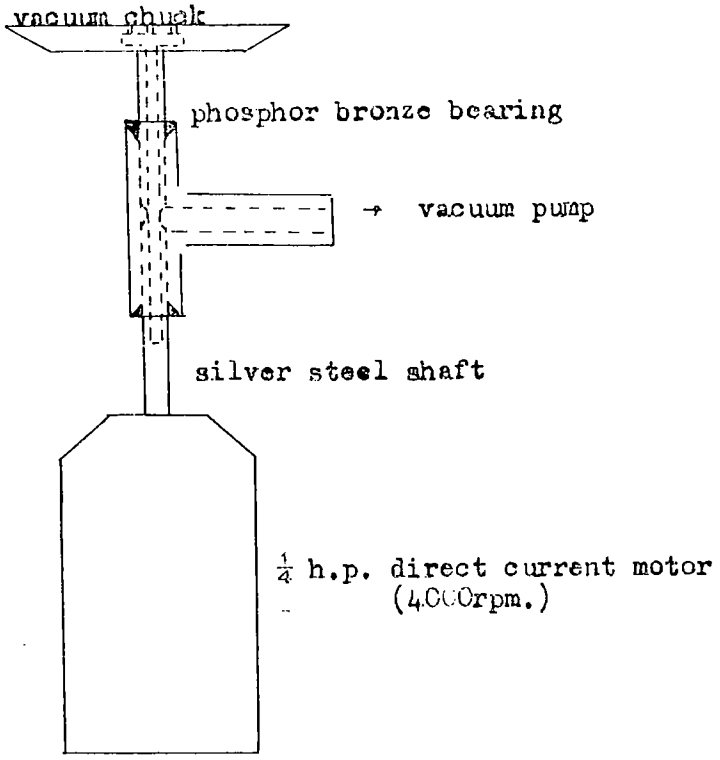

FIG A2.1 SPINNER FOR APPLYING PHOTO-RESIST

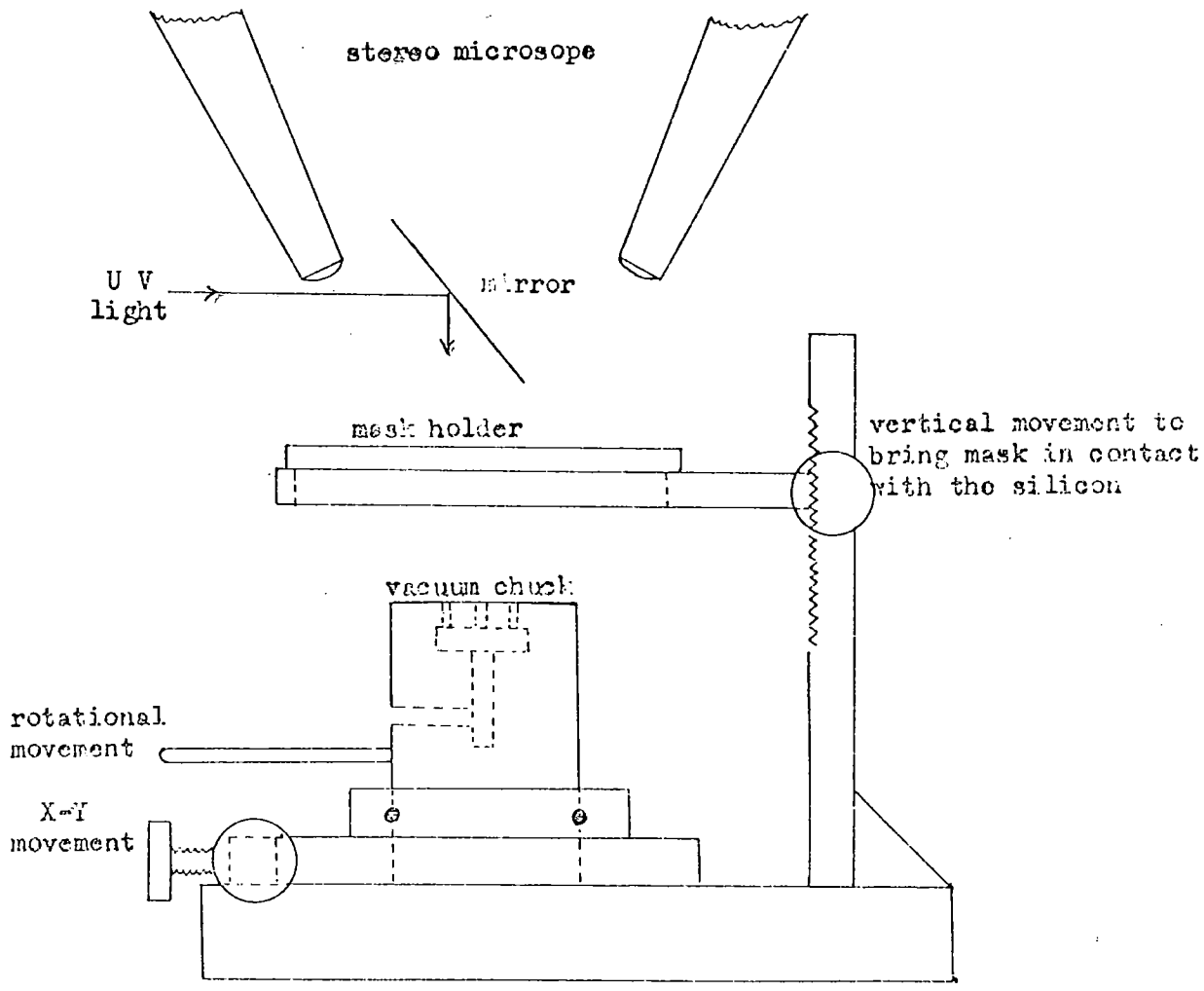

FIG A2.2 MASK ALIGNMENT EQUIPMENT

REFERENCES

1. Anon. Electronics, May 1971
2. Edwards, G. S. Ph. D. Thesis, University of Durham, 1970
3. Edwards, G. S. and A. N. Rushby, J. Mat. Science, 6, 225, 1971
4. Morant, M. J. Departmental Report of the Luminescent Properties of Willemite, 1972
5. Klik, C. C. Brit. J. Appl. Phys. Suppl. 4, 74, 1955
6. Garlick, G. F. J. Luminescence, Handbuch der Physik, Vol. 26, pp 1 - 128, 1958.
7. Klik, C. C. and J. H. Schulman, J. Opt. Soc. America, 42, 910, 1952
8. Verwey, J. F. J. Appl Phys, 43, 2273, 1972
9. Kailsel, S. F. and C. B. Clark, J. Opt. Soc. America, 44, 134, 1954
10. Schrader, R. E. and S. F. Kaisel, J. Opt. Soc. America, 44, 135, 1954
11. McKay, K. G., Phys. Rev. 94, 877, 1954
12. Wolff, P. A., Phys. Rev. 95, 1415, 1954
13. Seitz, F., Phys. Rev. 73, 550, 1948
14. McKay, K. G. and K. B. McAfee, Phys. Rev. 91, 1079, 1953
15. Chynoweth, A. G. J., Appl. Phys., 31, 1161, 1960
16. Shockley, W. S., S. S. E., 2, 35, 1961
17. Baraff, G. A., Phys. Rev., 128, 2507, 1962
18. Sewards, T. V. and W. W. Grannemann, New Mexico Univ., Albuquerque, Report Bureau of Engineering, 1971
19. Hodgkinson, R. J., Brit. J. Appl. Phys., 15, 1483, 1964
20. Bartelink, D. J., J. C. Moll and N. I. Meyer, Phys. Rev., 130, 972, 1963
21. Monch, W., Phys. Stat. Sol., 36, 9, 1969
22. Lawrence, J. E. J. Elec. Chem. Soc., 112, 796, 1968
23. Chynoweth, A. G. and P. L. Pearson, J. Appl. Phys., 29, 1103, 1958
24. Matare, H. F., Defect Electronics in Semiconductors, (Wiley) p. 442
25. Newman, R., Phys. Rev., 100, 700, 1955
26. Wolff, P. A., J. Phys. Chem. Solids, 16, 184, 1960
27. Figielski, T. and A. Toran, Proc. Internat. Conf. Phys. Semiconductors, Exeter, p. 863, 1962
28. Wolff, H. F., Silicon Semiconductor Data, p. 20 (Pergaman Press) 1969
29. Chynoweth, A. G. and K. G. McKay, J. Appl. Phys., 30, 1811, 1959
30. McIntyre, R. J., J. Appl. Phys., 32, 983, 1961
31. Haitz, R. H., J. Appl. Phys., 35, 1370, 1964
32. Aladinskii, V. K., Sov. Phys. Semiconductors, 6, 1731, 1973
33. Phillips, A. B., Transistor Engineering, McGraw-Hill, p. 216, 1962

34. Maeda, K. and K. Suzuki, Jap. Appl. Phys., 1, 193, 1962
35. Haitz, R. H. A. Goetzberger, R.M. Scarlett and W. Shockley, J. Appl. Phys., 34, 1581, 1963
36. Goetzberger, A., B. McDonald, R. H. Haitz, and R. M. Scarlett, J. Appl. Phys., 34, 1591, 1963.
37. Haitz, R. H. and A. Goetzberger, S. S. E., 6, 678, 1964
38. Burton, J. A., Phys. Rev. 108, 1342, 1957
39. Simon, R. E. and W. E. Spicer, Phys. Rev. 119, 621, 1960
40. Elinson, and Lutski, Sov. Phys.-Solid State, 6, 1857, 1965
41. Goffaux, R. Journal de Physique et le Radium, 2, 94, 1960
42. Patrick, L. and W. J. Choyke, Phys. Rev. Letters, 2,48, 1959
43. Tauc, J., Nature, 181, 38, 1958
44. Senitzkey, B., Phys. Rev., 116, 874, 1959
45. Bok, J. and J. Klien, Phys. and Chem. of Solids, 27, 295, 1966
46. Hodgkinson, R. J., Brit. J. Appl. Phys., 15, 1483, 1964
47. Walder, M., J. Appl, Phys., 36, 188, 1965
48. Lamb, D. R., Electrical Conduction Mechanisms InThin Insulating Films (Methuen and Co. London) 1967
49. Goodman, A. M. Phys. Rev., 164, 1145, 1967
50. Goodman, A. M. and J. J. O'Neill, Jr. J. Appl. Phys., 37, 3580, 1966
51. Williams, R. Phys. Rev., 140, A. 569, 1965
52. Berglund, C. N. and R. J. Powell, J. Appl. Phys., 42, 573, 1971
53. Thomas, J. H. and F. J. Feigl, S. S. E., 8, 1669, 1970
54. Thomas, J. H. and F. J. Feigl, J. Phys, Chem. Solids, 33, 2197, 1972
55. DiMaria, D. J. F. J. Feigl and S. R. Butler, App., Phys. Letters, 24, 459, 1974
56. Lenzlinger, M. and E. H. Snow, J. Appl. Phys., 40, 278, 1969
57. Osburn, C. M. and E. J. Weitzman, J. Elec. Chem. Soc., 119, 603, 1972
58. Balk, P., J. Elec. Chem. Soc., 112, 185C, 1965
59. Peel, J. L., R. A. Kjar and R. C. Eden, App. Phys. Letters, 17, 3, 1970
60. Di Stefano T. H. and J. M. Vicciano, IBM J. Res. and Dev., 18, 94, 1974
61. Conti, M. and A. Vanin, Thin Solid Films, 14, 211, 1972
62. Ferris, A., I.B.M. J. Res. Dev., 17, 125, 1973
63. Nicollian, E. H., A. Goetzberger and C. N. Berglund, Appl. Phys. Letters, 15, 174, 1969
64. Nicollian, E. H. and C. N. Berglund, J. Appl. Phys., 141, 3052, 1970
65. Nicollian, E. H., C. N. Berglund, P. F. Schmidt and J. M. Andrews, J. Appl. Phys. 42, 5654, 1971

66. Erb, D. M., H. G. Dill, and T. N. Toombs, I.E.E. Trans. Electron Devices, ED - 18, 105, 1971
67. Verwey, J. F., J. Appl. Phys., 44, 2681, 1973
68. Hara, H. Y. Okamoto, H. Oknoma, Jap. J. Appl. Phys., 9,1103, 1970
69. Frohman - Bentchkowsky, D., S.S.E., 17, 517, 1974.
70. Verwey, J. F. and B. J. De Maagt, I.E.E. Trans. Electron Devices, ED. -19, 245, 1972.
71. Pepper, M., J. Phys. D: Appl. Phys. 6, 2124, 1974
72. De Graaff, H. C., Philips Res. Rep., 25, 21, 1970
73. Bulucea, C., S.S.E., 18, 363, 1975
74. Bulucea, C., S.S.E., 18, 381, 1975
75. Armstrong, H. L., I.R.E. Trans. on Electron Devices, ED-4, 15, 1957
76. Kennedy, D.P. and R.R. O'Brien, I.R.E. Trans. on Electron Devices, ED-9, 478, 1962
77. Kennedy, D.P. and P.C. Murley, Proc. I.E.E., (Corresp) 54, 620, 1964
78. Washburn, J., G. Thomas, and H. J. Queisser, J. Electrochemical Technol., 35, 1909, 1964
79. Heynes, M.S.R. and J.T. Wilkerson, J. Electrochemical Technol., 5, 464, 1967
80. Morton, B. R., Quart, J., Mech. and Appl. Maths, 12, 410, 1959
81. McDonald, B. and A. Goetzberger, J. Elec. Chem. Soc., 109, 141, 1962
82. Irvin, J. C., Bell Syst. Tech. J., 41, 387, 1962
83. Deal, B. E. and M. Sklar, J. Elec. Chem. Soc., 112, 430. 1965
84. Thomas, J. E. and D. R. Young, I.B.M. J. Res. Dev., 8, 368, 1964
85. Stickler, R. and J. W. Faust Jr., J. Electrochemical Technol., 4, 70, 1966
86. Evseev, Yu. A., I. N. Magden, A. E. Radechko, and V. E. Chelnokov, Sov. Phys. Semiconductors, 4,1226, 1970
87. O'Dwyer, J. J., J. Appl. Phys., 40,3887, 1969
88. Szedon, J. R. and R. M. Handy, J. Vacuum Science and Technol, 6, 1, 1968
89. Fowler, R. H. and L. Nordheim, Proc. Royal Soc. A. 119, 173, 1928
90. Stratton, R., Proc. Phys. Soc. (London), B68, 746, 1955.
91. Grove, A. S., Physics and Technology of Semiconductor Devices, Wiley, p.p. 172 - 180, 1967
92. Bulucea, C. and D. C. Prisecaru, I.E.E.E. Trans. Electron Devices, ED-20, 692, 1973
93. Hill, R. M., Thin Solid Films, 1,39, 1967
94. Verwey, J. F. and B. J. De Maagt, S.S.E., 17, 963, 1974.

95. Davies, G. D., M. Sc. Thesis 'The Preparation and Properties of Thin Films of Willemite on Silicon', Univ. of London, 1975

96. Davies, G. D., Internal Report, Dept. of Applied Physics and Electronics, Univ. of Durham, 1972

97. Morant, M. J. and G. S. Edwards, S.S.E., 16,173, 1972

98. Errington, D., PhD. Thesis. Univ. of Durham, (To be presented)

99. Pfeiffer, H. G. and G. R. Fonda, J. Elec. Soc. 99,140, 1952

100. Goetzberger, A. and W. Shockley, J. Appl. Phys. 31,1821, 1960

101. Champlin, K. S., J. Appl. Phys. 30,1039, 1959

102. Grove, A. S., Physics and Technology of Semiconductor Devices, p. 39, (Wiley) 1967

103. Jain, R. K. and R. J. Van Overstralten, Phys. Stat. Sol. 25, 125, 1974

104. Wolf, H. F., Silicon Semiconductor Data, p. 150, (Pergamon Press) 1969

105. Meyer, N. I. and F. P. Jensen, J. Appl. Phys., 37,4297, 1966

106. Rawlins, T. G. R., and R. J. Woodward, J. Mat. Science, 7,257, 1972

107. Husain, M. R. Ph.D., Thesis, University of Durham. 1974

108. HAWKES, J. F. B. J. of Luminescence. 11, 129, 1975

experimental points lie on a straight line indicating a deviation from the simple image force lowering theory at high fields. From the slope of the straight line part of the plot an estimate of the effective temperature of the assumed Maxwellian distribution of electron energies can be obtained and compared with previous worker's results. A value of 3.9 was used for the dielectric constant for silicon dioxide and a value for kT_e of 0.12eV was calculated from the slope. This is very close to the 0.11eV calculated from Wolff's [12] theory of avalanche breakdown is silicon and to the estimate of 0.18eV made by Chynoweth [15] from the radiation emission spectrum of a microplasma. It is however lower than the estimate of 0.45eV made by Bartelink[20] and the value of 0.5 eV from Bok and Klien[45]. These values, however, come from the direct measurement of the energies of electrons emitted into vacuum and therefore represent the high energy tail of the electron population rather than that of the total avalanching electron population. Furthermore, the background doping of the bulk p-type silicon in Bartelink's and Bok's devices was of the order of $10^{18}/cm^3$. In the present work the doping was $5 \times 10^{15}/cm^3$ thus giving a lower critical field at breakdown. According to Bartelink's theory the effective energy of the charge carrier population is given by

$$kT_e = \frac{E_0}{\frac{1}{2} + \left(\frac{1}{4} + \frac{E_0}{rE_r}\right)^{1/2}} \qquad ((6.13))$$

where

$$E_0 = \frac{(qF_A l_r)^2}{rE_r} \qquad ((6.14))$$

and F_A is the field at avalanche breakdown.
In the present work F_A is approximately 3×10^5 V/cm compared with Bartelink's 10^6V/cm. Taking Bartelinks values of r = 3.2, Er=0.063eV, l_r = 60 Å gives,

$$kT_e = 0.11 \text{ eV}$$

It is concluded therefore that the value of 0.12 eV derived from the present results is consistent with the best avalanche theories.

We now turn to the situation at higher oxide fields. It is apparent from Fig. 6.2, that for fields greater than 1.4×10^6V/cm the injected oxide current no longer follows a linear relationship with $\sqrt{F(x)}$. This can be interpreted as a deviation away from a dependence on the image force lowering of the barrier to one in which the oxide current is increasingly dominated by electron tunnelling through the barrier.

The transmission coefficient of an electron through a triangular barrier has been considered by Fowler and Nordheim [89] who show that if,

a large emitting area and a depletion field directed normal, towards the surface, leading to a higher injected efficiency.

3.2 Impurity Profiles and Junction Breakdown

The reverse voltage at which a planar p-n junction breaks down has been shown by Armstrong [75] to be dependent on the depth of diffusion. This is a result of the edge curvature of the junction. The shallower a junction is, the smaller the radius of curvature and the higher the localised field causing edge breakdown. Edge breakdown can be prevented by diffusing a deep guard ring around the shallow region (Fig. 3.3). Because of the depth of the guard ring the junction field is not increased by the geometry and the breakdown voltage approaches that of a plane junction, dependent only on the doping concentration profile. For an abrupt junction the breakdown voltage is controlled by the background impurity concentration. However, planar diffused junctions are not usually abrupt and the breakdown voltage is also a function of the impurity concentration gradient at the junction boundary. (Fig. 3.1) With appropriate design it has been possible to arrange the guard ring breakdown to occur at a higher voltage than the shallow layer so that controlled avalanching is possible.

Appendix 1 considers the mathematical expressions for these impurity profiles of diffused junctions.

From Equation A1.8 the concentration gradient for a Guassion distribution is given by:-

$$\left.\frac{\partial N}{\partial x}\right|_{x,\ t} = \frac{-x}{2Dt} \cdot (N(x.t))$$

where N is the impurity concentration at depth x after a diffusion time t.

D is the appropriate diffusion coefficient.

At the junction boundary,

$$x = x_j$$

Putting $\frac{\partial N}{\partial x} = a = -x_j N_B/2Dt$ ((3·1))

where N_B = substrate doping

From Equation ((A1·10))

$$x_j = (4Dt \log_e (N_B R_s q \mu_{av} \sqrt{\pi Dt}))^{\frac{1}{2}} \quad ((3\cdot2))$$

$$\therefore a = N_B/\sqrt{Dt}\,(\log_e (N_B R_s q \mu_{av} \sqrt{\pi Dt}))^{\frac{1}{2}} \quad ((3\cdot3))$$

where R_s is the sheet resistance of the diffused layer,

μ_{av} is the average electron mobility